Aus dem Walther-Straub-Institut für Pharmakologie und Toxikologie

Institutsvorstand: Prof. Dr. med. Thomas Gudermann

Targeting cardiac arrhythmia by enhancing mitochondrial Ca^{2+} uptake

Habilitationsschrift

vorgelegt von

Johann Schredelseker PhD

München, 2020

From the Walther Straub Institute for Pharmacology and Toxicology

Head: Prof. Dr. med. Thomas Gudermann

Targeting cardiac arrhythmia by enhancing mitochondrial Ca^{2+} uptake

Habilitation thesis

submitted by

Johann Schredelseker PhD

Munich, 2020

Index

Summary

Cardiovascular diseases remain the number one cause for morbidity and mortality worldwide with an estimated half of cardiovascular disease-related deaths being attributed to cardiac arrhythmia. Despite this enormous importance for public health, existing antiarrhythmic drugs are still far from being ideal as they display perilous side effects and can not be administered over extended time periods. It is thus a major endeavor of cardiovascular research to identify novel safer drug targets and therapeutic strategies for the treatment of cardiac arrhythmia.

Since cardiac rhythmicity is directly dependent on a tight regulation of intracellular Ca^{2+} and cardiac arrhythmia is often associated with disturbances in Ca^{2+} homeostasis, we used an unbiased approach to identify novel regulators of cardiac Ca^{2+} handling and modulators thereof. A library of newly synthesized, organic-like compounds was screened for their ability to restore rhythmic cardiac contractions in a zebrafish model for cardiac fibrillation. From this screen we identified the small ester compound efsevin, which binds to the voltage-dependent anion channel 2 (VDAC2) in the outer mitochondrial membrane. We demonstrated that treatment with efsevin enhances mitochondrial Ca^{2+} uptake and thereby prevents propagation of spontaneous intracellular Ca^{2+} release events in cardiomyocytes, the triggers for ectopic excitations and arrhythmia. Since this work presented a novel role for VDAC2 in cardiomyocytes we analyzed the structure of VDAC2 by crystallography to identify elements that promote specificity of this isoform over VDAC1 and VDAC3. Though we could not detect large structural differences, we identified moieties that interact with regulatory proteins, which differ between the isoforms, and could thus explain the distinct role of VDAC2 in cardiomyocytes. We then used the crystal structure of VDAC2 to identify the binding site of efsevin by

computational modeling and identified a binding pocket located between the wall of the VDAC2 pore and the pore-lining α helix, that was previously suggested to promote channel gating. In planar lipid bilayers we demonstrated that efsevin promotes gating of the channel from an anion-selective high conductance state into a more cation-selective low conductance state, thereby explaining the enhanced mitochondrial Ca^{2+} uptake induced by efsevin.

To analyze the translational potential of efsevin, we tested efsevin in experimental models for the human cardiac arrhythmia catecholaminergic polymorphic ventricular tachycardia (CPVT). Efsevin reduced spontaneous diastolic Ca^{2+} signals and action potentials in cardiomyocytes isolated from CPVT mice and significantly reduced episodes of ventricular tachycardia in *in vivo*. Furthermore, efsevin reduced spontaneous, diastolic Ca^{2+} signals in induced pluripotent stem cell derived cardiomyocytes from a CPVT patient. Because efsevin lacks several features essential for druggability like e.g. a nanomolar affinity to the target and key pharmacokinetic properties like oral bioavailability, we then screened a library of clinically approved compounds for additional mitochondrial Ca^{2+} uptake enhancers. We identified increased uptake of Ca^{2+} into mitochondria of cardiomyocytes upon treatment with either the cholesterol uptake inhibitor ezetimbe or disulfiram, used for the treatment of alcohol abuse. Both were active at significantly lower concentrations compared to efsevin and showed efficacy experimental models for cardiac arrhythmia.

Taken together, this thesis (i) establishes the outer mitochondrial membrane as a regulated barrier for Ca^{2+}, (ii) establishes mitochondrial Ca^{2+} uptake as a novel regulator of cardiac rhythmicity and (iii) provides a novel candidate structure and lead substances for the development of a treatment for human cardiac arrhythmia.

Introduction

Therapy of cardiac arrhythmia

Cardiovascular diseases (CVDs) continue to dominate mortality and morbidity rates worldwide (Nichols et al., 2012; Benjamin et al., 2018). Despite a general decline of CVD-associated deaths over the last years, mortality rates for cardiac arrhythmia in particular are still increasing (Klawki et al., 2018). Almost half of all CVD related deaths are attributed to sudden cardiac death mainly caused by ventricular tachyarrythmias (Mehra, 2007). This is in part due to the insufficiency of currently used antiarrhythmic drugs, which display perilous side effects and are thus difficult to apply.

Cardiac arrhythmias originate at focal areas in the myocardium induced by structural abnormalities, such as infarct wounds and anatomical obstructions, or as a result of physiological abnormalities such as a disturbed cellular ion homeostasis (***Figure 1***). The latter might be caused by maladaptations of the mycardium to preexisting conditions like heart failure, ion channel mutations, or drug intake. The resulting focal activity of the myocardium gives rise to a propagating ectopic excitation wave along the heart and creates a reentry circuit, the physiological underpinning of tachycardias.

Commonly used antiarrhythmic drugs of Vaughan Williams classes I-IV and cardiac glycosides directly or indirectly target ion channels in the cardiomyocyte membrane to modify the cardiac conduction system and thereby block expansion of ectopic excitations along the myocardium (***Figure 1***). However, by blocking cardiac de- or repolarization and thereby modulating cardiac conduction speed all of these

drugs, with the exception of beta blockers, are prone to proarrhythmic and negative inotropic side effects. It is thus a major focus of cardiovascular research to identify novel targets and strategies for a safer treatment of cardiac arrhythmia.

A major line of research for the development of such therapies lies on intracellular target structures, in particular the cellular Ca^{2+} handling network, but not only because cardiac arrhythmias are often associated with disturbances in cellular Ca^{2+}. Also, by targeting intracellular structures the cardiac action potential is expected to remain unaffected and therapies targeting intracellular structures could thus be less prone to proarrhythmic side effects.

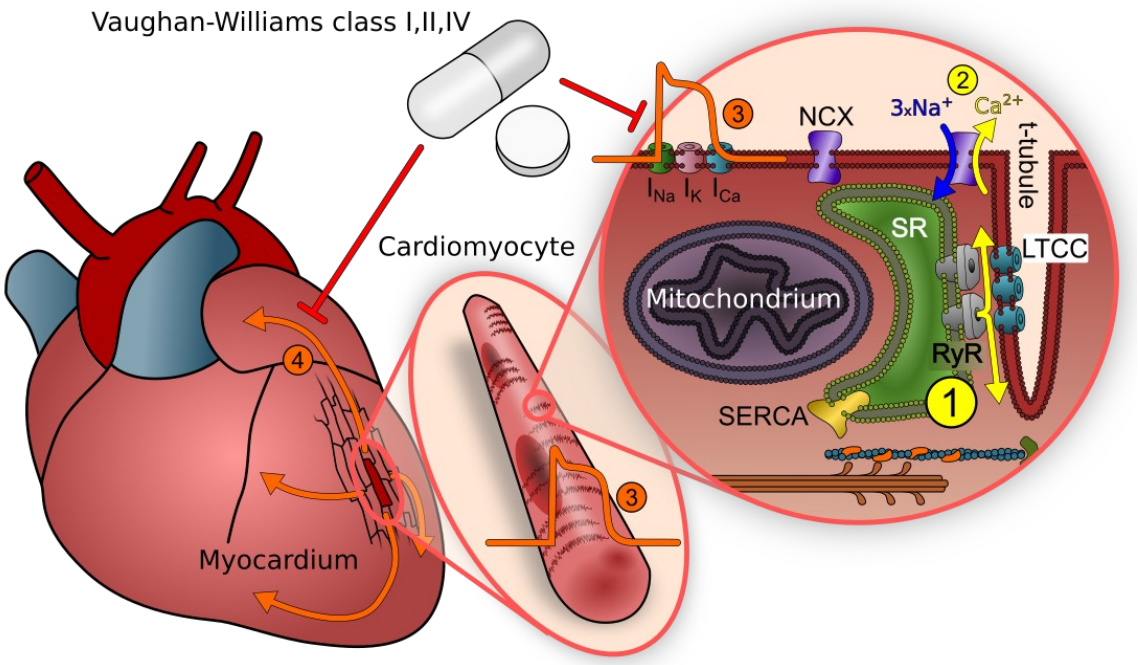

Figure 1. Cardiac arrhythmogenesis and treatment. *Ca^{2+}-associated arrhythmias are triggered by the spontaneous release of Ca^{2+} during diastole (**1**). This spontaneous Ca^{2+} release triggers the influx of Na^{+} (**2**) through NCX and finally a spontaneous depolarization of the cardiomyocyte (**3**). This diastolic excitation is propagated along the electrical syncytium of the myocardium and triggers an ectopic beat (**4**). Currently used antiarrhythmic drugs of Vaughan-Williams classes I,III, and IV target ion channels in the myocardium to prevent propagation of the excitation (**3,4**) rather then targeting the intracellular origin of the arrhythmia (**1**).*

Cardiac Ca^{2+} cycling and arrhythmia

Cardiac rhythmicity and contractility critically depend on a tight regulation of intracellular Ca^{2+} in the cells of the myocardium, the cardiomyocytes. During diastole the concentration of resting Ca^{2+} inside the cell is in the low nanomolar range, while the cell is extracellularly surrounded by approximately 2 mM Ca^{2+} (Bers, 2008; Fearnley et al., 2011). In this phase the cell maintains a membrane potential of approximately -80mV. During systolic excitation the cell is depolarized to roughly 20-30 mV causing L-type Ca^{2+} channels to open and Ca^{2+} to passively enter the cell. The L-type Ca^{2+} channels are located in clusters inside the t-tubuli, deep invaginations of the cell membrane into the cellular lumen. The t-tubular membrane is tightly coupled to the membrane of the sarcoplasmic reticulum (SR), the main Ca^{2+} store inside cardiac muscle cell. Inside these couplons the L-type Ca^{2+} channel clusters in the t-tubular membrane are closely juxtaposed to clusters of ryanodine receptors (RyRs) on the surface of the SR. In a process called Ca^{2+}-induced Ca^{2+} release (CICR) Ca^{2+} entering the cell through L-type channels binds to RyRs causing them to open and to release large amounts of Ca^{2+} from the SR into the cytosol. The transient rise in intracellular Ca^{2+} leads to activation of the myofilaments and consecutively muscle contraction. Thereafter, Ca^{2+} is actively extruded from the cell by the sarcolemmal Na^{+}/Ca^{2+} exchanger NCX and pumped back into the SR by the sarco-/endoplasmatic reticulum Ca^{2+} pump (SERCA) to return to resting conditions (for a review see Bers, 2002).

Certain conditions such as mutations in ion channels, imbalances in ion homeostasis or defects in post-translational regulation can lead to uncontrolled Ca^{2+} fluxes in the cell. Erratic Ca^{2+} release during diastole induced by mutations in RyR or due to elevated cytosolic Ca^{2+} levels can be the trigger for severe arrhythmias

(***Figure 1***). Specifically, individual clusters of RyRs on the surface of the SR spontaneously activate during diastole and release small quantities of Ca^{2+} from the SR as a locally restricted event. These elementary Ca^{2+} release events were first discovered by using Ca^{2+} sensitive dyes and were contiguously named Ca^{2+} sparks (Cheng et al., 1993). Once the rate of Ca^{2+} sparks reaches a certain threshold, Ca^{2+} from one spark activates the neighboring cluster of RyRs and a saltatory expansion of Ca^{2+} inside the cells occurs, called a Ca^{2+} wave. The elevated level of Ca^{2+} inside the cell drives NCX through which Na^{+} enters the cell in a 1:3 Ca^{2+} over Na^{+} ratio, yielding a net influx of positive charges, and thus depolarization of the cell (Allen et al., 1984). If sufficiently large these delayed afterdepolarizations (DADs) can spread along the myocardium and cause ectopic excitations and finally arrhythmia.

Regulation of cardiac Ca^{2+} cycling

Apart from these main players, a plethora of regulatory proteins and pathways fine tune intracellular Ca^{2+} handling to guarantee a meticulously regulated Ca^{2+} homeostasis at rest and during adaption to higher workload.

These Ca^{2+} regulatory mechanisms range from post-translational modifications of the key players such as the L-type Ca^{2+} channel or the RyR, to additional regulatory proteins such as subunits of these channels or structural proteins, which anchor the essential cell compartments together to finally entire organelles that interact with the aforementioned cellular structures. For example, lysosomes and mitochondria were both described to form close contacts to the SR at Ca^{2+} release sites and to vividly interact with the SR (Hajnóczky et al., 2000; Aston et al., 2017). Especially mitochondria were shown to be capable of sequestering large amounts of Ca^{2+} into their matrix (Hajnóczky et al., 2000).

These regulatory mechanisms are still under intensive research and while some of them are well described, others were just recently discovered and are still poorly understood. However, these intracellular regulatory mechanisms bare the potential to serve as novel drug targets, since they have the power to modulate and regulate Ca^{2+} release and by this to suppress erratic Ca^{2+} release without affecting the cardiac conduction system.

The central thesis of the project

In this work we present mitochondrial Ca^{2+} uptake as a novel regulatory mechanism of cardiac rhythmicity and a potential drug target.

By applying an unbiased screening approach we identified the novel compound efsevin by its ability to restore rhythmic cardiac contractions in otherwise fibrillating heart of a zebrafish arrhythmia model (Shimizu et al., 2015). A pull-down assay identified the voltage-dependent anion channel 2 (VDAC2) to be the target of efsevin. VDAC2 is a large pore forming protein in the outer mitochondrial membrane, which in cardiomyocytes is positioned in close proximity to the Ca^{2+} release sites of the SR. It is composed of a β-sheet barrel and a pore-lining α-helix that was proposed to be responsible for channel gating (Schredelseker et al., 2014). Efsevin binds to the hinge region of this helix and facilitates gating of VDAC2 from the open state into less anion selective gated states and thereby enhances influx of Ca^{2+} into mitochondria (Wilting et al., 2020).

With this data, we formulated the following central hypothesis: Arrhythmogenic signals in cardiomyocytes are generated by erratic diastolic Ca^{2+} release starting with a Ca^{2+} spark, the spontaneous opening of a single cluster of RyRs (***Figure 2***). Under

pathological conditions Ca^{2+} released from this elementary event triggers opening of neighboring Ca^{2+} release sites to initiate an arrhythmogenic Ca^{2+} wave, which propagates along the cardiomyocyte. Mitochondria, which are located in close proximity to the Ca^{2+} release sites of the SR, have the ability to take up Ca^{2+} and thereby provide a Ca^{2+} buffering compartment to shape cellular Ca^{2+} signals. When mitochondrial Ca^{2+} uptake is pharmacological activated a fraction of the released Ca^{2+} is buffered into mitochondria leading to a spacial and temporal restriction of the spark. By this mechanism the cell can tolerate a higher spark frequency without generation of arrhythmogenic Ca^{2+} waves (***Figure 2***).

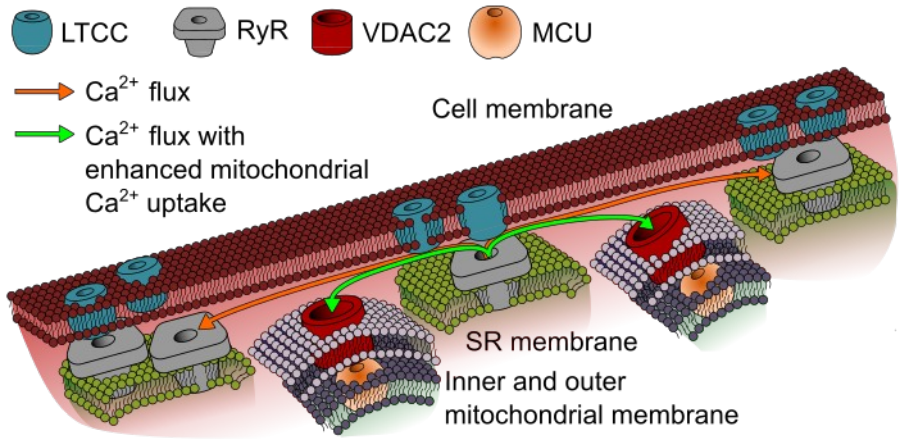

Figure 2. Model for mitochondrial Ca^{2+} uptake mediated suppression of arrhythmia. *Ca^{2+} released by the spontaneous opening of a cluster of ryanodine receptors (RyR) during diastole diffuse laterally inside the cytoplasm and induces saltatoric propagation of a Ca^{2+} wave by activating neighboring Ca^{2+} release units (orange arrow). Upon activation of mitochondrial Ca^{2+} uptake the Ca^{2+} signal is buffered into mitochondria and the saltatoric propagation is interrupted (green arrow).*

To prove this hypothesis we evaluated the effect of efsevin on Ca^{2+} sparks and waves in ventricular cardiomyocytes. Indeed, efsevin enhanced cytosolic Ca^{2+} clearance and thus led to a spatial and temporal restriction of individual Ca^{2+} sparks

(Shimizu et al., 2015; Schweitzer et al., 2017). Thereby it suppressed the generation of Ca^{2+} waves and finally arrhythmogenic action potentials in these cells. This effect was blocked in the presence of the mitochondrial Ca^{2+} uptake inhibitor Ru360. To prove the general validity of this hypothesis we identified and tested distinct enhancers of mitochondrial Ca^{2+} uptake (MiCUps) acting on different proteins within the mitochodrial Ca^{2+} uptake complex (Schweitzer et al., 2017, Sander et al., submitted). Independent of the molecular target all of these enhancers suppressed arrhythmogenic Ca^{2+} waves in cardiomyocytes.

This mechanism was potent enough to suppress arrhythmogenesis also in translational models for human cardiac arrhythmias (Schweitzer et al., 2017, Sander et al., submitted). In catecholaminergic polymorphic ventricular tachycardia (CPVT) a increased propensity of spontaneous SR Ca^{2+} release induced by mutations in RyR leads to the occurrence of episodes of life-threatening ventricular tachycardia under physical or emotional stress. In cardiomyocytes from a CPVT mouse model MiCUps significantly suppressed arrhythmogenic Ca^{2+} waves and action potentials. MiCUps also reduced episodes of ventricular tachycardia in CPVT mice *in-vivo* and efficiently suppressed arrhythmogenic Ca^{2+} waves in induced pluripotent stem cell derived cardiomyocytes from a CPVT patient.

Taken together, this thesis presents a novel regulatory mechanism in cardiomyocytes which can be pharmacologically activated to suppress arrhythmogenesis. It is potent enough to suppress arrhythmia in translational arrhythmia models and is thus a promising candidate for future pre-clininal and clinical studies.

In the following chapter the key steps leading to the success of the project are discussed coherently.

Coherent discussion of individual project related publications

Identification of VDAC2 as a novel regulator of cardiac rhythmicity

Shimizu, H.*, **Schredelseker, J**.*, Huang, J.*, Lu, K.*, Naghdi, S., Lu, F., Franklin, S., Fiji, H. D., Wang, K., Zhu, H., Tian, C., Lin, B., Nakano, H., Ehrlich, A., Nakai, J., Stieg, A. Z., Gimzewski, J. K., Nakano, A., Goldhaber, J. I., Vondriska, T. M., Hajnóczky, G., Kwon, O., and Chen, J.-N. (2015) Mitochondrial Ca^{2+} uptake by the voltage-dependent anion channel 2 regulates cardiac rhythmicity. *Elife*. **4**, e04801 (*...shared first authorship)

With the aim to identify novel candidate structures for a safer antiarrhythmic therapy, we set out to screen for novel cellular regulators of cardiac rhythmicity and chemical modulators thereof through an unbiased approach. To this aim we used the zebrafish cardiac fibrillation model *tremblor* (tre^{tc318}). Homozygous *tremblor* embryos carry a null-mutation for a cardiac specific isoform of the Na^+/Ca^{2+} exchanger NCX (Ebert et al., 2005; Langenbacher et al., 2005) and are characterized by a hyper-contracted myocardium with only chaotic contractions. We used these embryos to screen a diversity-oriented library of approximately 200 newly synthesized organic-like compounds. One compound, hereafter called efsevin, potently restored rhythmic cardiac contractions in *tremblor* hearts. Using a pull-down assay with immobilized efsevin on embryonic protein lysate we identified the voltage-dependent anion channel 2 (VDAC2) as the protein target of efsevin. Transient knockdown of VDAC2 in *tremblor* embryos abolished the efsevin induced phenotype rescue, while transient VDAC2 overexpression phenocopied it, confirming VDAC2 as the effective target of efsevin.

VDACs are the most abundant proteins in the outer mitochondrial membrane (OMM). They are large pore-forming channels that mediate the transfer of metabolites and ions over the OMM. Although they are often considered freely permeable due to their large pore diameter an increasing number of reports present VDACs as regulated barrier in the OMM (Rapizzi et al., 2002; Báthori et al., 2006). In cardiomyocytes the OMM is in close contact with the SR and and intensive crosstalk between the two organelles exist (Hajnóczky et al., 2000; Ruiz-Meana et al., 2010). Molecular tethers link mitochondria to the SR (García-Pérez et al., 2008) in close vicinity to the SR Ca^{2+} release units (De la Fuente et al., 2016) and mitochondria express several distinct transporters and channels for Ca^{2+} uptake and release. A gradual rise in mitochondrial matrix Ca^{2+} was reported to enhance enzymes of the TCA cycle under higher workload (Brandes and Bers, 1997), however, the role of an observed rapid beat-to-beat Ca^{2+} uptake remains elusive.

We therefore rationalized that the Ca^{2+} uptake of mitochondria could be altered by efsevin binding and that this could explain the antiarrhythmic effect of efsevin. Indeed efsevin as well as overexpression of VDAC2 enhanced mitochondrial Ca^{2+} uptake in HeLa cells. To investigate the effect of the enhanced mitochondrial Ca^{2+} uptake on mechanisms of arrhythmogenesis in cardiomyocytes we recorded cytosolic Ca^{2+} signals in isolated murine cardiomyocytes. The elementary Ca^{2+} release event in cardiomyocytes is the Ca^{2+} spark that is induced by the opening of one cluster of RyRs (Cheng et al., 1993). We found that in murine cardiomyocytes efsevin had no influence on the frequency or amplitude of Ca^{2+} sparks indicating no effect on SR Ca^{2+} release. Most strikingly however, the decay of the Ca^{2+} spark was significantly accelerated leading to shorter and narrower sparks. To test if this spacial and temporal restriction of Ca^{2+} sparks could prevent saltatory expansion of Ca^{2+} release inside the cardiomyocyte we induced spontaneous Ca^{2+} waves in cardiomyocytes by

raising extracellular Ca^{2+}. We found a significant, dose-dependent reduction in spontaneous Ca^{2+} waves with efsevin. Since Ca^{2+} waves underlie delayed afterdepolarizations and thus arrhythmia this effect explains the antiarrhythmic effect of efsevin.

Based on our results we formulated the following research hypothesis: Fast uptake of Ca^{2+} into mitochondria represents a buffering compartment adjacent to the Ca^{2+} release sites of the sarcoplasmic reticulum, which can be enhanced by pharmacological activation of VDAC2 as a molecular compartment of the mitochondrial Ca^{2+} uptake complex. Arrhythmogenic signals in cardiomyocytes are generated under conditions where RyRs become leaky, e.g. by elevated intracelluar Ca^{2+} levels. Under these conditions the spark frequency raises until a certain threshold is reached after which Ca^{2+} released from a spark triggers opening of neighboring Ca^{2+} release sites to initiate a Ca^{2+} wave. By activating mitochodrial Ca^{2+} uptake in close vicinity to the spark, a fraction of the released Ca^{2+} is transported into mitochondria leading to a spacial and temporal restriction of the spark. By this mechanism the cell can tolerate a higher spark frequency without generation of arrhythmogenic Ca^{2+} waves.

This study identified VDAC2 and mitochondrial Ca^{2+} uptake in general as a potent regulator of cardiac rhythmicity and a potential drug target for arrhythmia. Against the common perception that VDAC constitutes freely permeable pores in the OMM, we present evidence that the uptake of Ca^{2+} into mitochondria is already regulated at the OMM. Furthermore, this study suggests an isoform-specific role for VDAC2 in cardiomyocytes. We therefore set out to investigate VDAC2 on a structural level with the aim to identify differences between VDAC2 and VDAC1 that could explain its specific role in Ca^{2+} transport.

The structure of VDAC2

Schredelseker, J., Paz, A., López, C. J., Altenbach, C., Leung, C. S., Drexler, M. K., Chen, J.-N., Hubbell, W. L., and Abramson, J. (2014) High-Resolution Structure and Double Electron-Electron Resonance of the Zebrafish Voltage Dependent Anion Channel 2 Reveal an Oligomeric Population. *J. Biol. Chem.* **289**, 12566–77

After our discovery of VDAC2 as a regulator of cardiomyocyte Ca^{2+} handling and cardiac rhythmicity, we set out to investigate the molecular basis for the cardiac-specific role of VDAC2. Three isoforms of VDAC are expressed in higher animals and expression patterns between cell types vary. Although the distinct physiological roles of the three isoforms are not fully understood, evidence points towards considerable differences between the three isoforms. Especially VDAC2 was repeatedly described to fulfill several strictly isoform-specific roles: most strikingly, VDAC2 knock-out mice are embryonic lethal (Cheng et al., 2003), while knock-out mice for VDAC1 and VDAC3 display relatively mild phenotypes (Anflous et al., 2001; Sampson et al., 2001). Furthermore, VDAC2 was shown to exclusively mediate mitochondrial import of pro-apoptotic Bcl-2 family members thereby inhibiting apoptosis (Naghdi et al., 2015). Most relevant for us was the finding that VDAC2 specifically mediates transfer of Ca^{2+} from the sarcoplasmic reticulum into mitochondrial in cardiomyocytes by us and others (Subedi et al., 2011; Min et al., 2012; Shimizu et al., 2015).

We therefore set out to investigate the molecular structure of VDAC2 with the aim to identify structural elements that could explain the unique physiological features of VDAC2 compared to isoforms 1 and 3. Using X-ray crystallography we resolved the structure of zebrafish VDAC2 at a 2.8 Å resolution. Comparable to VDAC1, VDAC2 forms a β-barrel composed from 19 antiparralel β-sheets, exept for sheets 1 and 19 which align parallel, and an N-terminal α-helix lining the pore. However, we did not

find major structural differences between VDAC1 and VDAC2, which could explain the different physiological behavior of the channel. Recent studies however propose that isoform differences could be attributed to differences in molecular interaction partners (Caterino et al., 2017) such as Bcl2 family members (Cheng et al., 2003). Indeed, we identified several structural elements that could serve as docking sites for molecular interactions partners which vary between the isoforms, mainly the loop connecting β-sheets 1 and 2 which is displaced by ~12 Å compared to VDAC1 and an electropositive cluster within the same loop which is electronegative in VDAC1.

In an effort to identify the efsevin binding site we also set out to co-crystallize VDAC2 together with efsevin. However, the limited solubility of efsevin did not allow us to achieve a molar amount of efsevin in the experimental setup high enough to efficiently bind one efsevin molecule to each molecule of VDAC2. Consistently the structure of efsevin could not be resolved in the co-crystallization attempts.

However, this work set the basis for a follow-up study in which we used purified VDAC2, generated with the protocol established here, and the determined VDAC2 structure to characterize the efsevin-VDAC2 interaction on a biophysical and structural level.

The VDAC2-efsevin interaction

Wilting F., Kopp R., Gurnev P.A., Schedel A., Dupper N. J., Kwon O., Nicke A., Gudermann T., and **Schredelseker J.** (2020) The antiarrhythmic compound efsevin directly modulates voltage-dependent anion channel 2 by binding to its inner wall and enhancing mitochondrial Ca^{2+} uptake, *Br J Pharmacol.* doi: 10.1111/bph.15022

After identifying efsevin as a potent suppressor of cardiac arrhythmia in zebrafish and isolated murine cardiomyocytes and subsequent determination of the VDAC2 structure we set out to investigate the efsevin mode-of-action on a molecular level. Therefore we inserted purified recombinant VDAC2 into planar lipid bilayers and measured single channel currents in response to 10s voltage steps from -60 to +60 mV. In line with previous reports on other VDAC isoforms, VDAC2 showed a single channel conductance of approx. 4 ns in the open state in 1M KCl (Colombini, 1989; Ujwal et al., 2008). At low potentials between -20 and +20 mV the channel almost exclusively resided in this 4 nS-open state, but displays vigorous gating behavior between the open state and two distinct gated states with conductances of 2 and 1 nS respectively at intermediate potentials around ±30 mV. At very low or high potentials below -40 mV or above +40 the channel is mostly gated and only scarcely opens into the open state. This translates into a bell-shaped conductance-voltage relationship that is typical for VDAC and is consistent with previous observations on other VDAC isoforms. Strikingly addition of efsevin strongly facilitated gating and significantly reduced the open probability of the channel. Even at the physiologically relevant low potentials the channel mainly shifts between the two gated states. We then measured ion selectivity of the open state and the efsevin-induced gated state and found that anion selectivity is reduced upon efsevin binding explaining the enhanced mitochondrial Ca^{2+} uptake observed previously.

To identify potential efsevin binding sites we used the previously solved molecular structure of VDAC2 (Schredelseker et al., 2014) for computational docking experiments and identified a pocket formed between the barrel wall and the hinge region of the N-terminal pore-lining helix. Since the N-terminal helix was repeatedly proposed to be involved in channel gating and since this would be in line with our electrophysiological data, we further validated this potential binding site by a mutagenesis approach. By mutating three key residues from the identified pocket to alanines, we completely eliminated efsevin-sensitivity of VDAC2 in planar lipid bilayer recordings.

To finally proof the hypothesis that efsevin enhances mitochondrial Ca^{2+} uptake by binding to this pocket and changing the ion selectivity of the channel, we established a heterologous expression system in cultured HL-1 cardiomyocytes. Therefore we first knocked down expression of the endogenous mVDAC2 by shRNA. Knock-down of mVDAC2 completely abolished SR-mitochondria Ca^{2+} transfer as analyzed by recording the intra-mitochondrial Ca^{2+} level during caffeine-induced SR Ca^{2+} release. Strikingly subsequent heterologous expression of VDAC2 or the efsevin-insensitive mutant $zVDAC2^{AAA}$ completely restored SR-mitochondria Ca^{2+} transfer but only wild-type zVDAC2 was sensitive to efsevin.

Taken together, this study describes the efsevin-VDAC2 interaction on a molecular level. We show that efsevin binds through a pocket located inside the channel pore and shifts the channel into a more cation selective state leading to enhanced transfer of Ca^{2+} from the SR into mitochondria. This supports our initial hypothesis that efsevin activates a mitochondrial buffering system to blunt cytosolic Ca^{2+} signals and to suppress arrhythmia.

The translational potential of enhancing mitochondrial Ca^{2+} uptake for the treatment of arrhythmia

Schweitzer, M. K., Wilting, F., Sedej, S., Dreizehnter, L., Dupper, N. J., Tian, Q., Moretti, A., My, I., Kwon, O., Priori, S. G., Laugwitz, K.-L., Storch, U., Lipp, P., Breit, A., Mederos y Schnitzler, M., Gudermann, T., and **Schredelseker, J.** (2017) Suppression of Arrhythmia by Enhancing Mitochondrial Ca^{2+} Uptake in Catecholaminergic Ventricular Tachycardia Models. *JACC Basic to Transl. Sci.* **2**, 737–746

After we had identified the mode of action of efsevin on a physiological and structural level, we next evaluated the translational potential of this novel pharmacological concept in experimental models for a human cardiac arrhythmia. To this aim we used two models for catecholaminergic polymorphic ventricular tachycardia (CPVT) as an example for a Ca^{2+}-triggered arrhythmia (Cerrone et al., 2009). CPVT is characterized by episodes of ventricular tachycardia in response to catecholaminergic stimulation induced by physical or emotional stress and is associated with mutations in cardiac Ca^{2+} handling proteins, predominantly RyR2 (CPVT1) or calsequestrin (CPVT2).

Mice heterozygous for a R4496C conversion in RyR2 ($RyR2^{R4496C/WT}$), a homolog to the human R4497C mutation associated with CPVT, recapitulate the human CPVT phenotype and show episodes of bidirectional ventricular tachycardia upon catecholaminergic stimulation (Cerrone et al., 2005). We recorded intracellular Ca^{2+} in freshly isolated cardiomyocytes of $RyR2^{R4496C/WT}$ mice and analyzed diastolic Ca^{2+} activity immediately after stopping rhythmic electrical stimulation of the cells. In line with the CPVT phenotype, isoproterenol induced the occurrence of spontaneous Ca^{2+} waves, the molecular basis for arrhythmogenesis within this diastolic phase. Strikingly efsevin completely abolished isoproterenol-induced diastolic Ca^{2+} waves without

affecting systolic Ca^{2+} transients. The diastolic Ca^{2+} waves are considered to trigger a transient sodium influx through the Na^{+}/Ca^{2+} exchanger initiating depolarization of the cell and thus spontaneous activity in form of a delayed afterdepolarization (DAD). To evaluate if efsevin can suppress DADs, we patch-clamped $RyR2^{R4496C/WT}$ cardiomyocytes and found a significant reduction of spontaneous diastolic action potentials after superfusion with efsevin. To evaluate our hypothesis that efsevin exerts its therapeutic effect by enhancing mitochondrial Ca^{2+} uptake we applied both, a loss-of-function and a gain-of-function approach. For the loss-of-function approach we repeated the above experiment in the presence of Ru360 a specific blocker of the mitochondrial Ca^{2+} uniporter (MCU) in the inner mitochondrial membrane. Indeed, in the presence of Ru360 efsevin was unable to suppress isoproterenol-induced diastolic Ca^{2+} waves. *Vice-versa*, we used a previously described enhancer of MCU, to prove the general concept that pharmacological enhancement of mitochondrial Ca^{2+} uptake could suppress arrhythmogenesis. Kaempferol, a naturally occurring flavonoid, was reported to enhance mitochondrial Ca^{2+} uptake in HeLa cells (Montero et al., 2004). After confirming that kaempferol enhances transfer of Ca^{2+} from the SR into mitochondria using our HL-1 cardiomyocyte mitochondrial Ca^{2+} uptake assay, we tested it on $RyR2^{R4496C/WT}$ cardiomyocytes and found that kaempferol suppresses diastolic Ca^{2+} waves comparable to efsevin. These results demonstrate that enhancing mitochondrial Ca^{2+} uptake could serve as a general pharmacological concept for the treatment of arrhythmia and is independent of the molecular target, which is VDAC2 for efsevin and MCU for kaempferol.

We then used both mitochondrial Ca^{2+} uptake enhancers (MiCUps), efsevin and kaempferol, *in-vivo* in $RyR2^{R4496C/WT}$ mice. Mice were implanted with an osmotic minipump releasing a constant dose of drug into the blood flow 3 days prior to undergoing an ECG recording. During the ECG recording mice were injected with a

bolus of epinephrine and caffeine to induce catecholaminergic stress and the ECG was evaluated for the occurrence of bidirectional ventricular tachycardia. Strikingly, all mice receiving vehicle control but only half of the mice treated with either efsevin or kaempferol developed ventricular tachyarrhythmia.

To finally prove efficacy of efsevin in human tissue we used pluripotent stem cell-derived cardiomyocytes from a CPVT patient (Jung et al., 2012) and again recorded spontaneous Ca^{2+} activity as a measure for arrhythmogenesis. Comparable to the data obtained from $RyR2^{R4496C/WT}$ mice, we found that both MiCUps, efsevin and kaempferol, significantly reduced spontaneous diastolic Ca^{2+} waves.

Taken together, our data from this study highlights the translational potential of enhancing mitochondrial Ca^{2+} uptake as a therapeutic concept for the treatment and prevention of Ca^{2+}-triggered cardiac arrhythmias. Through targeting different components of the mitochondrial Ca^{2+} uptake complex, both MiCUps, efsevin and kaempferol, significantly suppressed arrhythmia in a murine and a human model for cardiac arrhythmia. However, both substances are still very experimental and not optimized for the use in human. For example, basic pharmacokinetic and pharmacodynamic parameters are largely undetermined or suggest impracticality for the use as drugs in human. We therefore set out to identify additional substances which activate mitochondrial Ca^{2+} uptake in a follow-up study.

Novel mitochondrial Ca^{2+} uptake enhancers

Sander P., Arduino D., Schweitzer M. K., Wilting F., Gutenthaler S., Dreizehnter L., Moretti A., Gudermann T., Perocchi F., and **Schredelseker J.** (2020) Approved drugs ezetimibe and disulfiram enhance mitochondrial Ca^{2+} uptake and suppress cardiac arrhythmogenesis, *submitted*

After we demonstrated that the two MiCUps efsevin and kaempferol significantly reduce arrhythmogenesis in translational models for human Ca^{2+}-triggered cardiac arrhythmia, we questioned if these substances are druggable for pre-clinical and clinical studies and finally the use as therapeutics. Analysis of the dose response curves of efsevin and kaempferol revealed an EC_{50} of approximately 2-5 µM for both drugs in our SR-mitochondria Ca^{2+} transfer assay, which is relatively high for the use as therapeutics since it makes binding of the drugs to unspecific targets likely. In this regard very little is known about efsevin. Though we identified VDAC2 as the primary target of efsevin relevant for the reduction of arrhythmogenesis, selectivity of the drug was never systematically addressed. Kaempferol was suggested to act on different targets including the NF-κB (Kadioglu et al., 2015), the fibroblast growth factor (Lee et al., 2018), and other signaling pathways (Yao et al., 2014; Kim et al., 2015; Wu et al., 2017).

To circumvent problems associated with the high EC_{50} of these drugs, we selectively screened a library of FDA and EMA approved drugs for their ability to enhance mitochondrial Ca^{2+} uptake using a HeLa based high-throughput assay (Arduino et al., 2017). From this screen we identified four substances, which enhanced mitochondrial Ca^{2+} uptake greater then 2.5-fold compared to control and have never been associated with mitochondrial Ca^{2+} before. We then validated these hits at different concentrations in HeLa cells and excluded cefatrizine as a false-positive.

Since we previously identified cardiac SR-mitochondria Ca^{2+} transfer as the molecular foundation for the antiarrhythmogenic activity of MiCUPs we evaluated the remaining three substances in our HL-1 cardiomyocyte Ca^{2+} transfer assay. In this assay two substances, namely ezetimibe, used to lower cholesterol and disulfiram, used for the treatment of alcohol abuse, significantly enhanced SR-mitochondria Ca^{2+} transfer at significantly lower concentrations compared to our previously established MiCUps efsevin and kaempferol. Interestingly, the natural compound honokiol, which scored highest in the HeLa assay failed to enhance SR-mitochondria Ca^{2+} transfer in cardiomyocytes, which might be explained by differences in the subunit composition (Raffaello et al., 2013; Patron et al., 2019) or subcellar localization (De la Fuente et al., 2016) of the mitochondrial Ca^{2+} uptake complex in this cell type.

We then tested ezetimbe and disulfiram for their antiarrhythmogenic activity in different arrhythmia models. As a first assay we tested both substances in *tremblor* zebrafish embryos as an *in-vivo* model for Ca^{2+} overload induced arrhythmia. Both significantly restored rhythmic cardiac contractions in *tremblor* comparable to efsevin (Shimizu et al., 2015) but at significantly lower concentrations. As a next step we tested ezetimibe and disulfiram for their potential to suppress arrhythmogenic diastolic Ca^{2+} waves in CPVT cardiomyocytes of $RyR2^{R4496C/WT}$ mice and human iPSC-derived cardiomyocytes (Schweitzer et al., 2017). Both significantly suppressed isoproterenol-induced diastolic Ca^{2+} waves dose-dependently and again at lower concentrations then efsevin and kaempferol. Interestingly, disulfiram induced side-effects in all tested models. Fish displayed severe malformations and cells displayed elevated cytosolic baseline Ca^{2+} concentrations and increased spontaneous activity, indicating that although effective, care has to be taking when disulfiram is used in pre-clinical and clinical applications.

This study presents two FDA and EMA approved drugs as novel enhancers of mitochondrial Ca^{2+} uptake. Both substances effectively suppress arrhythmia in experimental models for human arrhythmia, however disulfiram shows indications of severe side effects. Both substances are promising candidates for future pre-clinical and clinical studies to evaluate the therapeutic potential of MiCUps for arrhythmia therapy.

Relevance of the work for the scientific field

Mitochondrial Ca^{2+} uptake as a regulator of cardiac rhythmicity

Already in the early 60s researchers noted that mitochondria can take up vast amounts of Ca^{2+} inside the mitochondrial matrix (DeLuca and Engstrom, 1961) but the physiological role of this uptake was discussed ever since. In principle, two mechanisms, a high affinity low conductance pathway for gradual Ca^{2+} uptake in response to changes in basal cytosolic Ca^{2+} levels and a low affinity high conductance pathway for the rapid uptake of Ca^{2+} were discussed (Waldeck-Weiermair et al., 2013). Today, it is widely appreciated that a slow and gradual uptake of Ca^{2+} into mitochondria stimulates enzymes of the TCA cycle to enhance energy production (McCormack and Denton, 1989; Brandes and Bers, 1997), while the role of the fast mitochondrial Ca^{2+} uptake remains elusive. Several reports suggest that the fast mitochondrial Ca^{2+} uptake represents a local buffering mechanism to shape intracellular Ca^{2+} signals (Hoth et al., 2000; Montero et al., 2000).

Rapid mitochondrial Ca^{2+} uptake was particularly investigated in cardiomyocytes, which constantly undergo rapid and large changes in intracellular Ca^{2+} levels and

where Ca^{2+} signaling represents a central part of the cell's physiology. In cardiomyocytes mitochondria comprise approximately 30% of the total cell volume (Barth et al., 1992; Kim et al., 1994) primarily to cover the high energy demand of the working myocardium. Conspicuously often however, they are located in close proximity to the Ca^{2+} release sites of the SR, and are tightly tethered to the SR membrane (Boncompagni et al., 2009; Hayashi et al., 2009). An extensive cross-talk between the two organelles exists (García-Pérez et al., 2008; Dorn and Scorrano, 2010) and mitochondria were reported to play an essential role in shaping intracellular Ca^{2+} signals (Parekh, 2003).

In this thesis we identified an immediate physiological role for rapid mitochondrial Ca^{2+} uptake in cardiomyocytes as a so far unappreciated important regulator of cardiac rhythmicity. We propose a mechanism in which spatially defined mitochondrial Ca^{2+} uptake in close vicinity to the cardiac Ca^{2+} release sites spatially and temporally restricts erratic diastolic Ca^{2+} sparks and thereby inhibits saltatory expansion of the signal in form of a Ca^{2+} wave. This hypothesis is supported by a previous report in which inhibition of mitochondrial Ca^{2+} uptake increased the propensity for propagating Ca^{2+} waves in cardiomyocytes (Seguchi et al., 2005) and the finding that VDAC2 closely interacts with the RyR (Subedi et al., 2011; Min et al., 2012). Our data thus supports the notion that rapid mitochondrial Ca^{2+} uptake is used to shape intracellular Ca^{2+} signals. Moreover, our study adds additional relevance to this mechanism, since we present this mechanism to be relevant for the pathogenesis and treatment of a human disease.

Surprisingly, in our experiments activation of mitochondrial Ca^{2+} uptake activates a mechanism to protect the cell during diastole while it has limited effects on systolic Ca^{2+} signals. This poses the question why mitochondrial Ca^{2+} uptake is limited under

physiological conditions. Future experiments are needed to address this question in long-term experiments and a detailed analysis of systolic Ca^{2+} transients at rest and under higher workload.

The mitochondrial outer membrane as a regulated Ca^{2+} barrier

Ever since mitochondrial Ca^{2+} uptake was first described in the 1960s (DeLuca and Engstrom, 1961) various studies speculated on the molecular entities mediating this large and highly selective current described as MCU (Kirichok et al., 2004). Numerous targets in the inner mitochondrial membrane were suggested to be involved in mitochondrial Ca^{2+} uptake including mitochondrial uncoupling proteins 2/3, Letm1, and RyR (Trenker et al., 2007; Waldeck-Weiermair et al., 2011). The picture changed in 2011 when the molecular identity of MCU was reported by two independent groups (Baughman et al., 2011; De Stefani et al., 2011). After this discovery, research on mitochondrial Ca^{2+} uptake has experienced a revival and new research tools, like gene-modified mice (Pan et al., 2013), became available. Numerous regulatory subunits of MCU were identified and intensively investigated.

However, on its way into mitochondria, Ca^{2+} has to pass two membranes, the outer and inner mitochondrial membrane. The transfer route of Ca^{2+} over the outer mitochondrial membrane is generally believed to be constituted by VDACs. Because of their large pore diameter of approx. 15 Å and their conductivity for large metabolites such as ATP and NADPH they were often depicted as unselective pores leading to the assumption that the outer mitochondrial membrane would be freely permeable for ions. However, several observations challenge this general belief and establish VDAC in the OMM as a second regulated barrier for Ca^{2+} in addition to

MCU: (i) VDAC was shown to be localized in close proximity to ER/SR Ca^{2+} release sites and even a direct link to Ca^{2+} release channels was proposed (Szabadkai et al., 2006; Min et al., 2012). (ii) Overexpression of VDAC1 enhanced transfer of Ca^{2+} from microdomains into mitochondria (Rapizzi et al., 2002). (iii) VDAC gating is modulated by Ca^{2+} (Báthori et al., 2006) and (iv) Ca^{2+} permeability through the VDAC pore depends on the the open state of the channel (Tan and Colombini, 2007).

In this thesis we demonstrate that pharmacological modulation of the outer mitochondrial membrane channel VDAC2 by efsevin enhances transfer of Ca^{2+} into mitochondria. This data supports the idea that uptake of Ca^{2+} into mitochondria is regulated already at the outer mitochondrial membrane, specifically through VDAC. Moreover, we present evidence that this regulatory step is highly relevant for the physiological regulation of the cell. In cardiomyocytes VDAC2 limits uptake of Ca^{2+} into mitochondria. Enhancement of VDAC2 Ca^{2+} conductance by efsevin enhances mitochondrial Ca^{2+} uptake and thereby creates an additional Ca^{2+} buffering compartment that protects the cell from arrhythmogenic diastolic Ca^{2+} signals.

Against the common belief that MCU is the sole regulator of mitochondrial Ca^{2+} uptake, we propose a situation in which VDAC2 works together with MCU in the inner mitochondrial membrane as a mitochondrial Ca^{2+} uptake supercomplex. We present evidence that overexpression of VDAC2 just like overexpression of MCU restores rhythmic cardiac contractions in *tremblor* embryos, while knockdown of MCU abolishes the rescuing effect of VDAC2 overexpression and *vice-versa* (Shimizu et al., 2015). This demonstrates that both channel depend on each other and regulate mitochondrial Ca^{2+} uptake in form of a two membrane tunnel. This idea is further supported by a recently identified physical interaction between VDAC and MCU (Liao et al., 2015).

Beyond this interaction, several studies suggest that the mitochondrial Ca^{2+} uptake complex is part of a bigger complex involving the Ca^{2+} release channel of the sarcoplasmic reticulum, i.e. the IP_3 receptor in non-excitable cells and the RyR in cardiomyocytes respectively (Rizzuto et al., 1998; Marchi et al., 2018; Xu et al., 2018). This is supported by the notion that due to the low-affinity of the MCU for Ca^{2+} , a threshold of approximately 1 µM - 3 µM Ca^{2+} is required for opening of the channel (Csordás et al., 2013), which is not reached by bulk cytosolic Ca^{2+} but only within nandomains in close proximity to the Ca^{2+} release sites of the ER/SR. Within these contact sites the outer mitochondrial membrane VDAC is tethered to the ER presumably through the anchoring protein GRP75 (Szabadkai et al., 2006), to form the center of the complex.

Taken together, this thesis together with other reports provides evidence that not MCU alone, but a macromolecular complex between the SR Ca^{2+} release channel, VDAC in the outer membrane, and MCU in the inner membrane regulates mitochondrial Ca^{2+} uptake. Therefore, care should be taken when investigating effects of mitochondrial Ca^{2+} uptake on cellular physiology solely by genetic or physiological manipulation of MCU under the assumption that the outer mitochondrial membrane is freely permeable to Ca^{2+}. Instead, VDAC and MCU should be treated as a complex spanning both membranes to regulate Ca^{2+} uptake in two consecutive steps. Future studies are needed however to investigate the nature of this complex in different tissues and the relative contribution of the outer and inner mitochondrial membrane to the regulation of mitochondrial Ca^{2+} uptake.

Mitochondrial Ca^{2+} uptake as a therapeutic strategy

By describing mitochondrial Ca^{2+} uptake as a pharmacologically targetable mechanism for the regulation of cardiac rhythmicity, this thesis presents an entirely new candidate structure for the development of novel antiarrhythmic therapies. We present four different candidate substances, out of which two are FDA and EMA approved drugs, which could serve as lead compounds for the generation of novel drugs. Furthermore, we show efficacy of this approach in models for cardiac arrhythmias including a Ca^{2+} overload model and models for inherited arrhythmias and including several species, namely *in-vivo* experiments on fish and mice and experiments on human cells.

Common antiarrhythmic therapies using Na^+, K^+, and Ca^{2+} channel blockers aim at inhibiting the propagation of an ectopic excitation along the myocardium by blocking channels of the cardiac conduction system. As such they influence cardiac de- or repolarization and are thus prone to proarrhythmic side effects. Because MiCUps target intracellular structures to suppress the generation of ectopic depolarizations and do not influence the cardiac action potential, they are expected be less prone to these proarrhythmic effects.

However, several further studies must be conducted before MiCUps can be used for clinical testing. Efsevin the first substance identified in our studies is a newly synthesized compound and basic pharmacokinetic parameters like oral bioavailability, plasma half-life time or volume of distribution are not known and need to be determined. While most of these parameters are known for kaempferol, both substances, efsevin and kaempferol, showed fairly high EC_{50} values in the low µM range in our mitochondrial Ca^{2+} uptake assay suggesting that fairly high amounts of the drugs need to be administered to achieve a therapeutic effect. At these high

concentrations binding of the drug to other targets becomes likely. While specificity of efsevin to other targets has never been assessed, kaempferol was suggested to interact with numerous proteins including the NF-κB (Kadioglu et al., 2015), the fibroblast growth factor (Lee et al., 2018), and other signaling pathways (Yao et al., 2014; Kim et al., 2015; Wu et al., 2017), suggesting that side effects are to be expected. In contrast, ezetimibe and disulfiram are clinically approved and EC_{50} values of mitochondrial Ca^{2+} uptake in our assay are in the low nM range, a range that is well suitable for their use as therapeutics. However, both substances have been approved for other indications based on their effect on their primary targets, i.e. the cholesterol transporter Niemann-Pick C1-like 1 (NPC1L1) for ezetimibe and the acetaldehyde dehydrogenase for disulfiram. Affinity of the drug for the mitochondrial Ca^{2+} uptake complex versus their primary targets has to be determined.

Furthermore it should be noted that mitochondrial Ca^{2+} uptake is a process presumably taking place in every cell of the body and not limited to cardiomyocytes. Though we assume that a special situation exists in cardiomyocytes due to the specific subcellular localization of the mitochondrial Ca^{2+} uptake complex in these cells (De la Fuente et al., 2016; De La Fuente et al., 2018) and the subunit composition of MCU (Raffaello et al., 2013; Lambert et al., 2019; Patron et al., 2019), effects of enhanced mitochondrial Ca^{2+} uptake in other tissues need to be excluded prior to clinical experiments.

For the above reasons, the identified drugs might need to be optimized through chemical modification. Our study identified the binding site for efsevin on the VDAC2 protein and thus provides a structural basis for the optimization of efsevin through structure-aided drug design. The protein target of kaempferol, ezetimbe and

disulfiram within the mitochondrial Ca^{2+} uptake complex still need to be determined, however, our work provides the tools to successfully address this question.

Taken together, this thesis provides the basis for the development of a novel generation of antiarrhythmic drugs, but also opens the door for a number of studies before clinical experiments can be started.

References

Allen, D.G., Eisner, D.A., and Orchard, C.H. (1984). Characterization of oscillations of intracellular calcium concentration in ferret ventricular muscle. J. Physiol. *352*: 113–28.

Anflous, K., Armstrong, D.D., and Craigen, W.J. (2001). Altered mitochondrial sensitivity for ADP and maintenance of creatine-stimulated respiration in oxidative striated muscles from VDAC1-deficient mice. J. Biol. Chem. *276*: 1954–60.

Arduino, D.M., Wettmarshausen, J., Vais, H., Navas-Navarro, P., Cheng, Y., Leimpek, A., et al. (2017). Systematic Identification of MCU Modulators by Orthogonal Interspecies Chemical Screening. Mol. Cell *67*: 711–723.e7.

Aston, D., Capel, R.A., Ford, K.L., Christian, H.C., Mirams, G.R., Rog-Zielinska, E.A., et al. (2017). High resolution structural evidence suggests the Sarcoplasmic Reticulum forms microdomains with Acidic Stores (lysosomes) in the heart. Sci. Rep. *7*: 40620.

Barth, E., Stämmler, G., Speiser, B., and Schaper, J. (1992). Ultrastructural quantitation of mitochondria and myofilaments in cardiac muscle from 10 different animal species including man. J. Mol. Cell. Cardiol. *24*: 669–81.

Báthori, G., Csordás, G., Garcia-Perez, C., Davies, E., and Hajnóczky, G. (2006). Ca^{2+}-dependent control of the permeability properties of the mitochondrial outer membrane and voltage-dependent anion-selective channel (VDAC). J. Biol. Chem. *281*: 17347–58.

Baughman, J.M., Perocchi, F., Girgis, H.S., Plovanich, M., Belcher-Timme, C.A., Sancak, Y., et al. (2011). Integrative genomics identifies MCU as an essential component of the mitochondrial calcium uniporter. Nature *476*: 341–5.

Benjamin, E.J., Virani, S.S., Callaway, C.W., Chamberlain, A.M., Chang, A.R., Cheng, S., et al. (2018). Heart Disease and Stroke Statistics—2018 Update: A Report From the American Heart Association. Circulation *137*: e67–e492.

Bers, D.M. (2002). Cardiac excitation-contraction coupling. Nature *415*: 198–205.

Bers, D.M. (2008). Calcium cycling and signaling in cardiac myocytes. Annu. Rev. Physiol. *70*: 23–49.

Boncompagni, S., Rossi, A.E., Micaroni, M., Beznoussenko, G. V, Polishchuk, R.S., Dirksen, R.T., et al. (2009). Mitochondria are linked to calcium stores in striated muscle by developmentally regulated tethering structures. Mol. Biol. Cell *20*: 1058–67.

Brandes, R., and Bers, D.M. (1997). Intracellular Ca^{2+} increases the mitochondrial NADH concentration during elevated work in intact cardiac muscle. Circ. Res. *80*: 82–7.

Caterino, M., Ruoppolo, M., Mandola, A., Costanzo, M., Orrù, S., and Imperlini, E. (2017). Protein-protein interaction networks as a new perspective to evaluate distinct functional roles of voltage-dependent anion channel isoforms. Mol. Biosyst. *13*:.

Cerrone, M., Colombi, B., Santoro, M., Barletta, M.R. di, Scelsi, M., Villani, L., et al. (2005). Bidirectional ventricular tachycardia and fibrillation elicited in a knock-in mouse model carrier of a mutation in the cardiac ryanodine receptor. Circ. Res. *96*: e77-82.

Cerrone, M., Napolitano, C., and Priori, S.G. (2009). Catecholaminergic polymorphic ventricular tachycardia: A paradigm to understand mechanisms of arrhythmias associated to impaired Ca^{2+} regulation. Heart Rhythm *6*: 1652–9.

Cheng, E.H.Y., Sheiko, T. V, Fisher, J.K., Craigen, W.J., and Korsmeyer, S.J. (2003). VDAC2 inhibits BAK activation and mitochondrial apoptosis. Science *301*: 513–7.

Cheng, H., Lederer, W., and Cannell, M. (1993). Calcium sparks: elementary events underlying excitation-contraction coupling in heart muscle. Science (80-.). *262*: 740–744.

Colombini, M. (1989). Voltage gating in the mitochondrial channel, VDAC. J. Membr. Biol. *111*: 103–11.

Csordás, G., Golenár, T., Seifert, E.L., Kamer, K.J., Sancak, Y., Perocchi, F., et al. (2013). MICU1 controls both the threshold and cooperative activation of the mitochondrial Ca^{2+} uniporter. Cell Metab. *17*: 976–87.

DeLuca, H.F., and Engstrom, G.W. (1961). Calcium uptake by rat kidney mitochondria. Proc. Natl. Acad. Sci. U. S. A. *47*: 1744–50.

Dorn, G.W., and Scorrano, L. (2010). Two close, too close: sarcoplasmic reticulum-mitochondrial crosstalk and cardiomyocyte fate. Circ. Res. *107*: 689–99.

Ebert, A.M., Hume, G.L., Warren, K.S., Cook, N.P., Burns, C.G., Mohideen, M.A., et al. (2005). Calcium extrusion is critical for cardiac morphogenesis and rhythm in embryonic zebrafish hearts. Proc. Natl. Acad. Sci. U. S. A. *102*: 17705–10.

Fearnley, C.J., Roderick, H.L., and Bootman, M.D. (2011). Calcium signaling in cardiac myocytes. Cold Spring Harb. Perspect. Biol. *3*: a004242.

García-Pérez, C., Hajnóczky, G., and Csordás, G. (2008). Physical coupling supports the local Ca^{2+} transfer between sarcoplasmic reticulum subdomains and the mitochondria in heart muscle. J. Biol. Chem. *283*: 32771–80.

Hajnóczky, G., Csordás, G., Madesh, M., and Pacher, P. (2000). The machinery of local Ca^{2+} signalling between sarco-endoplasmic reticulum and mitochondria. J. Physiol. *529*: 69–81.

Hayashi, T., Martone, M.E., Yu, Z., Thor, A., Doi, M., Holst, M.J., et al. (2009). Three-dimensional electron microscopy reveals new details of membrane systems for Ca^{2+} signaling in the heart. J. Cell Sci. *122*: 1005–13.

Hoth, M., Button, D.C., and Lewis, R.S. (2000). Mitochondrial control of calcium-channel gating: a mechanism for sustained signaling and transcriptional activation in T lymphocytes. Proc. Natl. Acad. Sci. U. S. A. *97*: 10607–12.

Jung, C.B., Moretti, A., Mederos y Schnitzler, M., Iop, L., Storch, U., Bellin, M., et al. (2012). Dantrolene rescues arrhythmogenic RYR2 defect in a patient-specific stem cell model of catecholaminergic polymorphic ventricular tachycardia. EMBO Mol. Med. *4*: 180–91.

Kadioglu, O., Nass, J., Saeed, M.E.M., Schuler, B., and Efferth, T. (2015). Kaempferol Is an Anti-Inflammatory Compound with Activity towards NF-κB Pathway Proteins. Anticancer Res. *35*: 2645–50.

Kim, H.-D., Kim, C.H., Rah, Bb.-J., Chung, H.-I., and Shim, T.-S. (1994). Quantitative study on the relation between structural and functional properties of the hearts from three different mammals. Anat. Rec. *238*: 199–206.

Kim, S.H., Park, J.G., Lee, J., Yang, W.S., Park, G.W., Kim, H.G., et al. (2015). The Dietary Flavonoid Kaempferol Mediates Anti-Inflammatory Responses via the Src, Syk, IRAK1, and IRAK4 Molecular Targets. Mediators Inflamm. *2015*: 1–15.

Kirichok, Y., Krapivinsky, G., and Clapham, D.E. (2004). The mitochondrial calcium uniporter is a highly selective ion channel. Nature *427*: 360–4.

Klawki, R., Schmidt, K., and Heinemann, M. (2018). Deutscher Herzbericht 2018 (Frankfurt am Main).

la Fuente, S. De, Fernandez-Sanz, C., Vail, C., Agra, E.J., Holmstrom, K., Sun, J., et al. (2016). Strategic positioning and biased activity of the mitochondrial calcium uniporter in cardiac muscle. J. Biol. Chem. *291*:.

La Fuente, S. De, Lambert, J.P., Nichtova, Z., Fernandez Sanz, C., Elrod, J.W., Sheu, S.-S., et al. (2018). Spatial Separation of Mitochondrial Calcium Uptake and Extrusion for Energy-Efficient Mitochondrial Calcium Signaling in the Heart. Cell Rep. *24*: 3099–3107.e4.

Lambert, J.P., Luongo, T.S., Tomar, D., Jadiya, P., Gao, E., Zhang, X., et al. (2019). MCUB Regulates the Molecular Composition of the Mitochondrial Calcium Uniporter Channel to Limit Mitochondrial Calcium Overload During Stress. Circulation *140*: 1720–1733.

Langenbacher, A.D., Dong, Y., Shu, X., Choi, J., Nicoll, D.A., Goldhaber, J.I., et al. (2005). Mutation in sodium-calcium exchanger 1 (NCX1) causes cardiac fibrillation in zebrafish. Proc. Natl. Acad. Sci. U. S. A. *102*: 17699–704.

Lee, C.-J., Moon, S.-J., Jeong, J.-H., Lee, S., Lee, M.-H., Yoo, S.-M., et al. (2018). Kaempferol targeting on the fibroblast growth factor receptor 3-ribosomal S6 kinase 2 signaling axis prevents the development of rheumatoid arthritis. Cell Death Dis. *9*: 401.

Liao, Y., Hao, Y., Chen, H., He, Q., Yuan, Z., and Cheng, J. (2015). Mitochondrial calcium uniporter protein MCU is involved in oxidative stress-induced cell death. Protein Cell *6*: 434–42.

Marchi, S., Patergnani, S., Missiroli, S., Morciano, G., Rimessi, A., Wieckowski, M.R., et al. (2018). Mitochondrial and endoplasmic reticulum calcium homeostasis and cell death. Cell Calcium *69*: 62–72.

McCormack, J.G., and Denton, R.M. (1989). The role of Ca^{2+} ions in the regulation of intramitochondrial metabolism and energy production in rat heart. Mol. Cell. Biochem. *89*: 121–5.

Mehra, R. (2007). Global public health problem of sudden cardiac death.

Min, C.K., Yeom, D.R., Lee, K.-E., Kwon, H.-K., Kang, M., Kim, Y.-S., et al. (2012). Coupling of ryanodine receptor 2 and voltage-dependent anion channel 2 is essential for Ca^{2+} transfer from the sarcoplasmic reticulum to the mitochondria in the heart. Biochem. J. *447*: 371–9.

Montero, M., Alonso, M.T., Carnicero, E., Cuchillo-Ibáñez, I., Albillos, A., García, A.G., et al. (2000). Chromaffin-cell stimulation triggers fast millimolar mitochondrial Ca^{2+} transients that modulate secretion. Nat. Cell Biol. *2*: 57–61.

Montero, M., Lobatón, C.D., Hernández-Sanmiguel, E., Santodomingo, J., Vay, L., Moreno, A., et al. (2004). Direct activation of the mitochondrial calcium uniporter by natural plant flavonoids. Biochem. J. *384*: 19–24.

Naghdi, S., Várnai, P., and Hajnóczky, G. (2015). Motifs of VDAC2 required for mitochondrial Bak import and tBid-induced apoptosis. Proc. Natl. Acad. Sci. U. S. A. *112*: E5590-9.

Nichols, M., Townsend, N., Luengo-Fernandez, R., Leal, J., Gray, A., Scarborogh, P., et al. (2012). European Cardiovascular Disease Statistics 2012 (Brussels, Sophia Antipolis).

Pan, X., Liu, J., Nguyen, T.T., Liu, C., Sun, J., Teng, Y., et al. (2013). The physiological role of mitochondrial calcium revealed by mice lacking the mitochondrial calcium uniporter. Nat. Cell Biol. *15*: 1464–72.

Parekh, A.B. (2003). Mitochondrial regulation of intracellular Ca^{2+} signaling: more than just simple Ca2+ buffers. News Physiol. Sci. *18*: 252–6.

Patron, M., Granatiero, V., Espino, J., Rizzuto, R., and Stefani, D. De (2019). MICU3 is a tissue-specific enhancer of mitochondrial calcium uptake. Cell Death Differ. *26*: 179–195.

Raffaello, A., Stefani, D. De, Sabbadin, D., Teardo, E., Merli, G., Picard, A., et al. (2013). The mitochondrial calcium uniporter is a multimer that can include a dominant-negative pore-forming subunit. EMBO J. *32*: 2362–76.

Rapizzi, E., Pinton, P., Szabadkai, G., Wieckowski, M.R., Vandecasteele, G., Baird, G., et al. (2002). Recombinant expression of the voltage-dependent anion channel enhances the transfer of Ca^{2+} microdomains to mitochondria. J. Cell Biol. *159*: 613–24.

Rizzuto, R., Pinton, P., Carrington, W., Fay, F.S., Fogarty, K.E., Lifshitz, L.M., et al. (1998). Close contacts with the endoplasmic reticulum as determinants of mitochondrial Ca^{2+} responses. Science *280*: 1763–6.

Ruiz-Meana, M., Fernandez-Sanz, C., and Garcia-Dorado, D. (2010). The SR-mitochondria interaction: a new player in cardiac pathophysiology. Cardiovasc. Res. *88*: 30–9.

Sampson, M.J., Decker, W.K., Beaudet, A.L., Ruitenbeek, W., Armstrong, D.D., Hicks, M.J., et al. (2001). Immotile sperm and infertility in mice lacking mitochondrial voltage-dependent anion channel type 3. J. Biol. Chem. *276*: 39206–12.

Schredelseker, J., Paz, A., López, C.J., Altenbach, C., Leung, C.S., Drexler, M.K., et al. (2014). High-Resolution Structure and Double Electron-Electron Resonance of the Zebrafish Voltage Dependent Anion Channel 2 Reveal an Oligomeric Population. J. Biol. Chem. *289*: 12566–77.

Schweitzer, M.K., Wilting, F., Sedej, S., Dreizehnter, L., Dupper, N.J., Tian, Q., et al. (2017). Suppression of Arrhythmia by Enhancing Mitochondrial Ca^{2+} Uptake in Catecholaminergic Ventricular Tachycardia Models. JACC Basic to Transl. Sci. *2*: 737–746.

Seguchi, H., Ritter, M., Shizukuishi, M., Ishida, H., Chokoh, G., Nakazawa, H., et al. (2005). Propagation of Ca^{2+} release in cardiac myocytes: role of mitochondria. Cell Calcium *38*: 1–9.

Shimizu, H., Schredelseker, J., Huang, J., Lu, K., Naghdi, S., Lu, F., et al. (2015). Mitochondrial Ca^{2+} uptake by the voltage-dependent anion channel 2 regulates cardiac rhythmicity. Elife *4*:.

Stefani, D. De, Raffaello, A., Teardo, E., Szabò, I., and Rizzuto, R. (2011). A forty-kilodalton protein of the inner membrane is the mitochondrial calcium uniporter. Nature *476*: 336–40.

Subedi, K.P., Kim, J.-C., Kang, M., Son, M.-J., Kim, Y.-S., and Woo, S.-H. (2011). Voltage-dependent anion channel 2 modulates resting Ca^{2+} sparks, but not action potential-induced Ca^{2+} signaling in cardiac myocytes. Cell Calcium *49*: 136–43.

Szabadkai, G., Bianchi, K., Várnai, P., Stefani, D. De, Wieckowski, M.R., Cavagna, D., et al. (2006). Chaperone-mediated coupling of endoplasmic reticulum and mitochondrial Ca^{2+} channels. J. Cell Biol. *175*: 901–11.

Tan, W., and Colombini, M. (2007). VDAC closure increases calcium ion flux. Biochim. Biophys. Acta *1768*: 2510–5.

Trenker, M., Malli, R., Fertschai, I., Levak-Frank, S., and Graier, W.F. (2007). Uncoupling proteins 2 and 3 are fundamental for mitochondrial Ca^{2+} uniport. Nat. Cell Biol. *9*: 445–52.

Ujwal, R., Cascio, D., Colletier, J.-P., Faham, S., Zhang, J., Toro, L., et al. (2008). The crystal structure of mouse VDAC1 at 2.3 A resolution reveals mechanistic insights into metabolite gating. Proc. Natl. Acad. Sci. U. S. A. *105*: 17742–7.

Waldeck-Weiermair, M., Deak, A.T., Groschner, L.N., Alam, M.R., Jean-Quartier, C., Malli, R., et al. (2013). Molecularly distinct routes of mitochondrial Ca^{2+} uptake are activated depending on the activity of the sarco/endoplasmic reticulum Ca^{2+} ATPase (SERCA). J. Biol. Chem. *288*: 15367–79.

Waldeck-Weiermair, M., Jean-Quartier, C., Rost, R., Khan, M.J., Vishnu, N., Bondarenko, A.I., et al. (2011). Leucine zipper EF hand-containing transmembrane protein 1 (Letm1) and uncoupling proteins 2 and 3 (UCP2/3) contribute to two distinct mitochondrial Ca^{2+} uptake pathways. J. Biol. Chem. *286*: 28444–55.

Wilting, F., Kopp, R., Gurnev, P.A., Schedel, A., Dupper, N.J., Kwon, O., et al. (2020). The antiarrhythmic compound efsevin directly modulates voltage-dependent anion channel 2 by binding to its inner wall and enhancing mitochondrial Ca^{2+} uptake . Br. J. Pharmacol.

Wu, Y., Zhang, Q., and Zhang, R. (2017). Kaempferol targets estrogen-related receptor α and suppresses the angiogenesis of human retinal endothelial cells under high glucose conditions. Exp. Ther. Med. *14*: 5576–5582.

Xu, H., Guan, N., Ren, Y.-L., Wei, Q.-J., Tao, Y.-H., Yang, G.-S., et al. (2018). IP3R-Grp75-VDAC1-MCU calcium regulation axis antagonists protect podocytes from apoptosis and decrease proteinuria in an Adriamycin nephropathy rat model. BMC Nephrol. *19*: 140.

Yao, K., Chen, H., Liu, K., Langfald, A., Yang, G., Zhang, Y., et al. (2014). Kaempferol targets RSK2 and MSK1 to suppress UV radiation-induced skin cancer. Cancer Prev. Res. (Phila). *7*: 958–967.

Acknowledgments

I'd like to express my sincere thanks to Thomas Gudermann for believing in this project and for giving me the opportunity to start my own lab at the Walther Straub Institute for Pharmacology and Toxicology. Without his constant support this project would not have been feasible.

The work presented in this thesis is by far not the work of a single man, but of a team of excellent scientists that I had the honor to work with and that have always shared my ambitions to make this story become successful. I want to express my deepest thanks to the entire Schredelseker lab, my doctoral students Maria K. Schweitzer, Fabiola Wilting, Paulina Sander, Simon Huber, Kira Steinhorst, Anna Schedel, and Sandra Fischbach, my technical assistants Brigitte Mayerhofer and Eva Vetter, and all the numerous master students and research fellows that have worked in the lab in the past years.

Even the best team can not do everything alone and so I'd like to thank all my collaborators who have contributed to the success of this project, the Chen lab, Abramson lab, and Kwon lab at UCLA, the Mederos y Schnitzler lab, Nicke lab, and Breit lab at LMU Munich, the Sedej lab at Graz Medical University, the Moretti lab at TU Munich, the Perocchi lab at the Helmholtz Center Munich, and all other collaborators who have provided expertise and experiments to the project.

Last but not least, I'd like to thank my entire family, especially my wife, Sabine Geiger-Schredelseker, who always followed me to where science led me, for supporting me and for sharing my enthusiasm for science and academia.

Appendices

The present habilitation project comprises 5 publications of the applicant. Print versions of these publications can be found as appendices to this thesis.

Appendix 1: Shimizu, H. et al. (2015) Mitochondrial Ca^{2+} uptake by the voltage-dependent anion channel 2 regulates cardiac rhythmicity. *Elife*.

Shimizu, H.*, Schredelseker, J.*, Huang, J.*, Lu, K.*, Naghdi, S., Lu, F., Franklin, S., Fiji, H. D., Wang, K., Zhu, H., Tian, C., Lin, B., Nakano, H., Ehrlich, A., Nakai, J., Stieg, A. Z., Gimzewski, J. K., Nakano, A., Goldhaber, J. I., Vondriska, T. M., Hajnóczky, G., Kwon, O., and Chen, J.-N. (2015) Mitochondrial Ca^{2+} uptake by the voltage-dependent anion channel 2 regulates cardiac rhythmicity. *Elife*. 4, e04801 (*...shared first authorship)

eLIFE elifesciences.org

RESEARCH ARTICLE

Mitochondrial Ca^{2+} uptake by the voltage-dependent anion channel 2 regulates cardiac rhythmicity

Hirohito Shimizu[1†], Johann Schredelseker[1†‡], Jie Huang[1†], Kui Lu[2†¶], Shamim Naghdi[3], Fei Lu[1], Sarah Franklin[4§], Hannah DG Fiji[2], Kevin Wang[1], Huanqi Zhu[2], Cheng Tian[1], Billy Lin[1], Haruko Nakano[1,5], Amy Ehrlich[3], Junichi Nakai[6], Adam Z Stieg[7,8], James K Gimzewski[2,7,8,9], Atsushi Nakano[1,5], Joshua I Goldhaber[10], Thomas M Vondriska[4], György Hajnóczky[3], Ohyun Kwon[2], Jau-Nian Chen[1]*

[1]Department of Molecular, Cell and Developmental Biology, University of California, Los Angeles, Los Angeles, United States; [2]Department of Chemistry and Biochemistry, University of California, Los Angeles, Los Angeles, United States; [3]MitoCare Center, Department of Pathology, Anatomy and Cell Biology, Thomas Jefferson University, Philadelphia, United States; [4]Department of Anesthesiology, University of California, Los Angeles, Los Angeles, United States; [5]Broad Center of Regenerative Medicine and Stem Cell Research, University of California, Los Angeles, Los Angeles, United States; [6]Brain Science Institute, Saitama University, Saitama, Japan; [7]California NanoSystems Institute, University of California, Los Angeles, Los Angeles, United States; [8]WPI Center for Materials Nanoarchitectonics, National Institute for Materials Science, Tsukuba, Japan; [9]School of Physics, Centre for Nanoscience and Quantum Information, University of Bristol, Bristol, UK; [10]Cedars-Sinai Heart Institute, Los Angeles, United States

***For correspondence:** chenjn@mcdb.ucla.edu

[†]These authors contributed equally to this work

Present address: [‡]Walther-Straub Institute for Pharmacology and Toxicology, Ludwig-Maximilians University, Munich, Germany; [¶]College of Bioengineering, Tianjin University of Science and Technology, Tianjin, China; [§]Department of Internal Medicine, Nora Eccles Harrison Cardiovascular Research and Training Institute, University of Utah, Salt Lake City, United States

Competing interests: The authors declare that no competing interests exist.

Funding: See page 17

Received: 17 September 2014
Accepted: 23 December 2014
Published: 15 January 2015

Reviewing editor: Jodi Nunnari, University of California, Davis, United States

Abstract Tightly regulated Ca^{2+} homeostasis is a prerequisite for proper cardiac function. To dissect the regulatory network of cardiac Ca^{2+} handling, we performed a chemical suppressor screen on zebrafish *tremblor* embryos, which suffer from Ca^{2+} extrusion defects. Efsevin was identified based on its potent activity to restore coordinated contractions in *tremblor*. We show that efsevin binds to VDAC2, potentiates mitochondrial Ca^{2+} uptake and accelerates the transfer of Ca^{2+} from intracellular stores into mitochondria. In cardiomyocytes, efsevin restricts the temporal and spatial boundaries of Ca^{2+} sparks and thereby inhibits Ca^{2+} overload-induced erratic Ca^{2+} waves and irregular contractions. We further show that overexpression of VDAC2 recapitulates the suppressive effect of efsevin on *tremblor* embryos whereas VDAC2 deficiency attenuates efsevin's rescue effect and that VDAC2 functions synergistically with MCU to suppress cardiac fibrillation in *tremblor*. Together, these findings demonstrate a critical modulatory role for VDAC2-dependent mitochondrial Ca^{2+} uptake in the regulation of cardiac rhythmicity.
DOI: 10.7554/eLife.04801.001

Introduction

During development, well-orchestrated cellular processes guide cells from diverse lineages to integrate into the primitive heart tube and establish rhythmic and coordinated contractions. While many genes and pathways important for cardiac morphogenesis have been identified, molecular

eLife digest The heart is a large muscle that pumps blood around the body by maintaining a regular rhythm of contraction and relaxation. If the heart loses this regular rhythm it works less efficiently, which can lead to life-threatening conditions.

Regular heart rhythms are maintained by changes in the concentration of calcium ions in the cytoplasm of the heart muscle cells. These changes are synchronised so that the heart cells contract in a controlled manner. In each cell, a contraction begins when calcium ions from outside the cell enter the cytoplasm by passing through a channel protein in the membrane that surrounds the cell. This triggers the release of even more calcium ions into the cytoplasm from stores within the cell. For the cells to relax, the calcium ions must then be pumped out of the cytoplasm to lower the calcium ion concentration back to the original level.

Shimizu et al. studied a zebrafish mutant—called *tremblor*—that has irregular heart rhythms because its heart muscle cells are unable to efficiently remove calcium ions from the cytoplasm. Embryos of the *tremblor* mutant were treated with a wide variety of chemical compounds with the aim of finding some that could correct the heart defect.

A compound called efsevin restores regular heart rhythms in *tremblor* mutants. Efsevin binds to a pump protein called VDAC2, which is found in compartments called mitochondria within the cell. Although mitochondria are best known for their role in supplying energy for the cell, they also act as internal stores for calcium. By binding to VDAC2, efsevin increases the rate at which calcium ions are pumped from the cytoplasm into the mitochondria. This restores rhythmic calcium ion cycling in the cytoplasm and enables the heart muscle cells to develop regular rhythms of contraction and relaxation. Increasing the levels of VDAC2 or another similar calcium ion pump protein in the heart cells can also restore a regular heart rhythm.

Efsevin can also correct irregular heart rhythms in human and mouse heart muscle cells, therefore the new role for mitochondria in controlling heart rhythms found by Shimizu et al. appears to be shared in other animals. The experiments have also identified the VDAC family of proteins as potential new targets for drug therapies to treat people with irregular heart rhythms.

DOI: 10.7554/eLife.04801.002

mechanisms governing embryonic cardiac rhythmicity are poorly understood. The findings that Ca^{2+} waves traveling across the heart soon after the formation of the primitive heart tube (***Chi et al., 2008***) and that loss of function of key Ca^{2+} regulatory proteins, such as the L-type Ca^{2+} channel, Na/K−ATPase and sodium-calcium exchanger 1 (NCX1), severely impairs normal cardiac function (***Rottbauer et al., 2001***; ***Shu et al., 2003***; ***Ebert et al., 2005***; ***Langenbacher et al., 2005***), indicate an essential role for Ca^{2+} handling in the regulation of embryonic cardiac function.

Ca^{2+} homoeostasis in cardiac muscle cells is tightly regulated at the temporal and spatial level by a subcellular network involving multiple proteins, pathways, and organelles. The release and reuptake of Ca^{2+} by the sarcoplasmic reticulum (SR), the largest Ca^{2+} store in cardiomyocytes, constitutes the primary mechanism governing the contraction and relaxation of the heart. Ca^{2+} influx after activation of the L-type Ca^{2+} channel in the plasma membrane induces the release of Ca^{2+} from the SR via ryanodine receptor (RyR) channels, which leads to an increase of the intracellular Ca^{2+} concentration and cardiac contraction. During diastolic relaxation, Ca^{2+} is transferred back into the SR by the SR Ca^{2+} pump or extruded from the cell through NCX1. Defects in cardiac Ca^{2+} handling and Ca^{2+} overload, for example during cardiac ischemia/reperfusion or in long QT syndrome, are well known causes of contractile dysfunction and many types of arrhythmias including early and delayed afterdepolarizations and Torsade des pointes (***Bers, 2002***; ***Choi et al., 2002***; ***Yano et al., 2008***; ***Greiser et al., 2011***).

Ca^{2+} crosstalk between mitochondria and ER/SR has been noted in many cell types and the voltage-dependent anion channel (VDAC) and the mitochondrial Ca^{2+} uniporter (MCU) serve as primary routes for Ca^{2+} entry through the outer and inner mitochondrial membranes, respectively (***Rapizzi et al., 2002***; ***Bathori et al., 2006***; ***Shoshan-Barmatz et al., 2010***; ***Baughman et al., 2011***; ***De Stefani et al., 2011***). In the heart, mitochondria are tethered to the SR and are located in close proximity to Ca^{2+} release sites (***García-Pérez et al., 2008***; ***Boncompagni et al., 2009***; ***Hayashi et al., 2009***). This subcellular architecture exposes the mitochondria near the Ca^{2+} release sites to a high local Ca^{2+} concentration

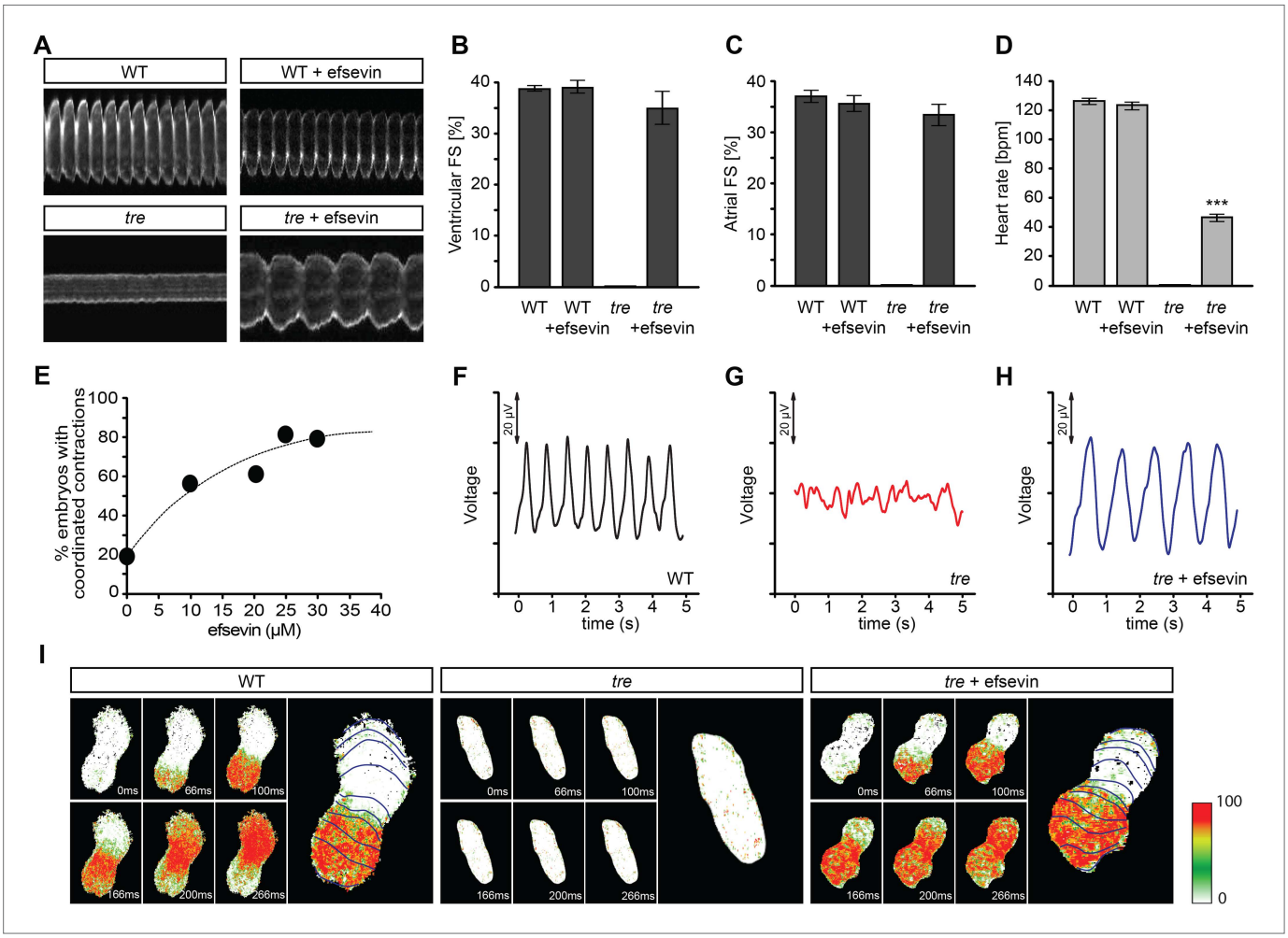

Figure 1. Efsevin restores rhythmic cardiac contractions in zebrafish tremblor embryos. (**A**) Line scans across the atria of *Tg(myl7:GFP)* embryonic hearts at 48 hpf. Rhythmically alternating systoles and diastoles are recorded from vehicle- (upper left) or efsevin- treated wild type (upper right) and efsevin-treated *tre* (lower right) embryos, while only sporadic unsynchronized contractions are recorded from vehicle-treated *tre* embryos (lower left). (**B**, **C**) Fractional shortening (FS) deduced from the line-scan traces. While cardiac contraction was not observed in *tre*, efsevin-treated wild type and *tre* hearts have similar levels of FS to those observed in control hearts. Ventricular FS of wild type v.s. wild type + efsevin vs tre + efsevin: 39 ± 0.6%, n = 8 vs 39 ± 1%, n = 10 vs 35 ± 3%, n = 6; and Atrial FS: 37 ± 1%, n = 11 vs 35 ± 2%, n = 11 vs 33 ± 2%, n = 15. (**D**) While efsevin restored a heart rate of 46 ± 2 beats per minute (bpm) in *tre* embryos, same treatment does not affect the heart rate in wild type embryos (126 ± 2 bpm in vehicle-treated embryos vs 123 ± 3 bpm in efsevin-treated wild-type embryos). ***, $p < 0.001$ by one-way ANOVA. (**E**) Dose-dependence curve for efsevin. The *tre* embryos were treated with various concentrations of efsevin from 24 hpf and cardiac contractions were analyzed at 48 hpf. (**F**–**H**) Representative time traces of local field potentials for wild type (**F**), *tre* (**G**) and efsevin-treated *tre* (**H**) embryos clearly display periods of regular, irregular, and restored periodic electrical activity. (**I**) In vivo optical maps of Ca^{2+} activation represented by isochronal lines every 33 ms recorded from 36 hpf wild type (left), *tre* (center) and efsevin-treated *tre* (right) embryos.

DOI: 10.7554/eLife.04801.003

that is sufficient to overcome the low Ca^{2+} affinity of MCU and facilitates Ca^{2+} crosstalk between SR and mitochondria (***García-Pérez et al., 2008***; ***Dorn and Scorrano, 2010***; ***Kohlhaas and Maack, 2013***). Increase of the mitochondrial Ca^{2+} concentration enhances energy production during higher workload and dysregulation of SR-mitochondrial Ca^{2+} signaling results in energetic deficits and oxidative stress in the heart and may trigger programmed cell death (***Brandes and Bers, 1997***; ***Maack et al., 2006***; ***Kohlhaas and Maack, 2013***). However, whether SR-mitochondrial Ca^{2+} crosstalk also contributes significantly to cardiac Ca^{2+} signaling during excitation-contraction coupling requires further investigation.

In zebrafish, the *tremblor* (*tre*) locus encodes a cardiac-specific isoform of the Na^{+}/Ca^{2+} exchanger 1, NCX1h (also known as slc8a1a) (***Ebert et al., 2005***; ***Langenbacher et al., 2005***). The *tre* mutant hearts

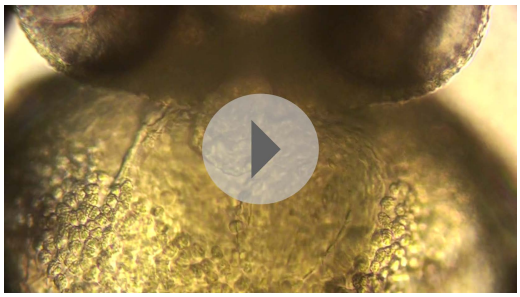

Video 1. The video shows a heart of a wild-type zebrafish embryo at 2 dpf. Robust rhythmic contractions can be observed in atrium and ventricle.
DOI: 10.7554/eLife.04801.004

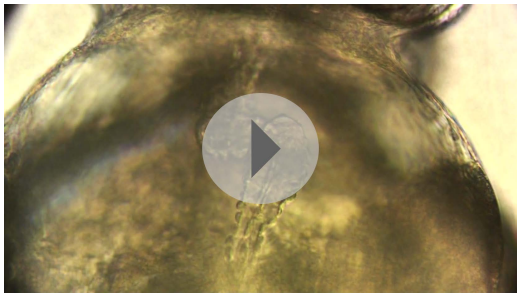

Video 2. This video shows a heart of a *tremblor* embryo at 2 dpf. Embryos of the mutant line *tremblor* display only local, unsynchronized contractions, comparable to cardiac fibrillation.
DOI: 10.7554/eLife.04801.005

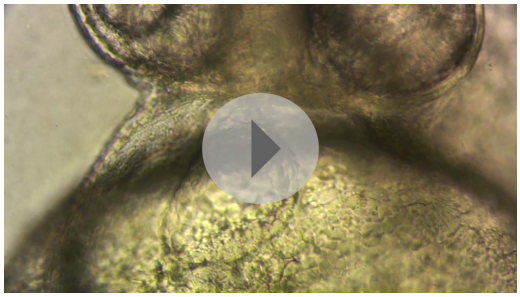

Video 3. This video shows a heart of a *tremblor* embryo at 2 dpf treated with efsevin. Treatment of *tremblor* embryos with efsevin restores rhythmic contractions with comparable atrial fractional shortening compared to wild-type embryos and approximately 40% of wild-type heart rate.
DOI: 10.7554/eLife.04801.006

lack rhythmic Ca^{2+} transients and display chaotic Ca^{2+} signals in the myocardium leading to unsynchronized contractions resembling cardiac fibrillation (***Langenbacher et al., 2005***). In this study, we used *tre* as an animal model for aberrant Ca^{2+} handling-induced cardiac dysfunction and took a chemical genetic approach to dissect the Ca^{2+} regulatory network important for maintaining cardiac rhythmicity. A synthetic compound named efsevin was identified from a suppressor screen due to its potent ability to restore coordinated contractions in *tre*. Using biochemical and genetic approaches we show that efsevin interacts with VDAC2 and potentiates its mitochondrial Ca^{2+} transporting activity and spatially and temporally modulates cytosolic Ca^{2+} signals in cardiomyocytes. The important role of mitochondrial Ca^{2+} uptake in regulating cardiac rhythmicity is further supported by the suppressive effect of VDAC2 and MCU overexpression on cardiac fibrillation in *tre*.

Results and discussion

Identification of a chemical suppressor of *tre* cardiac dysfunction

Homozygous *tre* mutant embryos suffer from Ca^{2+} extrusion defects and manifest chaotic cardiac contractions resembling fibrillation (***Ebert et al., 2005***; ***Langenbacher et al., 2005***). To dissect the regulatory network of Ca^{2+} handling in cardiomyocytes and to identify mechanisms controlling embryonic cardiac rhythmicity, we screened the BioMol library and a collection of synthetic compounds for chemicals that are capable of restoring heartbeat either completely or partially in *tre* embryos. A dihydropyrrole carboxylic ester compound named efsevin was identified based on its ability to restore persistent and rhythmic cardiac contractions in *tre* mutant embryos in a dose-dependent manner (***Figure 1A,E***, and ***Videos 1–4***). To validate the effect of efsevin, we assessed cardiac performance of wild type, *tre* and efsevin-treated *tre* embryos (***Nguyen et al., 2009***). Fractional shortening of efsevin treated *tre* mutant hearts was comparable to that of their wild type siblings and heart rate was restored to approximately 40% of that observed in controls (***Figure 1B–D***). Periodic local field potentials accompanying each heartbeat were detected in wild type and efsevin-treated *tre* embryos using a microelectrode array (***Figure 1F–H***). Furthermore, while only sporadic Ca^{2+} signals were detected in *tre* hearts, in vivo Ca^{2+} imaging revealed steady Ca^{2+} waves propagating through efsevin-treated *tre* hearts (***Figure 1I***, ***Videos 5–7***), demonstrating that cardiomyocytes are functionally coupled and that efsevin treatment restores regular Ca^{2+} transients in *tre* hearts.

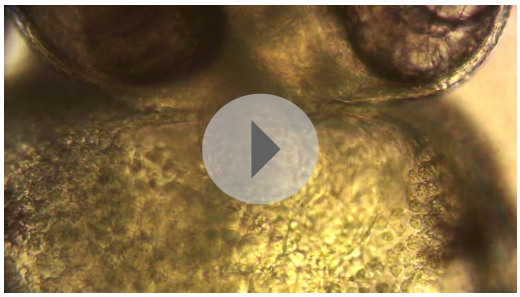

Video 4. The video shows a heart of a wild-type zebrafish embryo at 2 dpf treated with efsevin. Treatment of wild-type embryos with efsevin did not affect cardiac performance, indicated by robust, rhythmic contractions comparable to untreated wild-type embryos.
DOI: 10.7554/eLife.04801.007

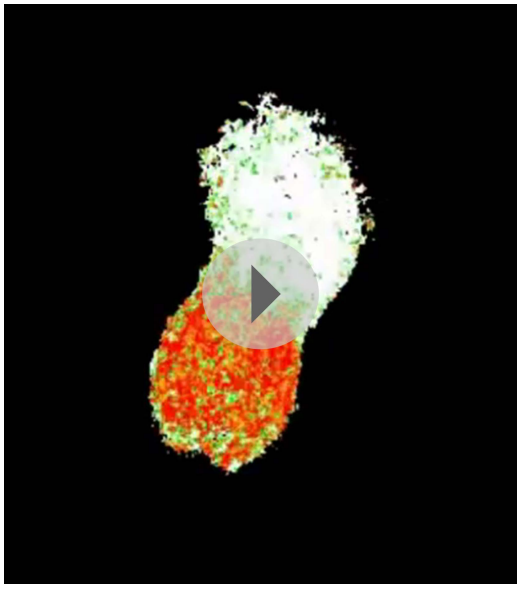

Video 5. Heat map of Ca^{2+} transients recorded in 1 day old wild type heart.
DOI: 10.7554/eLife.04801.008

Efsevin suppresses Ca^{2+} overload-induced irregular contraction

We next examined whether efsevin could suppress aberrant Ca^{2+} homeostasis-induced arrhythmic responses in mammalian cardiomyocytes. Mouse embryonic stem cell-derived cardiomyocytes (mESC-CMs) establish a regular contraction pattern with rhythmic Ca^{2+} transients (***Figure 2A,B,E,F***). Mimicking Ca^{2+} overload by increasing extracellular Ca^{2+} levels was sufficient to disrupt normal Ca^{2+} cycling and induce irregular contractions in mESC-CMs (***Figure 2C,E,F***). Remarkably, efsevin treatment restored rhythmic Ca^{2+} transients and cardiac contractions in these cells (***Figure 2D–F***). Similar effect was observed in human embryonic stem cell-derived cardiomyocytes (hESC-CMs) (***Figure 2G***). Together, these findings suggest that efsevin targets a conserved Ca^{2+} regulatory mechanism critical for maintaining rhythmic cardiac contraction in fish, mice and humans.

VDAC2 mediates the suppressive effect of efsevin on *tre*

To identify the protein target of efsevin, we generated a N-Boc-protected 2-aminoethoxyethoxyethylamine linker-attached efsevin ($efsevin^{L}$) (***Figure 3A,C***). This modified compound retained the activity of efsevin to restore cardiac contractions in *ncx1h* deficient embryos (***Figure 3B,D***) and was used to create efsevin-conjugated agarose beads ($efsevin^{LB}$). A 32kD protein species was detected from zebrafish lysate due to its binding ability to $efsevin^{LB}$ and $OK\text{-}C125^{LB}$, an active efsevin derivative conjugated to beads, but not to beads capped with ethanolamine alone or beads conjugated with an inactive efsevin analog ($OK\text{-}C19^{LB}$) (***Figure 3A–E***). Furthermore, preincubation of zebrafish lysate with excess efsevin prevented the 32kD protein from binding to $efsevin^{LB}$ or $OK\text{-}C125^{LB}$ (***Figure 3E***). Mass spectrometry analysis revealed that this 32kD band represents a zebrafish homologue of the mitochondrial voltage-dependent anion channel 2 (VDAC2) (***Figure 3F*** and ***Figure 3—figure supplement 1***).

VDAC2 is expressed in the developing zebrafish heart (***Figure 4A***), making it a good candidate for mediating efsevin's effect on cardiac Ca^{2+} handling. To examine this possibility, we injected in vitro synthesized VDAC2 RNA into *tre* embryos and found that the majority of these embryos had coordinated cardiac contractions similar to those subjected to efsevin treatment (***Figure 4B***, ***Videos 8–11***). In addition, we generated *myl7:VDAC2* transgenic fish in which VDAC2 expression can be induced in the heart by tebufenozide (TBF) (***Figure 4C***). Knocking down NCX1h in *myl7:VDAC2* embryos results in chaotic cardiac movement similar to *tre*. Like efsevin treatment, induction of VDAC2 expression by TBF treatment restored coordinated and rhythmic contractions in *myl7:VDAC2;NCX1h MO* hearts (***Figure 4D***, ***Videos 12,13***). Conversely, knocking down VDAC2 in *tre* hearts attenuated the suppressive effect of efsevin (***Figure 4E***, ***Videos 14–16***). Furthermore, we generated VDAC2 null embryos by the Zinc Finger Nuclease gene targeting approach (***Figure 4G***). Similar to that observed in morpholino knockdown embryos, homozygous $VDAC2^{LA2256}$ embryos do not exhibit noticeable morphological

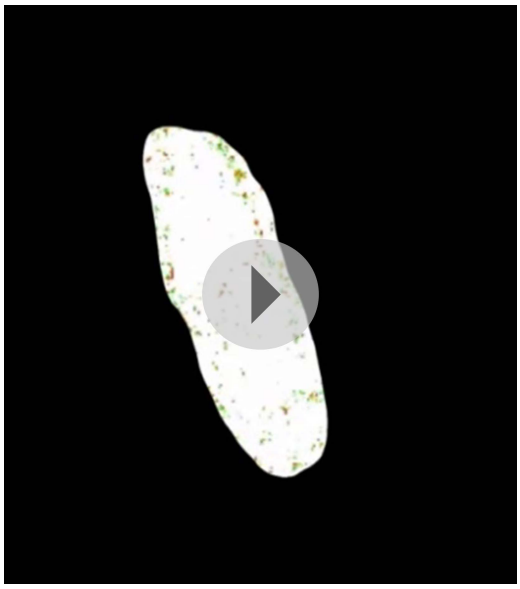

Video 6. Heat map of Ca^{2+} transients recorded in 1 day old *tremblor* heart.
DOI: 10.7554/eLife.04801.009

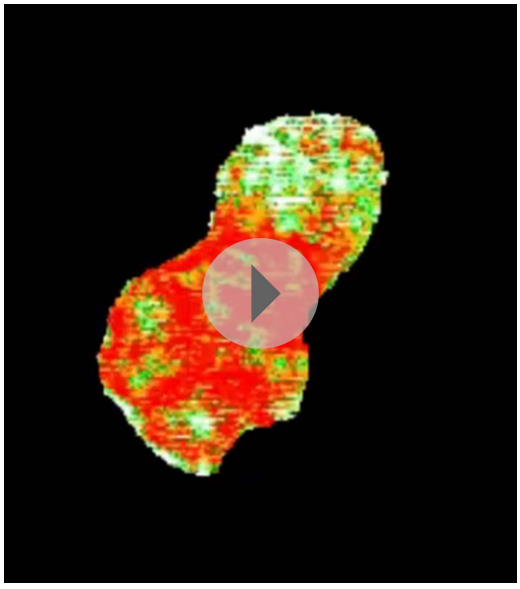

Video 7. Heat map of Ca^{2+} transients recorded in 1 day old efsevin treated *tremblor* heart.
DOI: 10.7554/eLife.04801.010

defects, but the suppressive effect of efsevin was attenuated in homozygous *VDAC2*^{LA2256}*; NCX1MO* embryos (***Figure 4F***). These findings demonstrate that VDAC2 is a major mediator for efsevin's effect on *ncx1h* deficient hearts.

VDAC2-dependent effect of efsevin on mitochondrial Ca^{2+} uptake

VDAC is an abundant channel located on the outer mitochondrial membrane serving as a primary passageway for metabolites and ions (***Figure 5A***) (***Rapizzi et al., 2002***; ***Bathori et al., 2006***; ***Shoshan-Barmatz et al., 2010***). At its close state, VDAC favours Ca^{2+} flux (***Tan and Colombini, 2007***). To examine whether efsevin would modulate mitochondrial Ca^{2+} uptake via VDAC2, we transfected HeLa cells with VDAC2. We noted increased mitochondrial Ca^{2+} uptake in permeabilized VDAC2 transfected and efsevin-treated cells after the addition of Ca^{2+} and the combined treatment further enhanced mitochondrial Ca^{2+} levels (***Figure 5B***).

Mitochondria are located in close proximity to Ca^{2+} release sites of the ER/SR and an extensive crosstalk between the two organelles exists (***García-Pérez et al., 2008***; ***Hayashi et al., 2009***; ***Brown and O'Rourke, 2010***; ***Dorn and Scorrano, 2010***; ***Kohlhaas and Maack, 2013***). We examined whether Ca^{2+} released from intracellular stores could be locally transported into mitochondria through VDAC2 in VDAC1/VDAC3 double knockout (V1/V3DKO) MEFs where VDAC2 is the only VDAC isoform being expressed (***Roy et al., 2009a***). While treatments with ATP, an IP3-linked agonist, and thapsigargin, a SERCA inhibitor, stimulated similar global cytoplasmic [Ca^{2+}] elevation in intact cells, only ATP induced a rapid mitochondrial matrix [Ca^{2+}] rise (***Figure 5—figure supplement 1***). This finding is consistent with observations obtained in other cell types (***Rizzuto et al., 1994***; ***Hajnóczky et al., 1995***) and suggests that Ca^{2+} was locally transferred from IP3 receptors to mitochondria through VDAC2 at the close ER-mitochondrial associations. We next investigated whether this process could be modulated by efsevin. In permeabilized V1/V3DKO MEFs, treatment with efsevin increased the amount of Ca^{2+} transferred into mitochondria during IP_3-induced Ca^{2+} release (***Figure 5C***). Also, in intact V1/V3 DKO MEFs, efsevin accelerated the transfer of Ca^{2+} released from intracellular stores into mitochondria during stimulation with ATP (***Figure 5D,E***).

Efsevin modulates Ca^{2+} sparks and suppresses erratic Ca^{2+} waves in cardiomyocytes

We next examined the effect of efsevin on cytosolic Ca^{2+} signals in isolated adult murine cardiomyocytes. We found that efsevin treatment induced faster inactivation kinetics without affecting the

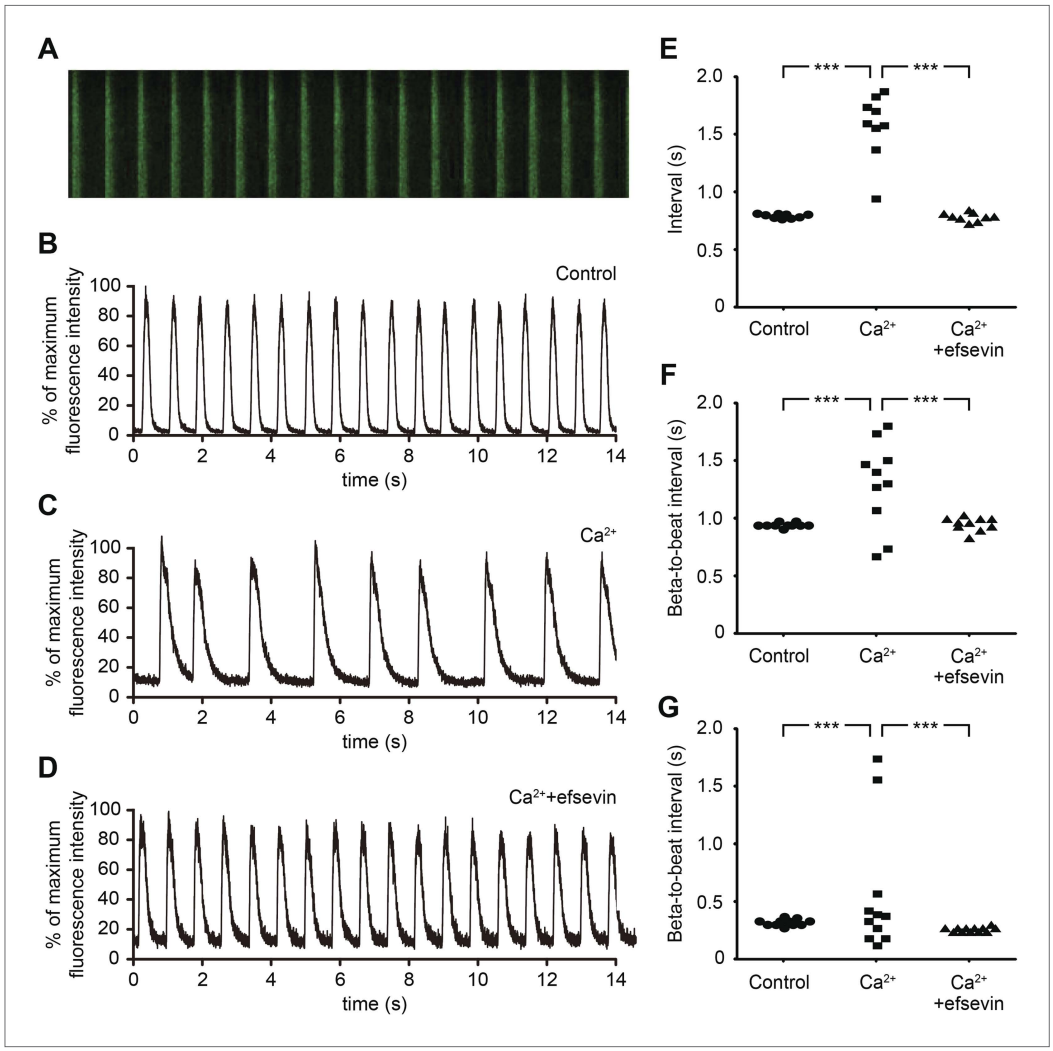

Figure 2. Efsevin reduces arrhythmogenic events in ES cell-derived cardiomyocytes. (**A**) Line-scan analysis of Ca^{2+} transients in mESC-CMs after 10 days of differentiation. (**B**–**D**) Representative graph of Ca^{2+} transients detected in mESC-CMs (**B**). After treatment with 10 mM Ca^{2+} for 10 min, the EB showed an irregular pattern of Ca^{2+} transients (**C**). Efsevin treatment restores regular Ca^{2+} transients under Ca^{2+} overload conditions in mESC-CMs (**D**). (**E**) Plotted intervals between peaks of Ca^{2+} signals detected in mESC-CMs prior to treatment (control), in 10 mM Ca^{2+}_{ext} (Ca^{2+}) and in 10 mM Ca^{2+}_{ext}+10 μM efsevin (Ca^{2+}+efsevin). (**F**, **G**) Plotted intervals of contractions detected in EBs prior to treatment (control), in 10 mM Ca^{2+}_{ext} (Ca^{2+}) and in 10 mM Ca^{2+}_{ext} + 10 μM efsevin (Ca^{2+} + efsevin) for mouse ESC-CMs (**F**) and 5 mM Ca^{2+}_{ext} (Ca^{2+}) and in 5 mM Ca^{2+}_{ext} + 5 μM efsevin (Ca^{2+} + efsevin) for human ESC-CMs (**G**). ***, $p < 0.001$ by F-test.

DOI: 10.7554/eLife.04801.011

amplitude or time to peak of paced Ca^{2+} transients (***Figure 6A***). Similarly, efsevin treatment did not significantly alter the frequency, amplitude or Ca^{2+} release flux of spontaneous Ca^{2+} sparks, local Ca^{2+} release events, but accelerated the decay phase resulting in sparks with a shorter duration and a narrower width (***Figure 6B***). These results indicate that by activating mitochondrial Ca^{2+} uptake, efsevin accelerates Ca^{2+} removal from the cytosol in cardiomyocytes and thereby restricts local cytosolic Ca^{2+} sparks to a narrower domain for a shorter period of time without affecting SR Ca^{2+} load or RyR Ca^{2+} release. Under conditions of Ca^{2+} overload, single Ca^{2+} sparks can trigger opening of neighbouring Ca^{2+} release units and thus induce the formation of erratic Ca^{2+} waves (***Figure 6C***). Efsevin treatment significantly reduced the number of propagating Ca^{2+} waves in a dosage-dependent manner (***Figure 6C,D***), demonstrating a potent suppressive effect of efsevin on the propagation of Ca^{2+} overload-induced Ca^{2+} waves and suggesting that efsevin could serve as a pharmacological tool to manipulate local Ca^{2+} signals.

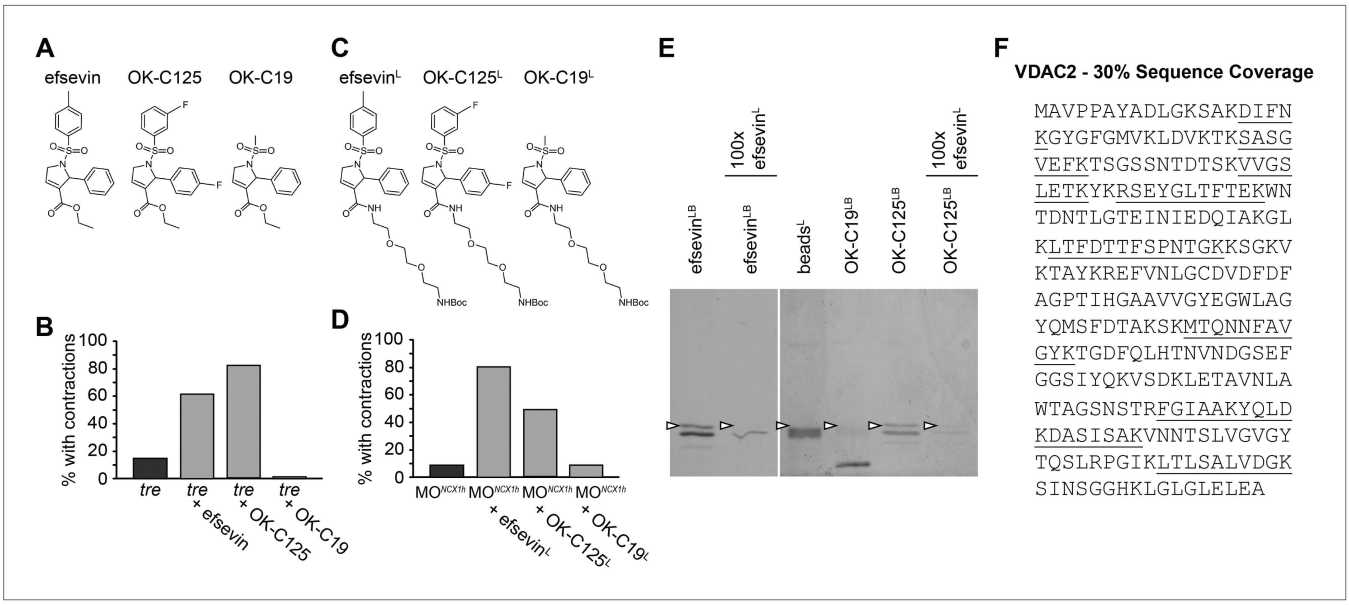

Figure 3. VDAC2 is a protein target of efsevin. (**A**) Structures of efsevin and two derivatives, OK-C125 and OK-C19. (**B**) Efsevin and OK-C125 restored rhythmic contractions in the majority of *tremblor* embryos, whereas OK-C19 failed to rescue the *tremblor* phenotype. (**C**) Structures of linker-attached compounds (indicated by superscript L). (**D**) Compounds efsevin^{L} and OK-C125^{L} retained their ability to restore rhythmic contractions in NCX1hMO injected embryos, while the inactive derivative OK-C19^{L} was still unable to induce rhythmic contraction. (**E**) Affinity agarose beads covalently linked with efsevin (efsevin^{LB}) or OK-C125 (OK-C125^{LB}) pulled down 2 protein species from zebrafish embryonic lysate, whereof one, the 32 kD upper band, was sensitive to competition with a 100-fold excess free efsevin^{L}. The 32 kD band was not detected in proteins eluted from beads capped with ethanolamine alone (beads^{C}) or beads linked to OK-C19 (OK-C19^{LB}). Arrowheads point to the 32kD bands. (**F**) Mass Spectrometry identifies the 32kD band as VDAC2. Peptides identified by mass spectrometry (underlined) account for 30% of the total sequence.

DOI: 10.7554/eLife.04801.012

The following figure supplement is available for figure 3:

Figure supplement 1. Mass Spectometry identifies VDAC2 as the target of efsevin.

DOI: 10.7554/eLife.04801.013

Mitochondrial Ca^{2+} uptake modulates embryonic cardiac rhythmicity

We hypothesize that efsevin treatment/VDAC2 overexpression suppresses aberrant Ca^{2+} handling-associated arrhythmic cardiac contractions by buffering excess Ca^{2+} into mitochondria. This hypothesis predicts that activating other mitochondrial Ca^{2+} uptake molecules would likewise restore coordinated contractions in *tre*. To test this model, we cloned zebrafish MCU and MICU1, an inner mitochondrial membrane Ca^{2+} transporter and its regulator (***Perocchi et al., 2010***; ***Baughman et al., 2011***; ***De Stefani et al., 2011***; ***Mallilankaraman et al., 2012***; ***Csordas et al., 2013***). In situ hybridization showed that MCU and MICU1 were expressed in the developing zebrafish heart (***Figure 7A***) and their expression levels were comparable between the wild type and *tre* hearts (***Figure 7—figure supplement 1***). Overexpression of MCU restored coordinated contractions in *tre*, akin to what was observed with VDAC2 (***Figure 7B***). In addition, *tre* embryos injected with suboptimal concentrations of MCU or VDAC2 had a fibrillating heart, but embryos receiving both VDAC2 and MCU at the suboptimal concentration manifested coordinated contractions (***Figure 7C***), demonstrating a synergistic effect of these proteins. Furthermore, overexpression of MCU failed to suppress the *tre* phenotype in the absence of VDAC2 activity and VDAC2 could not restore coordinated contractions in *tre* without functional MCU (***Figure 7B,D***). Similar results were observed by manipulating MICU1 activity (***Figure 7E,F***). Together, these findings indicate that mitochondrial Ca^{2+} uptake mechanisms on outer and inner mitochondrial membranes act cooperatively to regulate cardiac rhythmicity.

Conclusion

In summary, we conducted a chemical suppressor screen in zebrafish to dissect the regulatory network critical for maintaining rhythmic cardiac contractions and to identify mechanisms underlying aberrant

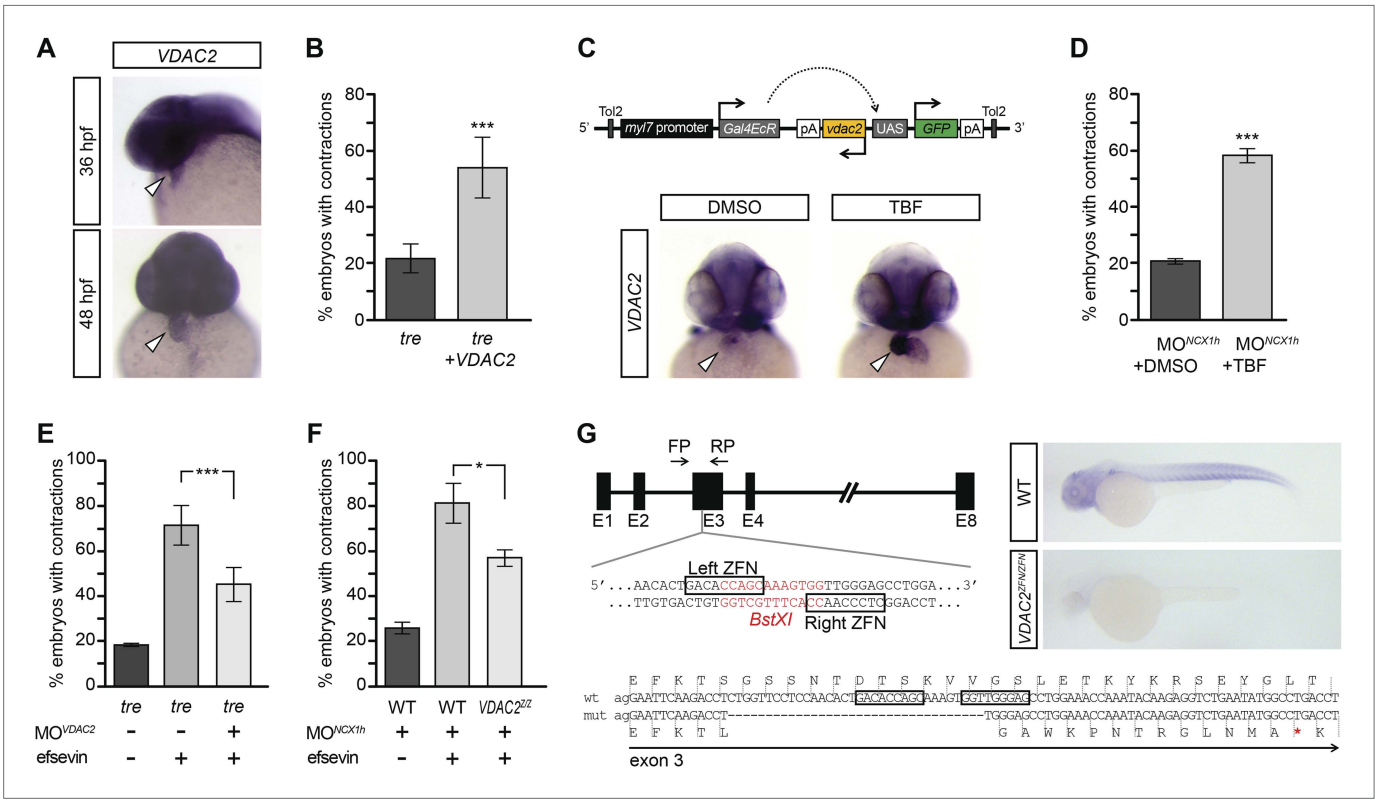

Figure 4. VDAC2 restores rhythmic cardiac contractions in *tre*. (**A**) In situ hybridization analysis showed that VDAC2 is expressed in embryonic hearts at 36 hpf (upper image) and 48 hpf (lower image). (**B**) Injection of 25 pg in vitro synthesized VDAC2 mRNA restored cardiac contractions in 52.9 ± 12.1% (n = 78) of 1-day-old *tre* embryos, compared to 21.8 ± 5.1% in uninjected siblings (n = 111). (**C**) Schematic diagram of *myl7:VDAC2* construct (top). In situ hybridization analysis showed that TBF treatment induces VDAC2 expression in the heart (lower panel). (**D**) While only ~20% of *myl7:VDAC2;NCX1hMO* embryos have coordinated contractions (n = 116), 52.3 ± 2.4% of these embryos established persistent, rhythmic contractions after TBF induction of VDAC2 (n = 154). (**E**) On average, 71.2 ± 8.8% efsevin treated embryos have coordinated cardiac contractions (n = 131). Morpholino antisense oligonucleotide knockdown of VDAC2 (MO^{VDAC2}) attenuates the ability of efsevin to suppress cardiac fibrillation in *tre* embryos (45.3 ± 7.4% embryos with coordinated contractions, n = 94). (**F**) Efsevin treatment restores coordinated cardiac contractions in 76.2 ± 8.7% NCX1MO embryos, only 54.1 ± 3.6% $VDAC2^{zfn/zfn}$;NCX1MO embryos have coordinated contractions (n = 250). (**G**) Diagram of Zinc finger target sites. $VDAC2^{zfn/zfn}$ carries a 34 bp deletion in exon 3 which results in a premature stop codon (red asterisk). In situ hybridization analysis showing loss of VDAC2 transcripts in $VDAC2^{zfn/zfn}$ embryos. White arrowheads point to the developing heart.

DOI: 10.7554/eLife.04801.014

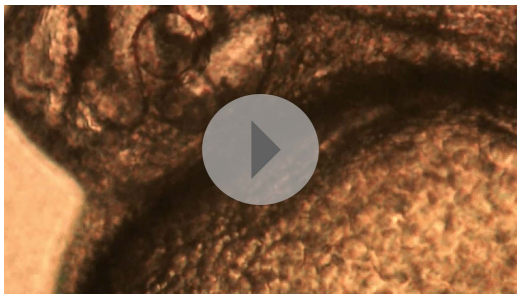

Video 8. This video shows a heart of a wild-type zebrafish embryo at 1 dpf. Robust rhythmic contractions can be observed in atrium and ventricle.

DOI: 10.7554/eLife.04801.015

Ca^{2+} handling-induced cardiac dysfunction. We show that activation of VDAC2 through overexpression or efsevin treatment potently restores rhythmic contractions in NCX1h deficient zebrafish hearts and effectively suppresses Ca^{2+} overload-induced arrhythmogenic Ca^{2+} events and irregular contractions in mouse and human cardiomyocytes. We provide evidence that potentiating VDAC2 activity enhances mitochondrial Ca^{2+} uptake, accelerates Ca^{2+} transfer from intracellular stores into mitochondria and spatially and temporally restricts single Ca^{2+} sparks in cardiomyocytes. The crucial role of mitochondria in the regulation of cardiac rhythmicity is further supported by the findings that VDAC2 functions in concert with MCU; these genes have a strong synergistic effect on suppressing cardiac fibrillation and loss of function of either gene abrogates the rescue effect of the other in *tre*.

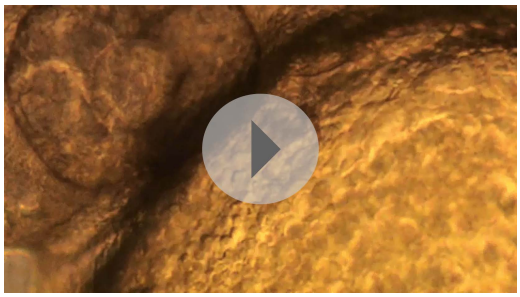

Video 9. This video shows a heart of a wild-type zebrafish embryo injected with zebrafish VDAC2 mRNA at 1 dpf. Robust rhythmic contractions can be observed in atrium and ventricle.
DOI: 10.7554/eLife.04801.016

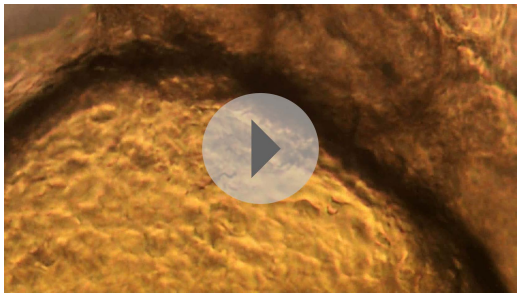

Video 10. This video shows a heart of a *tremblor* embryo at 1 dpf. *Tremblor* embryos display only local, unsynchronized contractions, comparable to cardiac fibrillation.
DOI: 10.7554/eLife.04801.017

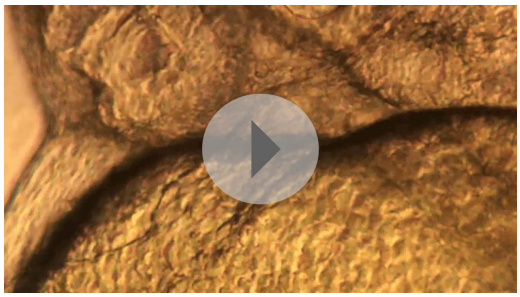

Video 11. This video shows a heart of a *tremblor* embryo injected with zebrafish VDAC2 mRNA at 1 dpf. Overexpression of zebrafish VDAC2 mRNA restores rhythmic contractions in *tremblor* embryos.
DOI: 10.7554/eLife.04801.018

The regulatory roles of mitochondrial Ca^{2+} in cardiac metabolism, cell survival and fate have been studied extensively (***Brown and O'Rourke, 2010***; ***Dorn and Scorrano, 2010***; ***Doenst et al., 2013***; ***Kasahara et al., 2013***; ***Kohlhaas and Maack, 2013***; ***Luo and Anderson, 2013***). Our study provides genetic and physiologic evidence supporting an additional role for mitochondria in regulating cardiac rhythmicity and reveals VDAC2 as a modulator of Ca^{2+} handling in cardiomyocytes. Our findings, together with recent reports of the physical interaction between VDAC2 and RyR2 (***Min et al., 2012***) and the close proximity of outer and inner mitochondrial membranes at the contact sites between the mitochondria and the SR (***García-Pérez et al., 2011***), suggest an intriguing model. We propose that mitochondria facilitate an efficient clearance mechanism in the Ca^{2+} microdomain, which modulates Ca^{2+} handling without affecting global Ca^{2+} signals in cardiomyocytes. In this model, VDAC facilitates mitochondrial Ca^{2+} uptake via MCU complex and thereby controls the duration and the diffusion of cytosolic Ca^{2+} near the Ca^{2+} release sites to ensure rhythmic cardiac contractions. This model is consistent with our observation that efsevin treatment induces faster inactivation kinetics of cytosolic Ca^{2+} transients without affecting the amplitude or the time to peak in cardiomyocytes and the reports that blocking mitochondrial Ca^{2+} uptake has little impact on cytosolic Ca^{2+} transients (***Maack et al., 2006***; ***Kohlhaas et al., 2010***). Further support for this model comes from the observation of the Ca^{2+} peaks on the OMM (***Drago et al., 2012***) and the finding that down-regulating VDAC2 extends Ca^{2+} sparks (***Subedi et al., 2011***; ***Min et al., 2012***) and that blocking mitochondrial Ca^{2+} uptake by Ru360 leads to an increased number of spontaneous propagating Ca^{2+} waves (***Seguchi et al., 2005***). Future studies on the kinetics of VDAC2-dependent mitochondrial Ca^{2+} uptake and exploring potential regulatory molecules for VDAC2 activity will provide insights into how the crosstalk between SR and mitochondria contributes to Ca^{2+} handling and cardiac rhythmicity.

Aberrant Ca^{2+} handling is associated with many cardiac dysfunctions including arrhythmia. Establishing animal models to study molecular mechanisms and develop new therapeutic strategies are therefore major preclinical needs. Our chemical suppressor screen identified a potent effect of efsevin and its biological target VDAC2 on manipulating cardiac Ca^{2+} handling and restoring regular cardiac contractions in fish and mouse and human cardiomyocytes. This success indicates that fundamental mechanisms regulating cardiac function are conserved among vertebrates despite the existence of species-specific features and suggests a new paradigm of using zebrafish cardiac disease models for the dissection of critical genetic pathways and the discovery of new therapeutic approaches. Future studies examining the effects of efsevin on other

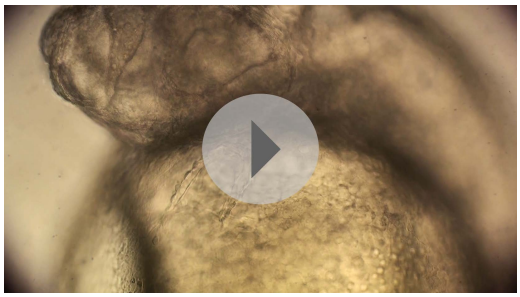

Video 12. This video shows a heart of a 2 dpf Tg-VDAC2 embryo injected with a morpholino targeting NCX1h. Morpholino knock-down of NCX1h results in a fibrillating heart.
DOI: 10.7554/eLife.04801.019

Video 13. This video shows a heart of a 2 dpf NCX1h morphant in the Tg-VDAC2 genetic background. TBF treatment induces VDAC2 expression and restores coordinated cardiac contractions.
DOI: 10.7554/eLife.04801.020

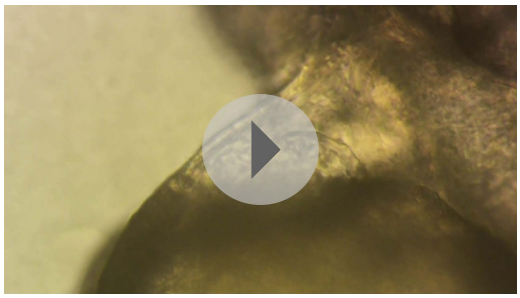

Video 14. This video shows a heart of a 2 dpf wild type zebrafish embryo injected with a morpholino targeting VDAC2. Morpholino knockdown of VDAC2 did not have obvious effects on cardiac performance.
DOI: 10.7554/eLife.04801.021

arrhythmia models would further elucidate the potential for efsevin as a pharmacological tool to treat cardiac arrhythmia associated with aberrant Ca^{2+} handling.

Materials and methods

Zebrafish husbandry and transgenic lines

Zebrafish of the mutant line *tremblor* (*tre*^{tc318}) were maintained and bred as described previously (***Langenbacher et al., 2005***). Transgenic lines, *myl7:gCaMP4.1*^{LA2124} and *myl7:VDAC2*^{LA2309} were created using the Tol2kit (***Esengil et al., 2007***; ***Kwan et al., 2007***; ***Shindo et al., 2010***). The *VDAC2*^{LA2256} was created using the zinc finger array OZ523 and OZ524 generated by the zebrafish Zinc Finger Consortium (***Foley et al., 2009a***, ***2009b***).

Molecular Biology

Full length VDAC2 cDNA was purchased from Open Biosystems (Huntsville, AL) and cloned into pCS2+ or pCS2+3XFLAG. Full length cDNA fragments of zebrafish MCU (Accession number: JX424822) and MICU1 (JX42823) were amplified from 2 dpf embryos and cloned into pCS2+. For mRNA synthesis, plasmids were linearized and mRNA was synthesized using the SP6 mMESSAGE mMachine kit according to the manufacturers manual (Ambion, Austin, TX.).

Zebrafish injections

VDAC2 mRNA and morpholino antisense oligos (5′-GGGAACGGCCATTTTATCTGTTAAA-3′) (Genetools, Philomath, OR) were injected into one-cell stage embryos collected from crosses of *tre*^{tc318} heterozygotes. Cardiac performance was analyzed by visual inspection on 1 dpf. The *tre* mutant embryos were identified either by observing the fibrillation phenotype at 2–3 dpf or by genotyping as previously described (***Langenbacher et al., 2005***).

Chemical screen

Chemicals from a synthetic library (***Castellano et al., 2007***; ***Choi et al., 2011***; ***Cruz et al., 2011***) and from Biomol International LP (Farmingdale, NY) were screened for their ability to partially or completely restore persistent heartbeat in *tre* embryos. 12 embryos collected from crosses of *tre*^{tc318} heterozygotes were raised in the presence of individual compounds at a concentration of 10 μM from 4 hpf (***Choi et al., 2011***). Cardiac function was analyzed by visual inspection at 1 and 2 dpf. The hearts of *tre*^{tc318} embryos manifest a chaotic movement resembling cardiac fibrillation with intermittent contractions in rare occasion (***Ebert et al., 2005***; ***Langenbacher et al., 2005***). Compounds that elicit persistent coordinated cardiac contractions were validated on large number of *tre* mutant embryos and NCX1h morphants (>500 embryos).

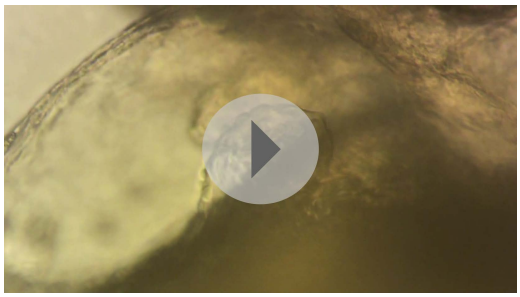

Video 15. This video shows a heart of a 2 dpf *tremblor* mutant embryo injected with a morpholino targeting VDAC2.
DOI: 10.7554/eLife.04801.022

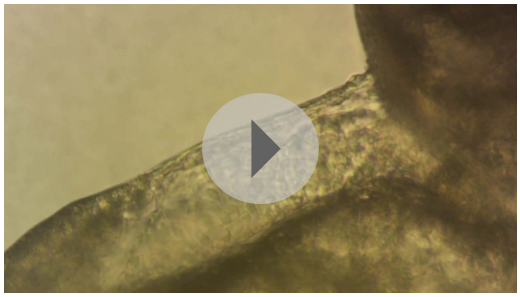

Video 16. This video shows a heart of a 2 dpf *tremblor* mutant embryo injected with a morpholino targeting VDAC2. Efsevin treatment cannot restore coordinated cardiac contractions in the absence of VDAC2.
DOI: 10.7554/eLife.04801.023

Zebrafish cardiac imaging

Videos of GFP-labelled *myl7:GFP* hearts were taken at 30 frames per second. Line-scan analysis was performed along a line through the atria or the ventricles of these hearts (***Nguyen et al., 2009***). Fraction of shortening was deduced from the ratio of diastolic and systolic width and heart rate was determined by beats per minute. Cardiac parameters were analyzed in *tremblor*^{tc318} and *VDAC2*^{LA2256} at 2 dpf.

Zebrafish optical mapping

36 hpf *myl7:gCaMP4.1* embryos were imaged at a frame rate of 30 ms/frame. Electromechanical isolation was achieved by tnnt2MO (***Milan et al., 2006***). The fluorescence intensity of each pixel in a 2D map was normalize to generate heat maps and isochronal lines at 33 ms intervals were obtained by identifying the maximal spatial gradient for a given time point (***Chi et al., 2008***).

Mouse and human embryonic stem cells

The mouse E14Tg2a ESC and human H9 ESC line were cultured and differentiated as previously described (***Blin et al., 2010***; ***Arshi et al., 2013***). At day 10 of differentiation, beating mouse EBs were exposed to external solution containing 10 mM $CaCl_2$ for 10 min before DMSO or efsevin (10 μM) treatment. Human EBs were differentiated for 15 days and treated with 5 mM $CaCl_2$ for 10 min before DMSO or efsevin (5 μM) treatment. Images of beating EBs were acquired at a rate of 30 frames/s and analyzed by motion-detection software. For calcium recording, the EBs were loaded with 10 μM fluo-4 AM in culture media for 30 min at 37°C. Line-scan analysis was performed and fluorescent signals were acquired by a Zeiss LSM510 confocal microscope.

Microelectrode array measurements

2-day-old wild type, *tre*, and efsevin-treated *tre* embryos were placed on uncoated, microelectrode arrays (MEAs) containing 120 integrated TiN electrodes (30 μm diameter, 200 μm interelectrode spacing). Local field potentials (LFPs) at each electrode were collected for three trials per embryo type over a period of three minutes at a sampling rate of 1 kHz using the MEA2100-HS120 system (Multichannel Systems, Reutiligen, Germany). Raw data was low-pass filtered at a cutoff frequency of 10 Hz using a third-order Butterworth filter. Data analysis was carried out using the MC_DataTool (Multichannel Systems) and Matlab (MathWorks).

Ca^{2+} imaging

Murine ventricular cardiomyocytes were isolated as previously described (***Reuter et al., 2004***). Cells were loaded with 5 μM fluo-4 AM in external solution containing: 138.2 mM NaCl, 4.6 mM KCl, 1.2 mM MgCl, 15 mM glucose, 20 mM HEPES for 1 hr and imaged in external solution supplemented with 2, 5 or 10 mM $CaCl_2$. For the recording of Ca^{2+} sparks and transients, the external solution contained 2 mM $CaCl_2$. For Ca^{2+} transients, cells were field stimulated at 0.5 Hz with a 5 ms pulse at a voltage of 20% above contraction threshold. For all measurements, efsevin was added 2 hr prior to the actual experiment. Images were recorded on a Zeiss LSM 5 Pascal confocal microscope. Data analysis was carried out using the Zeiss LSM Image Browser and ImageJ with the SparkMaster plugin (***Picht et al., 2007***). Cells were visually inspected prior to and after each recording. Only those recordings from

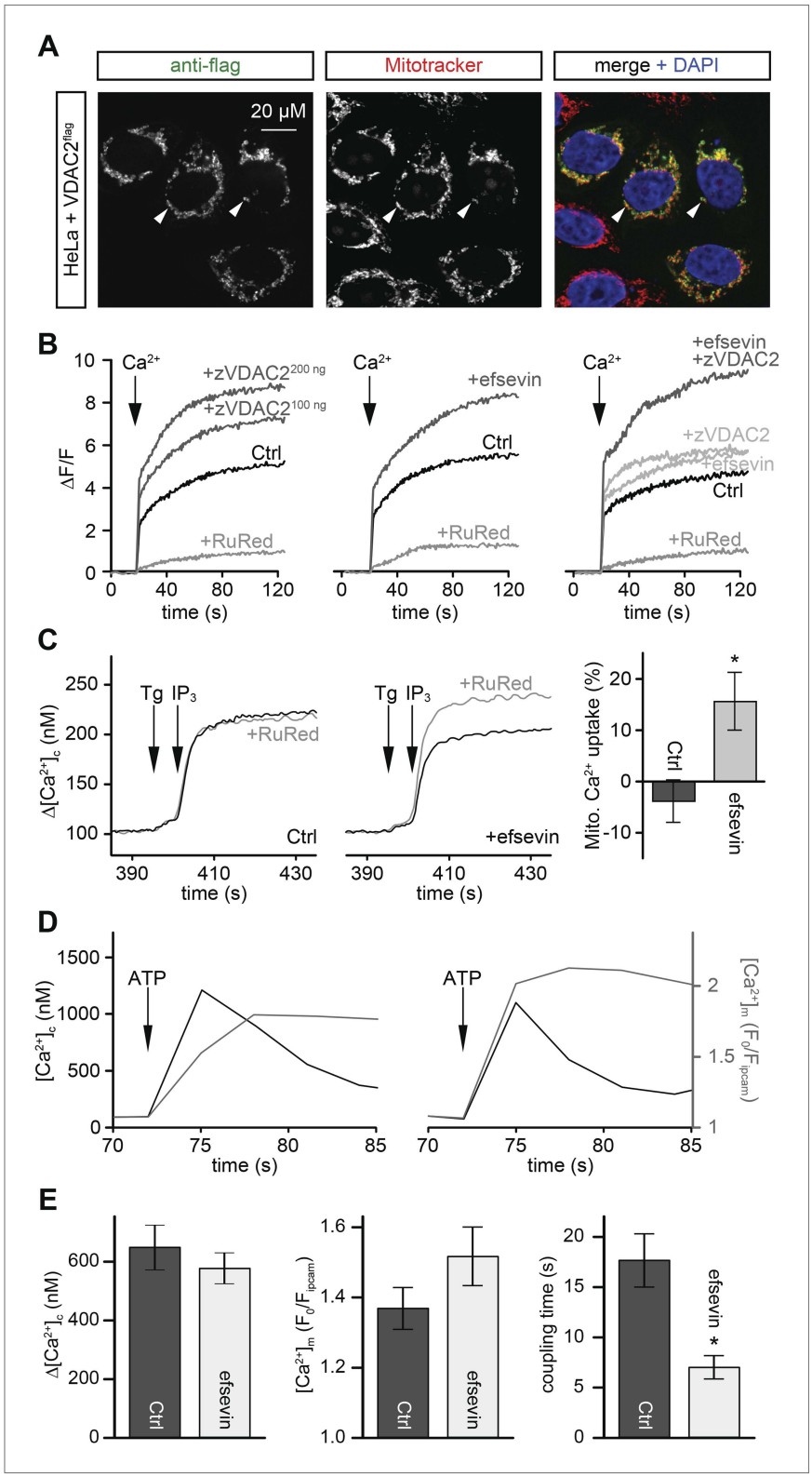

Figure 5. Efsevin enhances mitochondrial Ca^{2+} uptake. (**A**) HeLa cells were transfected with a flag-tagged zebrafish VDAC2 ($VDAC2^{flag}$), immunostained against the flag epitope and counterstained for mitochondria with MitoTracker Orange and for nuclei with DAPI. (**B**) Representative traces of mitochondrial matrix $[Ca^{2+}]$ ($[Ca^{2+}]_m$) detected by

Figure 5. Continued on next page

Figure 5. Continued

Rhod2. Arrows denote the addition of Ca^{2+}. Mitochondrial Ca^{2+} uptake was assessed when VDAC2 was overexpressed (left), cells were treated with 1 μM efsevin (middle) and combination of both at suboptimal doses (right). Control-traces with ruthenium red (RuRed) show mitochondrial specificity of the signal. (**C**) Representative traces of cytosolic $[Ca^{2+}]$ ($[Ca^{2+}]_c$) changes upon the application of 7.5 μM IP_3 in the presence (+) or absence (−) of RuRed. Mitochondrial Ca^{2+} uptake was assessed by the difference of the – and + RuRed conditions normalized to the total release (n = 4; mean ± SE). (**D**) MEFs overexpressing zebrafish VDAC2 (polycistronic with mCherry) were stimulated with 1 μM ATP in a nominally Ca^{2+} free buffer. Changes in $[Ca^{2+}]_c$ and $[Ca^{2+}]_m$ were imaged using fura2 and mitochondria-targeted inverse pericam, respectively. Black and gray traces show the $[Ca^{2+}]_c$ (in nM) and $[Ca^{2+}]_m$ (F_0/F mtpericam) time courses in the absence (left) or present (right) of efsevin. (**E**) Bar charts: Cell population averages for the peak $[Ca^{2+}]_c$ (left), the corresponding $[Ca^{2+}]_m$ (middle), and the coupling time (time interval between the maximal $[Ca^{2+}]_c$ and $[Ca^{2+}]_m$ responses) in the presence (black, n = 24) or absence (gray, n = 28) of efsevin.
DOI: 10.7554/eLife.04801.024
The following figure supplement is available for figure 5:

Figure supplement 1. Local Ca^{2+} delivery between IP3 receptors and VDAC2.
DOI: 10.7554/eLife.04801.025

healthy looking cells with distinct borders, uniform striations and no membrane blebs or granularity were included in the analysis.

Biochemistry

For pull down assays mono-N-Boc protected 2,2'-(ethylenedioxy)bis(ethylamine) was attached to the carboxylic ester of efsevin and its derivatives through the amide bond. After removal of the Boc group using TFA, the primary amine was coupled to the carboxylic acid of Affi-Gel 10 Gel (Biorad, Hercules, CA). 2-day-old zebrafish embryos were deyolked by centrifugation before being lysed with Rubinfeld's lysis buffer (***Rubinfeld et al., 1993***). The lysate was precleaned by incubation with Affi-Gel 10 Gel to eliminate non-specific binding. Precleaned lysate was incubated with affinity beads overnight. Proteins were eluted from the affinity beads and separated on SDS-PAGE. Protein bands of interest were excised. Gel plugs were dehydrated in acetonitrile (ACN) and dried completely in a Speedvac. Samples were reduced and alkylated with 10 mM dithiotreitol and 10 mM TCEP solution in 50 mM NH_4HCO_3 (30 min at 56°C) and 100 mM iodoacetamide (45 min in dark), respectively. Gel plugs were washed with 50 mM NH_4HCO_3, dehydrated with ACN, and dried down in a Speedvac. Gel pieces were then swollen in digestion buffer containing 50 mM NH_4HCO_3, and 20.0 ng/μl of chymotrypsin (25°C, overnight). Peptides were extracted with 0.1% TFA in 50% ACN solution, dried down and resuspended in LC buffer A (0.1% formic acid, 2% ACN).

Mass spectrometry analyses and database searching

Extracted peptides were analyzed by nano-flow LC/MS/MS on a Thermo Orbitrap with dedicated Eksigent nanopump using a reversed phase column (New Objective, Woburn, MA). The flow rate was 200 nl/min for separation: mobile phase A contained 0.1% formic acid, 2% ACN in water, and mobile phase B contained 0.1% formic acid, 20% water in ACN. The gradient used for analyses was linear from 5% B to 50% B over 60 min, then to 95% B over 15 min, and finally keeping constant 95% B for 10 min. Spectra were acquired in data-dependent mode with dynamic exclusion where the instrument selects the top six most abundant ions in the parent spectra for fragmentation. Data were searched against the *Danio rerio* IPI database v3.45 using the SEQUEST algorithm in the BioWorks software program version 3.3.1 SP1. All spectra used for identification had deltaCN>0.1 and met the following Xcorr criteria: >2 (+1), >3 (+2), >4 (+3), and >5 (+4). Searches required full cleavage with the enzyme, $\leq$4 missed cleavages and were performed with the differential modifications of carbamidomethylation on cysteine and methionine oxidation.

In situ hybridization

In situ hybridization was performed as previously described (***Chen and Fishman, 1996***). DIG-labeled RNA probe was synthesized using the DIG RNA labeling kit (Roche, Indianapolis, IN).

Immunostaining

HeLa cells were transfected with a C-terminally flag-tagged zebrafish VDAC1 or VDAC2 in plasmid pCS2+ using Lipofectamine 2000 (Invitrogen). After staining with MitoTracker Orange (Invitrogen)

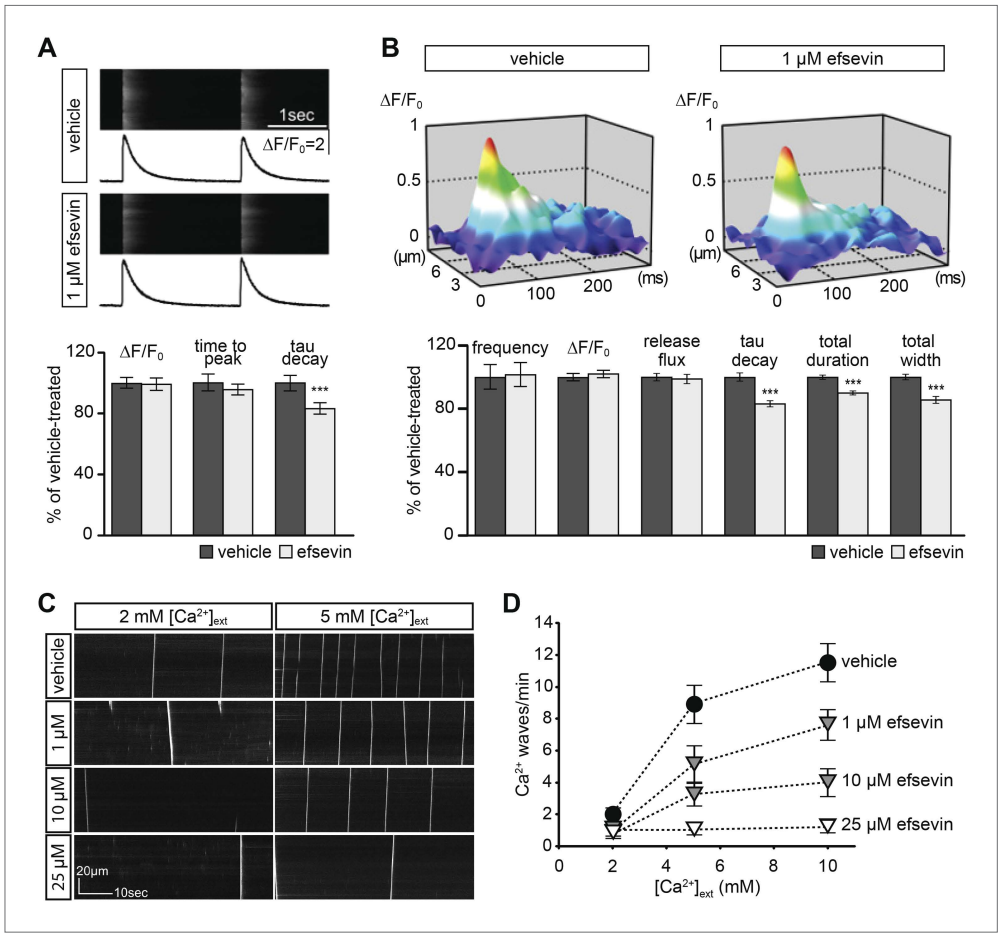

Figure 6. Effects of efsevin on isolated cardiomyocytes. (**A**) Electrically paced Ca^{2+} transients at 0.5 Hz (top). Normalized quantification of Ca^{2+} transient parameters reveals no difference for transient amplitude (efsevin-treated at 98.6 ± 4.5% of vehicle-treated) and time to peak (95 ± 3.9%), but a significant decrease for the rate of decay (82.8 ± 4% of vehicle- for efsevin-treated) (lower panel). (**B**) Representation of typical Ca^{2+} sparks of vehicle- and efsevin treated cardiomyocytes (top). No differences were observed for spark frequency (101.1 ± 7.7% for efsevin- compared to vehicle-treated), maximum spark amplitude (101.6 ± 2.5%) and Ca^{2+} release flux (98.7 ± 2.8%). In contrast, the decay phase of the single spark was significantly faster in efsevin treated cells (82.5 ± 2.1% of vehicle-treated). Consequently, total duration of the spark was reduced to 85.7 ± 2% and the total width was reduced to 89.5 ± 1.4% of vehicle-treated cells. *, $p < 0.05$; ***, $p < 0.001$. (**C**) Increasing concentrations of extracellular Ca^{2+} induced a higher frequency of spontaneous propagating Ca^{2+} waves in isolated adult murine ventricular cardiomyocytes. Efsevin treatment reduced Ca^{2+} waves in a dose-dependent manner. (**D**) Quantitative analysis of spontaneous Ca^{2+} waves spanning more than half of the entire cell. Addition of 1 µM efsevin reduced Ca^{2+} waves to approximately half. Increasing the concentration of efsevin to 10 µM further reduced the number of spontaneous Ca^{2+} waves and 25 µM efsevin almost entirely blocked the formation of Ca^{2+} waves.

DOI: 10.7554/eLife.04801.026

cells were fixed in 3.7% formaldehyde and permeabilized with acetone. Immunostaining was performed using primary antibody ANTI-FLAG M2 (Sigma Aldrich, St. Luis, MO) at 1:100 and secondary antibody Anti-Mouse IgG1-FITC (Southern Biotechnology Associates, Birmingham, AL) at 1:200. Cells were mounted and counterstained using Vectashield Hard Set with DAPI (Vector Laboratories, UK).

Mitochondria Ca^{2+} uptake assay in HeLa cells

HeLa cells were transfected with zebrafish VDAC2 using Lipofectamine 2000 (Invitrogen, Carlsbad, CA). 36 hrs after transfection, cells were loaded with 5 µM Rhod2-AM (Invitrogen), a Ca^{2+} indicator preferentially localized in mitochondria, for 1 hr at 15°C followed by a 30 min de-esterification period at 37°C. Subsequently, cells were permeabilized with 100 µM digitonin for 1 min at room temperature.

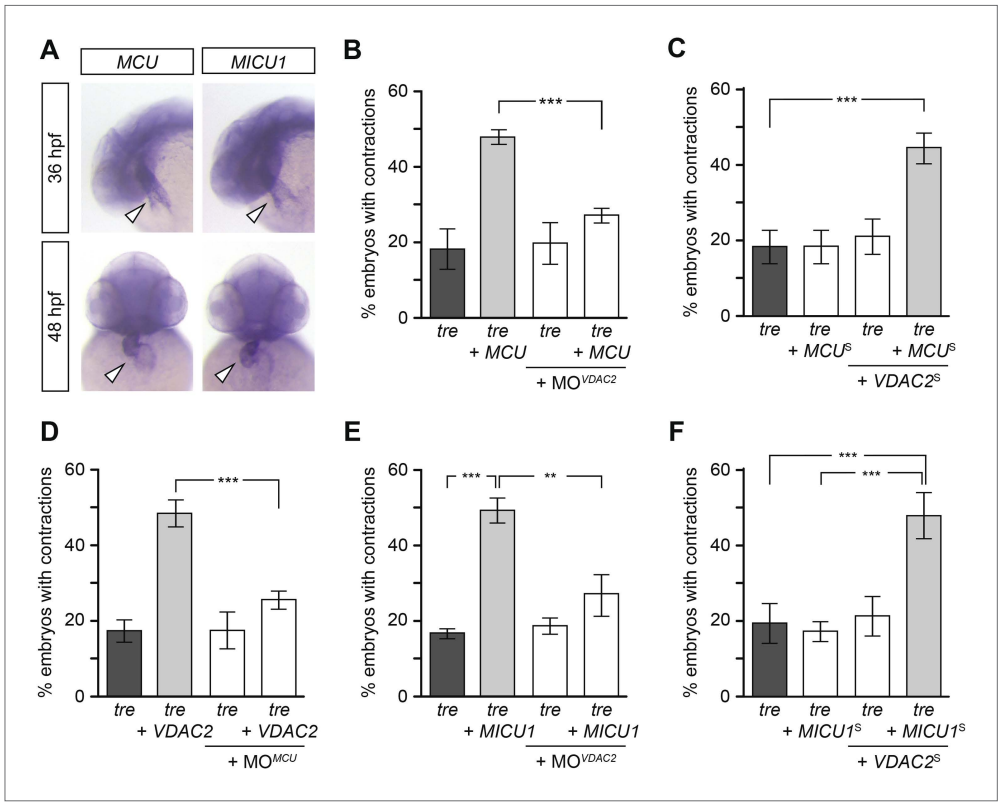

Figure 7. Mitochondria regulate cardiac rhythmicity through a VDAC2-dependent mechanism. (**A**) MCU and MICU1 are expressed in the developing zebrafish hearts (arrowhead). (**B**) Overexpression of MCU is sufficient to restore coordinated cardiac contractions in *tre* embryos (47.1 ± 1.6% embryos, n = 112 as opposed to 18.3 ± 5.3% of uninjected siblings, n = 64) while this effect is significantly attenuated when co-injected with morpholino antisense oligonucleotide targeted to VDAC2 (27.1 ± 1.9% embryos, n = 135). (**C**) Suboptimal overexpression of MCU (MCU^S) and VDAC2 ($VDAC2^S$) in combination is able to suppress cardiac fibrillation in *tre* embryos (42.9 ± 2.6% embryos, n = 129). (**D**) The ability of VDAC2 to restore rhythmic contractions in *tre* embryos (48.5 ± 3.5% embryos, n = 111) is significantly attenuated when MCU is knocked down by antisense oligonucleotide (MO^{MCU}) (25.6 ± 2.4% embryos, n = 115). (**E**) Overexpression of MICU1 is sufficient to restore rhythmic cardiac contractions in *tre* embryos (49.3 ± 3.4% embryos, n = 127 compared to 16.8 ± 1.4% of uninjected siblings, n = 150). This effect is abrogated by VDAC2 knockdown (MO^{VDAC2}, 25.3 ± 5.5% embryos, n = 97). (**F**) Suboptimal overexpression of MICU1 ($MICU1^S$) and VDAC2 ($VDAC2^S$) in combination is able to restore rhythmic cardiac contractions in *tre* embryos (48.6 ± 6.0%, n = 106). Error bars represent s.d.; *p < 0.05; ***p < 0.001.

DOI: 10.7554/eLife.04801.027

The following figure supplement is available for figure 7:

Figure supplement 1. Expression of MCU, MICU1 and VDAC2.

DOI: 10.7554/eLife.04801.028

Fluorescence changes in Rhod2 (ex: 544 nm, em: 590 nm) immediately after the addition of Ca^{2+} (final free Ca^{2+} concentration is calculated to be approximately 10 μM using WEBMAXC at http://web.stanford.edu/~cpatton/webmaxcS.htm) were monitored in internal buffer (5 mM K-EGTA, 20 mM HEPES, 100 mM K-aspartate, 40 mM KCl, 1 mM $MgCl_2$, 2 mM maleic acid, 2 mM glutamic acid, 5 mM pyruvic acid, 0.5 mM KH_2PO_4, 5 mM MgATP, pH adjusted to 7.2 with Trizma base) using a FLUOSTAR plate reader (BMG Labtech, Germany).

Mitochondria Ca^{2+} uptake assay in VDAC1/VDAC3 double knockout (V1/V3 DKO) MEFs

V1/V3 DKO MEFs were cultured as previously described (***Roy et al., 2009a***). Efsevin-treated (15 μM for 30 min) or mock-treated MEFs were used for measurements of $[Ca^{2+}]_c$ in suspensions of permeabilized cells or imaging of $[Ca^{2+}]_m$ simultaneously with $[Ca^{2+}]_c$ in intact single cells. Permeabilization of the

plasma membrane was performed by digitonin (40 μM/ml). Changes in $[Ca^{2+}]$ in the cytoplasmic buffer upon IP_3 (7.5 μM) addition in the presence or absence of ruthenium red (3 μM) was measured by fura2 in a fluorometer (***Csordás et al., 2006***; ***Roy et al., 2009b***). To avoid endoplasmic reticulum Ca^{2+} uptake 2 μM thapsigargin was added before IP_3. For imaging of $[Ca^{2+}]_m$ and $[Ca^{2+}]_c$, MEFs were co-transfected with plasmids encoding polycistronic zebrafish VDAC2 with mCherry and mitochondria-targeted inverse pericam for 40 hr. Cells were sorted to enrich the transfected cells and attached to glass coverslips. In the final 10 min, of the efsevin or mock-treatment, the cells were also loaded with fura2AM (2.5 μM) and subsequently transferred to the microscope stage. Stimulation with 1 μM ATP was carried out in a normimally Ca^{2+} free buffer. Changes in $[Ca^{2+}]_c$ and $[Ca^{2+}]_m$ were imaged using fura2 (ratio of ex:340 nm–380 nm) and mitochondria-targeted inverse pericam (ex: 495 nm), respectively (***Csordas et al., 2010***).

Statistics

All values are expressed as mean ± SEM, unless otherwise specified. Significance values are calculated by unpaired student's t-test unless noted otherwise.

Acknowledgements

The authors thank Kenneth D Philipson, James N Weiss and Adam D Langenbacher for comments on the manuscript, Janice Ahn for assisting the initial chemical screen and Lingling Peng for the synthesis and Yi Chiao Fan for the characterization of efsevin and its derivatives. We also thank Jing Huang, James N Weiss and the UCLA cardiovascular research laboratory for reagents and infrastructure, and Jinghua Tang of UCLA-BSCRC for technical assistance on human ES cell works. We thank William Craigen for providing V1/V3 DKO MEFs.

Additional information

Funding

Funder	Grant reference number	Author
National Heart, Lung, and Blood Institute	HL081700 and HL096980	Jau-Nian Chen
National Institute of General Medical Sciences	GM071779 and P41GM081282	Ohyun Kwon
The Nakajima Foundation	Graduate Student Fellowship	Hirohito Shimizu
China Scholarship Council	Graduate Student Fellowship	Fei Lu
University of California, Los Angeles	Philip Whitcome Training Program, Graduate Student Fellowship	Fei Lu
Laubisch Foundation	Faculty Award	Jau-Nian Chen
Austrian Science Fund	Erwin-Schrodinger Stipendium Postdoctoral Fellowship	Johann Schredelseker
University of California, Los Angeles	Broad Stem Cell Research Center Faculty Award	Atsushi Nakano
National Heart, Lung, and Blood Institute	HL105699	Thomas M Vondriska
National Heart, Lung, and Blood Institute	HL107674	Sarah Franklin
National Heart, Lung, and Blood Institute	HL070828	Joshua I Goldhaber
National Institute of General Medical Sciences	GM059419	György Hajnóczky

The funders had no role in study design, data collection and interpretation, or the decision to submit the work for publication.

Author contributions

HS, Designed, performed, analyzed, and interpreted experiments, Wrote the manuscript, Conception and design, Acquisition of data, Analysis and interpretation of data, Drafting or revising the article;

JS, Designed, performed, analyzed, and interpreted experiments, Wrote the manuscript, Acquisition of data, Analysis and interpretation of data, Drafting or revising the article; JH, Designed, performed, analyzed, and interpreted experiments, Conception and design, Acquisition of data, Analysis and interpretation of data; KL, Designed and synthesized the compound library and all efsevin used for experiments, Conception and design, Acquisition of data; SN, AE, Examined mitochondrial Ca^{2+} uptake in V1/V3KO MEFs, Acquisition of data, Analysis and interpretation of data; FL, KW, CT, Performed, analyzed, and interpreted experiments, Acquisition of data, Analysis and interpretation of data; SF, Designed and performed the mass-spec analysis, Acquisition of data, Analysis and interpretation of data; HDGF, Designed and synthesized the compound library and all efsevin used for experiments, Acquisition of data, Analysis and interpretation of data; HZ, Designed and performed MEA analysis, Acquisition of data, Analysis and interpretation of data; BL, Performed, analyzed, and interpreted experiments, Acquisition of data; HN, Designed and performed hESC-CM experiments, Acquisition of data, Analysis and interpretation of data; JN, Provided gCaMP construct, Contributed unpublished essential data or reagents; AZS, JKG, Designed and interpreted MEA analysis, Analysis and interpretation of data; AN, Designed and performed hESC-CM experiments, Analysis and interpretation of data; JIG, Supervised physiological analysis, Analysis and interpretation of data; TMV, Designed and performed the mass-spec analysis, Analysis and interpretation of data; GH, Examined mitochondrial Ca^{2+} uptake in V1/V3KO MEFsDesigned and formulated hypothesis, Designed and synthesized the compound library and all efsevin used for experiments, Analysis and interpretation of data; OK, Designed and synthesized the compound library and all efsevin used for experiments, Conception and design, Analysis and interpretation of data; J-NC, Designed and formulated hypothesis, Performed, analyzed, and interpreted experiments, Wrote the manuscript, Conception and design, Acquisition of data, Analysis and interpretation of data, Drafting or revising the article

Author ORCIDs
Adam Z Stieg, http://orcid.org/0000-0001-7312-9364

Ethics
Animal experimentation: This study was performed in strict accordance with the recommendations in the Guide for the Care and Use of Laboratory Animals of the National Institutes of Health. All of the animals were handled according to approved institutional animal care and use committee (IACUC) protocols of the University of California, Los Angeles and the Cedars-Sinai Hospital. The protocols were approved by the Cedars-Sinai Institutional Animal Care and Use Committee (#003574 for the use of mouse cardiomyocytes), the Office of Animal Research Oversight that oversees the Ethics of Animal Experiments (ARC# 2000-051-43B for the use of zebrafish) and Embryonic Stem Cell Research Oversight (#2009-006-06 for the use of ES cells) of the University of California, Los Angeles. Every effort was made to minimize suffering.

References
Arshi A, Nakashima Y, Nakano H, Eaimkhong S, Evseenko D, Reed J, Stieg AZ, Gimzewski JK, Nakano A. 2013. Rigid microenvironments promote cardiac differentiation of mouse and human embryonic stem cells. *Science and Technology of Advanced Materials* **14**:pii: 025003. doi: 10.1088/1468-6996/14/2/025003.

Bathori G, Csordas G, Garcia-Perez C, Davies E, Hajnoczky G. 2006. Ca2+-dependent control of the permeability properties of the mitochondrial outer membrane and voltage-dependent anion-selective channel (VDAC). *The Journal of Biological Chemistry* **281**:17347–17358. doi: 10.1074/jbc.M600906200.

Baughman JM, Perocchi F, Girgis HS, Plovanich M, Belcher-Timme CA, Sancak Y, Bao XR, Strittmatter L, Goldberger O, Bogorad RL, Koteliansky V, Mootha VK. 2011. Integrative genomics identifies MCU as an essential component of the mitochondrial calcium uniporter. *Nature* **476**:341–345. doi: 10.1038/nature10234.

Bers DM. 2002. Cardiac excitation-contraction coupling. *Nature* **415**:198–205. doi: 10.1038/415198a.

Blin G, Nury D, Stefanovic S, Neri T, Guillevic O, Brinon B, Bellamy V, Rucker-Martin C, Barbry P, Bel A, Bruneval P, Cowan C, Pouly J, Mitalipov S, Gouadon E, Binder P, Hagège A, Desnos M, Renaud JF, Menasché P, Pucéat M. 2010. A purified population of multipotent cardiovascular progenitors derived from primate pluripotent stem cells engrafts in postmyocardial infarcted nonhuman primates. *The Journal of Clinical Investigation* **120**:1125–1139. doi: 10.1172/JCI40120.

Boncompagni S, Rossi AE, Micaroni M, Beznoussenko GV, Polishchuk RS, Dirksen RT, Protasi F. 2009. Mitochondria are linked to calcium stores in striated muscle by developmentally regulated tethering structures. *Molecular Biology of the Cell* **20**:1058–1067. doi: 10.1091/mbc.E08-07-0783.

Brandes R, Bers DM. 1997. Intracellular Ca2+ increases the mitochondrial NADH concentration during elevated work in intact cardiac muscle. *Circulation Research* **80**:82–87. doi: 10.1161/01.RES.80.1.82.

Brown DA, O'Rourke B. 2010. Cardiac mitochondria and arrhythmias. *Cardiovascular Research* **88**:241–249. doi: 10.1093/cvr/cvq231.
Castellano S, Fiji HD, Kinderman SS, Watanabe M, Leon P, Tamanoi F, Kwon O. 2007. Small-molecule inhibitors of protein geranylgeranyltransferase type I. *Journal of the American Chemical Society* **129**:5843–5845. doi: 10.1021/ja070274n.
Chen JN, Fishman MC. 1996. Zebrafish tinman homolog demarcates the heart field and initiates myocardial differentiation. *Development* **122**:3809–3816.
Chi NC, Shaw RM, Jungblut B, Huisken J, Ferrer T, Arnaout R, Scott I, Beis D, Xiao T, Baier H, Jan LY, Tristani-Firouzi M, Stainier DY. 2008. Genetic and physiologic dissection of the vertebrate cardiac conduction system. *PLOS Biology* **6**:e109. doi: 10.1371/journal.pbio.0060109.
Choi BR, Burton F, Salama G. 2002. Cytosolic Ca2+ triggers early afterdepolarization and Torsade de Pointes in rabbit hearts with type 2 long QT syndrome. *The Journal of Physiology* **543**:615–631. doi: 10.1113/jphysiol.2002.024570.
Choi J, Mouillesseaux K, Wang Z, Fiji HD, Kinderman SS, Otto GW, Geisler R, Kwon O, Chen JN. 2011. Aplexone targets the HMG-CoA reductase pathway and differentially regulates arterovenous angiogenesis. *Development* **138**:1173–1181. doi: 10.1242/dev.054049.
Cruz D, Wang Z, Kibbie J, Modlin R, Kwon O. 2011. Diversity through phosphine catalysis identifies octahydro-1,6-naphthyridin-4-ones as activators of endothelium-driven immunity. *Proceedings of the National Academy of Sciences of USA* **108**:6769–6774. doi: 10.1073/pnas.1015254108.
Csordas G, Golenar T, Seifert EL, Kamer KJ, Sancak Y, Perocchi F, Moffat C, Weaver D, de la Fuente Perez S, Bogorad R, Koteliansky V, Adijanto J, Mootha VK, Hajnóczky G. 2013. MICU1 controls both the Threshold and Cooperative activation of the mitochondrial Ca^{2+} uniporter. *Cell Metabolism* **17**:976–987. doi: 10.1016/j.cmet.2013.04.020.
Csordás G, Renken C, Varnai P, Walter L, Weaver D, Buttle KF, Balla T, Mannella CA, Hajnoczky G. 2006. Structural and functional features and significance of the physical linkage between ER and mitochondria. *The Journal of Cell Biology* **174**:915–921. doi: 10.1083/jcb.200604016.
Csordas G, Varnai P, Golenar T, Roy S, Purkins G, Schneider TG, Balla T, Hajnoczky G. 2010. Imaging interorganelle contacts and local calcium dynamics at the ER-mitochondrial interface. *Molecular Cell* **39**:121–132. doi: 10.1016/j.molcel.2010.06.029.
De Stefani D, Raffaello A, Teardo E, Szabo I, Rizzuto R. 2011. A forty-kilodalton protein of the inner membrane is the mitochondrial calcium uniporter. *Nature* **476**:336–340. doi: 10.1038/nature10230.
Doenst T, Nguyen TD, Abel ED. 2013. Cardiac metabolism in heart failure: implications beyond ATP production. *Circulation Research* **113**:709–724. doi: 10.1161/CIRCRESAHA.113.300376.
Dorn GW II, Scorrano L. 2010. Two close, too close: sarcoplasmic reticulum-mitochondrial crosstalk and cardiomyocyte fate. *Circulation Research* **107**:689–699. doi: 10.1161/CIRCRESAHA.110.225714.
Drago I, De Stefani D, Rizzuto R, Pozzan T. 2012. Mitochondrial Ca2+ uptake contributes to buffering cytoplasmic Ca2+ peaks in cardiomyocytes. *Proceedings of the National Academy of Sciences of USA* **109**:12986–12991. doi: 10.1073/pnas.1210718109.
Ebert AM, Hume GL, Warren KS, Cook NP, Burns CG, Mohideen MA, Siegal G, Yelon D, Fishman MC, Garrity DM. 2005. Calcium extrusion is critical for cardiac morphogenesis and rhythm in embryonic zebrafish hearts. *Proceedings of the National Academy of Sciences of USA* **102**:17705–17710. doi: 10.1073/pnas.0502683102.
Esengil H, Chang V, Mich JK, Chen JK. 2007. Small-molecule regulation of zebrafish gene expression. *Nature Chemical Biology* **3**:154–155. doi: 10.1038/nchembio858.
Foley JE, Maeder ML, Pearlberg J, Joung JK, Peterson RT, Yeh JR. 2009a. Targeted mutagenesis in zebrafish using customized zinc-finger nucleases. *Nature Protocols* **4**:1855–1867. doi: 10.1038/nprot.2009.209.
Foley JE, Yeh JR, Maeder ML, Reyon D, Sander JD, Peterson RT, Joung JK. 2009b. Rapid mutation of endogenous zebrafish genes using zinc finger nucleases made by Oligomerized Pool ENgineering (OPEN). *PLOS ONE* **4**:e4348. doi: 10.1371/journal.pone.0004348.
García-Pérez C, Hajnóczky G, Csordás G. 2008. Physical coupling supports the local Ca2+ transfer between sarcoplasmic reticulum subdomains and the mitochondria in heart muscle. *The Journal of Biological Chemistry* **283**:32771–32780. doi: 10.1074/jbc.M803385200.
García-Pérez C, Schneider TG, Hajnoczky G, Csordas G. 2011. Alignment of sarcoplasmic reticulum-mitochondrial junctions with mitochondrial contact points. *American Journal of Physiology Heart and Circulatory Physiology* **301**:H1907–H1915. doi: 10.1152/ajpheart.00397.2011.
Greiser M, Lederer WJ, Schotten U. 2011. Alterations of atrial Ca(2+) handling as cause and consequence of atrial fibrillation. *Cardiovascular Research* **89**:722–733. doi: 10.1093/cvr/cvq389.
Hajnóczky G, Robb-Gaspers LD, Seitz MB, Thomas AP. 1995. Decoding of cytosolic calcium oscillations in the mitochondria. *Cell* **82**:415–424. doi: 10.1016/0092-8674(95)90430-1.
Hayashi T, Martone ME, Yu Z, Thor A, Doi M, Holst MJ, Ellisman MH, Hoshijima M. 2009. Three-dimensional electron microscopy reveals new details of membrane systems for Ca2+ signaling in the heart. *Journal of Cell Science* **122**:1005–1013. doi: 10.1242/jcs.028175.
Kasahara A, Cipolat S, Chen Y, Dorn GW II, Scorrano L. 2013. Mitochondrial fusion directs cardiomyocyte differentiation via calcineurin and Notch signaling. *Science* **342**:734–737. doi: 10.1126/science.1241359.
Kohlhaas M, Liu T, Knopp A, Zeller T, Ong MF, Bohm M, O'Rourke B, Maack C. 2010. Elevated cytosolic Na+ increases mitochondrial formation of reactive oxygen species in failing cardiac myocytes. *Circulation* **121**:1606–1613. doi: 10.1161/CIRCULATIONAHA.109.914911.
Kohlhaas M, Maack C. 2013. Calcium release microdomains and mitochondria. *Cardiovascular Research* **98**:259–268. doi: 10.1093/cvr/cvt032.

Kwan KM, Fujimoto E, Grabher C, Mangum BD, Hardy ME, Campbell DS, Parant JM, Yost HJ, Kanki JP, Chien CB. 2007. The Tol2kit: a multisite gateway-based construction kit for Tol2 transposon transgenesis constructs. *Developmental Dynamics* **236**:3088–3099. doi: 10.1002/dvdy.21343.

Langenbacher AD, Dong Y, Shu X, Choi J, Nicoll DA, Goldhaber JI, Philipson KD, Chen JN. 2005. Mutation in sodium-calcium exchanger 1 (NCX1) causes cardiac fibrillation in zebrafish. *Proceedings of the National Academy of Sciences of USA* **102**:17699–17704. doi: 10.1073/pnas.0502679102.

Luo M, Anderson ME. 2013. Mechanisms of altered Ca^{2+} handling in heart failure. *Circulation Research* **113**: 690–708. doi: 10.1161/CIRCRESAHA.113.301651.

Maack C, Cortassa S, Aon MA, Ganesan AN, Liu T, O'Rourke B. 2006. Elevated cytosolic Na+ decreases mitochondrial Ca2+ uptake during excitation-contraction coupling and impairs energetic adaptation in cardiac myocytes. *Circulation Research* **99**:172–182. doi: 10.1161/01.RES.0000232546.92777.05.

Mallilankaraman K, Doonan P, Cardenas C, Chandramoorthy HC, Muller M, Miller R, Hoffman NE, Gandhirajan RK, Molgo J, Birnbaum MJ, Rothberg BS, Mak DO, Foskett JK, Madesh M. 2012. MICU1 is an essential gatekeeper for MCU-mediated mitochondrial Ca(2+) uptake that regulates cell survival. *Cell* **151**:630–644. doi: 10.1016/j.cell.2012.10.011.

Milan DJ, Giokas AC, Serluca FC, Peterson RT, MacRae CA. 2006. Notch1b and neuregulin are required for specification of central cardiac conduction tissue. *Development* **133**:1125–1132. doi: 10.1242/dev.02279.

Min CK, Yeom DR, Lee KE, Kwon HK, Kang M, Kim YS, Park ZY, Jeon H, Kim do H. 2012. Coupling of ryanodine receptor 2 and voltage-dependent anion channel 2 is essential for Ca^{2+} transfer from the sarcoplasmic reticulum to the mitochondria in the heart. *The Biochemical Journal* **447**:371–379. doi: 10.1042/BJ20120705.

Nguyen CT, Qing L, Wang Y, Chen J-N. 2009. Zebrafish as a model for cardiovascular development and disease. *Drug Discovery Today Disease Models* **5**:135–140. doi: 10.1016/j.ddmod.2009.02.003.

Perocchi F, Gohil VM, Girgis HS, Bao XR, McCombs JE, Palmer AE, Mootha VK. 2010. MICU1 encodes a mitochondrial EF hand protein required for Ca(2+) uptake. *Nature* **467**:291–296. doi: 10.1038/nature09358.

Picht E, Zima AV, Blatter LA, Bers DM. 2007. SparkMaster: automated calcium spark analysis with ImageJ. *American Journal of Physiology Cell Physiology* **293**:C1073–C1081. doi: 10.1152/ajpcell.00586.2006.

Rapizzi E, Pinton P, Szabadkai G, Wieckowski MR, Vandecasteele G, Baird G, Tuft RA, Fogarty KE, Rizzuto R. 2002. Recombinant expression of the voltage-dependent anion channel enhances the transfer of Ca2+ microdomains to mitochondria. *The Journal of Cell Biology* **159**:613–624. doi: 10.1083/jcb.200205091.

Reuter H, Han T, Motter C, Philipson KD, Goldhaber JI. 2004. Mice overexpressing the cardiac sodium-calcium exchanger: defects in excitation-contraction coupling. *The Journal of Physiology* **554**:779–789. doi: 10.1113/jphysiol.2003.055046.

Rizzuto R, Bastianutto C, Brini M, Murgia M, Pozzan T. 1994. Mitochondrial Ca2+ homeostasis in intact cells. *The Journal of Cell Biology* **126**:1183–1194. doi: 10.1083/jcb.126.5.1183.

Rottbauer W, Baker K, Wo ZG, Mohideen MA, Cantiello HF, Fishman MC. 2001. Growth and function of the embryonic heart depend upon the cardiac-specific L-type calcium channel alpha1 subunit. *Developmental Cell* **1**:265–275. doi: 10.1016/S1534-5807(01)00023-5.

Roy SS, Ehrlich AM, Craigen WJ, Hajnoczky G. 2009a. VDAC2 is required for truncated BID-induced mitochondrial apoptosis by recruiting BAK to the mitochondria. *EMBO Reports* **10**:1341–1347. doi: 10.1038/embor.2009.219.

Roy SS, Madesh M, Davies E, Antonsson B, Danial N, Hajnoczky G. 2009b. Bad targets the permeability transition pore independent of Bax or Bak to switch between Ca2+-dependent cell survival and death. *Molecular Cell* **33**:377–388. doi: 10.1016/j.molcel.2009.01.018.

Rubinfeld B, Souza B, Albert I, Muller O, Chamberlain SH, Masiarz FR, Munemitsu S, Polakis P. 1993. Association of the APC gene product with beta-catenin. *Science* **262**:1731–1734. doi: 10.1126/science.8259518.

Seguchi H, Ritter M, Shizukuishi M, Ishida H, Chokoh G, Nakazawa H, Spitzer KW, Barry WH. 2005. Propagation of Ca2+ release in cardiac myocytes: role of mitochondria. *Cell Calcium* **38**:1–9. doi: 10.1016/j.ceca.2005.03.004.

Shindo A, Hara Y, Yamamoto TS, Ohkura M, Nakai J, Ueno N. 2010. Tissue-tissue interaction-triggered calcium elevation is required for cell polarization during Xenopus gastrulation. *PLOS ONE* **5**:e8897. doi: 10.1371/journal.pone.0008897.

Shoshan-Barmatz V, De Pinto V, Zweckstetter M, Raviv Z, Keinan N, Arbel N. 2010. VDAC, a multi-functional mitochondrial protein regulating cell life and death. *Molecular Aspects of Medicine* **31**:227–285. doi: 10.1016/j.mam.2010.03.002.

Shu X, Cheng K, Patel N, Chen F, Joseph E, Tsai HJ, Chen JN. 2003. Na,K-ATPase is essential for embryonic heart development in the zebrafish. *Development* **130**:6165–6173. doi: 10.1242/dev.00844.

Subedi KP, Kim JC, Kang M, Son MJ, Kim YS, Woo SH. 2011. Voltage-dependent anion channel 2 modulates resting Ca^{2+} sparks, but not action potential-induced Ca^{2+} signaling in cardiac myocytes. *Cell Calcium* **49**: 136–143. doi: 10.1016/j.ceca.2010.12.004.

Tan W, Colombini M. 2007. VDAC closure increases calcium ion flux. *Biochimica Et Biophysica Acta* **1768**: 2510–2515. doi: 10.1016/j.bbamem.2007.06.002.

Yano M, Yamamoto T, Kobayashi S, Ikeda Y, Matsuzaki M. 2008. Defective Ca2+ cycling as a key pathogenic mechanism of heart failure. *Circulation Journal* **72**:A22–A30. doi: 10.1253/circj.CJ-08-0070.

Appendix 2: Schredelseker, J. et al. (2014) High-Resolution Structure and Double Electron-Electron Resonance of the Zebrafish Voltage Dependent Anion Channel 2 Reveal an Oligomeric Population. *J. Biol. Chem.*

Schredelseker, J., Paz, A., López, C. J., Altenbach, C., Leung, C. S., Drexler, M. K., Chen, J.-N., Hubbell, W. L., and Abramson, J. (2014) High-Resolution Structure and Double Electron-Electron Resonance of the Zebrafish Voltage Dependent Anion Channel 2 Reveal an Oligomeric Population. *J. Biol. Chem.* 289, 12566–77

THE JOURNAL OF BIOLOGICAL CHEMISTRY VOL. 289, NO. 18, pp. 12566–12577, May 2, 2014

High Resolution Structure and Double Electron-Electron Resonance of the Zebrafish Voltage-dependent Anion Channel 2 Reveal an Oligomeric Population*

Received for publication, June 27, 2013, and in revised form, March 11, 2014 Published, JBC Papers in Press, March 13, 2014, DOI 10.1074/jbc.M113.497438

Johann Schredelseker[‡§¶1], Aviv Paz[§1], Carlos J. López[‖1], Christian Altenbach[‖], Calvin S. Leung[§], Maria K. Drexler[¶], Jau-Nian Chen[‡2], Wayne L. Hubbell[‖3], and Jeff Abramson[§4]**

*From the [‡]Department of Molecular, Cell and Developmental Biology, the [§]Department of Physiology, and the [¶]Walther Straub-Institut für Pharmakologie und Toxikologie, Ludwig-Maximilians-Universität München, Munich 80336, Germany, the [‖]Jules Stein Eye Institute and Department of Chemistry and Biochemistry, UCLA, Los Angeles, California 90095, and the **The Institute for Stem Cell Biology and Regenerative Medicine (inStem), National Centre for Biological Sciences-Tata Institute of Fundamental Research, GKVK Bellary Road, Bangalore-560065, Karnataka, India*

Background: Biochemical characterization of voltage-dependent anion channel 2 (VDAC2) is limited due to an inability to obtain functional protein.
Results: The crystal structure of VDAC2 suggests a dimer interface that is confirmed by double electron-electron resonance and cross-linking.
Conclusion: zfVDAC2 has a fractional dimeric population.
Significance: VDAC isoforms are structurally similar, but this study has identified a number of hot spots that require further exploration.

In recent years, there has been a vast increase in structural and functional understanding of VDAC1, but VDAC2 and -3 have been understudied despite having many unique phenotypes. One reason for the paucity of structural and biochemical characterization of the VDAC2 and -3 isoforms stems from the inability of obtaining purified, functional protein. Here we demonstrate the expression, isolation, and basic characterization of zebrafish VDAC2 (zfVDAC2). Further, we resolved the structure of zfVDAC2 at 2.8 Å resolution, revealing a crystallographic dimer. The dimer orientation was confirmed in solution by double electron-electron resonance spectroscopy and by cross-linking experiments disclosing a dimer population of ~20% in lauryldimethine amine oxide detergent micelles, whereas in lipidic bicelles a higher population of dimeric and higher order oligomers species were observed. The present study allows for a more accurate structural comparison between VDAC2 and its better-studied counterpart VDAC1.

Mitochondria are often depicted as the cell's "powerhouse" because they generate ATP from ADP and inorganic phosphate through the oxidative phosphorylation process. It is now firmly established that mitochondria have a far more expansive role in cellular function, including signaling, cell death/survival, and differentiation (1–3). As such, mitochondria are central to normal human physiology as well as disease. The most abundant proteins in the outer mitochondrial membrane, the voltage-dependent anion channels (VDACs),[5] are large pore-forming proteins that mediate the efficient exchange of metabolites and ions between the cytosol and the mitochondrial intermembrane space (IMS). In mammals, there are three VDAC isoforms (VDAC1–3), which have a high degree of sequence homology, yet their relative ratios and distribution between cell types are varied.

The sequence identity/similarity between human VDAC1 (hVDAC1), hVDAC2 and hVDAC3 is 75%/91% and 67%/85%, respectively (Fig. 1). Undoubtedly, VDAC1 is the best characterized isoform. After decades of struggle, three groups independently resolved the high resolution structure of VDAC1 (4–6). Using the lipidic bicelle crystallization technique (6–8), we solved a high resolution x-ray structure of mouse VDAC1 (mVDAC1) at a resolution of 2.3 Å. All reported high resolution structures of VDAC1 revealed a novel fold of a 19-stranded β-barrel with an N-terminal α-helix lying inside the pore. This helix is aligned nearly parallel to the membrane plane, causing a partial narrowing of the pore. Numerous studies have established the functional importance of the N-terminal α-helix in regulating the flux of metabolites through the channel (9, 10), and the observation that it is localized within the pore makes it

* This work was supported, in whole or in part, by National Institutes of Health Grants RO1 GM078844 (to J. A.) and 5R01 EY005216 (to C. J. L.). This work was also supported by Austrian Science Fund FWF Erwin-Schrödinger Fellowship J3065-B11 (to J. S.), Jules Stein Eye Institute Training Grant 2T32EY007026-36A1 (to C. J. L.), and the Jules Stein Professor Endowment (to W. L. H.).
This work is dedicated to the memory of Armand S. Vartanian, a colleague and friend.
The atomic coordinates and structure factors (code 4BUM) have been deposited in the Protein Data Bank (http://wwpdb.org/).
[1] These authors contributed equally to this work.
[2] To whom correspondence may be addressed. E-mail: chenjn@mcdb.ucla.edu.
[3] To whom correspondence may be addressed. E-mail: hubbellw@jsei.ucla.edu.
[4] To whom correspondence may be addressed. E-mail: jabramson@mednet.ucla.edu.

[5] The abbreviations used are: VDAC, voltage-dependent anion channel; hVDAC, zfVDAC, and mVDAC, human, zebrafish, and mouse VDAC, respectively; CHAPSO, 3-[(3-cholamidopropyl)dimethylammonio]-2-hydroxy-1-propanesulfonic acid; IMS, intermembrane space; DEER, double electron-electron resonance; LDAO, lauryldimethyl amine oxide; CW, continuous wave; DEF, dipolar evolution function.

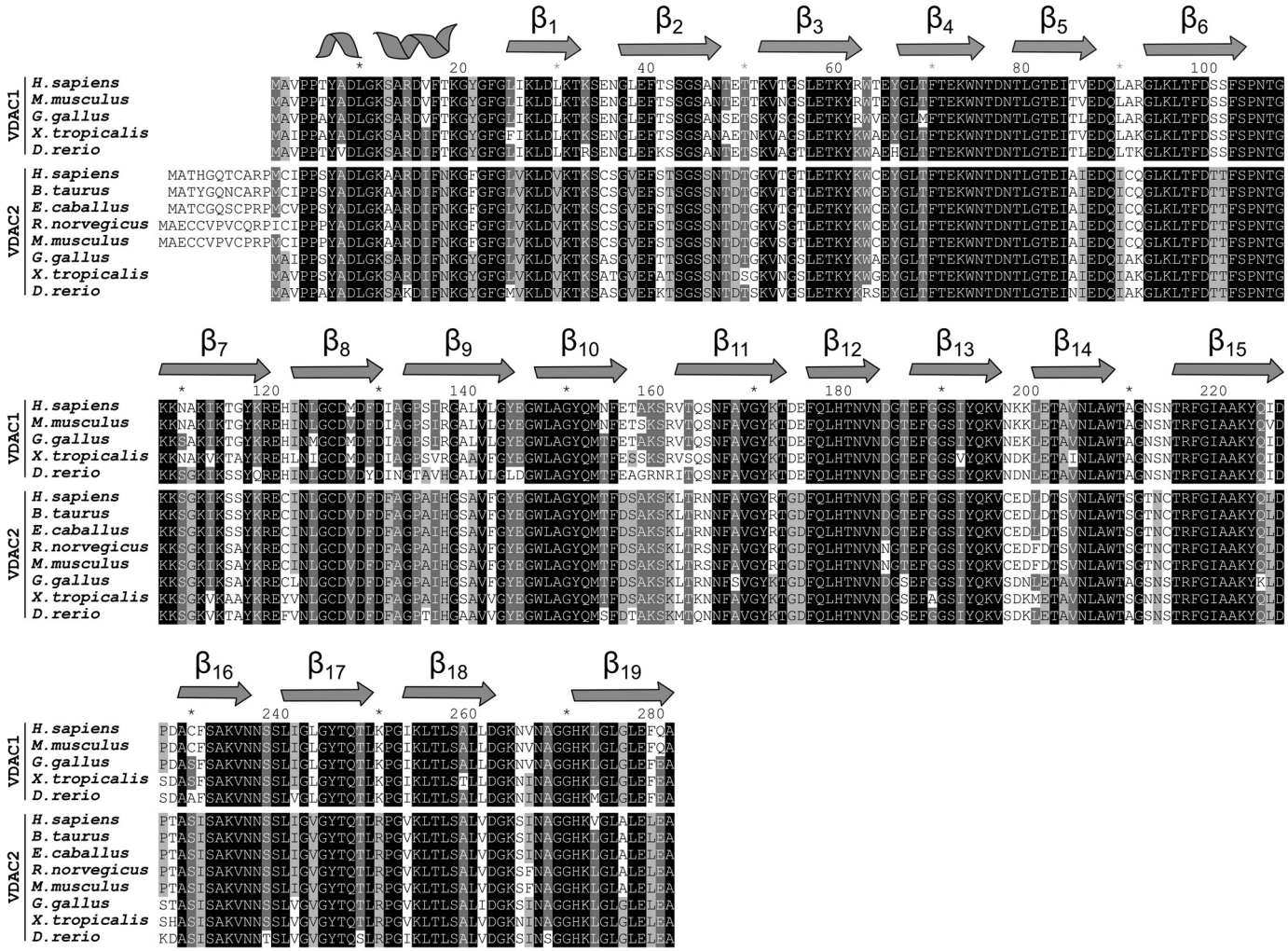

FIGURE 1. **Sequence alignment between VDAC1 and -2.** A select set of VDAC1 and -2 sequences are aligned. For reference, the secondary structure elements are represented as *two-dimensional schematics above* sequences.

ideally suited to regulate the passage of ions and metabolites through the pore. Based on molecular dynamics simulations and a series of cross-linking studies, the structure is believed to reside in the "open" conformation, facilitating the passage of ATP and other nucleotides (11, 12).

In contrast to VDAC1, structural and biochemical characterization of VDAC2 and -3 is rather limited, yet these isoforms have distinct physiological functions. In particular, VDAC2 null mice are embryonic lethal (13), whereas null mice of VDAC1 and -3 isoforms display mild phenotypes (14, 15). Furthermore, VDAC2 has been shown to interact and inhibit the proapoptotic protein BAK, thereby hampering mitochondrial apoptosis (13). In cardiomyocytes, VDAC2 specifically interacts with the ryanodine receptor and mediates Ca^{2+} transfer from the sarcoplasmic reticulum into mitochondria (16), implicating a role for VDAC2 in cardiac Ca^{2+} homeostasis. Additionally, the small quinazolinone agent erastin, an anti-tumor compound, interacts with VDAC2 to induce cell death in tumor cells expressing mutant RAS (17, 18). In total, there is significant evidence that despite the high sequence identity in this family, VDAC2 has a specific phenotype, which is distinct from those of the other two VDAC isoforms.

To gain insight into the structure and function of VDAC2, we expressed and purified zfVDAC2. The purified protein forms active channels in lipid planar bilayers, and we were able to determine the structure at 2.8 Å resolution. The overall structure is very similar to VDAC1, revealing a dimer interface between β17, β18, β19, β1, and β3. Using double electron-electron resonance (DEER) measurements and cross-linking experiments, we confirmed the dimer topology in solution and found a fractional dimer content of ~20% in detergent micelles and ~40% in lipidic bicelles.

EXPERIMENTAL PROCEDURES

Cloning of pQE60-zfVDAC2^{C127A} and Single-cysteine Mutants—The full-length zfVDAC2 ORF was purchased from Open Biosystems and PCR-amplified. PCR primers were used to add an NcoI site (5′) and a His_6 tag followed by a HindIII site (3′) for subsequent NcoI/HindIII cloning into the pQE60 expression plasmid. For DEER experiments, we created construct pQE60-zfVDAC2$^{C127A/S232C}$. Three individual PCRs were used to create three overlapping fragments of the zfVDAC2 ORF and to introduce the C127A and S232C mutations, respectively, by mutagenesis primers. Individual PCR fragments were fused by

splicing by overlap extension-PCR, and the resulting product was ligated into the pQE60 backbone using NcoI/HindIII. All PCR-amplified products were fidelity-checked by sequencing (Laragen, Inc., Culver City, CA).

To create single-Cys mutants for cross-linking experiments, the Cys-less backbone pQE60-zfVDAC2^{C127A} was created by fusion of base pairs 427–870 of the ORF from pQE60-zfVDAC2 into pQE60-zfVDAC2$^{C127A/S232C}$ using PstI and HindIII, thereby eliminating the S232C mutation. Single-cysteine mutants were subsequently generated in the pQE60-zfVDAC2^{C127A} backbone by mutagenesis PCR. For pQE60-zfVDAC2$^{C127A/V27C}$, pQE60-zfVDAC2$^{C127A/D50C}$, pQE60-zfVDAC2$^{C127A/S52C}$, and pQE60-zfVDAC2$^{C127A/T83C}$ mutation primers were used to introduce the respective mutations in two independent PCRs, which were then fused in a splice overlap extension PCR. Final PCR products were ligated into pQE60-zfVDAC2^{C127A} using XhoI and PstI. For pQE60-zfVDAC2$^{C127A/Q196C}$, pQE60-zfVDAC2$^{C127A/L251C}$, pQE60-zfVDAC2$^{C127A/I255C}$, and pQE60-zfVDAC2$^{C127A/I257C}$ mutagenesis PCR was performed as described above, but PCR products were ligated into pQE60-zfVDAC2^{C127A} using PstI and NheI. All PCR-amplified products were fidelity-checked by sequencing (Eurofins MWG Operon, Ebersberg, Germany).

Expression and Purification of zfVDAC2—Cloning, expression, and purification of zfVDAC2 followed the previously reported protocol for mVDAC1 (6). In short, M15 *Escherichia coli* cells carrying pQE60-zfVDAC2 were grown in Luria broth with agitation at 37 °C, induced at an OD of 1 with 0.4 mM isopropyl-1-thio-β-D-galactopyranoside and grown for an additional 4–5 h. Cells were harvested by centrifugation and resuspended in 50 mM Tris·HCl (pH 8.0), 2 mM EDTA, 20% sucrose. The cell slurry was lysed by consecutive incubation with 12.5 μg/ml lysozyme and 0.6% Triton X-100 followed by sonication. Inclusion bodies were obtained through centrifugation at 12,000 × *g* for 15 min, washed, and solubilized in 20 mM Tris·HCl (pH 8.0), 300 mM NaCl, 6 M guanidinium hydrochloride. zfVDAC2 protein was purified using a Talon metal affinity column and refolded in a three-step dialysis at 10 mg/ml. Dialysis buffers were as follows: 1) 20 mM Tris·HCl (pH 8.0), 300 mM NaCl, 1 mM DTT, 3 M guanidinium hydrochloride; 2) 20 mM Tris·HCl (pH 8.0), 300 mM NaCl, 1 mM DTT, 0.1% LDAO; and 3) 20 mM Tris·HCl (pH 8.0), 50 mM NaCl, 1 mM DTT, 0.1% LDAO. 2% LDAO was added to the protein solution prior to the second dialysis step. Refolded protein was concentrated, ultracentrifuged (355,000 × *g*, 30 min) to remove aggregated protein, and passed over a Superdex 200 column in 150 mM NaCl, 0.1% LDAO, 20 mM Tris·HCl (pH 8.0) to obtain a homogenous protein population (Fig. 2, *A* and *B*). For crystallization, fractions containing the non-aggregated zfVDAC2 peak were collected, concentrated, and buffer changed to 50 mM NaCl, 0.1% LDAO, 20 mM Tris·HCl (pH 8.0) using an Amicon Ultra-30k (Millipore) concentrator.

Crystallization—Crystals of ~0.6 × 0.2 × 0.1 mm were grown by the hanging drop vapor diffusion method using the Mosquito crystallization robot. A 12 mg/ml protein solution was mixed (1:1) with a well solution of 100 mM Tris·HCl (pH 8.0), 100 mM KCl, and PEG 2000 ranging between 19 and 24%. Subsequent optimization was performed by the addition of *n*-undecyl-β-D-thiomaltopyranoside at its critical micelle concentration (0.011%). Crystals were cryoprotected by transferring them for 10 s into a solution containing 100 mM Tris·HCl (pH 8.0), 100 mM KCl, 50% PEG 2000, 0.011% *n*-undecyl-β-D-thiomaltopyranoside prior to flash freezing in liquid nitrogen.

Lipid Planar Bilayer—Lipid bilayer experiments were performed as described previously (6). In brief, recordings were performed in diphytanoyl phosphatidylcholine bilayers across a 0.1-mm hole in 10 mM Tris·HCl (pH 7.4), 1 M KCl, 5 mM $CaCl_2$. After channel insertion, currents were recorded in response to test pulses between −50 and +50 mV. Total point histograms at each applied voltage were plotted to calculate the conductance (G) of open and closed states (Fig. 2*C*).

X-ray Data Collection and Processing—X-ray diffraction data were collected to 2.7 Å on flash-frozen crystals (−180 °C) at the Advanced Light Source (Berkeley, CA) (beam line 5.0.2). Indexing and integration were performed with XDS (19), using data up to 2.8 Å, and the space group was determined to be $P3_221$ with the following unit cell dimensions: $a = 72.47$ Å, $b = 72.47$ Å, and $c = 177.95$ Å ($\alpha = \beta = 90°$ and $\gamma = 120°$). One molecule is present per asymmetric unit with an estimated solvent content of 70.4% ($V_m = 4.15$ Å^3/Da) based on the Matthews probability calculator (20, 21). The structure was solved by molecular replacement using the murine VDAC1 coordinates (Protein Data Bank code 3EMN) as the search model in PHENIX (21). After generation of the initial model, it was manually rebuilt using Coot (22), followed by iterative rounds of refinement in PHENIX (21). The final model (Protein Data Bank code 4BUM) contained 283 amino acids, six water molecules, and one LDAO molecule with a final *R*-factor and *R*-free of 0.246 and 0.282, respectively. Data collection and refinement statistics are listed in Table 1. All figures containing structures were generated using PyMOL (23) or Chimera (24).

Spin Labeling, Continuous Wave (CW) EPR Spectroscopy, and DEER Experiments—For CW and DEER experiments, DTT was removed during the size exclusion chromatography step, and the protein was incubated with a 5-fold molar excess of 1-oxyl-2,2,5,5-tetramethylpyrroline-3-methyl methanethiosulfonate for 16 h at 4 °C to generate the R1 side chain (25). Excess spin label was removed by repeated washes using an Amicon Ultra-30k (Millipore) concentrator in 20 mM Tris·HCl (pH 8.0), 50 mM NaCl, 0.1% LDAO, 20% glycerol. For zfVDAC2$^{C127A/S232C}$, the fraction of spin-labeled protein was >98% as estimated from a 4,4′-dithiodipyridine titration for free thiol after the spin labeling reaction (26). A fraction of the spin-labeled zfVDAC2$^{C127A/S232C}$ was reconstituted in bicelles by mixing the protein with bicelles in a 4:1 ratio with a 35% (2.8:1) L-α-dimyristoylphosphatidylcholine/CHAPSO bicellar solution.

The CW EPR spectra of zfVDAC2 232R1 in LDAO and bicelles were recorded at room temperature on a Varian E-109 spectrometer fitted with a two-loop one-gap resonator; samples of 5 μl were contained in a borosilicate capillary tube (0.64-mm inner diameter × 0.84-mm outer diameter; VitroCom Inc.). For LDAO, a second spectrum was recorded with the sample containing 30% (w/w) sucrose solution. The spectra were recorded using 2-milliwatt microwave power and 1-G field modulation at 100 kHz.

Four-pulse DEER experiments (27) at Q band were conducted at 80 K on a Bruker ELEXSYS 580 spectrometer fitted with a Bruker EN5107D2 resonator. The protein concentration during the DEER experiments was maintained at or below 200 μM. 20 μl of spin-labeled protein reconstituted in LDAO or bicelles containing 20% (v/v) glycerol were loaded into a borosilicate capillary tube (1.4-mm inner diameter × 1.7-mm outer diameter; VitroCom) and subsequently flash-frozen in liquid nitrogen. A 36-ns π-pump pulse was set at the maximum absorption spectra, and the observer $\pi/2$ (16-ns) and π (32-ns) pulses were positioned 50 MHz (17.8 G) up-field. Distance distributions were obtained from the raw dipolar evolution time using the program LongDistances (available at the Hubbell Laboratory Web site). A dipolar evolution function (DEF) was obtained after applying an exponentially decaying background function (using a dimensionality of 3) to correct for random intermolecular dipolar interactions. The DEF was fit to obtain interspin distance distributions (Fig. 7, *B* and *C*).

In addition to the distribution of distances between interacting spins, the average number of interacting spins in a molecular entity, n_m, can be determined according to Equation 1 (28),

$$n_m = 1 + (\ln(1 - \Delta))/C \qquad \text{(Eq. 1)}$$

where Δ is the "depth of modulation" (shown in Fig. 7, *B* and *C*), and *C* is a constant that depends on the pump pulse profile, the resonator, and the spectral line shape of the nitroxide spin label (28). In the present experiments, *C* was determined using double cysteine mutants of T4 lysozyme (N68C/T109C and T109C/V131C) known to be quantitatively labeled with R1 as judged by determination of free thiols after the labeling reaction using a 4,4′-dithiodipyridine assay (26). From the depth of modulation and using $n_m = 2$, *C* is obtained from Equation 1; the values obtained from the two T4 lysozyme mutants agreed to within 1%. From the experimentally determined depth of modulation and *C*, the value of n_m for VDAC2 in LDAO or bicelles can be determined.

Cross-linking Experiments—Disulfide bonds between single-cysteine mutants were induced with the oxidizing reagent dichloro(1,10-phenanthroline)Cu(II). zfVDAC2 mutants were diluted to 15 μM in buffer containing 150 mM NaCl, 20 mM Tris·HCl (pH 8.0), 5 mM DTT, and 0.1% LDAO. The oxidizing reaction was performed with 5 mM dichloro(1,10-phenanthroline)Cu(II) at 4 °C for 2 min and subsequently quenched with 10 mM EDTA and 10 mM *N*-ethylmaleimide. The results were analyzed on 12% SDS-polyacrylamide gels stained with a Coomassie-based InstantBlue reagent (Expedeon).

RESULTS

Protein Purification and Lipid Bilayer Conductance—Native recombinant zfVDAC2 protein with a His tag fused to the C terminus was prepared using a two-step column purification that consisted of 1) solubilized inclusion bodies that were applied to a Talon metal affinity column and eluted with 150 mM imidazole and 2) concentrated protein that was refolded and applied to a Superdex 200 column to remove aggregation and obtain a homogenous protein population (Fig. 2, *A* and *B*). Purified zfVDAC2 protein was inserted in planar lipid bilayers,

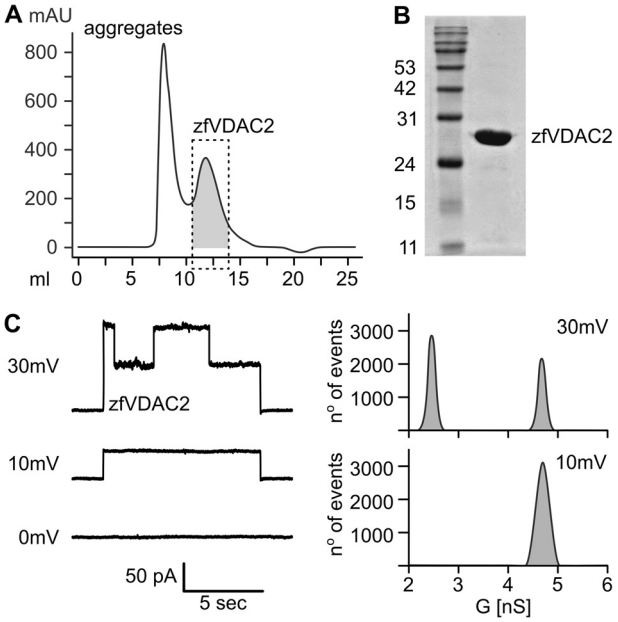

FIGURE 2. **Functional characterization of zfVDAC2.** *A*, size exclusion chromatography of zfVDAC2. The *dashed box* represents a non-aggregated homogenous population of protein used for further characterization. *B*, 12% SDS-polyacrylamide gel stained with Coomassie Brilliant Blue showing a pure sample of zfVDAC2. *C*, electrophysiology recordings of zfVDAC2 in diphytanoyl phosphatidylcholine bilayers in 10 mM Tris·HCl (pH 7.4), 1 M KCl, 5 mM $CaCl_2$. Total point histograms at each applied voltage were plotted to calculate the conductance (G) of the open and closed state. *mAU*, milliabsorbance units.

where it exhibited a single channel conductance of 4.2 ± 0.5 nanosiemens at 10 mV in 1 M KCl (open state; Fig. 2*C*). As the applied voltage was increased to ±30 mV, the channel presented distinct gating behavior between the open and closed states with a conductance of 1.7 ± 0.2 nanosiemens (Fig. 2*C*). This behavior is in good agreement with recordings from VDAC1 isolated from rats (29) and indicates that zfVDAC2, from our preparation, forms active channels. To further understand the functional aspects of ion and metabolite trafficking as well as the relation of zfVDAC2 to previously reported VDAC1, we pursued a high resolution structure of zfVDAC2.

Structural Overview—Optimized crystals of zfVDAC2 belong to the trigonal space group $P3_221$ with one molecule per asymmetric unit. The structure was determined by molecular replacement using the original mVDAC1 coordinates (Protein Data Bank code 3EMN) as a search model. The only part of the model that required manual rebuilding following the molecular replacement procedure was the loop between β-strands 1 and 2. The model was ultimately refined from merged data to a resolution of 2.8 Å with an *R*-free of 24.6% and an *R*-work of 28.2% (Table 1). 282 of the 283 amino acids of zfVDAC2 were assigned along with six water molecules and one copy of LDAO. Further details regarding the crystallization and structure determination can be found under "Experimental Procedures." A refined electron density map is shown in Fig. 3*C*.

The structure of zfVDAC2 is similar to that of mVDAC1 (Protein Data Bank code 3EMN), forming a β-barrel composed of 19 β-strands (Fig. 3). All of the strands exhibit an antiparallel pattern with the exception of strands 1 and 19, which associate in a parallel manner to seal the barrel. The maximal height and

width of the β-barrel are 35 and 40 Å, respectively. The correct orientation of the protein within the outer membrane of the mitochondria is still debated, with multiple studies producing conflicting results on the endogenous position of the N and C termini (30–32); however, a recent study has shown the C terminus to reside in the IMS (33). The N terminus of the protein forms a distorted α-helix that is aligned nearly parallel to the plane of the membrane, causing a partial narrowing of the pore (Fig. 3). The pore forms a large pathway that traverses the entire length of the protein. There have now been a number of studies confirming that this conformation probably resides in the "open" state of the channel (11, 12).

A structural alignment between the crystal structure of zfVDAC2 and mVDAC1 (Protein Data Bank code 3EMN) showed a root mean square deviation of 0.98 Å (Fig. 4*A*). The well aligned structures, including the N-terminal segment, indicate that these proteins share many similar properties and

TABLE 1
Crystallography statistics for zfVDAC2

Data collection	
Space group	$P3_221$
Cell dimensions	
a, *b*, *c* (Å)	72.47, 72.47, 177.95
α, β, γ (degrees)	90, 90, 120
Resolution (Å)	51.29–2.701
R_{sym} or R_{merge}	0.08 (0.76)[a]
$I/\sigma I$	12.99 (1.95)
Completeness (%)	97.98 (97.3)
Redundancy	3.5 (3.4)
Refinement	
Resolution (Å)	50–2.8
No. of reflections	53,149
R_{work}/R_{free}	24.55/28.22 (31.23/35.34)
No. of atoms	2151
Protein	2133
Ligand/ion	12
Water	6
B-Factors	
Protein	51.0
Ligand/ion	58.3
Water	24.4
Ramachandran favored (%)	94
Ramachandran outliers (%)	0.71
Root mean square deviations	
Bond lengths (Å)	0.004
Bond angles (degrees)	0.87

[a] Values in parentheses are for the highest resolution shell.

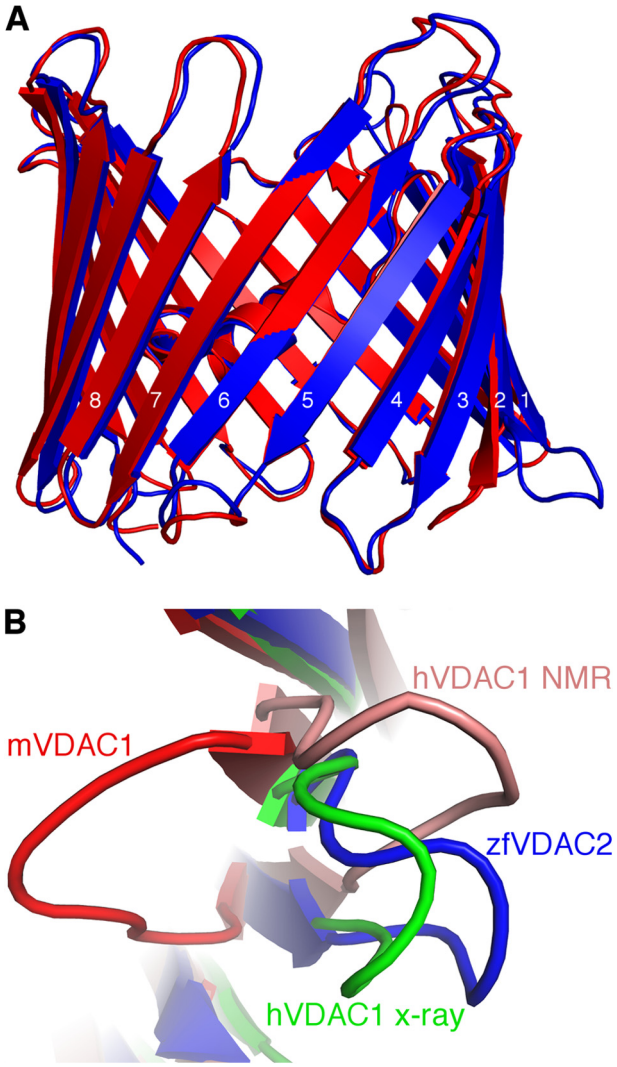

FIGURE 4. **Superposition of zfVDAC2 and VDAC1.** *A*, zfVDAC2 in *blue* and mVDAC1 (Protein Data Bank code 3EMN) in *red* were aligned with a C_α root mean square deviation of 0.98 Å. There is a large displacement (~12 Å) in the loop between β-strands 1 and 2. *B*, an IMS view of the loop between β-strands 1 and 2, including zfVDAC2 in *blue*, mVDAC1 in *red*, hVDAC1 (Protein Data Bank code 2JK4) in *green*, and a representative NMR conformer of hVDAC1 (Protein Data Bank code 2K4T) in *salmon*.

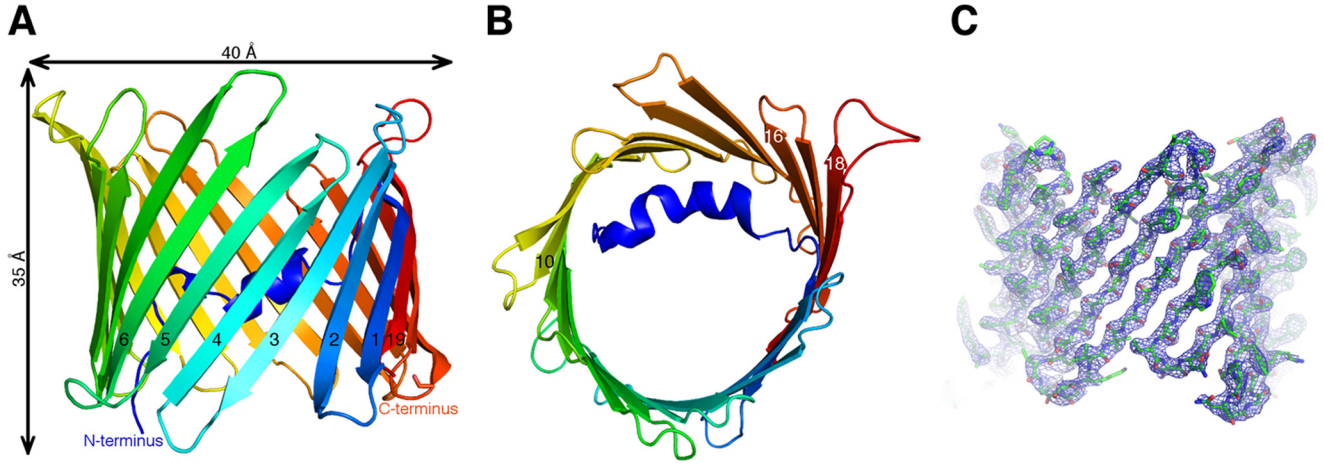

FIGURE 3. **Overall structure of zfVDAC2.** Shown are *cartoon representations* of zfVDAC2 viewed perpendicular to the membrane plane (*A*) and in the membrane plane (*B*). The protein backbone is *rainbow-colored* from the N terminus (*blue*) to the C terminus (*red*). A $2F_o - F_c$ map contoured at 1.5σ is displayed in a *blue wire frame* with the zfVDAC2 model shown in *sticks* (*C*).

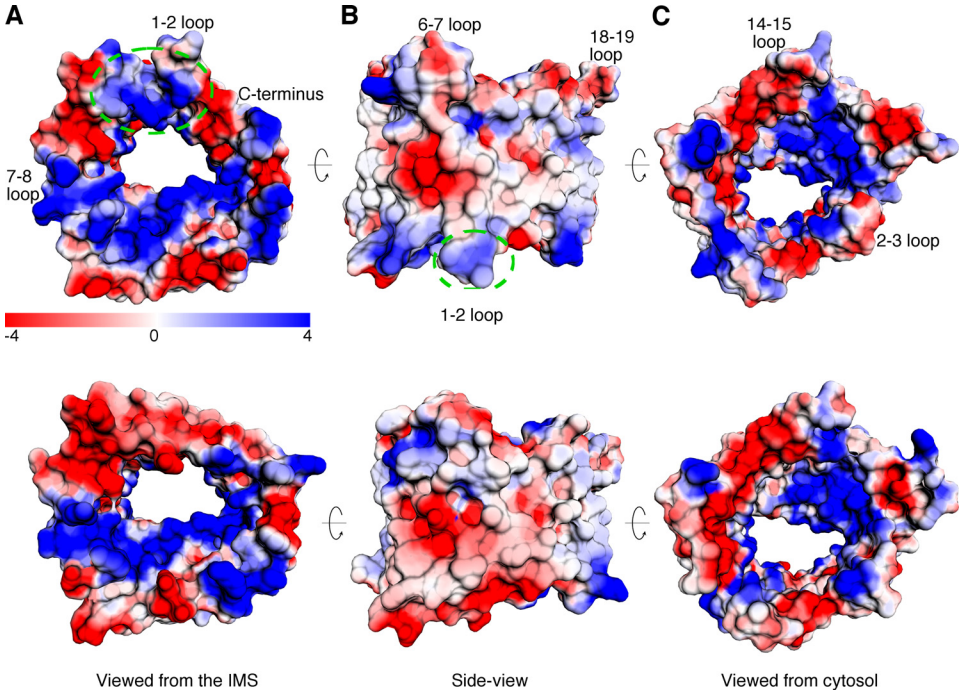

FIGURE 5. **Electrostatic potentials of zfVDAC2 and mVDAC1.** Electrostatic potentials for zfVDAC2 (*top row*) and mVDAC1 (*bottom row*) are shown. *A*, a view from the IMS. There is an elongated electronegative patch extending from the C terminus of mVDAC1 through the loops of β-strands 1–6, which is interrupted by positive charges in zfVDAC2 (*dashed green circle*). *B*, a side view. *C*, a view from the cytosolic side.

functions. The sole exception is a large displacement (~12 Å) of the loop between strands 1 and 2 (Fig. 4*B*). Further comparison using Columbic electrostatic calculations (Fig. 5) revealed a continuous electronegative patch on the cytosolic lip of mVDAC1 extending from the C terminus of the protein (β19) and within the loops connecting β1 to β2, β3 to β4, and β5 to β6. In zfVDAC2, the loop connecting β1 to β2 is electropositive, disrupting the electronegative continuity. In addition, there are a number of other subtle differences. Residues 61–65 in β-strand 3 contain four positive residues in zfVDAC2 (KYKRS) as opposed to two positive residues in mVDAC1 (KYRWT); residues 280–282, at the C terminus of the protein, contain two negative residues in zfVDAC2 (Glu-Leu-Glu) as opposed to one in mVDAC1 (Glu-Phe-Gln); and Glu-36, which resides in mVDAC1 in the mobile loop connecting β-strands 1 and 2, is substituted to an Ala in zfVDAC2. Additional hydrophobicity analysis did not show any significant difference between the two isoforms.

Dimer Interface—The oligomeric organization of VDAC has been strongly correlated with its physiological function. Numerous studies have demonstrated that VDAC can achieve a number of oligomeric populations, depending on the cell's environment, including monomers, dimers, trimers, tetramers, hexamers, and even higher order oligomers (34). More recently, this arrangement has been shown to be dynamic and further influenced by the lipidic environment (35). As was done with hVDAC1 (5), a zfVDAC2 dimer was constructed using crystal symmetry operators. zfVDAC2 forms crystals of a space symmetry group $P3_221$, which leads to three distinct zfVDAC2 symmetry-related interfaces. The most extensive surface, with a buried surface area of 554 $Å^2$ and a solvation free energy gain of $\Delta G = -14.9$ kcal/mol, is formed by buried hydrophobic residues in strands β17 (Arg-252 and Leu-251), β18 (Leu-259, Leu-257, and Ile-255), β19 (Leu-281, Leu-279, Leu-277, and Leu-275), β1 (Val-31, Leu-29, and Val-27), and β3 (Val-54, Ser-52, Asp-50, Thr-49, and Ser-47) (Fig. 6).

To confirm the dimer interface of zfVDAC2 in solution *and* the relative abundance of zfVDAC2 oligomers, we generated a cysteine-less construct by replacing the endogenous cysteine residue with alanine (C127A) and subsequently engineered a cysteine at position 232, which is the N-terminal residue of β16. This mutant was then spin-labeled with 1-oxyl-2,2,5,5-tetramethylpyrroline-3-methyl methanethiosulfonate reagent to generate an R1 side chain, and the interspin distance distribution was measured using DEER spectroscopy in LDAO and in lipidic bicelles. The DEER experiment measures the dipolar interaction between unpaired electrons in the range of 17–70 Å (27) and thus can be used to detect the presence of homodimers or higher oligomers in a solution of singly labeled proteins. Residue 232 was selected for this study because modeling of the R1 side chain at site 232 in the crystallographic dimer shown in Fig. 6 suggests a distance between R1 labels of ~31 Å (Fig. 7*A*), which is well within the range of interspin distance that can be reliably measured with DEER spectroscopy.

In the DEER experiment, magnetic interactions between randomly distributed spins in different molecular entities give rise to an exponentially decaying "background" signal (*red traces* in the *left-hand panels* of Fig. 7, *B* and *C*). The experimental DEER signals (*black* and *cyan traces* in the *left-hand panels* of Fig. 7, *B* and *C*) deviate from the background at short evolution times, unequivocally demonstrating the presence of specific oligomers in solutions of both LDAO and bicelles. Removal of the background signal from the raw data gives the corresponding DEFs (*right-hand panels* of Fig. 7, *B* and *C*),

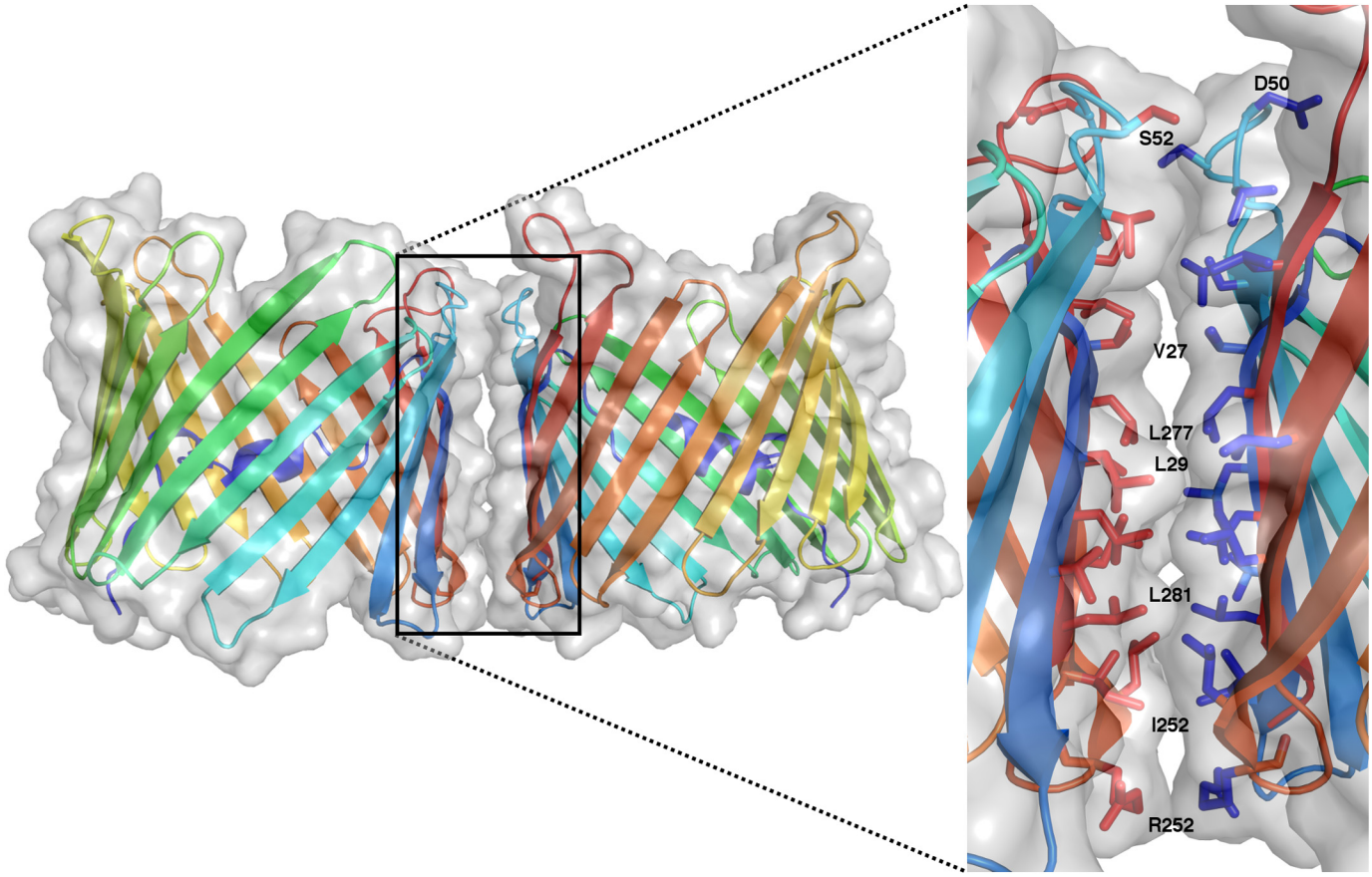

FIGURE 6. **zfVDAC2 dimer.** A symmetry-related dimer of zfVDAC2 is presented in a *transparent space-filling model on top of* a *cartoon representation* (same *coloring* as in Fig. 3). The *expanded view* shows the interaction site composed of residues from strands 1, 3, and 17–19 presented in *stick representations*.

which can be fit to obtain a probability distribution of interspin distances (Fig. 7*D*). In LDAO, the distance distribution is broad with a full width at half-height of nearly 20 Å, which exceeds the width anticipated from a distribution of R1 rotamers (34) and suggests flexibility in the region of β16. The broad distribution may also arise from heterogeneity regarding the relative orientation of each molecule in the dimer. However, some of the local maxima in the broad distribution could arise from distinct rotamers of R1. The median of the distribution is 30.5 Å, close to that determined from modeling of R1 in the crystallographic dimer.

In bicelles, the median of the distribution is 32.4 Å (the most probable distance is 30.3), again close to that expected from the crystallographic dimer. However, there is a small population near 55 Å (*arrow* in Fig. 7*D*). The shape of the distribution is not well determined due to the limited data collection time of 2.5 μs, but a detectable population at long distance is required to fit the data. A distance in this range cannot correspond to any possible homodimer but must originate from higher order oligomers.

The depth of modulation of the DEF (Δ; Fig. 7, *B* and *C*) is <4% for VDAC2 232R1 in either LDAO or bicelles, compared with ~10% for the doubly labeled T4 lysozyme pairs used for determination of the constant *C* under identical conditions (see "Experimental Procedures"). The low depth of modulation could be due to incomplete labeling of the protein and/or due to a small fraction of protein in oligomeric form (28). Because labeling was found to be quantitative (see "Experimental Procedures"), it is concluded that only a small fraction of the protein exists in oligomeric form, consistent with recent spectroscopy studies on hVDAC1 (35).

The distance distribution for 232R1 in LDAO clearly supports the formation of a homodimer. Within the context of this model, the fraction of VDAC2 in dimer form, f_d, can be estimated from the modulation depth of the DEER signal according to Refs. 24 and 25 ($f_d = n - 1 = \ln(1 - \Delta)/C$, which gives ~18%.

The depth of modulation for VDAC2 232R1 in bicelles is larger than for the protein in LDAO (compare delta values in *panels B* and *C* of Fig. 7), which indicates a higher fraction of total oligomeric species (~40%). The larger depth of modulation arises due to the existence of higher order oligomers (indicated by the 55 Å population in the distance distribution) and possibly a larger value for fd. An increase in the oligomeric population in bicelles compared with LDAO micelles is in agreement with previous studies, which reported that the percentage of dimer is influenced by detergent or lipidic environments (35).

To obtain information on the relative mobility of the 232R1 side chain in LDAO and bicelles, CW EPR spectra were recorded for the protein in the two environments. In both cases, the spectra show a dominant component reflecting restricted mobility of the R1 side chain (Fig. 7*E*, *top spectra*, *i*), and a second component reflecting higher mobility (*m*). The two spectral components can arise from slow exchange (microsec-

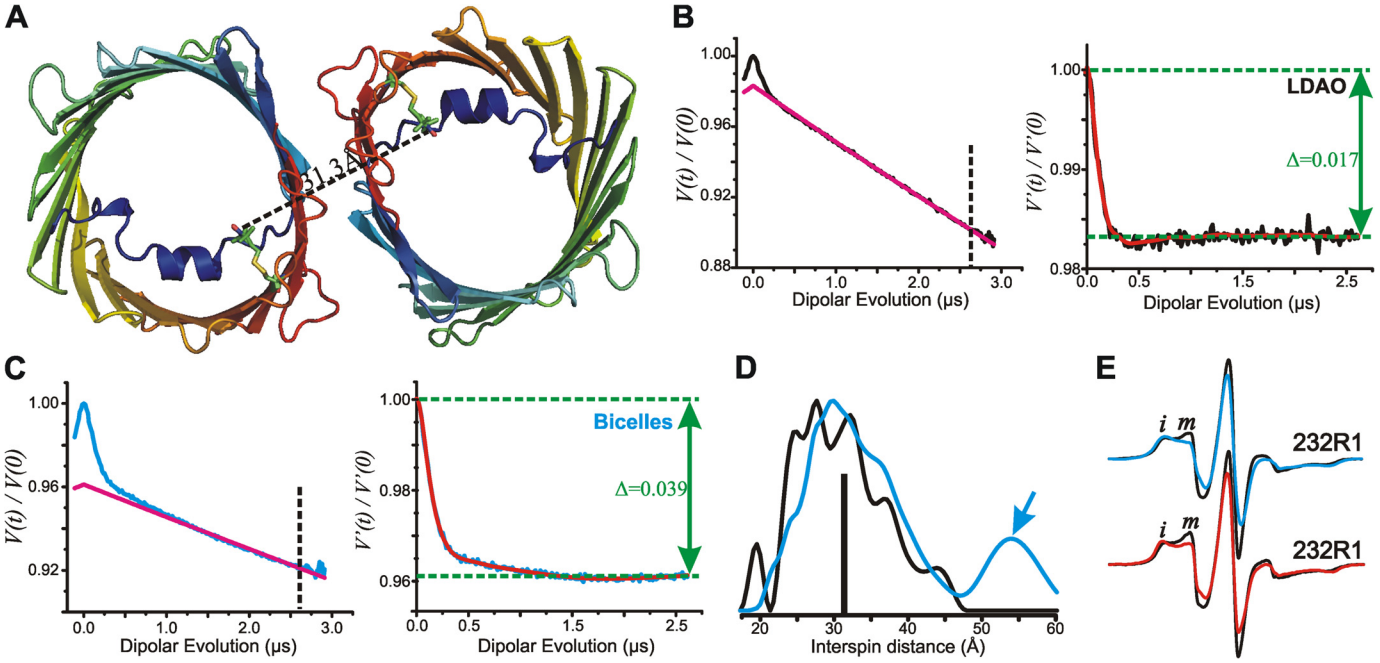

FIGURE 7. **Interspin distance measurements of zfVDAC2 232R1.** *A*, *cartoon representation* of zfVDAC2 232R1 showing the expected distance based on modeling of R1 on the zfVDAC2 structure. Models of the R1 side chain at site 232 are shown as *stick representations*. The *black dashed line* shows the expected interspin distance in the crystallographic dimer. *B*, *left*, raw data (*black*) and exponentially decaying background signal (*magenta*) arising from random intermolecular distances in LDAO. For analysis, the raw data were truncated beyond 2.6 μs (*vertical dashed line*) to suppress the artifact caused by pulse overlap. *Right*, background-corrected DEF of zfVDAC2 232R1 reconstituted in LDAO. The fit of the DEF is shown in *red*. Δ, "depth of modulation" see "Experimental Procedures." *C*, *left*, raw data (*cyan*) and exponentially decaying background signal (*magenta*) of DEER data in bicelles. The raw data were truncated beyond 2.6 μs (*vertical dashed line*) to suppress artifact. *Right*, background-corrected DEF of zfVDAC2 232R1 reconstituted in bicelles. *D*, distance distributions of zfVDAC2 232R1 reconstituted in LDAO and bicelles are shown in *black* and *cyan*, respectively. The *vertical black bar* indicates the expected distance from modeling the R1 side chain at site 232 shown in *A*. *E*, *top spectra*, EPR signals of 232R1 in LDAO (*black*) and bicelles (*cyan*). *Bottom spectra*, EPR spectra of osmolyte perturbations for residue 232R1 in LDAO recorded in buffer (*black*) and in buffer containing 30% sucrose (*red*). Spectral intensities corresponding to relatively immobile (*i*) and mobile states (*m*) of R1 are indicated.

ond to millisecond time scale) between protein conformational substates or from rotameric equilibria of R1 (36). It has been shown that stabilizing osmolytes, such as sucrose, shift protein conformational equilibria but have little effect on rotameric equilibria of R1. For 232R1, the addition of sucrose shifts the relative population toward the more immobilized state, suggesting that the two components arise from slow (microsecond to millisecond) exchange between conformational substates differing in structure at, or in the vicinity of, the N-terminal region of β16 (Fig. 7*E*, *bottom spectra*).

To further validate the data obtained by DEER, we employed cross-linking experiments of single-cysteine mutants in an effort to better define the dimer interface in solution. We generated three cysteine mutants that were part of the putative dimer interface close to the cytoplasmic side of VDAC at positions Val-27, Asp-50, and Ser-52 and another set of three mutants close to the IMS at positions Leu-251, Ile-255, and Leu-257 (Figs. 6 and 8). These mutants were designed in loop regions and on β-strands at S–S distance ranges of 3.7–11.1 Å. In addition, two cysteine mutants were generated at sites that should reside outside of the putative dimer interface at positions Thr-83 and Gln-196 (Fig. 8*A*). Upon the addition of dichloro(1,10-phenanthroline)Cu(II), significant cross-linking was observed at all six sites that are part of the putative dimer interface (Fig. 8, *B* and *C*), indicative of disulfide formation between monomeric proteins as opposed to the control sites that did not display appreciable cross-linking (Fig. 8*D*).

DISCUSSION

In recent years, there has been a vast increase in structural and functional understanding of VDAC1, but VDAC2 and -3 have been understudied. zfVDAC2 is a good structural model for mammalian VDAC2 due to a high degree of sequence homology (*e.g.* 83.0% identity and 93.0% similarity) between zfVDAC2 and hVDAC2 with no sequence gaps (Fig. 1 shows a zfVDAC2 alignment against selected mammalian VDAC sequences). Most of the minor sequence differences reside in the exposed loop regions where the transmembrane segments remain conserved (Fig. 9, *top row*). Interestingly, mammalian VDAC2s have a small 11-amino acid N-terminal extension that is not present in zfVDAC2. However, this N-terminal extension was shown not to be essential in mediating VDAC2-specific properties of the channel, such as tBid-induced cytochrome *c* release (37). Most of these minor sequence differences reside in the exposed loop regions where the transmembrane segments remain conserved (Fig. 9, *top row*). In total, zfVDAC is a good model for mammalian VDAC2.

VDAC2 has a number of unique and specific protein-interacting partners, including the proapoptotic protein BAK (13), the ryanodine receptor (16), and erastin and tubulin (38). A logical assumption is that these specific interactions would be governed by structural differences. However, a structural comparison between VDAC1 and -2 reveals few differences on a positional (Fig. 9, *bottom row*) or electrostatic basis (Fig. 5). The

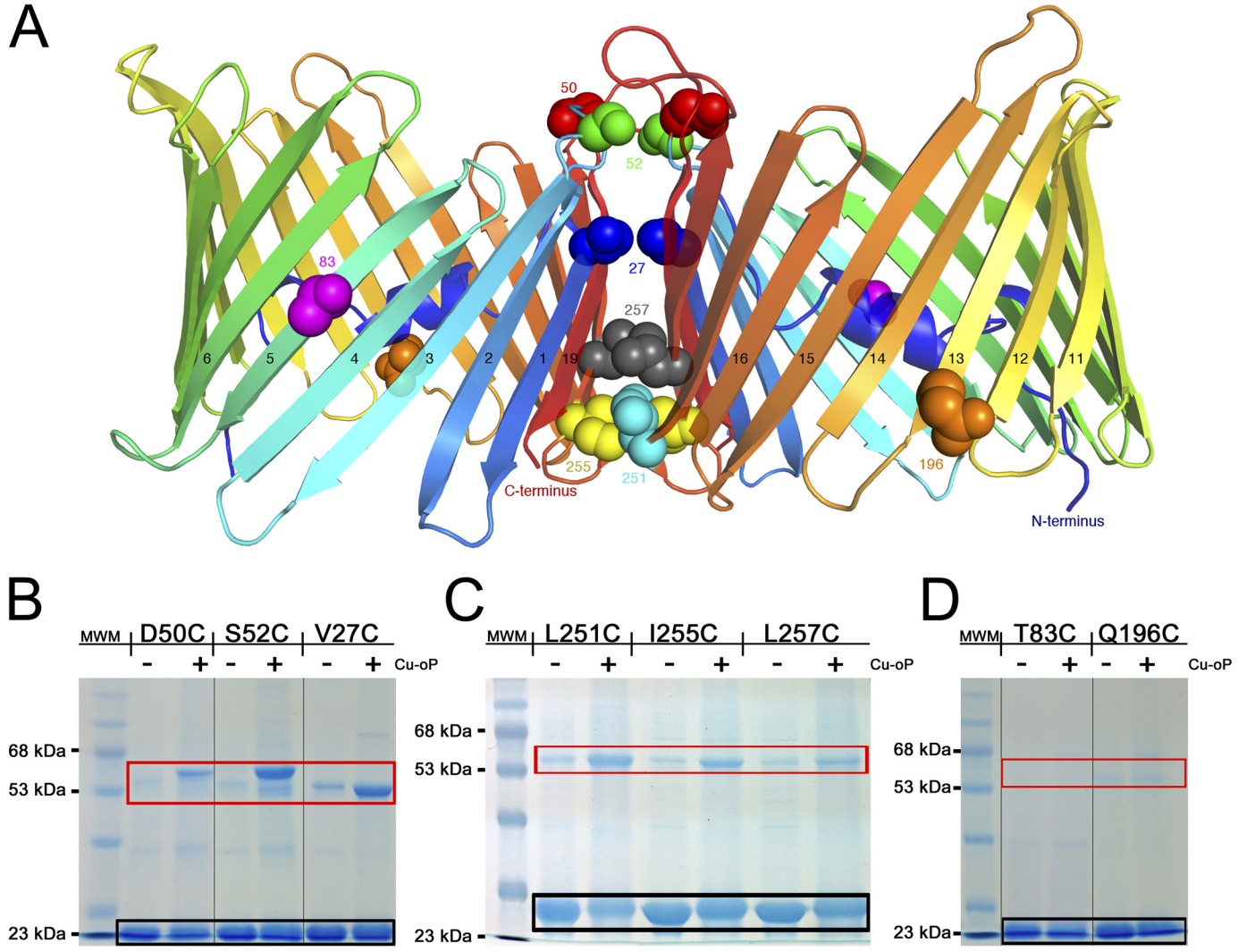

FIGURE 8. **Cross-linking experiments validate the dimer interface.** *A*, *cartoon representation* of the zfVDAC2 putative dimer with sites of cysteine mutations displayed in *spheres*, *differently colored* by position. *B*, 12% SDS-PAGE for zfVDAC2 single-cysteine mutants close to the cytosolic side. *C*, 12% SDS-PAGE for zfVDAC2 single-cysteine mutants close to the IMS. *D*, 12% SDS-PAGE of non-cross-linking single-cysteine mutants at positions outside of the putative dimer interface. *Black box*, monomeric zfVDAC2; *red box*, dimeric forms. *MWM*, molecular weight markers. Cu-oP, dichloro(1,10-phenanthroline)Cu(II) Groupings of images from different parts of the same gels are marked by *vertical lines*.

sole exceptions are large displacements of the loop between strands 1 and 2 (amino acid sequence 32–40) and the loop connecting β-strand 5 and β-strand 6 (amino acid sequence 88–95) as well as a change in the electrostatic properties on the cytosolic lip of VDAC. Indeed, differences between VDAC1 and VDAC2 accounting for the VDAC2-specific tBid-induced cytochrome *c* release were previously mapped to the N-terminal two-thirds, namely amino acids 13–188 (39). The loop connecting β-strand 1 and β-strand 2 is extended 12 Å away from the pore in the zfVDAC2 structure as compared with mVDAC1 (Protein Data Bank code 3EMN). In the hVDAC1 x-ray structure (Protein Data Bank code 2JK4), this loop occupies a position quite similar to that in the zfVDAC2, and the NMR structure of hVDAC1 has this loop even farther away from the mVDAC1 position (Fig. 4*B*). Interestingly, there is an amino acid divergence at position 36 located at the apex of this mobile loop. For VDAC1, there is a highly conserved Glu, but in VDAC2 the residue is primarily an Ala or a Cys. To date, this residue, as far as we know, has not been subjected to functional analysis.

The loop connecting β-strands 5 and 6 in the human x-ray structure is located ~13 Å internally from the position in mVDAC1 and zfVDAC2 x-ray structures. In the NMR model, this loop resides in the middle of these two positions. In the case of zfVDAC2, this loop is pushed away due to the presence of a symmetry-related molecule.

It would seem that loop displacements between β-strands 1 and 2 and β-strands 5 and 6, as observed here, would not suffice to explain the vast phenotypic differences between isoforms. However, the dynamic and electrostatic properties of these loops could play a key role in establishing protein-protein interactions and generate protein complexes or modulate gating properties and thus alter the function of VDACs. Indeed, binding of partner proteins was shown to vary substantially between VDAC isoforms, with compelling evidence that VDAC2 has a greater repertoire of binding partners (40–42).

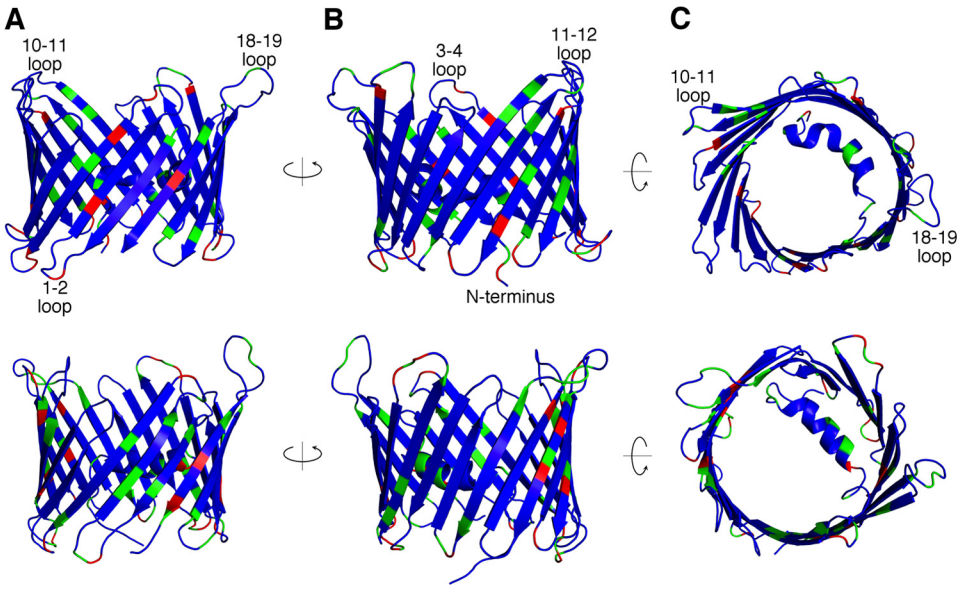

FIGURE 9. **Mapping the sequence diversity in VDAC isoforms.** The sequence diversity between zfVDAC2 and hVDAC2 (*top row*) is shown utilizing a *cartoon representation* of the zfVDAC2 structure and the sequence diversity between hVDAC1 and hVDAC2 (*bottom row*) is shown utilizing a schematic representation of the hVDAC1 structure. The views displayed from *left* to *right* are a side view (*A*), a 180° rotated side view (*B*), and a cytosolic view (*C*). *Blue*, sequence identity; *green*, sequence similarity; *red*, unconserved sequence substitutions.

Another aspect of VDAC physiology that has major implications, in particular for apoptotic events, is the protein's oligomeric state. Current research has strongly implicated a dimeric organization of hVDAC1 by analysis of crystal packing (5, 7), chemical cross-linking (43), and fluorescence cross-correlation spectroscopy (35). However, these studies have been lacking for VDAC2.

Using crystallographic symmetry operators, we identified a parallel dimer interface for zfVDAC2 that is virtually identical to the one suggested for hVDAC1 with a buried surface area of 554 Å^2. The interface is formed by strands β17, β18, β19, β1, and β3 (Figs. 6 and 8). Here we show that ~18% of the protein exists in a dimeric form in solution, as demonstrated by DEER spectroscopy for a singly R1-labeled mutant of zfVDAC2 reconstituted in LDAO; similar dimers exist in bicelles, apparently along with higher order oligomers (Fig. 7*B*). Remarkably, previous fluorescence cross-correlation spectroscopy studies done by Betaneli *et al.* (35) on hVDAC1 reconstituted in giant unilamellar vesicles showed a ~15% dimer population, comparable with that observed here for zfVDAC2 in LDAO.

The interspin distance distributions centered on ~30 Å observed in DEER are consistent with the interspin distance expected from modeling of the R1 side chain in the x-ray structure presented here, but the broad distributions indicate significant protein flexibility. The main probability distributions for VDAC2 232R1 in LDAO and bicelles are similar but not identical, showing that the structure of the dimer in both environments is similar.

The 55 Å population for the protein in bicelles, but not in LDAO detergent micelles, cannot arise from a homodimer. A possible oligomeric configuration could be drawn from crystal packing analysis of mVDAC1 crystals originating in bicelles (7). This structure reveals a more elaborate hexameric arrangement mimicking the native oligomeric packing observed in EM (44) and atomic force microscopy (45) images of the outer mitochondria membrane. Intramolecular distances between side chain 232R1 in this hexamer identify a likely origin for both the ~30 Å and 55 Å populations (Fig. 10).

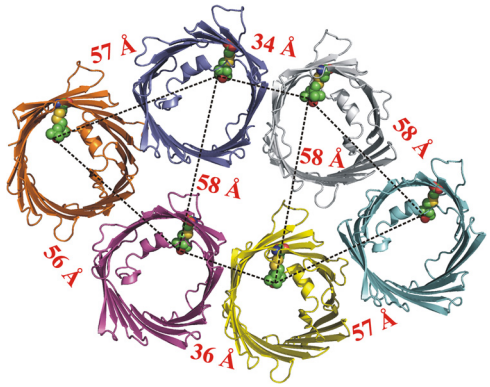

FIGURE 10. **Interspin distances of mVDAC1 hexamer at position 232.** A *cartoon representation* of mVDAC1 232R1 shows the expected distances based on modeling of R1 on the mVDAC1 structure. Models of the R1 side chain at site 232 are shown in *spherical representations*. The *black dashed line* shows the expected interspin distance in the crystallographic hexamer. Interspin distances of >70 Å are outside the range that can be reliably determined with the DEER data recorded in this study and thus are not shown.

Comparison of the CW EPR spectra of residue 232R1 in LDAO and bicelles shows an increase in the relative population of a more mobile state in LDAO (Fig. 7*C*), and osmolyte perturbation indicates that the two-component spectra probably arise from multiple conformational substates in equilibrium. Thus, the small differences that do exist in the distance distributions for LDAO and bicelles may be due to differences in conformational flexibility of the protein at or near residue 232R1.

The cross-linking experiments strongly support the validity of the suggested dimer interface in zfVDAC2. The two cysteine mutants designed outside of the dimer interface displayed no cross-linking, whereas mutants in the dimer interface displayed distinct levels of cross-linking. The highest levels of cross-link-

ing were observed for mutants in long flexible loop regions (D50C with S–S located 11.1 Å apart and S52C with an S–S distance of 6.8 Å and for an internal mutant located in the cytosolic side of β1 (V27C), which is the closest cysteine mutant in this set of cross-linking experiments (S–S distance of only 3.7 Å). The other three mutants on the mitochondrial IMS side that displayed lower cross-linking efficiencies were designed in rigid β-strands or just at the interface between short loops and β17 and β18 situated at relatively long S-S distance ranges of 6.4–8.9 Å.

Although the present study advances our structural understanding in the VDAC field, in particular VDAC2, there are still many unanswered questions that will need to be addressed. Perhaps the varied phenotype is not purely structural but depends on different affinities to partner proteins, expression patterns, subcellular localization of the distinct isoforms, or differences in the intrinsic flexibility of functionally important structural elements between the different isoforms. There is plenty of evidence for different physiological roles of the three isoforms, but the search for the underlying mechanisms has to be further explored. The structural characterization of VDAC2, however, provides blueprints to test many hypotheses and identifies a loop between strands 1 and 2 as a plausible dynamic structural element, as judged by changes in its relative position in structures of different VDAC isoforms, and identifies an area with a change in the electrostatic surface potential between zfVDAC2 and mVDAC1.

Acknowledgments—We thank Armand S. Vartanian and Vinod Nayak for fruitful discussions.

REFERENCES

1. Colombini, M., Blachly-Dyson, E., and Forte, M. (1996) VDAC, a channel in the outer mitochondrial membrane. *Ion Channels* **4,** 169–202
2. Rostovtseva, T. K., Sheldon, K. L., Hassanzadeh, E., Monge, C., Saks, V., Bezrukov, S. M., and Sackett, D. L. (2008) Tubulin binding blocks mitochondrial voltage-dependent anion channel and regulates respiration. *Proc. Natl. Acad. Sci. U.S.A.* **105,** 18746–18751
3. Colombini, M. (2004) VDAC: the channel at the interface between mitochondria and the cytosol. *Mol. Cell Biochem.* **256,** 107–115
4. Hiller, S., Garces, R. G., Malia, T. J., Orekhov, V. Y., Colombini, M., and Wagner, G. (2008) Solution structure of the integral human membrane protein VDAC-1 in detergent micelles. *Science* **321,** 1206–1210
5. Bayrhuber, M., Meins, T., Habeck, M., Becker, S., Giller, K., Villinger, S., Vonrhein, C., Griesinger, C., Zweckstetter, M., and Zeth, K. (2008) Structure of the human voltage-dependent anion channel. *Proc. Natl. Acad. Sci. U.S.A.* **105,** 15370–15375
6. Ujwal, R., Cascio, D., Colletier, J. P., Faham, S., Zhang, J., Toro, L., Ping, P., and Abramson, J. (2008) The crystal structure of mouse VDAC1 at 2.3 Å resolution reveals mechanistic insights into metabolite gating. *Proc. Natl. Acad. Sci. U.S.A.* **105,** 17742–17747
7. Ujwal, R., Cascio, D., Chaptal, V., Ping, P., and Abramson, J. (2009) Crystal packing analysis of murine VDAC1 crystals in a lipidic environment reveals novel insights on oligomerization and orientation. *Channels* **3,** 167–170
8. Ujwal, R., and Abramson, J. (2012) High-throughput crystallization of membrane proteins using the lipidic bicelle method. *J. Vis. Exp.* **59,** e3383
9. Guo, X. W., Smith, P. R., Cognon, B., D'Arcangelis, D., Dolginova, E., and Mannella, C. A. (1995) Molecular design of the voltage-dependent, anion-selective channel in the mitochondrial outer membrane. *J. Struct. Biol.* **114,** 41–59
10. Mannella, C. A. (1998) Conformational changes in the mitochondrial channel protein, VDAC, and their functional implications. *J. Struct. Biol.* **121,** 207–218
11. Choudhary, O. P., Ujwal, R., Kowallis, W., Coalson, R., Abramson, J., and Grabe, M. (2010) The electrostatics of VDAC: implications for selectivity and gating. *J. Mol. Biol.* **396,** 580–592
12. Teijido, O., Ujwal, R., Hillerdal, C. O., Kullman, L., Rostovtseva, T. K., and Abramson, J. (2012) Affixing N-terminal α-helix to the wall of the voltage-dependent anion channel does not prevent its voltage gating. *J. Biol. Chem.* **287,** 11437–11445
13. Cheng, E. H., Sheiko, T. V., Fisher, J. K., Craigen, W. J., and Korsmeyer, S. J. (2003) VDAC2 inhibits BAK activation and mitochondrial apoptosis. *Science* **301,** 513–517
14. Anflous, K., Armstrong, D. D., and Craigen, W. J. (2001) Altered mitochondrial sensitivity for ADP and maintenance of creatine-stimulated respiration in oxidative striated muscles from VDAC1-deficient mice. *J. Biol. Chem.* **276,** 1954–1960
15. Sampson, M. J., Decker, W. K., Beaudet, A. L., Ruitenbeek, W., Armstrong, D., Hicks, M. J., and Craigen, W. J. (2001) Immotile sperm and infertility in mice lacking mitochondrial voltage-dependent anion channel type 3. *J. Biol. Chem.* **276,** 39206–39212
16. Min, C. K., Yeom, D. R., Lee, K. E., Kwon, H. K., Kang, M., Kim, Y. S., Park, Z. Y., Jeon, H., Kim do, H. (2012) Coupling of ryanodine receptor 2 and voltage-dependent anion channel 2 is essential for Ca^{2+} transfer from the sarcoplasmic reticulum to the mitochondria in the heart. *Biochem. J.* **447,** 371–379
17. Yagoda, N., von Rechenberg, M., Zaganjor, E., Bauer, A. J., Yang, W. S., Fridman, D. J., Wolpaw, A. J., Smukste, I., Peltier, J. M., Boniface, J. J., Smith, R., Lessnick, S. L., Sahasrabudhe, S., and Stockwell, B. R. (2007) RAS-RAF-MEK-dependent oxidative cell death involving voltage-dependent anion channels. *Nature* **447,** 864–868
18. Bauer, A. J., Gieschler, S., Lemberg, K. M., McDermott, A. E., and Stockwell, B. R. (2011) Functional model of metabolite gating by human voltage-dependent anion channel 2. *Biochemistry* **50,** 3408–3410
19. Otwinowski, Z., and Minor, W. (1997) Processing of X-ray diffraction data collected in oscillation mode. *Methods Enzymol.* **276,** 307–326
20. Kantardjieff, K. A., and Rupp, B. (2003) Matthews coefficient probabilities: improved estimates for unit cell contents of proteins, DNA, and protein-nucleic acid complex crystals. *Protein Sci.* **12,** 1865–1871
21. Adams, P. D., Afonine, P. V., Bunkóczi, G., Chen, V. B., Davis, I. W., Echols, N., Headd, J. J., Hung, L. W., Kapral, G. J., Grosse-Kunstleve, R. W., McCoy, A. J., Moriarty, N. W., Oeffner, R., Read, R. J., Richardson, D. C., Richardson, J. S., Terwilliger, T. C., and Zwart, P. H. (2010) PHENIX: a comprehensive Python-based system for macromolecular structure solution. *Acta Crystallogr. D Biol. Crystallogr.* **66,** 213–221
22. Emsley, P., and Cowtan, K. (2004) Coot: model-building tools for molecular graphics. *Acta Crystallogr. D Biol. Crystallogr.* **60,** 2126–2132
23. DeLano, W. L. (2010) *The PyMOL Molecular Graphics System*, version 1.3r1, Schrodinger, LLC, New York
24. Pettersen, E. F., Goddard, T. D., Huang, C. C., Couch, G. S., Greenblatt, D. M., Meng, E. C., and Ferrin, T. E. (2004) UCSF Chimera: a visualization system for exploratory research and analysis. *J. Comput. Chem.* **25,** 1605–1612
25. Hubbell, W. L., Mchaourab, H. S., Altenbach, C., and Lietzow, M. A. (1996) Watching proteins move using site-directed spin labeling. *Structure* **4,** 779–783
26. Fleissner, M. R., Bridges, M. D., Brooks, E. K., Cascio, D., Kálai, T., Hideg, K., and Hubbell, W. L. (2011) Structure and dynamics of a conformationally constrained nitroxide side chain and applications in EPR spectroscopy. *Proc. Natl. Acad. Sci. U.S.A.* **108,** 16241–16246
27. Jeschke, G., and Polyhach, Y. (2007) Distance measurements on spin-labelled biomacromolecules by pulsed electron paramagnetic resonance. *Phys. Chem. Chem. Phys.* **9,** 1895–1910
28. Hilger, D., Jung, H., Padan, E., Wegener, C., Vogel, K. P., Steinhoff, H. J., and Jeschke, G. (2005) Assessing oligomerization of membrane proteins by four-pulse DEER: pH-dependent dimerization of NhaA Na^+/H^+ antiporter of *E. coli*. *Biophys. J.* **89,** 1328–1338
29. Colombini, M. (1989) Voltage gating in the mitochondrial channel, VDAC. *J. Membr. Biol.* **111,** 103–111

30. De Pinto, V., Prezioso, G., Thinnes, F., Link, T. A., and Palmieri, F. (1991) Peptide-specific antibodies and proteases as probes of the transmembrane topology of the bovine heart mitochondrial porin. *Biochemistry* **30,** 10191–10200
31. Engelhardt, H., Meins, T., Poynor, M., Adams, V., Nussberger, S., Welte, W., and Zeth, K. (2007) High-level expression, refolding and probing the natural fold of the human voltage-dependent anion channel isoforms I and II. *J. Membr. Biol.* **216,** 93–105
32. Stanley, S., Dias, J. A., D'Arcangelis, D., and Mannella, C. A. (1995) Peptide-specific antibodies as probes of the topography of the voltage-gated channel in the mitochondrial outer membrane of *Neurospora crassa*. *J. Biol. Chem.* **270,** 16694–16700
33. Tomasello, M. F., Guarino, F., Reina, S., Messina, A., and De Pinto, V. (2013) The voltage-dependent anion selective channel 1 (VDAC1) topography in the mitochondrial outer membrane as detected in intact cell. *PloS One* **8,** e81522
34. Gonçalves, R. P., Buzhynskyy, N., Prima, V., Sturgis, J. N., and Scheuring, S. (2007) Supramolecular assembly of VDAC in native mitochondrial outer membranes. *J. Mol. Biol.* **369,** 413–418
35. Betaneli, V., Petrov, E. P., and Schwille, P. (2012) The role of lipids in VDAC oligomerization. *Biophys. J.* **102,** 523–531
36. López, C. J., Fleissner, M. R., Guo, Z., Kusnetzow, A. K., and Hubbell, W. L. (2009) Osmolyte perturbation reveals conformational equilibria in spin-labeled proteins. *Protein Sci.* **18,** 1637–1652
37. Naghdi, S., Varnai, P., Hunyady, L., and Hajnoczky, G. (2012) The isoform specific N terminus of VDAC2 is dispensable for tBid induced cytochrome *c* release. *Biophys. J.* **102,** 437A
38. Maldonado, E. N., Sheldon, K. L., DeHart, D. N., Patnaik, J., Manevich, Y., Townsend, D. M., Bezrukov, S. M., Rostovtseva, T. K., and Lemasters, J. J. (2013) Voltage-dependent anion channels modulate mitochondrial metabolism in cancer cells: regulation by free tubulin and erastin. *J. Biol. Chem.* **288,** 11920–11929
39. Naghdi, S., Varnai, P., Roy, S. S., Hunyady, L., and Hajnoczky, G. (2013) Which domain of VDAC2 is necessary for Bak insertion to the outer mitochondrial membrane and tBid-induced cytochrome *c* release? *Biophys. J.* **104,** 656A
40. Alvira, C. M., Umesh, A., Husted, C., Ying, L., Hou, Y., Lyu, S. C., Nowak, J., and Cornfield, D. N. (2012) Voltage-dependent anion channel-2 interaction with nitric oxide synthase enhances pulmonary artery endothelial cell nitric oxide production. *Am. J. Respir. Cell Mol. Biol.* **47,** 669–678
41. Roy, S. S., Ehrlich, A. M., Craigen, W. J., and Hajnóczky, G. (2009) VDAC2 is required for truncated BID-induced mitochondrial apoptosis by recruiting BAK to the mitochondria. *EMBO Rep.* **10,** 1341–1347
42. Palaniappan, K. K., Hangauer, M. J., Smith, T. J., Smart, B. P., Pitcher, A. A., Cheng, E. H., Bertozzi, C. R., and Boyce, M. (2013) A chemical glycoproteomics platform reveals *O*-GlcNAcylation of mitochondrial voltage-dependent anion channel 2. *Cell Rep.* **5,** 546–552
43. Geula, S., Naveed, H., Liang, J., and Shoshan-Barmatz, V. (2012) Structure-based analysis of VDAC1 protein: defining oligomer contact sites. *J. Biol. Chem.* **287,** 2179–2190
44. Mannella, C. A. (1982) Structure of the outer mitochondrial membrane: ordered arrays of porelike subunits in outer-membrane fractions from *Neurospora crassa* mitochondria. *J. Cell Biol.* **94,** 680–687
45. Hoogenboom, B. W., Suda, K., Engel, A., and Fotiadis, D. (2007) The supramolecular assemblies of voltage-dependent anion channels in the native membrane. *J. Mol. Biol.* **370,** 246–255

Appendix 3: Wilting F., et al. (2020) The antiarrhythmic compound efsevin directly modulates voltage-dependent anion channel 2 by binding to its inner wall and enhancing mitochondrial Ca^{2+} uptake, *Br J Pharmacol.*

Wilting F., Kopp R., Gurnev P.A., Schedel A., Dupper N. J., Kwon O., Nicke A., Gudermann T., and Schredelseker J. (2020) The antiarrhythmic compound efsevin directly modulates voltage-dependent anion channel 2 by binding to its inner wall and enhancing mitochondrial Ca^{2+} uptake, *Br J Pharmacol.* doi: 10.1111/bph.15022

Received: 12 April 2019 | Revised: 20 January 2020 | Accepted: 29 January 2020

DOI: 10.1111/bph.15022

RESEARCH PAPER

The antiarrhythmic compound efsevin directly modulates voltage-dependent anion channel 2 by binding to its inner wall and enhancing mitochondrial Ca^{2+} uptake

Fabiola Wilting[1] | Robin Kopp[1] | Philip A. Gurnev[2] | Anna Schedel[1] | Nathan J. Dupper[3] | Ohyun Kwon[3] | Annette Nicke[1] | Thomas Gudermann[1,4] | Johann Schredelseker[1]

[1]Walther Straub Institute of Pharmacology and Toxicology, Faculty of Medicine, LMU Munich, Munich, Germany

[2]Section on Molecular Transport, Eunice Kennedy Shriver National Institute of Child Health and Human Development, National Institutes of Health, Bethesda, Maryland

[3]Department of Chemistry and Biochemistry, University of California Los Angeles, Los Angeles, California

[4]Deutsches Zentrum für Herz-Kreislauf-Forschung (DZHK), Partner Site Munich Heart Alliance (MHA), Munich, Germany

Correspondence
Johann Schredelseker, Walther Straub Institute of Pharmacology and Toxicology, LMU Munich, Munich 80336, Germany.
Email: johann.schredelseker@lmu.de

Funding information
Deutsche Forschungsgemeinschaft, Grant/Award Number: SCHR 1471/1-1; U.S. National Institute of Health, Grant/Award Number: R01GM071779

Background and Purpose: The synthetic compound efsevin was recently identified to suppress arrhythmogenesis in models of cardiac arrhythmia, making it a promising candidate for antiarrhythmic therapy. Its activity was shown to be dependent on the voltage-dependent anion channel 2 (VDAC2) in the outer mitochondrial membrane. Here, we investigated the molecular mechanism of the efsevin–VDAC2 interaction.

Experimental Approach: To evaluate the functional interaction of efsevin and VDAC2, we measured currents through recombinant VDAC2 in planar lipid bilayers. Using molecular ligand-protein docking and mutational analysis, we identified the efsevin binding site on VDAC2. Finally, physiological consequences of the efsevin-induced modulation of VDAC2 were analysed in HL-1 cardiomyocytes.

Key Results: In lipid bilayers, efsevin reduced VDAC2 conductance and shifted the channel's open probability towards less anion-selective closed states. Efsevin binds to a binding pocket formed by the inner channel wall and the pore-lining N-terminal α-helix. Exchange of amino acids N207, K236 and N238 within this pocket for alanines abolished the channel's efsevin-responsiveness. Upon heterologous expression in HL-1 cardiomyocytes, both channels, wild-type VDAC2 and the efsevin-insensitive $VDAC2^{AAA}$ restored mitochondrial Ca^{2+} uptake, but only wild-type VDAC2 was sensitive to efsevin.

Conclusion and Implications: In summary, our data indicate a direct interaction of efsevin with VDAC2 inside the channel pore that leads to modified gating and results in enhanced SR-mitochondria Ca^{2+} transfer. This study sheds new light on the function of VDAC2 and provides a basis for structure-aided chemical optimization of efsevin.

Abbreviations: CPVT, catecholaminergic polymorphic ventricular tachycardia; DPhPC, 1,2-diphytanoyl-sn-glycero-3-phosphatidylcholine; hVDAC2, human voltage-dependent anion channel 2; IRES, internal ribosome entry site; MCU, mitochondrial calcium uniporter; MOI, multiplicity of infection; mVDAC2, mouse voltage-dependent anion channel 2; OMM, outer mitochondrial membrane; P_O, open probability; RuR, ruthenium red; shRNA, short hairpin RNA; SR, sarcoplasmic reticulum; VDAC, voltage-dependent anion channel; zVDAC2, zebrafish voltage-dependent anion channel 2.

1 | INTRODUCTION

Cardiovascular diseases represent the primary cause of death and hospitalization worldwide (Benjamin et al., 2018). Especially, Cardiac arrhythmias are difficult to treat due to major side effects of common antiarrhythmic drugs. It is thus a major focus of cardiovascular research to identify novel, safer therapies for cardiac arrhythmia.

Using a chemical suppressor screen on the zebrafish cardiac arrhythmia model *tremblor* (Ebert et al., 2005; Langenbacher et al., 2005), we have previously identified the synthetic compound efsevin, a dihydropyrrole carboxylic ester compound, which potently restored rhythmic cardiac contractions in otherwise fibrillating zebrafish embryonic hearts (Shimizu et al., 2015). We further demonstrated efficacy of efsevin in translational models for catecholaminergic polymorphic ventricular tachycardia (CPVT; Schweitzer et al., 2017). Here, efsevin reduced episodes of tachycardia in vivo in CPVT mice and suppressed arrhythmogenic events in induced pluripotent stem cell-derived cardiomyocytes from a CPVT patient (Schweitzer et al., 2017). These findings make efsevin a promising lead structure for human antiarrhythmic therapy.

In a pull-down assay with immobilized efsevin, the outer mitochondrial membrane (OMM) voltage-dependent anion channel 2 (VDAC2) was identified as the primary molecular target of efsevin (Shimizu et al., 2015). Voltage-dependent anion channels are large pore-forming proteins in the outer mitochondrial membrane. They represent the main pathway for ions and metabolites over the outer mitochondrial membrane. Three isoforms of voltage-dependent anion channels are expressed in vertebrates out of which VDAC2 was described to have a specific role in the heart. While a global knockout of VDAC2 in mice is embryonically lethal (Cheng, Sheiko, Fisher, Craigen, & Korsmeyer, 2003), a conditional heart-specific VDAC2 knockout mouse was reported to develop post-natal cardiac defects and to die shortly after birth (Raghavan, Sheiko, Graham, & Craigen, 2012). In cardiomyocytes, VDAC2 was described to interact with the **ryanodine receptor** (RyR; Min et al., 2012) and to modulate cytosolic Ca^{2+} signals (Shimizu et al., 2015; Subedi et al., 2011). In arrhythmic *tremblor* zebrafish embryos, efsevin induced a restoration of rhythmic cardiac contractions. Transient knock-down of VDAC2 abolished the efsevin induced phenotype restoration while overexpression of VDAC2 recovered it. In cultured cells, efsevin enhanced uptake of Ca^{2+} into mitochondria. A direct link between the enhanced mitochondrial Ca^{2+} uptake and efsevin's anti-arrhythmic properties was established by two lines of experiments: (a) Pharmacological inactivation of mitochondrial Ca^{2+} uptake by Ru360, an inhibitor of the mitochondrial Ca^{2+} uniporter (MCU), abolished efsevin's protective effect in CPVT cardiomyocytes and (b) kaempferol, an activator of the mitochondrial Ca^{2+} uniporter, reduced arrhythmogenic Ca^{2+} signals comparable to efsevin (Schweitzer et al., 2017).

However, biophysical and structural determinants of the efsevin–VDAC2 interaction have remained unexplored. It is still unclear whether efsevin directly interacts with the VDAC2 peptide and thereby modulates the electrophysiological properties of the channel or if the observed effects require a yet unidentified protein partner. To address this issue, we expressed and purified recombinant zebrafish VDAC2 (zVDAC2) protein and inserted it into planar lipid bilayers. We found a pronounced effect of efsevin on channel gating and opening probability, indicating a direct effect of efsevin on the channel. To analyse the structural basis of the efsevin VDAC2 interaction, we performed computational protein-ligand docking using the crystal structure of zVDAC2 (Schredelseker et al., 2014). VDAC2 is formed by a barrel-like structure consisting of 19 antiparallel β-sheets (β-sheets 1-19) and an N-terminal α-helix lining the inner channel wall (Schredelseker et al., 2014). We identified an efsevin binding site located in a groove between the inner channel wall and the pore-lining α-helix and formed by hydrogen bonds and hydrophobic interactions between efsevin and the zVDAC2 peptide. Replacement of three residues (N207, K236 and N238) from this binding site with alanines ($zVDAC2^{AAA}$) resulted in a complete loss of efsevin sensitivity. To evaluate the physiological consequence of the observed efsevin-induced biophysical changes in VDAC2, we heterologously expressed wild-type zVDAC2 and the efsevin-insensitive $zVDAC2^{AAA}$ mutant in cultured HL-1 cardiomyocytes. We demonstrate that the observed changes in zVDAC2 electrophysiology translate into enhanced mitochondrial Ca^{2+} uptake and thereby explain the antiarrhythmic effect of efsevin. Our data provide novel insights into VDAC2 function and provide a basis for structure-aided chemical optimization of efsevin as a lead structure for the development of novel antiarrhythmic drugs.

What is already known

- The synthetic compound efsevin suppresses arrhythmogenesis in cardiac arrhythmia models.
- Efsevin binds to the mitochondrial voltage-dependent anion channel anion channel 2 (VDAC2).

What this study adds

- Efsevin binds into a pocket formed by the channel wall and the pore-lining helix.
- Efsevin facilitates VDAC2 gating into a less anion-selective state and enhances Ca^{2+} flux.

What is the clinical significance

- Identification of mode of action and binding pocket allows for future structure aided-drug optimization.

2 | METHODS

2.1 | Expression and purification of zVDAC2

Expression and purification of zVDAC2 were performed as previously described (Schredelseker et al., 2014) with minor modifications: Histidine-tagged zVDAC2 was purified on an Äkta pure chromatography system using a HisPrep FF 16/10 column. After refolding dialysis, size exclusion chromatography was performed on a HiLoad 16/600 Superdex200 pg column equilibrated with 150-mM NaCl, 1-mM DTT, 0.1% LDAO, and 20-mm Tris-HCl (pH = 8.0). Integrity of the purified zVDAC2 was confirmed by SDS-PAGE analysis on a 12% gel.

2.2 | Planar lipid bilayer recordings

Painted planar lipid bilayers were formed on an Ionovation Bilayer Explorer lipid bilayer set-up across a 120-μm diameter opening with 1,2-diphytanoyl-sn-glycero-3-phosphatidylcholine (DPhPC) dissolved in *n*-decane at 12.5 mg·ml^{-1}. Both chambers were filled with 1-M KCl, 5-mM $CaCl_2$, and 10-mM Tris-HCl (pH = 7.2) To facilitate insertion, purified zVDAC2 was inserted into lipidic bicelles (Ujwal, 2012). After formation of a stable bilayer, zVDAC2 containing bicelles were added to the cis chamber. After insertion of a channel, the membrane was clamped to 0 mV, and 10 s pulses to test potentials from −60 mV to +60 mV were applied. The signal was sampled at 10 kHz and filtered at 2 kHz. Efsevin (50-μM stock in recording solution) was added to the cis chamber to a final concentration of 8 μM. Data analysis was performed using Nest-o-Patch (Dr. V. Nesterov, https://sourceforge.netq/projects/nestopatch/).

zVDAC2 ion selectivity was measured using folded planar membranes formed from opposition of two monolayers made of 5 mg·ml^{-1} solution of DPhPC in pentane, as described (Rostovtseva, Gurnev, Chen, & Bezrukov, 2012). Recordings were performed in the buffer described above. Channel insertion was achieved by adding zVDAC2 in a 2.5% Triton X-100 solution to the cis compartment while stirring. After single channel was inserted in symmetrical solutions, the cis side was perfused with Tris-HCl (pH 7.2) buffer solution to achieve 0.2-M KCl. The exact KCl concentration of 0.2 M in the cis compartment after perfusion was verified at the end of each selectivity experiment using a conductivity meter CDM230 (Radiometer analytical). Ion selectivity of zVDAC2 conductance states was calculated from the reversal potential (V_{rev}). Permeability ratio between Cl^-, and K^+, I^-/I^+, was calculated according to the Goldman–Hodgkin–Katz equation (Hille, 2001):

$$I^-/I^+ = \left(1 - \frac{V_{rev}}{\frac{k_B T}{e} \cdot ln\frac{a_{trans}}{a_{cis}}}\right) \cdot \left(1 + \frac{V_{rev}}{\frac{k_B T}{e} \cdot ln\frac{a_{trans}}{a_{cis}}}\right)^{-1},$$

where k_B, T, and e have their usual meaning of Boltzmann constant, absolute temperature, and electron charge, and KCl solution activities were a_{cis} = 0.144 for 0.2-M KCl and a_{trans} = 0.604 for 1-M KCl, respectively (Lide, 2006).

2.3 | Molecular docking

The three-dimensional (3D) structure of efsevin was generated using MarvinSketch (v15.1.9, ChemAxon) and saved in the .pdb format. The crystal structure of zVDAC2 was obtained from the Research Collaboratory for Structural Bioinformatics Protein Data Bank (PDB ID: 4BUM). Gasteiger charges and hydrogens were added to protein and ligand using AutoDockTools (v1.5.6; Morris et al., 2009), and AutoDock Vina was used to perform the molecular docking simulations (Trott & Olson, 2010). The term "independent docking experiment" used in this text refers to independent software runs of AutoDock Vina. Each run starts from a random conformation that is independent from the previous one and yields nine likely conformations. To determine the best hypothetical binding mode of efsevin on zVDAC2, the flexible form of efsevin was first docked to the rigid zVDAC2 structure. After 15 iterative dockings with a grid centred to ensure coverage of the entire channel, analysis of 135 binding conformations showed that the binding site with the lowest binding energy was found in the region between the inner channel wall and the highly flexible N-terminal α-helix. Since zVDAC2 might undergo conformational changes upon binding of efsevin, the side chains facing the potential binding site were kept flexible for subsequent dockings (N19, Y22, F24, N207, R218, K236, N238, L242 and L262). The grid box was narrowed to 24 Å × 20 Å × 20 Å to cover this region. After additional 15 iterative dockings with flexible side chains, the best binding poses were selected based on the predicted binding affinities. Interactions were analysed with LigPlot+ (Laskowski & Swindells, 2011).

2.4 | Molecular cloning

To introduce N207A, K236A and N238A into pQE60-zVDAC2 for recombinant expression and purification construct pQE60-zVDAC2^{AAA} was created by two mutagenesis PCR reactions using pQE60-zVDAC2 (Schredelseker et al., 2014) as a template. The two PCR fragments were fused by overlap extension PCR and the resulting product was ligated into pQE60-zVDAC2 with PstI and NheI.

For the creation of pCClc-CMV-zVDAC2-IRES-nlsEGFP for virus production and following transduction of zVDAC2 into HL-1 cells, eGFP with a nuclear localization signal (nls-eGFP) together with an internal ribosome entry site (IRES) was PCR-amplified from p3E-IRES-nlsEGFPpA (Kwan et al., 2007) and subcloned into pCS2+ containing the zVDAC2 open reading frame (Shimizu et al., 2015). The zVDAC2-IRES-nlsEGFP construct was fused into pCCLc-CMV using the In-Fusion HD Cloning Kit (TaKaRa).

For the creation of pCClc-CMV-zVDAC2^{AAA}-IRES-nlsEGFP, zVDAC2 was exchanged for zVDAC2^{AAA} in pCS2+-zVDAC2 (Shimizu

et al., 2015) by PCR amplification of the zVDAC2^{AAA} open reading frame from PQE60-zVDAC2^{AAA} following ligation with BamHI and ClaI. The open reading frame of zVDAC2^{AAA} was PCR-amplified from pCS2+-zVDAC2^{AAA} fused to the IRES PCR-amplified from pCClc-CMV-zVDAC2-IRES-nlsEGFP by SOE PCR and the resulting fragment was fused into pCClc-CMV-zVDAC2-IRES-nlsGFP using the In-Fusion HD Cloning Kit (TaKaRa).

2.5 | Production of lentiviruses

Recombinant lentiviruses were produced in HEK 293T cells. Briefly, cells at 40% confluency were cotransfected with pCCLc-CMV-zVDAC2-IRES-nlsEGFP or pCCLc-CMV-zVDAC2^{AAA}-IRES-nlsEGFP together with pCMVΔ8.91 (coding for gag, pol, rev) and pCAGGS-VSV-G at a 5:5:1 ratio using TransIT®-293 (Mirus). Cells were induced with 10-mM sodium butyrate on the following day. The supernatant containing the virus was collected on Day 3 after transfection, filtered through a 0.45-μm syringe filter, and stored at −80°C. Viral titres were determined using the Lenti-X™ qRT-PCR Titration Kit (Takara).

2.6 | HL-1 culture and creation of cell lines

HL-1 cells were cultured as described previously (Claycomb et al., 1998). Briefly, HL-1 cells were grown on fibronectin (0.02%) / gelatin (10 μg·ml^{-1}) coated flasks in Claycomb medium supplemented with 10% FBS, 100 μg·ml^{-1} penicillin/streptomycin, 0.1-mM norepinephrine, and 2-mM L-glutamine. Stable knockdown of the endogenous mVDAC2 in HL-1 cardiomyocytes was performed by lentiviral transduction with shLenti2.4G-mVDAC2 or shLenti2.4G-Ctrl as described previously (Subedi et al., 2011) In brief, HL-1 cells were transduced in serum-free Claycomb medium with lentivirus at a multiplicity of infection (MOI) of 30 in the presence of 8 μg·ml^{-1} polybrene. Three days after transduction, cells were selected with 2 μg·ml^{-1} puromycin for 10 days and cultured for additional three passages. For overexpression of zVDAC2 and zVDAC2^{AAA}, transduction was performed as described above using a MOI of 25. After 4 days, nlsEGFP-positive cells were selected by FACS sorting on a BD FACS Aria III.

2.7 | SR-mitochondria Ca^{2+} transfer

Fluorescence-based measurements of mitochondrial Ca^{2+} were performed as previously described (Schweitzer et al., 2017). In brief, HL-1 cells (RRID:CVCL_0303) were plated in 96-well plates 1 day prior to the experiment. To monitor mitochondrial Ca^{2+}, cells were stained with Rhod-2, AM (Thermo Fisher, Darmstadt, Germany) and permeabilized using digitonin. Mitochondrial Ca^{2+} was constantly monitored in a fluorescence plate reader (Infinite® 200 PRO multimode reader, Tecan, Maennedorf, Switzerland), and SR Ca^{2+} release was induced by superfusion with 10-mM caffeine.

2.8 | Metabolic stability assay

Efsevin (10 mM in DMSO) was co-incubated with human liver microsomes at 37°C at an initial concentration of 1 μM. The reaction was initiated by addition of 1-mM NADPH; 0, 5, 10, 30, and 60 minutes after starting the reaction, small aliquots were transferred into ice-cold acetonitrile and centrifuged at 16000× *g* for 10 min. Supernatants were analysed by LC–MS/MS. Experiments were performed as contract research at 3D BioOptima Co., Ltd., Suzhuo, China.

2.9 | Data and statistical analysis

The data and statistical analysis comply with the recommendations of the *British Journal of Pharmacology* on experimental design and analysis in pharmacology (Curtis et al., 2018). zVDAC2 channels were inserted into lipid bilayers and measured before and after addition of efsevin in recording solution, thus leading groups of equal size. In some instances, membranes ruptured during the recording explaining smaller sample size for recordings with efsevin. The recording before efsevin addition served as a control. Since efsevin was the only drug investigated and was added in measuring solution, randomization and blinding were not applied. All traces were equally analysed for predefined parameters like average current or open state to exclude operators bias. For Ca^{2+} uptake experiments on HL-1 cardiomyocytes, wells were randomly assigned to control, efsevin and **ruthenium red** (RuR) group to generate groups of equal size. Wells were microscopically inspected after the experiment, and those in which cells have detached were excluded from the analysis. No data transformation or outlier removal was performed, and all traces were equally analysed for maximum response by a predefined script to exclude operators bias. Since nature and magnitude of the effects of efsevin on zVDAC2 were unknown before the experiment and not predictable, a sample size evaluation was not feasible.

Statistical analysis was only performed for sample sizes >5 from independent experiments (i.e. individual insertions in lipid bilayers, individual runs of computational docking, and individual cultures of HL-1 cardiomyocytes), and the obtained data were used for statistical analysis without normalization and outlier removal. Statistical analysis was performed using Prism 7 (GraphPad Software, San Diego, USA). Data are presented as mean ± *SEM* of *n* individual experiments (no technical replicates). Normality of data was determined by Shapiro–Wilk test. Tests for statistical significance were conducted as indicated and where unpaired student's t-test for comparison of two groups with normal distribution of data, Mann Whitney U test for comparison of two groups with non-normal distribution of data, and Kruskal-Wallis test with Dunn's post hoc test for multigroup comparison with non-normal data distribution. Statistical significance of $P < .05$ is indicated as *.

2.10 | Materials

Efsevin was synthesized as described before (Henry et al., 2014). Protein purification was performed on an Äkta pure, and all Äkta

material was purchased from GE Healthcare, Munich, Germany; LDAO was obtained from VWR, Darmstadt, Germany. The lipid bilayer set-up and all consumables including 1,2-diphytanoyl-sn-glycero-3-phosphatidylcholine (DPhPC) were purchased from Ionovation, Osnabrück, Germany. Ruthenium red and caffeine used for the HL-1 Ca^{2+} uptake assay were purchased from Sigma-Aldrich (Munich, Germany). Plasmids pCCLc-CMV, pCMVΔ8.91 and pCAGGS-VSV-G were obtained as a gift from Dr. Donald Kohn, University of California Los Angeles, USA; plasmid shLenti2.4G-mVDAC2 and shLenti2.4G-Ctrl were generously provided by Dr. Yeon Soo Kim from Inje University, Gimhae, South Korea. HL-1 cardiomyocytes were obtained as a gift from Dr. William Claycomb, Louisiana State University, New Orleans, USA; Claycomb medium and all cell culture supplies were obtained from Sigma-Aldrich (Munich, Germany).

2.11 | Nomenclature of targets and ligands

Key protein targets and ligands in this article are hyperlinked to corresponding entries in http://www.guidetopharmacology.org, the common portal for data from the IUPHAR/BPS Guide to PHARMACOLOGY (Harding et al., 2018), PHARMACOLOGY.

3 | RESULTS

3.1 | Efsevin reduces currents through zVDAC2

Recombinant zVDAC2 protein was purified from *Escherichia coli* as previously described (Schredelseker et al., 2014) and inserted into diphytanoylphosphatidylcholine (DPhPC) planar lipid bilayers. Currents were measured in response to 10 s test pulses to potentials from −60 to +60 mV in 1-M KCl. As shown in Figure 1a, typical average currents of 41 ± 3pA were recorded at 10 mV, where the channel almost exclusively resides in its open state (Colombini, 1989; Schredelseker et al., 2014). VDAC-typical flattening of the current–voltage relationship (*I*–*V* curve) was observed starting at approximately ±30 mV (Figure 1b), where the channel starts gating until finally being preferentially in its closed state at potentials above +50 mV or below −50 mV (Figure 1a,b). The observed *I*–*V* curve for zVDAC2 translates into a bell-shaped conductance–voltage

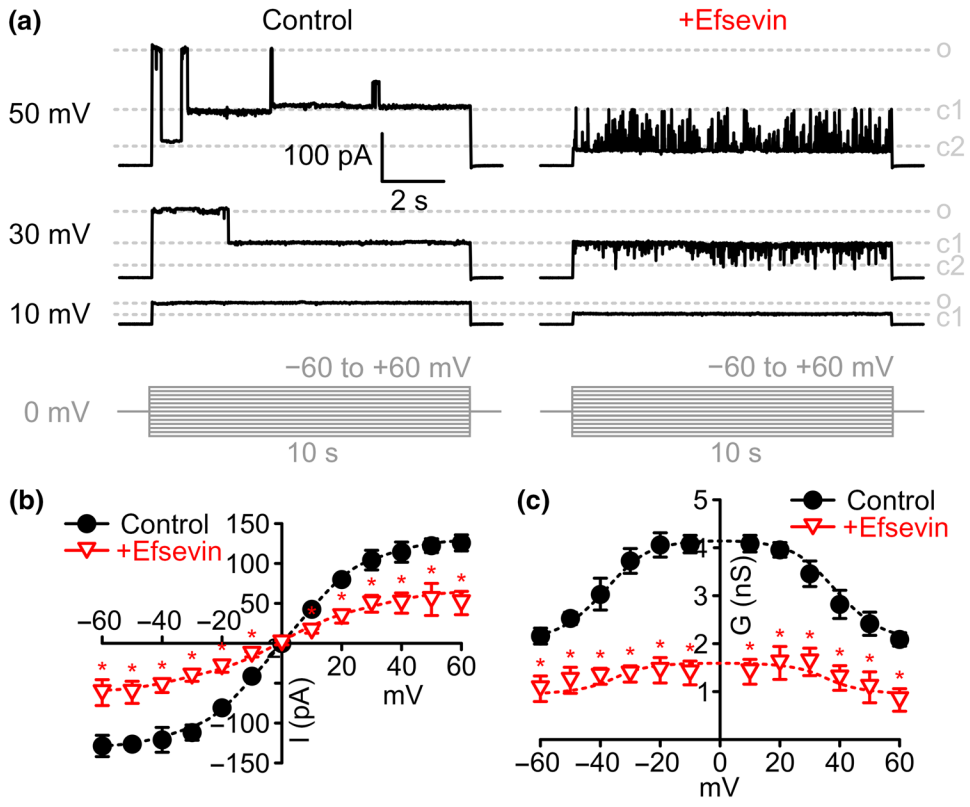

FIGURE 1 Effects of efsevin on zVDAC2 currents in planar lipid bilayers. (a) Typical current recordings from zVDAC2 inserted into painted planar DPhPC lipid bilayers in 1-M KCl in response to 10 s test pulses from 0 to 10, 40, and 50 mV, respectively, under control conditions (left) and after addition of 8-μM efsevin (right) to the same channel. Gating between three major states open (o), closed1 (c1) and closed2 (c2) and few subconductance states can be observed (pulse protocol in shown in grey). (b) Current–voltage relationship of average zVDAC2 currents before (n = 9 individual channels, black circles) and after addition of efsevin (n = 6 individual channels, red triangles, Unpaired Student's t-test). (c) Conductance–voltage relationship of zVDAC2 before (n = 9 individual channels, black circles) and after addition of efsevin (n = 6 individual channels, red triangles, Unpaired Student's t-test)

relationship that is characteristic of VDACs (Figure 1c). Strikingly, addition of 8-μM efsevin destabilized the channel's high conductance state and dramatically reduced currents through zVDAC2 by about 50% across all voltages.

3.2 | Efsevin reduces zVDAC2 open probability and shifts the channel towards closed states

Since efsevin profoundly reduced average zVDAC2 conductance, we further analysed the biophysical properties of zVDAC2 single channel currents to dissect the effects of efsevin on single channel conductance versus open probability of the channel. VDAC has been shown to undergo voltage-dependent gating between an anion-selective high-conductance state, referred to as the classical open state and several cation-selective low-conductance states, referred to as closed states (Colombini, 1989; Guardiani et al., 2018; Menzel et al., 2009; Mertins et al., 2012). Under control conditions, we observed gating of the channel between the classical open state with a conductance 4.2 ± 0.2 ns and two closed states with conductances of 2.0 ± 0.1 ns for closed state 1 and 1.2 ± 0.04 ns for closed state 2 (Figure 2a,b). Efsevin shifts the channel mainly into closed states 1 and 2 with only a few scarce openings of the channel into the open state, already at low potentials. Conductances of the three states remained comparable to control conditions (open: 4.1 ± 0.1 ns; closed1: 2.1 ± 0.2 ns; closed2: 1.0 ± 0.04 ns; Figure 2b). The shift towards the closed states becomes most obvious when plotting the open probability (P_O) of the channel against voltage (Figure 2c). Interestingly, at the physiologically relevant low potentials of ±30 mV (Lemeshko, 2006; Porcelli et al., 2005), the apo-form of the channel resides mainly in the open state, while the efsevin-bound form is preferentially closed (Figure 2d). The VDAC closed states were previously defined as more cation-selective compared to the open state (Tan & Colombini, 2007; Zachariae et al., 2012). We therefore measured the ion selectivity of the dominant states, the open

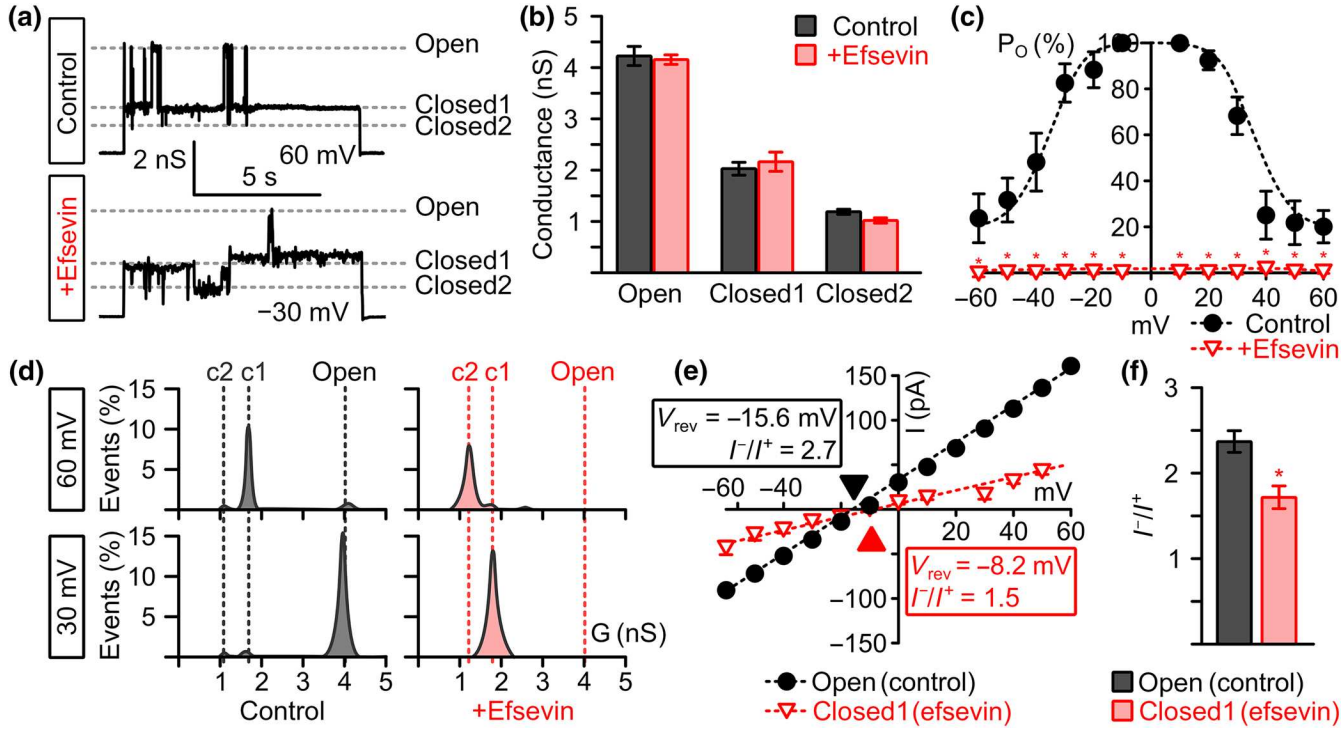

FIGURE 2 Effects of efsevin on zVDAC2 conductance and open probability (P_O). (a) Representative recordings of zVDAC2 in a painted lipid bilayer under control conditions (upper trace) and after addition of 8-μM efsevin (lower trace) at potentials where typical gating behaviour between the three states is observed, that is, very low/high potentials under control conditions and moderate potentials after addition of efsevin. Currents through the open and two distinct closed states of the channel are indicated by dashed lines. (b) Addition of 8-μM efsevin does not change the conductance of the three distinct conductance states of zVDAC2 (n = 12 individual channels for control and 6 individual channels after addition of efsevin). (c) Analysis of the open probability (P_O) of zVDAC2 shows a significant shift of the channel towards the closed states across all voltages after addition of efsevin (n = 12 for control and n = 6 for efsevin, Mann–Whitney U test). (d) Representative conductance histograms from recordings of zVDAC2 with and without efsevin at 30 mV and 60 mV show a shift of the channel from the classical open state to the closed states. (e,f) Current–voltage plots for the open and the efsevin-induced closed state 1 obtained from zVDAC2 in a folded lipid bilayer using a 0.2-M to 1-M KCl gradient reveal a shift in the reversal potential (V_{rev}). (f) Quantitative analysis of selectivity measurements reveals a significant reduction in anion selectivity for the efsevin-induced closed state 1 (n = 6 for control, n = 5 for efsevin, Unpaired Student's t- test)

state of the apo-form and closed state 1 of the efsevin-bound channel using salt gradient conditions (0.2-M [cis] vs. 1-M [trans] KCl) and found a change in the Cl^- to K^+ permeability ratio I^-/I^+ from 2.38 ± 0.13 for the open state to 1.71 ± 0.14 for the efsevin-bound closed state 1 (Figure 2e,f). In conclusion, our data indicate that efsevin binding facilitates channel closure and induces a shift of zVDAC2 towards the less anion-selective low conductance states.

3.3 | Molecular docking reveals an efsevin binding site between the inner channel wall and the pore-lining N-terminal α-helix

To identify the interaction between efsevin and zVDAC2 at the molecular level, we performed protein-ligand docking using AutoDock Vina (Trott & Olson, 2010). By docking the flexible form of efsevin into the rigid crystal structure of zVDAC2 (Schredelseker et al., 2014), a binding pocket formed between the inner channel wall and the N-terminal α-helix of zVDAC2 repeatedly showed the lowest binding energies in 15 independent dockings yielding 135 conformations (Figures 3a and S1). To further investigate molecular interactions between zVDAC2 and efsevin within this pocket, we performed subsequent docking simulations in which residues facing this binding site were made flexible. We identified multiple conformations with binding affinities below −8.0 kcal·mol^{-1} in which the dihydropyrrole of the efsevin core with the ethoxycarbonyl and phenyl substituents was always interacting with residues in the channel wall, while the *p*-tolyl substituent of the sulphonamide group faces the lumen of the pore and interacts with the hinge region of the N-terminal α-helix. Interactions of efsevin with zVDAC2 were identified with residues F18, N19, Y22, G23, F24 and M26 in the N-terminal α-helix and with residues N207, L208, A209, R218, F219, G220, K236, V237, N238, L242, G244 and L262 in the β-barrel, whereof asparagine 207, lysine 236 and asparagine 238 were the most prominent interaction partners. Hydrogen bonds and hydrophobic interactions with these three amino acids were present in the majority of conformations (Figure 3b). Figure 3c,d shows one representative conformation in which efsevin is held in place by N207, K236 and N238 in the channel wall and interacts with the α-helix through hydrophobic interactions with residues F18, N19, Y22, G23 and F24. To finally investigate translatability of the docking results to the human channel, we created

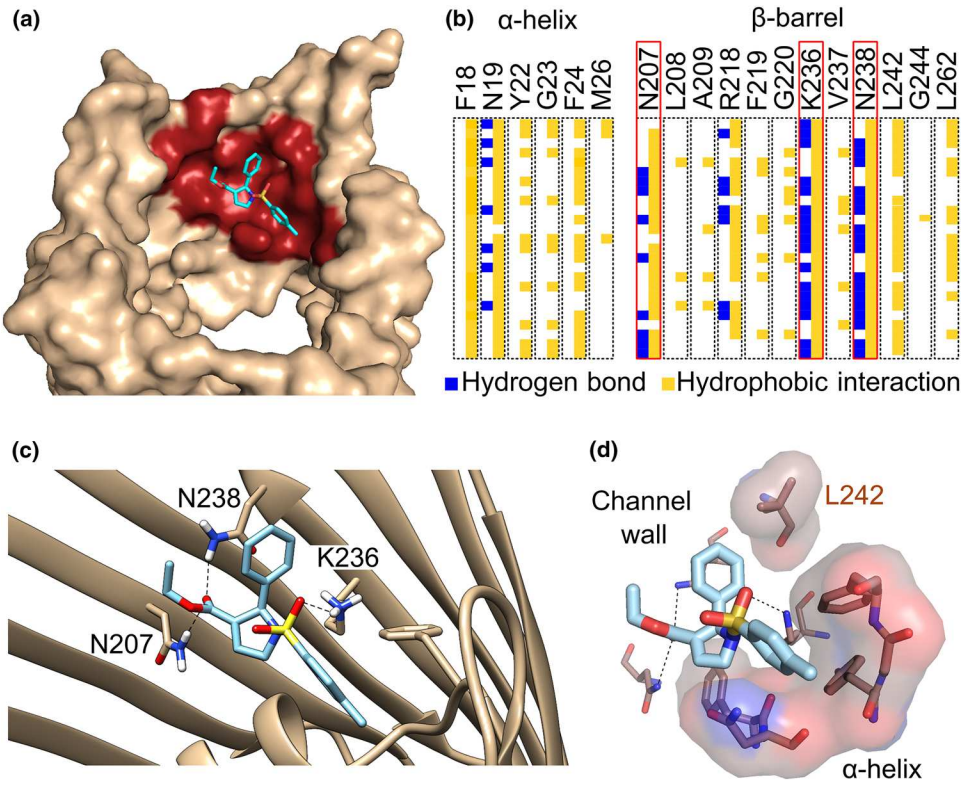

FIGURE 3 Predicted binding site of efsevin on zVDAC2 obtained by molecular docking. (a) Side view of the channel (pdb: 4bum, light brown) displays a binding pocket (red) for efsevin (light blue) located in the interspace between the inner channel wall and the N-terminal pore-lining α-helix. (b) Analysis of 25 different molecular dockings (rows) reveals interactions between efsevin and 18 amino acid rests of zVDAC2 (columns) through hydrogen bonds (blue) and hydrophobic interactions (yellow). Residues with the most interactions (N207 in β-sheet 14, K236, and N238 in β-sheet 16 of the barrel) are boxed in red. (c) Detailed view of one representative docking with efsevin binding to the channel through hydrogen bonds between the most prominent amino acids highlighted in (b) and efsevin. (d) Surface representation of residues forming hydrophobic interactions in the conformation shown in (c) reveals a cavity that accommodates the *p*-tolyl group of efsevin on the hinge of the flexible N-terminal α-helix. Nitrogen is shown in blue, oxygen in red, and sulfur in yellow

a model of human VDAC2 (hVDAC2) by homology modelling using SWISS-MODEL (Waterhouse et al., 2018) since no experimentally determined structure for hVDAC2 is currently available. In eight out of 10 independent docking experiments, the conformation with the lowest binding energy was found in the same binding pocket like in zVDAC2 indicating that this binding pocket is conserved among species (Figure S2).

3.4 | Elimination of residues N207, K236 and N238 abolishes the efsevin sensitivity of zVDAC2

To confirm the predicted efsevin binding site by mutational analysis, we created a zVDAC2 mutant in which residues N207, K236 and N238 were substituted by alanine residues, zVDAC2$^{N207A/K236A/N238A}$ (zVDAC2^{AAA}). Lipid bilayer recordings of this mutant showed that it forms a functional channel with a similar conductance–voltage relationship, single channel conductance and P_O compared to wild-type zVDAC2 (Figure S3). Most strikingly however, the channel was insensitive to efsevin, demonstrated by comparable values for the conductance–voltage relationship, single channel conductance and P_O before and after addition of efsevin (Figure 4).

3.5 | Efsevin mediates SR-mitochondria Ca^{2+} transfer by binding to the N207/K236/N238 binding site

To evaluate if the observed efsevin-induced electrophysiological changes can explain the enhanced mitochondrial Ca^{2+} uptake observed previously for HeLa cells and HL-1 cardiomyocytes (Schweitzer et al., 2017; Shimizu et al., 2015), we developed a heterologous expression system for zVDAC2. To this aim, we created a stable HL-1 cardiomyocyte line in which the endogenous mouse VDAC2 (mVDAC2) was knocked down by stable expression of shRNA (Subedi et al., 2011; Figure S4) and overexpressed shRNA-insensitive zVDAC2 constructs by lentiviral transduction. Ca^{2+} uptake into mitochondria upon caffeine-induced Ca^{2+} release from the sarcoplasmic reticulum (SR) was then measured in permeabilized Rhod-2 stained cells (Figure 5). In line with previous experiments, knock-down of the endogenous mVDAC2 eliminated transfer of Ca^{2+} from the sarcoplasmic reticulum into mitochondria (Subedi et al., 2011). While wild-type HL-1 cardiomyocytes displayed maximum $\Delta F/F_0$ values of 0.14 ± 0.02 that were enhanced to 0.38 ± 0.03 by 10-μM efsevin, shRNA-expressing cells displayed $\Delta F/F_{0\ max}$ values of 0.04 ± 0.03, which were indistinguishable from those obtained from cells treated with the mitochondrial Ca^{2+} uptake blocker ruthenium red (RuR; $\Delta F/F_{0\ max}$ = 0.06 ± 0.02) or efsevin ($\Delta F/F_{0\ max}$ = 0.06 ± 0.01, not significant). Though lack of VDAC2 was previously described to induce apoptosis and we can thus not rule out downstream effects induced by mVDAC2 knock down in these cells, the shmVDAC2 cell line was stable for the time of our experiments and thus suitable for heterologous overexpression experiments. Overexpression of zVDAC2 completely restored sarcoplasmic reticulum-mitochondria Ca^{2+} transfer to $\Delta F/F_{0\ max}$ = 0.14 ± 0.02, which was sensitive to modulation by efsevin ($\Delta F/F_{0\ max}$ = 0.34 ± 0.02). Strikingly, zVDAC2^{AAA} likewise restored mitochondrial Ca^{2+} uptake to levels indistinguishable from wild-type zVDAC2 ($\Delta F/F_{0\ max}$ = 0.15 ± 0.02) but was insensitive to treatment with efsevin ($\Delta F/F_{0\ max}$ = 0.16 ± 0.02). These data strongly indicate that the efsevin induced changes in zVDAC2 electrophysiology account for the enhanced mitochondrial Ca^{2+} uptake in cardiomyocytes.

4 | DISCUSSION

Here, we describe the efsevin–zVDAC2 interaction at a biophysical and structural level. Efsevin was previously shown to enhance mitochondrial Ca^{2+} uptake and to be a powerful modulator of cardiac rhythmicity and a potent suppressor of cardiac arrhythmia. Efsevin suppresses arrhythmogenesis in both, models for Ca^{2+} overload and models for inherited arrhythmias like catecholaminergic polymorphic

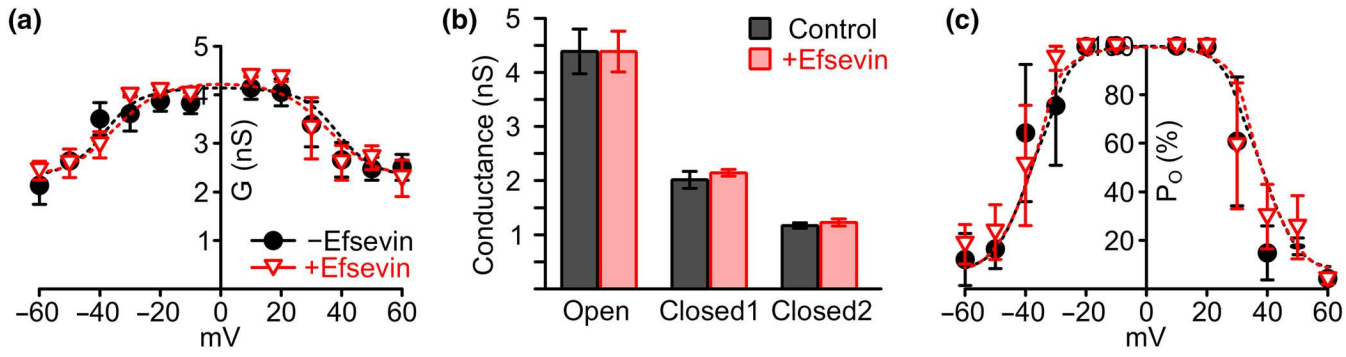

FIGURE 4 Effects of efsevin on conductance, and open probability (P_O) of zVDAC2^{AAA} in lipid bilayers. (a) Conductance–voltage relation of zVDAC2^{AAA} in painted bilayer recordings reveals a comparable shape before and after addition of 8-μM efsevin. (b) No differences in single channel conductance for open and closed states of zVDAC2^{AAA} were observed after addition of efsevin. (c) Finally, in zVDAC2^{AAA}, efsevin was unable to induce the reduction of P_O observed for wild-type zVDAC2 (n = 4 individual channels for control and 3 individual channels after addition of efsevin)

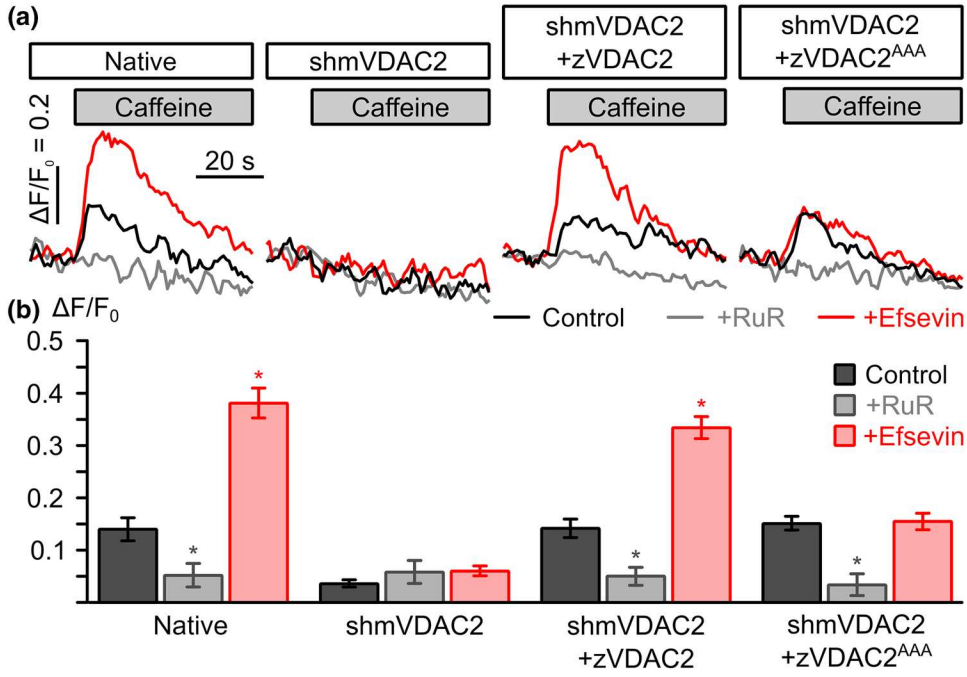

FIGURE 5 Sarcoplasmic reticulum (SR)-mitochondria Ca^{2+} transfer upon heterologous expression of zVDAC2 and zVDAC2^{AAA} in HL-1 cardiomyocytes. (a) Representative recordings of mitochondrial Ca^{2+} upon application of 10-mM caffeine to induce SR calcium release from permeabilized HL-1 cardiomyocytes. Traces from control conditions (black), recordings in the presence of 10-μM ruthenium red to block mitochondrial Ca^{2+} uptake (RuR, grey) and in the presence of 10-μM efsevin (red) are shown for native HL-1 cells (native), cells transduced with shRNA targeting the endogenous mouse mVDAC2 (shmVDAC2), and cells overexpressing zVDAC2 and zVDAC2^{AAA}, respectively. (b) Statistical analysis of SR-mitochondria Ca^{2+} transfer experiments. While native HL-1 cardiomyocytes showed an efsevin-sensitive uptake of Ca^{2+} into mitochondria (n = 21 for control, n = 7 for RuR, and n = 18 for efsevin), this uptake was abolished upon knock-down of the endogenous mVDAC2 (shmVDAC2, n = 24 for control, n = 8 for RuR, n = 15 for efsevin). Subsequent heterologous expression of zVDAC2 (shmVDAC2, n = 21 for control, n = 7 for RuR, n = 15 for efsevin) and zVDAC2^{AAA} (shmVDAC2^{AAA}, n = 18 for control, n = 6 for RuR, n = 18 for efsevin) revealed restoration of SR-mitochondria Ca^{2+} transfer. However, only zVDAC2 but not zVDAC2^{AAA} was sensitive to efsevin (Kruskal–Wallis test with Dunn's post hoc test)

ventricular tachycardia. In a murine model for CPVT, efsevin significantly reduced episodes of ventricular tachycardia, while no adverse effects of efsevin were observed after up to 8 days of continuous treatment. VDAC2, which was previously described as an essential component of the mitochondrial Ca^{2+} uptake machinery of the heart (Subedi et al., 2011), was identified as the primary target of efsevin (Shimizu et al., 2015). These findings make VDAC2-mediated mitochondrial Ca^{2+} uptake a promising therapeutic target for the development of a novel class of antiarrhythmic drugs with efsevin as a lead candidate. However, efsevin was identified in a chemical screen using 168 newly synthesized diversity-oriented compounds (Shimizu et al., 2015) without further compound optimization. In our HL-1-based sarcoplasmic reticulum-mitochondria Ca^{2+} transfer assay, efsevin showed a half-maximal activity at 2.2 μM (Figure S5A). Preliminary results on efsevin's pharmacokinetics show that it is hydrolysed rapidly in liver microsomes (Figure S5B). Furthermore, binding of efsevin to other targets, including VDAC isoforms 1 and 3, was never tested. Thus, its unknown selectivity, the low stability of efsevin and the relatively high EC_{50} value indicate the need for chemical optimization of the compound before further preclinical and clinical studies are performed. In this study, we present a molecular model of the efsevin binding site on zVDAC2 and thereby provide a basis for structure-based drug optimization in future experiments.

When discussing VDAC2 as a potential drug target for cardiac arrhythmia, it should be noted that the transfer of Ca^{2+} from the sarcoplasmic reticulum into mitochondria is most likely a specialized role of VDAC2 in cardiomyocytes, presumably accomplished by a functional or even physical coupling to the ryanodine receptor (Min et al., 2012; Shimizu et al., 2015; Subedi et al., 2011) and might be less relevant or maybe accomplished by other VDAC isoforms in other cell types. In fact, VDAC1 was previously reported to promote Ca^{2+} transfer from the endoplasmic reticulum into mitochondria in non-excitable cells through coupling to the **IP_3 receptor** (De Stefani et al., 2012; Rapizzi et al., 2002; Szabadkai et al., 2006). It is thus conceivable that despite the ubiquitous expression of VDACs in the body, efsevin-mediated effects are most pronounced or even limited to cardiomyocytes due to the specialized role of VDAC2 in this tissue. This effect might also explain the lack of major side effects that were observed previously in translational models (Schweitzer et al., 2017). However, future studies are needed to evaluate the role of the efsevin-mediated effects on other VDAC2-mediated effects like

apoptosis or regulation of bioenergetics (for a review, see Naghdi & Hajnóczky, 2016). Furthermore, although VDAC2 was identified as the primary target of efsevin and efsevin-induced antiarrhythmic effects were shown to depend on VDAC2 (Shimizu et al., 2015), interaction of efsevin with other VDAC isoforms were never investigated. Given a high sequence conservation of the residues involved in VDAC2 binding identified in this study, it is conceivable that efsevin binds to VDAC isoforms 1 and 3. This effect might be less relevant during short-term treatment of mice and fish but might have long-term impacts on, for example, bioenergetics and thus needs to be investigated in future studies.

Using computational docking on the crystal structure of zVDAC2, we identified a binding pocket formed by the inner channel wall and the N-terminal helix. The putative binding site was confirmed by replacing three prominent residues inside the pocket by alanines which resulted in insensitivity of the channel to efsevin in lipid bilayers. It is of note that we used a C-terminal His_6-tag for purification of the channel for subsequent bilayer experiments which is not present in the structure used for computational docking. It is thus conceivable that the His_6-tag interferes with efsevin and promotes effects seen in bilayer experiments. However, the His_6-tag is located approximately 25 Å away from the proposed binding site on the opposed mouth of the channel making interference unlikely. Furthermore, we evaluated the proposed binding site by heterologous expression of zVDAC2 without the C-terminal His_6-tag in HL-1 cardiomyocytes and found that efsevin sensitivity of the channel was again promoted through the proposed binding site. To prove translatability of the results obtained from zVDAC2, we created a homology model of hVDAC2 using zVDAC2 as a template and found that the lowest bind energy was calculated in the same pocket in eight out of 10 individual docking experiments. The mammalian channel includes additional 11 amino acids on the N-terminus of the channel. Unfortunately, no homologous structures of this additional sequence have been resolved so far, and coordinates for homology modelling are missing. It is thus again conceivable that the additional N-terminus in mammalian channels could interfere with efsevin binding. However, in HL-1 cardiomyocytes, we observe very similar effects of efsevin on native cells expressing the endogenous mVDAC2, which includes the N-terminal extension and heterologously expressed zVDAC2. Although these data do not rule out the possibility that efsevin promotes its effects on the two distinct channels differently, it argues against it.

Our data indicate that efsevin binds to the inner wall of the β-barrel in close proximity to the N-terminal α-helix and thereby affects channel conductance and gating. Although still not fully resolved, various models were proposed to explain gating of VDACs. Almost all models include a role of the N-terminal α-helix ranging from relatively small movements of the helix inside the barrel (Mertins et al., 2012; Shuvo, Ferens, & Court, 2016) to a large movement that place the helix outside of the barrel, which then collapses to induce channel closure (Choudhary et al., 2010; Zachariae et al., 2012). Furthermore, a fixation of the helix inside the pore through disulfate bridges was reported as a possible mechanism to regulate channel gating by redox sensing (Okazaki et al., 2015; Reina et al., 2016). Our data identified a binding pocket for efsevin located in a groove between the N-terminal α-helix and the inner channel wall. In all our predicted binding conformations, efsevin is bound to the channel wall through hydrogen bonds provided by N19, N207, R218, K236 or N238 plus additional hydrophobic interactions and interacts with a binding pocket located on the hinge of the α-helix. Interestingly, one of the residues in the channel wall, K236, was previously reported to form a hydrogen bond with F18 in the α-helix (Ujwal et al., 2008), a residue that interacts with efsevin upon efsevin binding. It is thus conceivable that efsevin interferes with the interaction between the barrel and the helix in zVDAC2 and consequently affects the movement of the α-helix required to modulate the channel. However, it should be noted that the binding of efsevin might induce a conformational change in the channel, which is not considered in our docking model. Further experimental and computational investigations, like molecular dynamics simulations and determination of the ligand-bound VDAC2 structure are thus needed to clarify the exact mode of gating and ion conduction through the channel in the presence and absence of efsevin.

Using an electrophysiological approach, we found efsevin-promoted gating of zVDAC2. Already at low potentials, the channel preferentially gates into the two closed states and only rarely returns to the open state. We demonstrate that the efsevin-induced low conducting states display less anion selectivity compared to the open state which translates into a higher Ca^{2+} flux and consequently into higher Ca^{2+} uptake into mitochondria in cardiomyocytes. This is in line with previous experimental (Tan & Colombini, 2007) and computational (Zachariae et al., 2012) studies, which have shown the closed states of VDAC to be more cation-selective. The observed shift from the open to the closed states is especially relevant at low potentials ranging from −40 to +40 mV. Though it is still under debate whether a membrane potential difference exists over the outer mitochondrial membrane, modelling data suggest a potential of approximately −20 to −27 mV (Lemeshko, 2006) and a study based on pH measurements suggests a potential of approximately −40 mV (Porcelli et al., 2005). This most likely explains the enhanced Ca^{2+} uptake into mitochondria seen in the presence of efsevin. The data presented in this study are thus in agreement with the concept of increased Ca^{2+} flux upon channel closure.

In this study, we present a binding pocket in zVDAC2 and an associated biophysical mechanism, namely, a modification of voltage gating and a shift towards the cation-selective closed states. VDACs were previously suggested as promising drug targets mainly because of their prominent role in apoptosis (for a review, see Magrì, Reina, & De Pinto, 2018). However, it remained unclear whether the role of VDAC in apoptosis was directly associated with the channel's gating behaviour or rather with a modified interaction with partner proteins such as hexokinase or members of the Bcl-2 family. In this study, we present evidence that the efsevin-induced change in gating facilitates transfer of Ca^{2+} from the SR into mitochondria. Interestingly, we never observed an involvement of the drug in apoptosis, neither in this study nor in previous studies (Schweitzer et al., 2017; Shimizu et al., 2015) despite a previously identified isoform-specific role for

VDAC2 in apoptosis through recruitment of Bax (Lauterwasser et al., 2016; Ma et al., 2014). Efsevin could thus serve as a tool to dissect these functions in future studies.

Taken together, we provide functional and structural data that explains the interaction between zVDAC2 and its modulator efsevin on a molecular basis. Our data provide new insights into VDAC2 function as well as a basis for computer-aided design of optimized compounds that could serve as research compounds and therapeutics for cardiac arrhythmia.

ACKNOWLEDGEMENTS

We would like to thank Brigitte Mayerhofer for technical assistance and Tatiana Rostovtseva and Anna Krautloher for help with data analysis. We thank Michael Hristov from the FACS core facility at the Institute for Cardiovascular Prevention at LMU Munich for performing FACS sorting of HL-1 cardiomyocytes. This work was supported by the Deutsche Forschungsgesellschaft DFG SCHR 1471/1-1 to J.S. and the U.S. National Institute of Health grant R01GM071779 to O.K.

CONFLICT OF INTEREST

The authors declare no conflicts of interest.

AUTHOR CONTRIBUTIONS

J.S. and T.G. conceptualized the study and acquired funding. F.W. and J.S. performed bilayer recordings and mitochondrial Ca^{2+} uptake experiments and analysed results. P.G. performed and analysed ion selectivity recordings. R.K. and A.S. performed molecular docking experiments. O.K. and N.J.D. synthesized efsevin. A.N. analysed data. J.S. wrote the manuscript. All authors commented on the manuscript.

DECLARATION OF TRANSPARENCY AND SCIENTIFIC RIGOUR

This Declaration acknowledges that this paper adheres to the principles for transparent reporting and scientific rigour of preclinical research as stated in the *BJP* guidelines for Design & Analysis, and as recommended by funding agencies, publishers and other organisations engaged with supporting research.

ORCID

Robin Kopp https://orcid.org/0000-0002-1639-2868

Johann Schredelseker https://orcid.org/0000-0002-6657-0466

REFERENCES

Benjamin, E. J., Virani, S. S., Callaway, C. W., Chamberlain, A. M., Chang, A. R., Cheng, S., … American Heart Association Council on Epidemiology and Prevention Statistics Committee and Stroke Statistics Subcommittee. (2018). Heart disease and stroke statistics—2018 update: A report from the American Heart Association. *Circulation*, *137*, e67–e492. https://doi.org/10.1161/CIR.0000000000000558

Cheng, E. H. Y., Sheiko, T. V., Fisher, J. K., Craigen, W. J., & Korsmeyer, S. J. (2003). VDAC2 inhibits BAK activation and mitochondrial apoptosis. *Science*, *301*, 513–517. https://doi.org/10.1126/science.1083995

Choudhary, O. P., Ujwal, R., Kowallis, W., Coalson, R., Abramson, J., & Grabe, M. (2010). The electrostatics of VDAC: Implications for selectivity and gating. *Journal of Molecular Biology*, *396*, 580–592. https://doi.org/10.1016/j.jmb.2009.12.006

Claycomb, W. C., Lanson, N. A., Stallworth, B. S., Egeland, D. B., Delcarpio, J. B., Bahinski, A., & Izzo, N. J. (1998). HL-1 cells: A cardiac muscle cell line that contracts and retains phenotypic characteristics of the adult cardiomyocyte. *Proceedings of the National Academy of Sciences of the United States of America*, *95*, 2979–2984. https://doi.org/10.1073/pnas.95.6.2979

Colombini, M. (1989). Voltage gating in the mitochondrial channel, VDAC. *Journal of Membrane Biology*, *111*, 103–111. https://doi.org/10.1007/bf01871775

Curtis, M. J., Alexander, S., Cirino, G., Docherty, J. R., George, C. H., Giembycz, M. A., … Ahluwalia, A. (2018). Experimental design and analysis and their reporting II: Updated and simplified guidance for authors and peer reviewers. *British Journal of Pharmacology*, *175*, 987–993. https://doi.org/10.1111/bph.14153

De Stefani, D., Bononi, A., Romagnoli, A., Messina, A., De Pinto, V., Pinton, P., & Rizzuto, R. (2012). VDAC1 selectively transfers apoptotic Ca^{2+} signals to mitochondria. *Cell Death and Differentiation*, *19*, 267–273. https://doi.org/10.1038/cdd.2011.92

Ebert, A. M., Hume, G. L., Warren, K. S., Cook, N. P., Burns, C. G., Mohideen, M. A., … Garrity, D. M. (2005). Calcium extrusion is critical for cardiac morphogenesis and rhythm in embryonic zebrafish hearts. *Proceedings of the National Academy of Sciences of the United States of America*, *102*, 17705–17710. https://doi.org/10.1073/pnas.0502683102

Guardiani, C., Magrì, A., Karachitos, A., Di Rosa, M. C., Reina, S., Bodrenko, I., … De Pinto, V. (2018). yVDAC2, the second mitochondrial porin isoform of *Saccharomyces cerevisiae*. *Biochimica et Biophysica Acta, Bioenergetics*, *1859*, 270–279. https://doi.org/10.1016/j.bbabio.2018.01.008

Harding, S. D., Sharman, J. L., Faccenda, E., Southan, C., Pawson, A. J., Ireland, S., … NC-IUPHAR. (2018). The IUPHAR/BPS Guide to pharmacology in 2018: Updates and expansion to encompass the new guide to immunopharmacology. *Nucleic Acids Research*, *46*, D1091–D1106. https://doi.org/10.1093/nar/gkx1121

Henry, C. E., Xu, Q., Fan, Y. C., Martin, T. J., Belding, L., Dudding, T., & Kwon, O. (2014). Hydroxyproline-derived pseudoenantiomeric [2.2.1] bicyclic phosphines: Asymmetric synthesis of (+)- and (–)-pyrrolines. *Journal of the American Chemical Society*, *136*, 11890–11893. https://doi.org/10.1021/ja505592h

Hille, B. (2001). *Ion channels of excitable membranes*. Sunderland, MA, USA: Sinauer Associates Inc.

Kirichok, Y., Krapivinsky, G. & Clapham, D. (2004). The mitochondrial calcium uniporter is a highly selective ion channel. *Nature*, *427*, 360–364.

Kwan, K. M., Fujimoto, E., Grabher, C., Mangum, B. D., Hardy, M. E., Campbell, D. S., … Chien, C. B. (2007). The Tol2kit: A multisite gateway-based construction kit for Tol2 transposon transgenesis constructs. *Developmental Dynamics*, *236*, 3088–3099. https://doi.org/10.1002/dvdy.21343

Langenbacher, A. D., Dong, Y., Shu, X., Choi, J., Nicoll, D. A., Goldhaber, J. I., … Chen, J. N. (2005). Mutation in sodium-calcium exchanger 1 (NCX1) causes cardiac fibrillation in zebrafish. *Proceedings of the National Academy of Sciences of the United States of America*, *102*, 17699–17704. https://doi.org/10.1073/pnas.0502679102

Laskowski, R. A., & Swindells, M. B. (2011). LigPlot+: Multiple ligand–protein interaction diagrams for drug discovery. *Journal of Chemical Information and Modeling*, *51*, 2778–2786. https://doi.org/10.1021/ci200227u

Lauterwasser, J., Todt, F., Zerbes, R. M., Nguyen, T. N., Craigen, W., Lazarou, M., … Edlich, F. (2016). The porin VDAC2 is the mitochondrial platform for Bax retrotranslocation. *Scientific Reports*, *6*, 32994. https://doi.org/10.1038/srep32994

Lemeshko, V. V. (2006). Theoretical evaluation of a possible nature of the outer membrane potential of mitochondria. *European Biophysics Journal*, *36*, 57–66. https://doi.org/10.1007/s00249-006-0101-7

Lide, D. R. (2006). *CRC handbook of chemistry and physics* (87th ed.). Boca Raton: CRC Press, Taylor & Francis Group.

Ma, S. B., Nguyen, T. N., Tan, I., Ninnis, R., Iyer, S., Stroud, D. A., … Dewson, G. (2014). Bax targets mitochondria by distinct mechanisms before or during apoptotic cell death: a requirement for VDAC2 or Bak for efficient Bax apoptotic function. *Cell Death and Differentiation*, *21*, 1925–1935. https://doi.org/10.1038/cdd.2014.119

Magrì, A., Reina, S., & De Pinto, V. (2018). VDAC1 as pharmacological target in cancer and neurodegeneration: Focus on its role in apoptosis. *Frontiers in Chemistry*, *6*, 108.

Menzel, V. A., Cassará, M. C., Benz, R., De Pinto, V., Messina, A., Cunsolo, V., … Hinsch, E. (2009). Molecular and functional characterization of VDAC2 purified from mammal spermatozoa. *Bioscience Reports*, *29*, 351–362. https://doi.org/10.1042/BSR20080123

Mertins, B., Psakis, G., Grosse, W., Back, K. C., Salisowski, A., Reiss, P., … Essen, L. O. (2012). Flexibility of the N-terminal mVDAC1 segment controls the channel's gating behavior. *PLoS ONE*, *7*, e47938. https://doi.org/10.1371/journal.pone.0047938

Min, C. K., Yeom, D. R., Lee, K.-E., Kwon, H.-K., Kang, M., Kim, Y.-S., … Kim, D. H. (2012). Coupling of ryanodine receptor 2 and voltage-dependent anion channel 2 is essential for Ca^{2+} transfer from the sarcoplasmic reticulum to the mitochondria in the heart. *The Biochemical Journal*, *447*, 371–379. https://doi.org/10.1042/BJ20120705

Morris, G. M., Huey, R., Lindstrom, W., Sanner, M. F., Belew, R. K., Goodsell, D. S., & Olson, A. J. (2009). AutoDock4 and AutoDockTools4: Automated docking with selective receptor flexibility. *Journal of Computational Chemistry*, *30*, 2785–2791. https://doi.org/10.1002/jcc.21256

Naghdi, S., & Hajnóczky, G. (2016). VDAC2-specific cellular functions and the underlying structure. *Biochimica et Biophysica Acta, Molecular Cell Research*, *1863*, 2503–2514. https://doi.org/10.1016/j.bbamcr.2016.04.020

Okazaki, M., Kurabayashi, K., Asanuma, M., Saito, Y., Dodo, K., & Sodeoka, M. (2015). VDAC3 gating is activated by suppression of disulfide-bond formation between the N-terminal region and the bottom of the pore. *Biochimica et Biophysica Acta (BBA)-Biomembranes*, *1848*, 3188–3196.

Porcelli, A. M., Ghelli, A., Zanna, C., Pinton, P., Rizzuto, R., & Rugolo, M. (2005). pH difference across the outer mitochondrial membrane measured with a green fluorescent protein mutant. *Biochemical and Biophysical Research Communications*, *326*, 799–804. https://doi.org/10.1016/j.bbrc.2004.11.105

Raghavan, A., Sheiko, T. V., Graham, B. H., & Craigen, W. J. (2012). Voltage-dependant anion channels: Novel insights into isoform function through genetic models. *Biochimica et Biophysica Acta-Biomembranes*, *1818*, 1477–1485. https://doi.org/10.1016/j.bbamem.2011.10.019

Rapizzi, E., Pinton, P., Szabadkai, G., Wieckowski, M. R., Vandecasteele, G., Baird, G., … Rizzuto, R. (2002). Recombinant expression of the voltage-dependent anion channel enhances the transfer of Ca^{2+} microdomains to mitochondria. *The Journal of Cell Biology*, *159*, 613–624. https://doi.org/10.1083/jcb.200205091

Reina, S., Checchetto, V., Saletti, R., Gupta, A., Chaturvedi, D., Guardiani, C., … de Pinto, V. (2016). VDAC3 as a sensor of oxidative state of the intermembrane space of mitochondria: The putative role of cysteine residue modifications. *Oncotarget*, *7*, 2249–2268. https://doi.org/10.18632/oncotarget.6850

Rostovtseva, T. K., Gurnev, P. A., Chen, M.-Y., & Bezrukov, S. M. (2012). Membrane lipid composition regulates tubulin interaction with mitochondrial voltage-dependent anion channel. *The Journal of Biological Chemistry*, *287*, 29589–29598. https://doi.org/10.1074/jbc.M112.378778

Schredelseker, J., Paz, A., López, C. J., Altenbach, C., Leung, C. S., Drexler, M. K., … Abramson, J. (2014). High-resolution structure and double electron-electron resonance of the zebrafish voltage dependent anion channel 2 reveal an oligomeric population. *The Journal of Biological Chemistry*, *289*, 12566–12577. https://doi.org/10.1074/jbc.M113.497438

Schweitzer, M. K., Wilting, F., Sedej, S., Dreizehnter, L., Dupper, N. J., Tian, Q., … Schredelseker, J. (2017). Suppression of arrhythmia by enhancing mitochondrial Ca^{2+} uptake in catecholaminergic ventricular tachycardia models. *JACC Basic to Translational Science*, *2*, 737–746. https://doi.org/10.1016/j.jacbts.2017.06.008

Shimizu, H., Schredelseker, J., Huang, J., Lu, K., Naghdi, S., Lu, F., … Chen, J. N. (2015). Mitochondrial Ca^{2+} uptake by the voltage-dependent anion channel 2 regulates cardiac rhythmicity. *eLife*, *4*. https://doi.org/10.7554/eLife.04801

Shuvo, S. R., Ferens, F. G., & Court, D. A. (2016). The N-terminus of VDAC: Structure, mutational analysis, and a potential role in regulating barrel shape. *Biochimica et Biophysica Acta-Biomembranes*, *1858*, 1350–1361. https://doi.org/10.1016/j.bbamem.2016.03.017

Subedi, K. P., Kim, J.-C., Kang, M., Son, M.-J., Kim, Y.-S., & Woo, S.-H. (2011). Voltage-dependent anion channel 2 modulates resting Ca^{2+} sparks, but not action potential-induced Ca^{2+} signaling in cardiac myocytes. *Cell Calcium*, *49*, 136–143. https://doi.org/10.1016/j.ceca.2010.12.004

Szabadkai, G., Bianchi, K., Várnai, P., De Stefani, D., Wieckowski, M. R., Cavagna, D., … Rizzuto, R. (2006). Chaperone-mediated coupling of endoplasmic reticulum and mitochondrial Ca^{2+} channels. *The Journal of Cell Biology*, *175*, 901–911. https://doi.org/10.1083/jcb.200608073

Tan, W., & Colombini, M. (2007). VDAC closure increases calcium ion flux. *Biochimica et Biophysica Acta*, *1768*, 2510–2515. https://doi.org/10.1016/j.bbamem.2007.06.002

Trott, O., & Olson, A. J. (2010). AutoDock Vina: Improving the speed and accuracy of docking with a new scoring function, efficient optimization, and multithreading. *Journal of Computational Chemistry*, *31*, 455–461. https://doi.org/10.1002/jcc.21334

Ujwal, R., & Abramson, J. (2012). High-throughput crystallization of membrane proteins using the lipidic bicelle method. *Journal of Visualized Experiments*, *59*, e3383.

Ujwal, R., Cascio, D., Colletier, J.-P., Faham, S., Zhang, J., Toro, L., … Abramson, J. (2008). The crystal structure of mouse VDAC1 at 2.3 Å resolution reveals mechanistic insights into metabolite gating. *Proceedings of the National Academy of Sciences of the United States of America*, *105*, 17742–17747. https://doi.org/10.1073/pnas.0809634105

Waterhouse, A., Bertoni, M., Bienert, S., Studer, G., Tauriello, G., Gumienny, R., … Schwede, T. (2018). SWISS-MODEL: Homology modelling of protein structures and complexes. *Nucleic Acids Research*, *46*, W296–W303. https://doi.org/10.1093/nar/gky427

Zachariae, U., Schneider, R., Briones, R., Gattin, Z., Demers, J.-P., Giller, K., … Lange, A. (2012). β-barrel mobility underlies closure of the voltage-dependent anion channel. *Structure*, *20*, 1540–1549. https://doi.org/10.1016/j.str.2012.06.015

SUPPORTING INFORMATION

Additional supporting information may be found online in the Supporting Information section at the end of this article.

How to cite this article: Wilting F, Kopp R, Gurnev PA, et al. The antiarrhythmic compound efsevin directly modulates voltage-dependent anion channel 2 by binding to its inner wall and enhancing mitochondrial Ca^{2+} uptake. *Br J Pharmacol*. 2020;1–12. https://doi.org/10.1111/bph.15022

Appendix 4: Schweitzer, M. K., et al. (2017) Suppression of Arrhythmia by Enhancing Mitochondrial Ca^{2+} Uptake in Catecholaminergic Ventricular Tachycardia Models. *JACC Basic to Transl. Sci.*

Schweitzer, M. K., Wilting, F., Sedej, S., Dreizehnter, L., Dupper, N. J., Tian, Q., Moretti, A., My, I., Kwon, O., Priori, S. G., Laugwitz, K.-L., Storch, U., Lipp, P., Breit, A., Mederos y Schnitzler, M., Gudermann, T., and **Schredelseker, J.** (2017) Suppression of Arrhythmia by Enhancing Mitochondrial Ca^{2+} Uptake in Catecholaminergic Ventricular Tachycardia Models. *JACC Basic to Transl. Sci.* **2**, 737–746

JACC: BASIC TO TRANSLATIONAL SCIENCE
VOL. 2, NO. 6, 2017
ISSN 2452-302X
https://doi.org/10.1016/j.jacbts.2017.06.008

PRECLINICAL RESEARCH

Suppression of Arrhythmia by Enhancing Mitochondrial Ca^{2+} Uptake in Catecholaminergic Ventricular Tachycardia Models

Maria K. Schweitzer, MSc,[a] Fabiola Wilting, MSc,[a] Simon Sedej, PhD,[b] Lisa Dreizehnter, PhD,[c] Nathan J. Dupper, BSc,[d] Qinghai Tian, PhD,[e] Alessandra Moretti, PhD,[c,f] Ilaria My, MD,[c] Ohyun Kwon, PhD,[d] Silvia G. Priori, MD, PhD,[g,h] Karl-Ludwig Laugwitz, MD,[c,f] Ursula Storch, PhD,[a] Peter Lipp, PhD,[e] Andreas Breit, PhD,[a] Michael Mederos y Schnitzler, PhD,[a,f] Thomas Gudermann, MD,[a,f] Johann Schredelseker, PhD[a]

VISUAL ABSTRACT

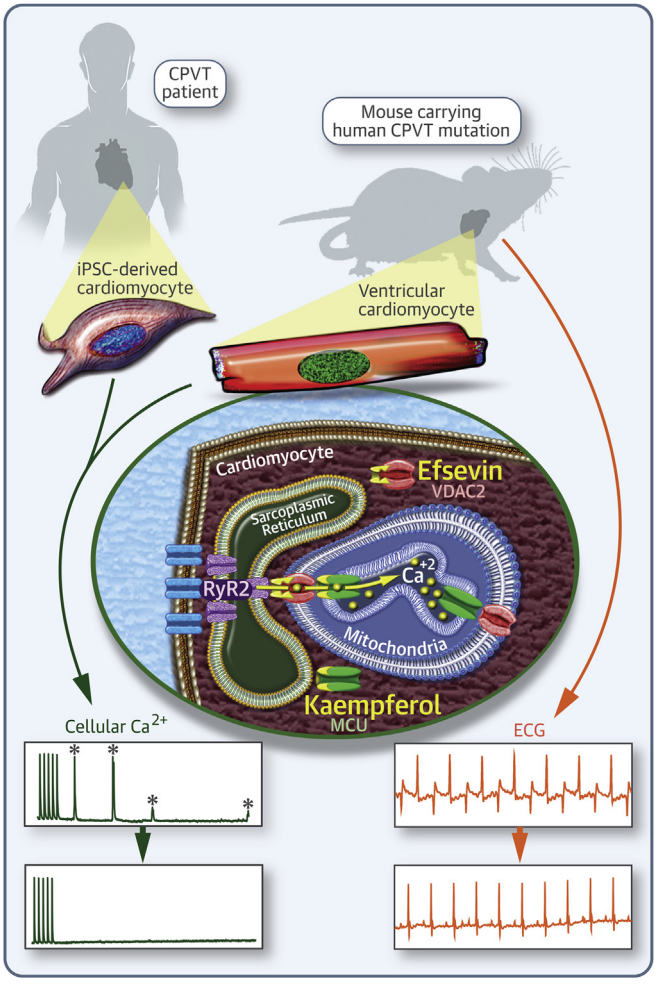

Schweitzer, M.K. et al. J Am Coll Cardiol Basic Trans Science. 2017;2(6):737–47.

HIGHLIGHTS

- Fast transfer of Ca^{2+} from the sarcoplasmic reticulum into mitochondria in cardiomyocytes can be enhanced by the MiCUps efsevin, targeting the VDAC2, and kaempferol, targeting the MCU.
- Enhancing sarcoplasmic reticulum-to-mitochondria Ca^{2+} transfer with MiCUps suppresses arrhythmogenic Ca^{2+} events and spontaneous action potentials in cardiomyocytes from a mouse model of CPVT.
- In vivo treatment of CPVT mice with MiCUps reduces episodes of ventricular tachycardia after adrenergic stimulation.
- In induced pluripotent stem cell-derived cardiomyocytes from a CPVT patient, both MiCUps reduce arrhythmogenic Ca^{2+} events.
- Our data establish fast mitochondrial Ca^{2+} uptake as a promising candidate structure for pharmacological treatment of human cardiac arrhythmia.

JACC: BASIC TO TRANSLATIONAL SCIENCE VOL. 2, NO. 6, 2017
DECEMBER 2017:737–47

ABBREVIATIONS AND ACRONYMS

CPVT = catecholaminergic polymorphic ventricular tachycardia

epi/caff = epinephrine/caffeine

iPSC = induced pluripotent stem cell

ISO = isoproterenol

MCU = mitochondrial calcium uniporter

MiCUp = mitochondrial calcium uptake enhancer

RyR2 = ryanodine receptor type 2

SR = sarcoplasmic reticulum

VDAC2 = voltage-dependent anion channel type 2

WT = wild type

SUMMARY

Cardiovascular disease-related deaths frequently arise from arrhythmias, but treatment options are limited due to perilous side effects of commonly used antiarrhythmic drugs. Cardiac rhythmicity strongly depends on cardiomyocyte Ca^{2+} handling and prevalent cardiac diseases are causally associated with perturbations in intracellular Ca^{2+} handling. Therefore, intracellular Ca^{2+} transporters are lead candidate structures for novel and safer antiarrhythmic therapies. Mitochondria and mitochondrial Ca^{2+} transport proteins are important regulators of cardiac Ca^{2+} handling. Here, the authors evaluated the potential of pharmacological activation of mitochondrial Ca^{2+} uptake for the treatment of cardiac arrhythmia. To this aim, the authors tested substances that enhance mitochondrial Ca^{2+} uptake for their ability to suppress arrhythmia in a murine model for ryanodine receptor 2 (RyR2)-mediated catecholaminergic polymorphic ventricular tachycardia (CPVT) in vitro and in vivo and in induced pluripotent stem cell-derived cardiomyocytes from a CPVT patient. In freshly isolated cardiomyocytes of $RyR2^{R4496C/WT}$ mice efsevin, a synthetic agonist of the voltage-dependent anion channel 2 (VDAC2) in the outer mitochondrial membrane, prevented the formation of diastolic Ca^{2+} waves and spontaneous action potentials. The antiarrhythmic effect of efsevin was abolished by blockade of the mitochondrial Ca^{2+} uniporter (MCU), but could be reproduced using the natural MCU activator kaempferol. Both mitochondrial Ca^{2+} uptake enhancers (MiCUps), efsevin and kaempferol, significantly reduced episodes of stress-induced ventricular tachycardia in $RyR2^{R4496C/WT}$ mice in vivo and abolished diastolic, arrhythmogenic Ca^{2+} events in human iPSC-derived cardiomyocytes. These results highlight an immediate potential of enhanced mitochondrial Ca^{2+} uptake to suppress arrhythmogenic events in experimental models of CPVT and establish MiCUps as promising pharmacological tools for the treatment and prevention of Ca^{2+}-triggered arrhythmias such as CPVT. (J Am Coll Cardiol Basic Trans Science 2017;2:737–47)

Cardiovascular diseases remain the leading cause of death worldwide (1). Approximately one-half of all cardiovascular deaths are attributed to severe cardiac arrhythmia (2). Cardiac rhythmicity critically depends on precisely regulated Ca^{2+} oscillations in cardiomyocytes (3), and cardiac arrhythmia is frequently associated with perturbations of cellular Ca^{2+} handling (4,5). Most currently used antiarrhythmic drugs target receptors and channels in the cell membrane (sarcolemma) to block the propagation of arrhythmic events along the myocardium but do not restore defective intracellular Ca^{2+} handling. Due to their modulatory effects on the cardiac action potential, these drugs often show pro-arrhythmic side effects. Therefore, intracellular Ca^{2+} transporters are candidate structures for novel and safer antiarrhythmic therapies.

Mitochondria occupy approximately 30% of the cardiomyocyte volume (6,7) and closely interact with the sarcoplasmic reticulum (SR) to absorb Ca^{2+}, which is released from the SR into the cytosol through cardiac ryanodine receptors (RyR2) (8,9). For that, mitochondria are equipped with a regulated network of Ca^{2+} transporters. While the mitochondrial calcium

From the [a]Walther Straub Institute of Pharmacology and Toxicology, Ludwig-Maximilians-Universität München, Munich, Germany; [b]Department of Cardiology, Medical University of Graz, Graz, Austria; [c]Department of Medicine (Cardiology), Klinikum rechts der Isar, Technische Universität München, Munich, Germany; [d]Department of Chemistry and Biochemistry, University of California Los Angeles, Los Angeles, California; [e]Institute for Molecular Cell Biology, University Medical Center, Saarland University, Homburg/Saar, Germany; [f]Deutsches Zentrum für Herz-Kreislauf-Forschung, Partner Site Munich Heart Alliance, Munich, Germany; [g]Molecular Cardiology, Istituto di ricovero e cura a carattere scientifico (IRCCS) Salvatore Maugeri Foundation, Pavia, Italy; and the [h]Department of Molecular Medicine, University of Pavia, Pavia, Italy. Supported by Deutsche Forschungsgemeinschaft (DFG), Bonn, Germany (SCHR 1471/1-1 to Dr. Schredelseker; TRR152 to Drs. Gudermann, Lipp, Moretti, and Laugwitz), the Friedrich-Baur-Stiftung, Munich, Germany (to Dr. Schredelseker), and U.S. National Institutes of Health (R01GM071779 to Dr. Kwon). Dr. Sedej is supported by the Austrian Science Fund FWF, Vienna, Austria (P27637-B28). Dr. Priori has received research support from Boston Scientific; and is a member of the advisory boards for General Electric and Audentes. All other authors have reported that they have no relationships relevant to the contents of this paper to disclose.
All authors attest they are in compliance with human studies committees and animal welfare regulations of the authors' institutions and Food and Drug Administration guidelines, including patient consent where appropriate. For more information, visit the *JACC: Basic to Translational Science* author instructions page.

Manuscript received April 10, 2017; revised manuscript received June 26, 2017, accepted June 27, 2017.

uniporter (MCU) has been identified as the main route for Ca^{2+} import in the inner mitochondrial membrane (10–12), the voltage-dependent anion channel 2 (VDAC2) in the outer mitochondrial membrane has only recently been shown to be a major part of the Ca^{2+} transport route from the SR into mitochondria (13–15). In addition to the 2 pore-forming channels, the mitochondrial Ca^{2+} uptake complex is regulated by several auxiliary subunits such as the essential MCU regulator EMRE or the mitochondrial Ca^{2+} uptake proteins MICU1 and -2 (16,17). While it is generally accepted that a slow and moderate rise of mitochondrial Ca^{2+} triggers enhanced energy production under higher workload (18), the immediate role of mitochondria in shaping cellular Ca^{2+} signals on a beat-to-beat level remains a matter of debate (19,20). Mitochondria have been demonstrated to be regulators of cardiac rhythmicity (21,22), but their potential to serve as therapeutic targets has not been evaluated so far. The synthetic compound efsevin has been newly identified to activate VDAC2 and to enhance mitochondrial Ca^{2+} uptake (15). Using efsevin, we demonstrated that cardiac rhythmicity in zebrafish embryos can be critically modulated by enhancing mitochondrial Ca^{2+} uptake (15).

This study evaluated the translational potential of pharmacological activation of mitochondrial Ca^{2+} uptake for the prevention and treatment of cardiac arrhythmia. To this end, we used 2 models of catecholaminergic polymorphic ventricular tachycardia (CPVT), exemplifying a Ca^{2+}-triggered arrhythmia. CPVT manifests in early adolescence and is characterized by episodes of life-threatening ventricular tachycardia upon catecholaminergic stimulation after physical exercise or emotional stress. The $RyR2^{R4496C/WT}$ mouse harbors an R4496C mutation in the SR Ca^{2+} release channel RyR2, homologous to the human R4497C mutation, which is associated with CPVT (23) and displays a CPVT phenotype (24). We show that activating mitochondrial Ca^{2+} uptake suppresses arrhythmia in $RyR2^{R4496C/WT}$ cardiomyocytes in vitro and in $RyR^{R4496C/WT}$ mice in vivo. Finally, we demonstrate that activating mitochondrial Ca^{2+} uptake is likewise efficient in blocking arrhythmogenesis in induced pluripotent stem cell (iPSC)-derived cardiomyocytes from a CPVT patient heterozygous for a different RyR2 mutation ($RyR2^{S406L}$).

METHODS

ISOLATION OF CARDIOMYOCYTES. Isolation of ventricular cardiomyocytes from heterozygous knock-in $RyR2^{R4496C/WT}$ mice (24) was performed using a Langendorff perfusion-based enzymatic digestion protocol (25) with minor modifications. Only excitable, rod-shaped, quiescent cells were used for experiments.

HUMAN iPSC-BASED MODEL. iPSCs from a skin biopsy from a CPVT patient carrying the $RyR2^{S406L/WT}$ mutation and from a healthy donor were differentiated into spontaneously beating explants (26,27) and enzymatically dissociated into single cardiomyocytes.

Ca^{2+} IMAGING. Ca^{2+} transients, spontaneous diastolic Ca^{2+} waves, and Ca^{2+} sparks were measured in cardiomyocytes loaded with Fluo-4 acetoxymethyl ester (AM) (Thermo Fisher Scientific, Darmstadt, Germany), using confocal microscopy in line scan mode. Cells were paced by extracellular electrodes at 0.5 Hz.

ELECTROPHYSIOLOGY. Action potentials were recorded in current clamp mode, using the perforated patch-clamp technique. Cells were paced by repetitive, depolarizing intracellular current injections at 0.5 Hz, followed by a 60-s pause to detect potentially proarrhythmic events during this diastolic phase.

cAMP ACCUMULATION ASSAY. For evaluation of intracellular cAMP levels, cardiomyocytes were labeled with ^{3}H-labeled adenine to measure accumulation of [^{3}H]cAMP over 15 min.

IN VIVO ARRHYTHMIA TESTING. Drugs were administered to $RyR2^{R4496C/WT}$ mice 8 to 12 weeks of age through osmotic minipumps, and subsequently, electrocardiography recordings were performed under light isoflurane anesthesia, to monitor ventricular tachycardia after bolus injection of epinephrine/caffeine (epi/caff). All animal procedures were performed in accordance with national and European ethical regulations (directive 2010/63/EU) and approved by the responsible government agency (BMWFW-66.010/0012-WF/V/3b/2015).

MITOCHONDRIAL Ca^{2+} UPTAKE. Mitochondrial Ca^{2+} uptake in response to 10 mM caffeine to open RyR2 was measured in Rhod-2 AM-loaded permeabilized HL-1 cardiomyocytes (28) on a fluorescence 96-well plate reader. The Ca^{2+} chelator 1,2-*bis*(*o*-aminophenoxy) ethane-*N*,*N*,*N*′,*N*′-tetraacetic acid (BAPTA) (1 mM) was used to restrict Ca^{2+} to the low micrometer range around RyR clusters (8,29).

STATISTICAL ANALYSIS. Data are mean ± standard error of the mean. Normality of data was determined by Shapiro-Wilk test, and respective tests for statistical significance were conducted as indicated. Post hoc tests were Dunn's test for Kruskal-Wallis tests and Tukey's multiple comparisons test for ANOVA. Significance for contingency tables was calculated using Fisher's exact test.

FIGURE 1 Efsevin Reduces Diastolic Ca^{2+} Waves and Spontaneous Action Potentials in $RyR2^{R4496C/WT}$ Cardiomyocytes

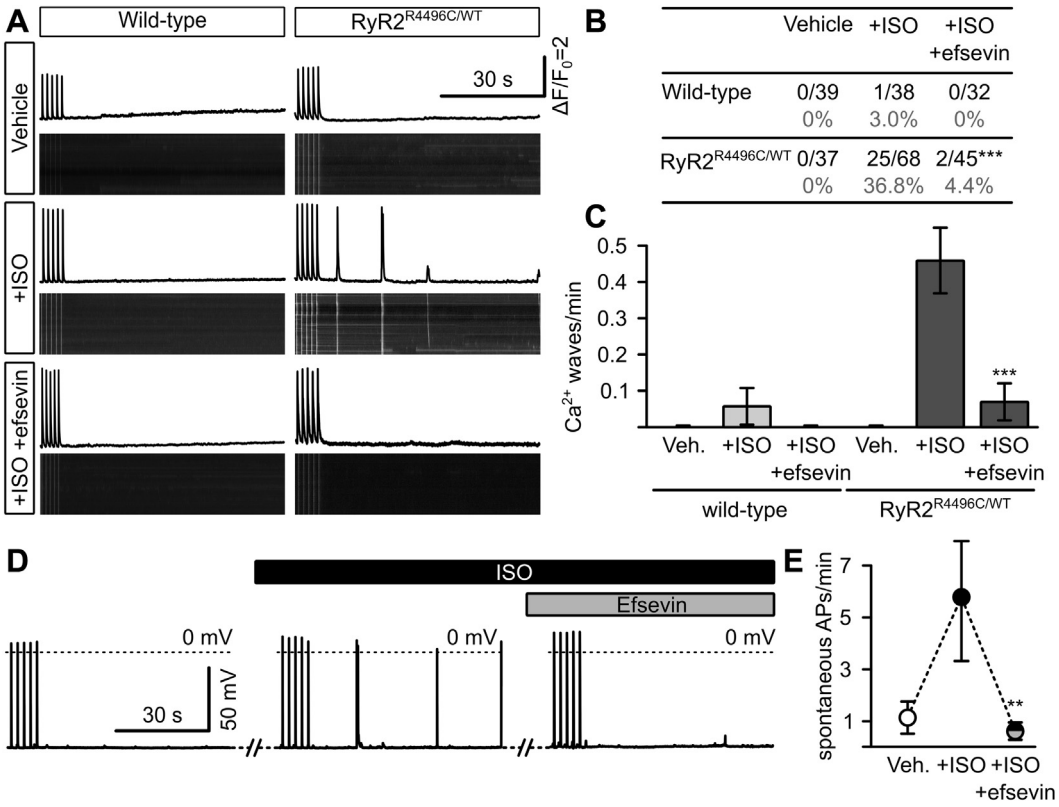

(A) Confocal line scans across the long axis of freshly isolated cardiomyocytes from wild-type and $RyR2^{R4496C/WT}$ mice loaded with Fluo-4 AM to measure intracellular Ca^{2+}. Images show line scans, and graphs depict fluorescence intensity plots. Cells were stimulated at 0.5 Hz for 30 s to reach steady state conditions (last 5 Ca^{2+} transients are shown) before pulsing was stopped and the diastolic phase was recorded for 90 s to screen for spontaneous diastolic Ca^{2+} waves. **(B)** While wild-type cells never showed a significant frequency of spontaneous diastolic Ca^{2+} waves, 25 of 68 $RyR2^{R4496C/WT}$ cardiomyocytes showed waves, which could be significantly reduced to 2 of 45 cells ($p < 0.001$, Fisher's exact test) by addition of 15 μM efsevin. **(C)** Average number of Ca^{2+} waves per minute was significantly enhanced from 0 in vehicle-treated $RyR2^{R4496C/WT}$ cardiomyocytes to 0.46 ± 0.09 waves/min in cells treated with 1 μM ISO ($p < 0.001$, Kruskal-Wallis test). Addition of 15 μM efsevin reduced the number of waves/minute to 0.07 ± 0.05 to levels indistinguishable from untreated cells ($p = 0.578$). **(D)** Patch clamp recordings from $RyR2^{R4496C/WT}$ cardiomyocytes showed an increase in spontaneous action potentials after superfusion with ISO, which were eliminated by addition of 15 μM efsevin. **(E)** Quantitative analysis of patch clamp recordings revealed a significant increase of spontaneous diastolic action potentials (APs) from 1.12 ± 0.62 APs/min under vehicle (Veh.) to 5.76 ± 2.45 APs/min after superfusion with ISO ($p = 0.018$, Friedman test, $n = 15$) and a significant reduction to 0.58 ± 0.34 APs/min when simultaneously treated with ISO and efsevin ($p = 0.011$). **$p < 0.01$; ***$p < 0.001$. ISO = isoproterenol.

Please see the detailed Methods in the Supplemental Appendix.

RESULTS

EFSEVIN REDUCES ARRHYTHMOGENIC Ca^{2+} WAVES IN $RyR2^{R4496C/WT}$ CARDIOMYOCYTES. The triggers for arrhythmia originating from imbalanced cellular Ca^{2+} homeostasis, such as CPVT, are intracellular Ca^{2+} waves during diastole, which arise from an increased SR Ca^{2+} leak through RyR2 (30). We therefore recorded diastolic Ca^{2+} waves in freshly isolated ventricular cardiomyocytes from $RyR2^{R4496C/WT}$ mice and their wild-type (WT) littermates. Under control conditions (vehicle), neither WT cardiomyocytes nor $RyR2^{R4496C/WT}$ cells showed spontaneous Ca^{2+} waves within 90 s after preceding electrical stimulation at 0.5 Hz. However, unlike WT cells, $RyR2^{R4496C/WT}$ cardiomyocytes displayed pronounced spontaneous, diastolic Ca^{2+} waves after stimulation with the catecholamine isoproterenol (ISO) (Figures 1A to 1C). Strikingly, application of 15 μM efsevin significantly reduced the number of cells displaying such Ca^{2+} waves and the average number of Ca^{2+} waves per

FIGURE 2 Efsevin Does Not Affect Beta-Adrenergic Stimulation in $RyR2^{R4496C/WT}$ Cardiomyocytes

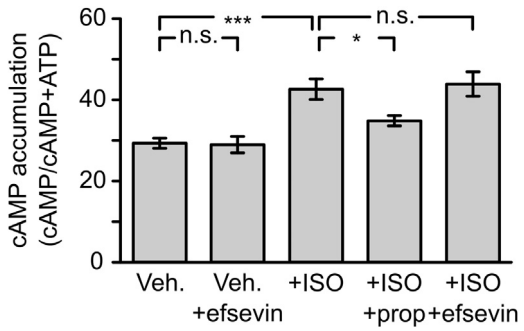

cAMP accumulation in freshly isolated $RyR2^{R4496C/WT}$ cardiomyocytes was measured in response to different stimuli. Efsevin had no effect on cellular cAMP levels ($p > 0.999$, Kruskal-Wallis test), whereas ISO induced a significant increase in cellular cAMP ($p < 0.001$). This increase could be blocked using the beta-adrenoreceptor blocker propranolol (prop) ($p = 0.036$), although efsevin had no effect on the ISO-induced increase in cellular cAMP ($p = 0.999$), indicating that efsevin neither activates nor blocks the beta-adrenergic system in cardiomyocytes. *$p < 0.05$; ***$p < 0.001$. Abbreviations as in Figure 1.

minute in $RyR2^{R4496C/WT}$ cardiomyocytes to levels of unstimulated $RyR2^{R4496C/WT}$ cells and WT cells. Notably, in contrast to previous data from unstimulated cells (15), efsevin did not exert any significant effects on the amplitude and kinetics of electrically evoked Ca^{2+} transients under ISO stimulation (Supplemental Figure 1).

EFSEVIN REDUCES SPONTANEOUS ACTION POTENTIALS IN $RyR2^{R4496C/WT}$ CARDIOMYOCYTES. Cardiac arrhythmia is triggered when Ca^{2+} waves activate the sarcolemmal sodium-calcium exchanger, leading to a transient depolarizing sodium inward current and finally spontaneous action potentials (31), which can propagate along the myocardium. Hence, we recorded spontaneous action potentials in patch-clamped $RyR2^{R4496C/WT}$ cardiomyocytes. We observed a significant increase in the frequency of spontaneous action potentials after cells were superfused with 1 μM ISO. Subsequent treatment with 15 μM efsevin effectively reduced these spontaneous depolarizations to baseline levels (**Figures 1D and 1E**). Notably, efsevin did not exert any effects on the resting membrane potential and amplitude of electrically evoked action potentials under ISO stimulation but caused a significant change of the repolarization phase (Supplemental Figure 1), namely a prolongation of the action potential duration at 50% repolarization (APD50) but not at 90% repolarization (APD90). To evaluate whether this effect seen on the fast, inactivating mouse action potential (32) could lead to QT prolongation in human cells, we recorded action potentials from human iPSC-derived cardiomyocytes in the presence of efsevin and found no changes in APD50 and APD90 compared to vehicle-treated cells (Supplemental Figures 2A and 2B). Furthermore, efsevin did not inhibit hERG channel activity in a heterologous expression system at relevant concentrations (Supplemental Figure 2C).

THE ANTIARRHYTHMIC EFFECT OF EFSEVIN IS MEDIATED BY MITOCHONDRIAL Ca^{2+} UPTAKE. We next investigated the mechanism of efsevin's antiarrhythmic effect. To exclude the possibility that efsevin directly blocks catecholaminergic stimulation by ISO, we measured cAMP accumulation in efsevin-treated $RyR2^{R4496C/WT}$ cardiomyocytes. Stimulation by ISO induced a significant increase in cellular cAMP, which was blocked by the beta-adrenoreceptor blocker propranolol. Addition of efsevin alone did not increase or decrease cellular cAMP concentrations, and addition of efsevin to stimulated cells had no effect on the ISO-induced cAMP increase, indicating that efsevin does not influence beta-adrenergic signaling in cardiomyocytes (**Figure 2**).

Efsevin significantly enhanced transfer of Ca^{2+} from the SR into mitochondria in a Ca^{2+} uptake assay in permeabilized cultured HL-1 cardiomyocytes. Mitochondrial Ca^{2+} was measured after addition of 10 mM caffeine to open RyR2s in the presence of the Ca^{2+} chelator BAPTA to restrict Ca^{2+} released from RyRs to the low micrometer range around RyR clusters (8,29) (**Figure 3A**). The efsevin-sensitive Ca^{2+} transfer between the SR and mitochondria was blocked by addition of the MCU blocker ruthenium red. To test whether the enhanced SR-mitochondria Ca^{2+} transfer was directly responsible for the reduction of diastolic Ca^{2+} wave frequency in $RyR2^{R4496C/WT}$ cardiomyocytes, we assessed whether blocking of mitochondrial Ca^{2+} uptake abolished the antiarrhythmic effect of efsevin. We measured catecholamine-induced Ca^{2+} waves in $RyR2^{R4496C/WT}$ myocytes under simultaneous blockade of mitochondrial Ca^{2+} uptake, using the MCU inhibitor Ru360 (**Figure 3B**). We observed a moderately higher Ca^{2+} wave frequency under all conditions, consistent with the idea that mitochondrial Ca^{2+} uptake prevents Ca^{2+} wave formation. Most strikingly, the ability of efsevin to suppress the ISO-induced increase in Ca^{2+} wave frequency was abolished in the presence of Ru360, indicating that the suppression of diastolic Ca^{2+} waves by efsevin is solely mediated by enhanced mitochondrial Ca^{2+} uptake.

FIGURE 3 Efsevin Acts Through Mitochondrial Ca^{2+} Uptake

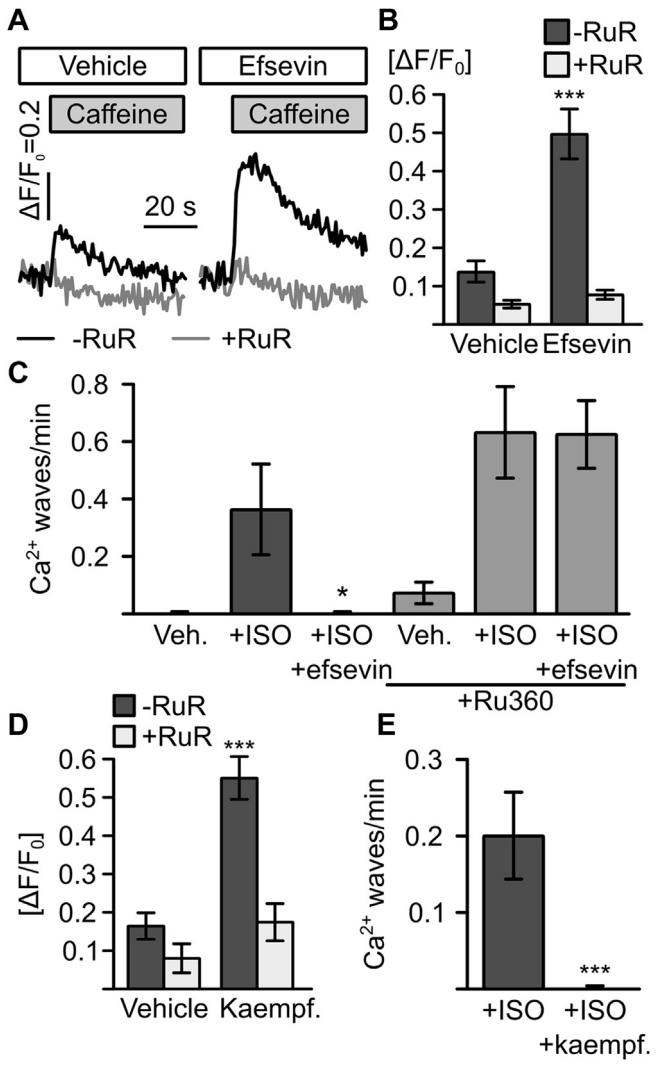

(A) Representative recordings of mitochondrial Ca^{2+} in permeabilized HL-1 cardiomyocytes. Superfusion with caffeine induced a rapid uptake of Ca^{2+} into mitochondria **(black trace)**, which was enhanced by 15 μM efsevin and blocked by 10 μM RuR **(gray trace)**. **(B)** Quantification of peak mitochondrial fluorescence showed a significant increase in mitochondrial Ca^{2+} uptake in cells treated with efsevin from $\Delta F/F_0 = 0.14 \pm 0.03$ ($n = 10$) to 0.50 ± 0.07 ($n = 19$, $p < 0.001$, ANOVA). **(C)** 15 μM efsevin reduces spontaneous propagating waves in $RyR2^{R4496C/WT}$ cardiomyocytes under ISO influence from 0.36 ± 0.16 waves/min ($n = 15$) to 0 **(black bars)** ($n = 21$, $p = 0.035$, Kruskal-Wallis test). In the presence of 8 μM of the mitochondrial Ca^{2+} uptake blocker Ru360, vehicle-treated cells showed 0.07 ± 0.04 waves/min ($n = 29$), which increased to 0.63 ± 0.16 under ISO influence ($n = 21$, $p < 0.001$) but could not be blocked with efsevin as shown by an indistinguishable value of 0.62 ± 0.12 waves/min under ISO influence together with efsevin **(gray bars)** ($n = 62$, $p = 0.354$ compared to that with ISO). **(D)** 10 μM of the MCU activator kaempferol significantly increased mitochondrial Ca^{2+} uptake after SR Ca^{2+} release from $\Delta F/F_0 = 0.16 \pm 0.04$ ($n = 9$) to 0.55 ± 0.05 ($n = 10$, $p < 0.001$, ANOVA) Ca^{2+} uptake was inhibited by 50 μM RuR **(gray bars)**. **(E)** Treatment of $RyR2^{R4496C/WT}$ cardiomyocytes with 10 μM kaempferol completely eliminated ISO-induced spontaneous diastolic Ca^{2+} waves from 0.19 ± 0.04 waves/min ($n = 49$) to 0 ($n = 45$; $p < 0.001$, Mann-Whitney *U* test). *$p < 0.05$; ***$p < 0.001$. $\Delta F/F_0$ = change in fluorescence over baseline fluorescence; MCU = mitochondrial Ca^{2+} uniporter; RuR = ruthenium red; SR = sarcoplasmic reticulum.

We next tested if enhancing mitochondrial Ca^{2+} uptake was a general pharmacological approach to suppress arrhythmogenic events or if it is limited to a specific effect of efsevin on VDAC2. To this purpose, we used another activator of mitochondrial Ca^{2+} uptake, the natural plant flavonoid kaempferol, which was reported to directly activate MCU in the inner mitochondrial membrane (33,34). Indeed, kaempferol increased SR-mitochondria Ca^{2+} transfer, comparable to efsevin (**Figure 3D**). To evaluate the antiarrhythmic potential of kaempferol, we measured diastolic Ca^{2+} waves in kaempferol-treated $RyR2^{R4496C/WT}$ cardiomyocytes under ISO to induce catecholaminergic stimulation. Strikingly, 10 μM kaempferol completely eliminated ISO-induced arrhythmogenic Ca^{2+} waves in $RyR2^{R4496C/WT}$ cardiomyocytes (**Figure 3E**).

It was previously reported that enhanced mitochondrial Ca^{2+} uptake in cardiomyocytes restricts diffusion of Ca^{2+} inside the cytosol (13) and thereby prevents propagation of cytosolic Ca^{2+} signals under conditions of Ca^{2+} overload (15). Because an enhanced RyR-mediated Ca^{2+} leak was reported to be the mechanism responsible for arrhythmogenesis in CPVT (35–37), we recorded Ca^{2+} sparks from $RyR2^{R4496C/WT}$ cardiomyocytes (**Figure 4**). We observed an increase in Ca^{2+} spark frequency and amplitude after treatment with ISO, consistent with previous work (36), thus explaining the enhanced Ca^{2+} wave frequency under catecholaminergic stimulation. Strikingly, the SR leak in cells treated with ISO together with efsevin was reduced compared to that in cells treated with ISO alone, as indicated by a decrease in Ca^{2+} spark frequency and amplitude. Also, we found removal of cytosolic Ca^{2+} was accelerated under efsevin stimulation, leading to a reduction of full width and full duration of Ca^{2+} sparks. Together, these effects explain the suppressive effect of efsevin on propagating Ca^{2+} waves.

MiCUps REDUCE EPISODES OF STRESS-INDUCED VENTRICULAR TACHYCARDIA IN VIVO. To assess the potency of both of the mitochondrial Ca^{2+} uptake enhancers (MiCUps), efsevin and kaempferol, to suppress arrhythmia in vivo, we administered efsevin and kaempferol to $RyR2^{R4496C/WT}$ mice, using implantable osmotic minipumps. All mice recovered well from surgery, and their behavior was grossly normal. Treated mice showed no signs of discomfort, stress, or abnormal behavior. After 3 days, efsevin and kaempferol showed no effect on electrocardiography (ECG) parameters such as the interval between atrial and ventricular depolarization (PR), the interval between ventricular depolarization and subsequent repolarization (QT), or conduction of ventricular

depolarization (QRS) and basal heart rate (Figures 5A and 5B). To activate their adrenergic response, we injected mice with a bolus of 2 mg/kg epinephrine and 120 mg/kg caffeine (epi/caff). The epi/caff injection induced a significant increase in heart rate in all 3 groups, but no differences were observed between vehicle-treated mice and mice treated with MiCUps. Most strikingly, both of the MiCUps significantly reduced episodes of bidirectional ventricular tachycardia under catecholaminergic stimulation. Injection of epi/caff provoked bidirectional ventricular tachycardia in all vehicle-treated control animals (n = 11) but only in 6 of 10 mice treated with efsevin and 6 of 11 mice treated with kaempferol (Figures 5D and 5E). Comparable results were obtained from mice treated with efsevin for 8 days (Supplemental Figure 3).

MiCUps REDUCE ARRHYTHMOGENIC Ca^{2+} WAVES IN iPSC-DERIVED CARDIOMYOCYTES FROM A CPVT PATIENT. In order to evaluate the translational potential of MiCUps for the treatment of CPVT, we used a human cell-based arrhythmia model for CPVT. Human iPSC-derived cardiomyocytes from a CPVT patient heterozygous for the $RyR2^{S406L}$ mutation associated with CPVT (26) were used to record arrhythmogenic Ca^{2+} waves, whereas cells obtained from a healthy 32-year-old female without history of cardiac disease served as control. In accordance with the CPVT phenotype, where patients show a normal ECG pattern under baseline conditions, only few untreated cells displayed Ca^{2+} waves (Figure 6), whereas beta-adrenergic stimulation induced by ISO led to a significant increase in diastolic Ca^{2+} waves in $RyR2^{S406L/WT}$ cells but did not induce Ca^{2+} waves in control cells. Treatment of $RyR2^{S406L}$ cells with either efsevin or kaempferol significantly reduced the number of cells displaying Ca^{2+} waves and the average frequency of Ca^{2+} waves per minute to baseline levels.

FIGURE 4 **Efsevin Reduces Intracellular Ca^{2+} Spark Frequency, Amplitude, and Cytosolic Ca^{2+} Clearance Leading to a Restriction of Individual Ca^{2+} Sparks**

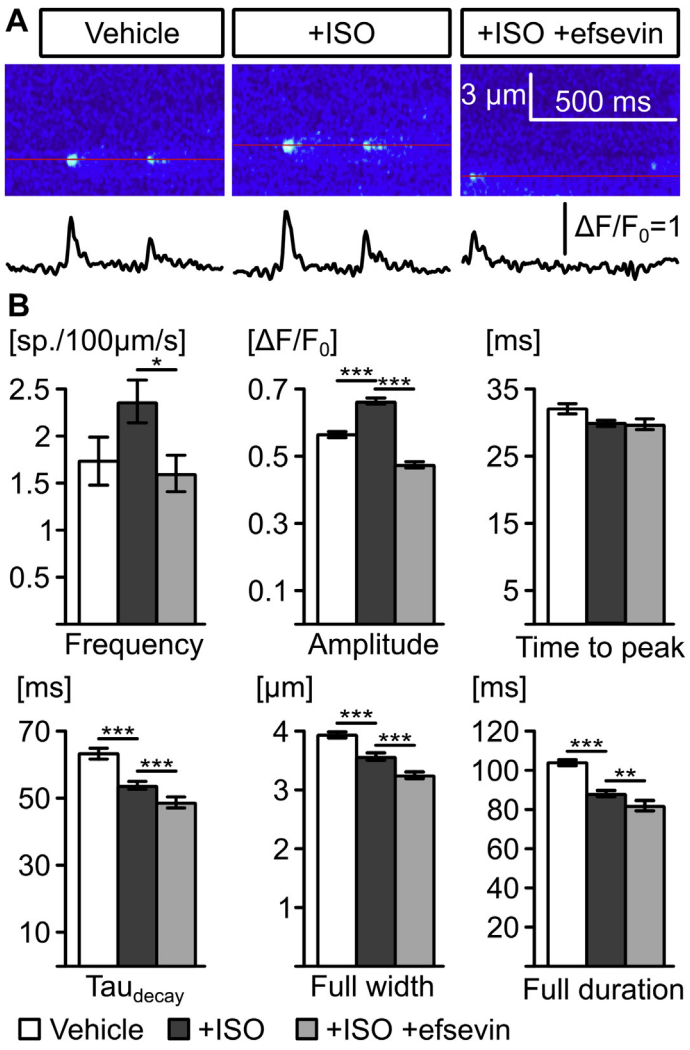

(A) Representative line scan confocal images from $RyR2^{R4496C/WT}$ cardiomyocytes show spontaneous Ca^{2+} sparks. **(B)** Treatment with ISO induced a higher spark frequency and amplitude and accelerated cytosolic Ca^{2+} removal (tau_{decay}) leading to narrower (full width) and shorter (full duration) sparks. Administration of efsevin reduced Ca^{2+} spark frequency ($p = 0.049$, Kruskal Wallis test) and amplitude ($p < 0.001$, Kruskal Wallis test) and limited spatial ($p < 0.001$, Kruskal Wallis test) and temporal ($p = 0.002$, Kruskal Wallis test) expansion of Ca^{2+} sparks. *$p < 0.05$; **$p < 0.01$; ***$p < 0.001$. Abbreviations as in Figure 1.

DISCUSSION

MITOCHONDRIA AS DRUG TARGETS. Mitochondria occupy approximately 30% of the cardiomyocyte volume (6,7). Although their crucial roles in ATP synthesis, regulation of respiratory rate, and apoptosis are well understood, mitochondrial contributions to cardiac Ca^{2+} handling are still under debate. While it is generally accepted that a gradual and moderate rise in mitochondrial Ca^{2+} enhances energy production (18), the role of a low-affinity/high-conductance, fast mitochondrial Ca^{2+} uptake remains unclear. Different experimental approaches suggest an immediate role for this uptake in the regulation of cardiomyocyte bioenergetics (38), contraction (39), and rhythmicity (15,21), but the potential of this rapid mitochondrial Ca^{2+} uptake mechanism to serve as a drug target in cardiovascular disease has not been sufficiently evaluated. It was proposed that inhibition of MCU by Ru360 ameliorates myocardial damage after ischemia reperfusion injury in rats, presumably by inhibiting depolarization of mitochondria and following opening of the mitochondrial permeability transition pore (40).

FIGURE 5 MiCUps Reduce Episodes of Ventricular Tachycardia in $RyR2^{R4496C/WT}$ Mice

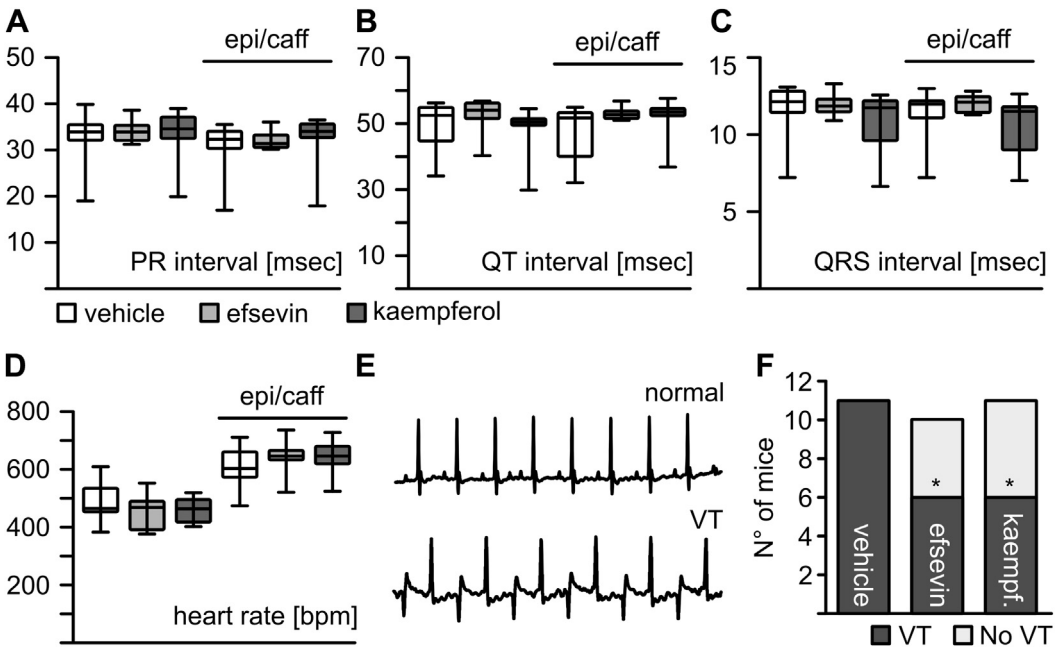

Three-lead surface ECGs from $RyR2^{R4496C/WT}$ mice receiving efsevin or kaempferol through an osmotic minipump are shown. After a baseline ECG was recorded, mice were injected with epi/caff as an adrenergic stimulus. Basic parameters of the ECG like PR **(A)**, QT **(B)**, and QRS **(C)** intervals were comparable between the vehicle-treated group and both of the MiCUp-treated groups at baseline and after epi/caff challenge (Kruskal-Wallis test). **(D)** Heart rate increased upon administration of epi/caff in all 3 groups but remained unaffected by the administration of MiCUps (Kruskal-Wallis test). **(E)** Examples of a normal ECG recording and a recording showing bidirectional ventricular tachycardia. **(F)** Episodes of bidirectional ventricular tachycardia were recorded in 11 of 11 vehicle-treated mice but were significantly reduced to 6 of 10 in mice with efsevin and 6 of 11 in mice with kaempferol ($p = 0.035$, Fisher's exact test). *$p < 0.05$. ECG = electrocardiography; epi/caff = epinephrine/caffeine; MiCUp = mitochondrial calcium uptake enhancer.

However, in healthy myocardium, the role of fast mitochondrial Ca^{2+} uptake remains elusive. Regarding arrhythmia, protective (22) as well as pro-arrhythmic (41) effects of activated mitochondria were discussed. We have recently identified the novel compound efsevin, which binds to the outer mitochondrial membrane VDAC2, enhances mitochondrial Ca^{2+} uptake, and restores rhythmic cardiac contractions in a zebrafish model for Ca^{2+}-induced cardiac arrhythmia (15). Here we show that enhancing mitochondrial Ca^{2+} uptake by using MiCUps efficiently suppresses arrhythmia in a murine and a human model of CPVT in vitro and in vivo. Our results establish pharmacological activation of rapid mitochondrial Ca^{2+} uptake as a novel preventive and therapeutic strategy against CPVT. We have previously shown that efsevin suppresses arrhythmia in cellular models for Ca^{2+} overload induced by high extracellular Ca^{2+} (15). Thus, due to their potent role of suppressing arrhythmogenic Ca^{2+} waves in both Ca^{2+} overload (15) and CPVT, it is conceivable that MiCUps may also be applied in other more common forms of Ca^{2+}-induced cardiac arrhythmias. These include arrhythmias in the setting of heart failure, which are triggered by cellular Ca^{2+} overload or atrial fibrillation, also linked to imbalances in cardiomyocyte Ca^{2+} handling (5). This study serves as a proof-of-principle, holding great promise for additional indications.

OPTIMIZED MiCUps. Our work shows that enhancing mitochondrial Ca^{2+} uptake efficiently reduces arrhythmia in experimental models of CPVT. In order to develop MiCUps toward human therapeutics, several steps of optimization must be taken. Candidate compounds need to be optimized to achieve a high affinity MiCUp with low side effects and suitable pharmacokinetics for application in human subjects. We show that the antiarrhythmic effect can be achieved by activation of at least 2 distinct target proteins within the mitochondrial Ca^{2+} uptake complex: efsevin, targeting VDAC2 in the outer mitochondrial membrane, and kaempferol, targeting MCU in the

FIGURE 6 MiCUps Reduce Spontaneous Ca^{2+} Waves in Human iPSC-derived Cardiomyocytes

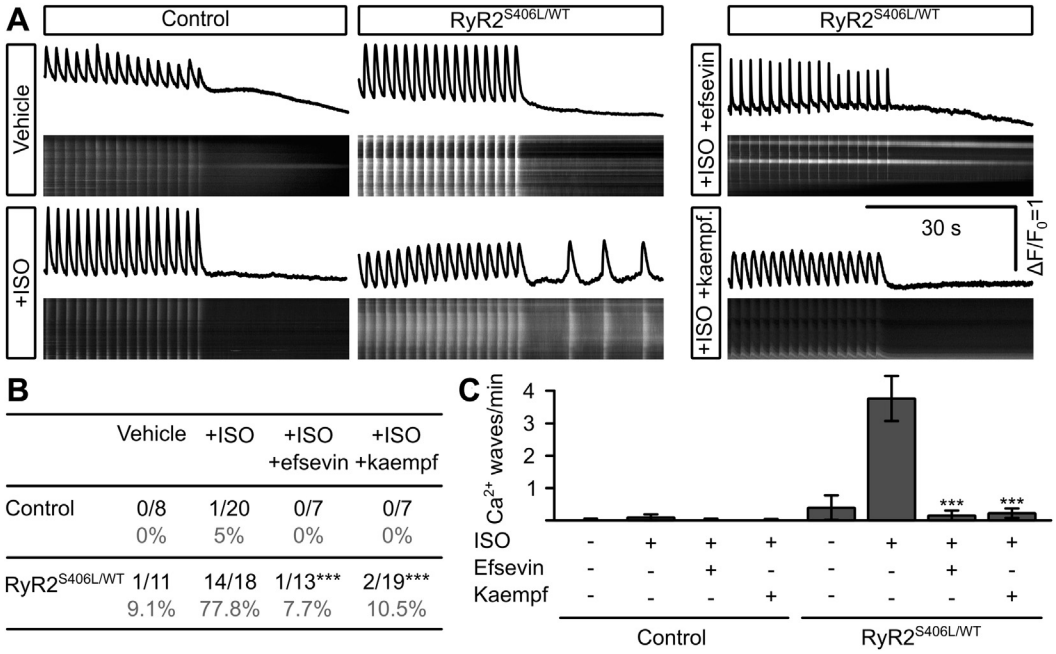

Confocal line scans of iPSC-derived human cardiomyocytes from a CPVT patient ($RyR2^{S406L/WT}$) and a healthy individual are shown (control). **(A)** Confocal line scans across iPSC-derived human cardiomyocytes loaded with Fluo-4 AM to measure intracellular Ca^{2+} and intensity plots show that stimulation with ISO does not induce spontaneous, diastolic Ca^{2+} waves in control cells but induced waves in $RyR2^{S406L/WT}$ cardiomyocytes. These waves can be blocked with either 15 μM efsevin **(upper right panel)** or 10 μM kaempferol **(lower right panel)**. **(B)** Quantitative analysis revealed a significant reduction in the number of $RyR2^{S406L/WT}$ cells showing ISO-induced Ca^{2+} waves upon treatment with MiCUps, to a level comparable to that of unstimulated cells (**asterisks** denote significance compared to $RyR2^{S406L/WT}$ +ISO by Fisher's exact test). **(C)** Quantification of waves/min reveal a significant reduction from 3.78 ± 0.72 waves/min in $RyR2^{S406L/WT}$ cardiomyocytes treated with ISO to levels indistinguishable from control after treatment with efsevin (0.15 ± 0.15; $p < 0.001$ compared to ISO: $p = 0.884$ compared to vehicle, Kruskal-Wallis test) or kaempferol, respectively (0.21 ± 0.14, $p < 0.001$ compared to ISO; $p = 0.980$ compared to vehicle, Kruskal-Wallis test). ***$p < 0.001$. CPVT = catecholaminergic polymorphic ventricular tachycardia; iPSC = induced pluripotent stem cell; other abbreviations as in Figure 1.

inner membrane. Suppression of arrhythmia is thus attributable to enhanced mitochondrial Ca^{2+} uptake and is independent of the molecular target protein within the fast mitochondrial Ca^{2+} uptake complex. Our work thus establishes the entire protein complex as a pharmacological target structure and allows for future optimization of this therapeutic concept through novel compounds and targets. Apart from VDAC2 and MCU, the auxiliary MCU regulators MICU1 and -2, MCUb, EMRE, and MCUR1 (16,17) may serve as future candidate targets.

SIDE EFFECTS. Mitochondrial Ca^{2+} uptake proteins such as VDAC2 and MCU are ubiquitously expressed. Regarding a therapeutic application, it is thus important to evaluate potential side effects of a MiCUp-based therapy. It is important to note that we did not observe any adverse effects of MiCUps in mice treated with efsevin or kaempferol for 3 to 8 consecutive days. Furthermore, kaempferol was previously used in animal experiments, and no adverse effects, even after up to 1 year of treatment or at high doses, were observed (42–44). However, further long-term experiments and large animal studies are needed to further evaluate safety of a MiCUp-based therapy. Although we did not observe changes in cytosolic Ca^{2+} in our experiments, long-term effects of enhanced mitochondrial Ca^{2+} uptake on a potential redistribution of cellular Ca^{2+} in the heart and other organs must be evaluated. Furthermore, because an enhanced mitochondrial Ca^{2+} uptake was observed to activate mitochondrial metabolism and reactive oxygen species production, special focus should be directed toward side effects related to changes in cellular bioenergetics.

Common side effects of actual antiarrhythmic drugs like Na^+, K^+, and Ca^{2+} channel blockers include

changes in cardiac electrophysiology like deceleration of cardiac de- or repolarization, the latter often expressed as a prolonged QT interval. We observed an effect of efsevin on the repolarization phase of the action potential in mice (Supplemental Figure 1), namely a prolongation of APD50 but not APD90. However, whereas repolarization in mice is carried mainly by fast potassium currents (I_{to}, $I_{K,\ slow}$), the human action potential displays a pronounced plateau phase, and phase 3 repolarization is carried predominantly by the delayed K^+ currents I_{Kr} and I_{ks} (32). To rule out the possibility that the observed prolongation of APD50 by efsevin in mice could be relevant for human therapy, we showed that efsevin does not influence action potential duration in human iPSC-derived cardiomyocytes and does not block hERG activity. It is thus conceivable that efsevin has a direct impact on the fast repolarizing currents in mice but does not influence the human action potential. Most importantly, however, we did not observe effects of MiCUp administration on ECG parameters like PR, QT, and QRS interval and heart rate in mice treated with MiCUps. Because MiCUps target intracellular structures to suppress the generation of ectopic depolarizations and do not influence the cardiac action potential, they might be less prone to severe side effects like, for example, the typical pro-arrhythmic effects observed with class I or III antiarrhythmic drugs. However, the murine repertoire of ion channels governing the cardiac action potential of mice varies from the human one, and additional experiments in other mammalian species are needed to solve this issue.

CONCLUSIONS

Common antiarrhythmic drugs aim at inhibiting expansion of ectopic activity and display perilous side effects. Because major arrhythmias are often associated with imbalanced intracellular Ca^{2+} homeostasis (3–5), intracellular Ca^{2+} transporters are attractive candidates for newer and safer therapies. Here we show that enhancing mitochondrial Ca^{2+} uptake by pharmacological agonists of the mitochondrial Ca^{2+} uptake proteins VDAC2 and MCU efficiently suppresses arrhythmia in a murine and a human model for CPVT. Our data establish MiCUps as attractive compounds for a novel preventive and therapeutic strategy to treat Ca^{2+}-triggered cardiac arrhythmias.

ACKNOWLEDGEMENTS The authors thank Brigitte Mayerhofer for technical assistance and Petra Eigner, Monika Mittermeier, and Clarinda Hofer and the staff of the Institute for Biomedical Research of the Medical University of Graz for animal husbandry.

ADDRESS FOR CORRESPONDENCE: Dr. Johann Schredelseker, Walther Straub Institute of Pharmacology and Toxicology, Ludwig-Maximilians-Universität München Nußbaumstrasse 26, D-80336 München, Germany. E-mail: johann.schredelseker@lmu.de.

PERSPECTIVES

COMPETENCY IN MEDICAL KNOWLEDGE: Mitochondria regulate cardiac rhythmicity. Pharmacological activation of mitochondrial Ca^{2+} uptake by MiCUps suppresses arrhythmogenesis in murine and human iPSC-based models for catecholaminergic polymorphic ventricular tachycardia.

TRANSLATIONAL OUTLOOK 1: Optimization of compounds and a careful investigation on pharmacokinetics and drug metabolism are needed to develop a potential MiCUp-based human therapy.

TRANSLATIONAL OUTLOOK 2: Additional experiments using models of other Ca^{2+}-triggered arrhythmias could further expand the application range of MiCUps.

REFERENCES

1. Mozaffarian D, Benjamin EJ, Go AS, et al. Heart disease and stroke statistics-2016 update. Circulation 2016;133:e38–360.

2. Mehra R. Global public health problem of sudden cardiac death. J Electrocardiol 2007;40: S118–22.

3. Bers DM. Calcium and cardiac rhythms: physiological and pathophysiological. Circ Res 2002;90: 14–7.

4. Choi B-R, Burton F, Salama G. Cytosolic Ca^{2+} triggers early afterdepolarizations and Torsade de Pointes in rabbit hearts with type 2 long QT syndrome. J Physiol 2002;543:615–31.

5. Greiser M, Lederer WJ, Schotten U. Alterations of atrial Ca^{2+} handling as cause and consequence of atrial fibrillation. Cardiovasc Res 2011;89:722–33.

6. Barth E, Stämmler G, Speiser B, Schaper J. Ultrastructural quantitation of mitochondria and myofilaments in cardiac muscle from 10 different animal species including man. J Mol Cell Cardiol 1992;24:669–81.

7. Kim H-D, Kim CH, Rah Bb-J, Chung H-I, Shim T-S. Quantitative study on the relation between structural and functional properties of the hearts from three different mammals. Anat Rec 1994;238: 199–206.

8. Szalai G, Csordás G, Hantash BM, Thomas AP, Hajnóczky G. Calcium signal transmission between ryanodine receptors and mitochondria. J Biol Chem 2000;275:15305–13.

9. Dorn GW, Maack C. SR and mitochondria: calcium cross-talk between kissing cousins. J Mol Cell Cardiol 2013;55:42–9.

10. Kirichok Y, Krapivinsky G, Clapham DE. The mitochondrial calcium uniporter is a highly selective ion channel. Nature 2004; 427:360–4.

11. Baughman JM, Perocchi F, Girgis HS, et al. Integrative genomics identifies MCU

as an essential component of the mitochondrial calcium uniporter. Nature 2011;476:341–5.

12. De Stefani D, Raffaello A, Teardo E, Szabò I, Rizzuto R. A forty-kilodalton protein of the inner membrane is the mitochondrial calcium uniporter. Nature 2011;476:336–40.

13. Subedi KP, Kim J-C, Kang M, Son M-J, Kim Y-S, Woo S-H. Voltage-dependent anion channel 2 modulates resting Ca^{2+} sparks, but not action potential-induced Ca^{2+} signaling in cardiac myocytes. Cell Calcium 2011;49:136–43.

14. Min CK, Yeom DR, Lee K-E, et al. Coupling of ryanodine receptor 2 and voltage-dependent anion channel 2 is essential for Ca^{2+} transfer from the sarcoplasmic reticulum to the mitochondria in the heart. Biochem J 2012;447:371–9.

15. Shimizu H, Schredelseker J, Huang J, et al. Mitochondrial Ca^{2+} uptake by the voltage-dependent anion channel 2 regulates cardiac rhythmicity. Elife 2015;4.

16. Jhun BS, Mishra J, Monaco S, et al. The mitochondrial Ca^{2+} uniporter: regulation by auxiliary subunits and signal transduction pathways. Am J Physiol Cell Physiol 2016;311:C67–80.

17. Marchi S, Pinton P. The mitochondrial calcium uniporter complex: molecular components, structure and physiopathological implications. J Physiol 2014;592:829–39.

18. Brandes R, Bers DM. Intracellular Ca^{2+} increases the mitochondrial NADH concentration during elevated work in intact cardiac muscle. Circ Res 1997;80:82–7.

19. Williams GSB, Boyman L, Chikando AC, Khairallah RJ, Lederer WJ. Mitochondrial calcium uptake. Proc Natl Acad Sci U S A 2013;110:10479–86.

20. O'Rourke B, Blatter LA. Mitochondrial Ca^{2+} uptake: tortoise or hare? J Mol Cell Cardiol 2009;46:767–74.

21. Seguchi H, Ritter M, Shizukuishi M, et al. Propagation of Ca^{2+} release in cardiac myocytes: role of mitochondria. Cell Calcium 2005;38:1–9.

22. Zhao Z, Gordan R, Wen H, Fefelova N, Zang W-J, Xie L-H. Modulation of intracellular calcium waves and triggered activities by mitochondrial ca flux in mouse cardiomyocytes. PLoS One 2013;8:e80574.

23. Priori SG, Napolitano C, Tiso N, et al. Mutations in the cardiac ryanodine receptor gene (hRyR2) underlie catecholaminergic polymorphic ventricular tachycardia. Circulation 2001;103:196–200.

24. Cerrone M, Colombi B, Santoro M, et al. Bidirectional ventricular tachycardia and fibrillation elicited in a knock-in mouse model carrier of a mutation in the cardiac ryanodine receptor. Circ Res 2005;96:e77–82.

25. O'Connell TD, Rodrigo MC, Simpson PC. Isolation and culture of adult mouse cardiac myocytes. Methods Mol Biol 2007;357:271–96.

26. Jung CB, Moretti A, Mederos y Schnitzler M, et al. Dantrolene rescues arrhythmogenic RYR2 defect in a patient-specific stem cell model of catecholaminergic polymorphic ventricular tachycardia. EMBO Mol Med 2012;4:180–91.

27. Moretti A, Bellin M, Welling A, et al. Patient-specific induced pluripotent stem-cell models for long-QT syndrome. N Engl J Med 2010;363:1397–409.

28. Claycomb WC, Lanson NA, Stallworth BS, et al. HL-1 cells: a cardiac muscle cell line that contracts and retains phenotypic characteristics of the adult cardiomyocyte. Proc Natl Acad Sci U S A 1998;95:2979–84.

29. Sharma VK, Ramesh V, Franzini-Armstrong C, Sheu SS. Transport of Ca^{2+} from sarcoplasmic reticulum to mitochondria in rat ventricular myocytes. J Bioenerg Biomembr 2000;32:97–104.

30. Paavola J, Viitasalo M, Laitinen-Forsblom PJ, et al. Mutant ryanodine receptors in catecholaminergic polymorphic ventricular tachycardia generate delayed afterdepolarizations due to increased propensity to Ca^{2+} waves. Eur Heart J 2007;28:1135–42.

31. Allen DG, Eisner DA, Orchard CH. Characterization of oscillations of intracellular calcium concentration in ferret ventricular muscle. J Physiol 1984;352:113–28.

32. Nerbonne JM, Nichols CG, Schwarz TL, Escande D. Genetic manipulation of cardiac K^+ channel function in mice: what have we learned, and where do we go from here? Circ Res 2001;89:944–56.

33. Montero M, Lobatón CD, Hernández-Sanmiguel E, et al. Direct activation of the mitochondrial calcium uniporter by natural plant flavonoids. Biochem J 2004;384:19–24.

34. Vay L, Hernández-Sanmiguel E, Santo-Domingo J, et al. Modulation of Ca^{2+} release and Ca^{2+} oscillations in HeLa cells and fibroblasts by mitochondrial Ca^{2+} uniporter stimulation. J Physiol 2007;580:39–49.

35. Jiang D, Xiao B, Zhang L, Chen SRW. Enhanced basal activity of a cardiac Ca^{2+} release channel (ryanodine receptor) mutant associated with ventricular tachycardia and sudden death. Circ Res 2002;91:218–25.

36. Fernández-Velasco M, Rueda A, Rizzi N, et al. Increased Ca^{2+} sensitivity of the ryanodine receptor mutant $RyR2^{R4496C}$ underlies catecholaminergic polymorphic ventricular tachycardia. Circ Res 2009;104:201–9.

37. Sedej S, Heinzel FR, Walther S, et al. Na^+-dependent SR Ca^{2+} overload induces arrhythmogenic events in mouse cardiomyocytes with a human CPVT mutation. Cardiovasc Res 2010;87:50–9.

38. Tomar D, Dong Z, Shanmughapriya S, et al. MCUR1 Is a scaffold factor for the MCU complex function and promotes mitochondrial bioenergetics. Cell Rep 2016;15:1673–85.

39. Drago I, De Stefani D, Rizzuto R, Pozzan T. Mitochondrial Ca^{2+} uptake contributes to buffering cytoplasmic Ca^{2+} peaks in cardiomyocytes. Proc Natl Acad Sci U S A 2012;109:12986–91.

40. García-Rivas G, de J, Carvajal K, Correa F, Zazueta C. Ru360, a specific mitochondrial calcium uptake inhibitor, improves cardiac post-ischaemic functional recovery in rats in vivo. Br J Pharmacol 2006;149:829–37.

41. Xie W, Santulli G, Reiken SR, et al. Mitochondrial oxidative stress promotes atrial fibrillation. Sci Rep 2015;5:11427.

42. Song H, Bao J, Wei Y, et al. Kaempferol inhibits gastric cancer tumor growth: An in vitro and in vivo study. Oncol Rep 2014;33:868–74.

43. Montero M, de la Fuente S, Fonteriz RI, Moreno A, Alvarez J. Effects of long-term feeding of the polyphenols resveratrol and kaempferol in obese mice. PLoS One 2014;9:e112825.

44. Shih T-Y, Young T-H, Lee H-S, Hsieh C-B, Hu OY-P. Protective effects of kaempferol on isoniazid- and rifampicin-induced hepatotoxicity. AAPS J 2013;15:753–62.

KEY WORDS CPVT, MCU, MiCUp, mitochondria, RyR2, VDAC2

APPENDIX For expanded Methods section as well as supplemental figures, please see the online version of this article.

Appendix 5: Sander P., et al. (2020) Approved drugs ezetimibe and disulfiram enhance mitochondrial Ca^{2+} uptake and suppress cardiac arrhythmogenesis, *submitted*

Sander P., Arduino D., Schweitzer M. K., Wilting F., Gutenthaler S., Dreizehnter L., Moretti A., Gudermann T., Perocchi F., and Schredelseker J. (2020) Approved drugs ezetimibe and disulfiram enhance mitochondrial Ca^{2+} uptake and suppress cardiac arrhythmogenesis, *submitted*

Approved drugs ezetimibe and disulfiram enhance mitochondrial Ca^{2+} uptake and suppress cardiac arrhythmogenesis

Paulina Sander[1], Daniela Arduino[2], Maria K. Schweitzer[1], Fabiola Wilting[1], Sophie M. Gutenthaler[1], Lisa Dreizehnter[3], Annette Nicke[1], Alessandra Moretti[3,4] Thomas Gudermann[1,4], Fabiana Perocchi[2,5,§], Johann Schredelseker[1,§]

[1] Walther Straub Institute of Pharmacology and Toxicology, Faculty of Medicine, LMU Munich, Munich, Germany.
[2] Institute for Diabetes and Obesity, Helmholtz Diabetes Center (HDC), Helmholtz Zentrum München, 85764 Neuherberg, Germany.
[3] First Department of Medicine, Cardiology, Klinikum rechts der Isar, Technische Universität München, Munich, Germany.
[4] Deutsches Zentrum für Herz-Kreislauf-Forschung, Partner Site Munich Heart Alliance, Munich, Germany.
[5] Munich Cluster for Systems Neurology, 81377 Munich, Germany.

[§] To whom correspondence should be addressed: johann.schredelseker@lmu.de; fabiana.perocchi@helmholtz-muenchen.de

Abstract

Efficacy and safety of common antiarrhythmic drugs are still limited due to perilous side effects. We previously demonstrated that pharmacological enhancement of mitochondrial Ca^{2+} uptake in cardiomyocytes represents a promising candidate strategy for safer treatment of cardiac arrhythmia. However, agonists of mitochondrial Ca^{2+} uptake are still limited. Here we screened a library of FDA and EMA approved drugs and identified ezetimibe and disulfiram as novel mitochondrial Ca^{2+} uptake enhancers (MiCUps). Both compounds were effective in stimulating mitochondrial Ca^{2+} uptake at significantly lower concentrations than previous activators such as kaempferol and the VDAC2 gating modifier efsevin. Importantly, both significantly suppressed arrhythmogenesis in a zebrafish Ca^{2+} overload model as well as in murine and human cardiomyocytes harboring mutations associated with human ventricular tachycardia. Our results establish ezetimibe and disulfiram as promising candidates for preclinical and clinical studies to evaluate the potential of MiCUps for treatment of cardiac arrhythmia.

Introduction

While mortality and morbidity rates related to cardiovascular diseases are generally declining, arrhythmia-related incidents are still on the rise (Benjamin *et al*, 2018). This is in part related to limited effectiveness and major side effects of common antiarrhythmic drugs. Antiarrhythmic drugs of Vaughan Williams class I, III, and IV act by targeting plasma membrane ion channels and suppressing propagation of ectopic signals. However, due to their effects on the cardiac action potential and thus cardiac conduction speed, they are prone to proarrhythmic side effects. Therefore, novel therapeutic strategies that suppress the initiation of arrhythmogenic signals inside cardiomyocytes are currently in focus of the search for novel and safer antiarrhythmic therapies.

We have recently demonstrated an important role of mitochondrial Ca^{2+} (mt-Ca^{2+}) uptake for the regulation of cardiac rhythmicity (Shimizu *et al*, 2015). The cardiac contraction cycle is initiated by influx of extracellular Ca^{2+} into cardiomyocytes and subsequent Ca^{2+} release predominantly from the sarcoplasmic reticulum (SR) to initiate muscle contraction (Bers, 2002, 2008). Mitochondria are located in close proximity to the SR (Rog-Zielinska *et al*, 2016) and can rapidly take up Ca^{2+} on a beat-to-beat interval (Robert *et al*, 2001) through a selective mitochondrial Ca^{2+} uptake pathway (MCUP) consisting of pore proteins in both mitochondrial membranes and several positive and negative regulators (Kirichok *et al*, 2004; Baughman *et al*, 2011; Waldeck-Weiermair *et al*, 2013; De Stefani *et al*, 2011). Under pathological conditions, erratic Ca^{2+} release during diastole leads to spontaneous contractions and arrhythmia (Allen *et al*, 1984). Pharmacological activation of mt-Ca^{2+} uptake locally buffers these events and thereby suppresses arrhythmogenic signals in cardiomyocytes, while systolic events remain unaltered (Shimizu *et al*, 2015). Indeed, treatment with agonists of mt-Ca^{2+} uptake suppressed episodes of arrhythmia in a murine model for catecholaminergic polymorphic ventricular tachycardia (CPVT) (Schweitzer *et al*, 2017). Modulation of mt-Ca^{2+} uptake could thus serve as novel pharmacological strategy for the treatment of human cardiac arrhythmias.

This can be accomplished by agonists of either the voltage-dependent anion channel 2 (VDAC2) in the outer mitochondrial membrane or the mitochondrial Ca^{2+} uniporter (MCU) in the inner mitochondrial membrane. Two such compounds, the VDAC2 gating modulator efsevin (Shimizu *et al*, 2015; Wilting *et al*, 2020) and the MCU agonist kaempferol (Montero *et al*, 2004) respectively, were found to be effective in reducing arrhythmia, thus providing a proof of concept that mitochondrial Ca^{2+} uptake enhancers (MiCUps) represent a pharmacologically highly relevant class of molecules. However, both drugs are so far only used experimentally and are currently too poorly characterized for having clinical potential. Furthermore, both are effective at concentrations around 10-20 μM at the target site *in-vitro* making them poor candidates for clinical use.

Here we screened a chemical library consisting of ~700 compounds with a history of use in human clinical trials for novel MiCUps. We identified two FDA and EMA approved drugs, ezetimibe and disulfiram, which significantly increased mt-Ca^{2+} uptake in permeabilized HeLa cells and SR-mitochondria Ca^{2+} transfer in cardiomyocytes. Both drugs exerted their effect at significantly lower concentrations than efsevin and kaempferol. Most importantly, both suppressed cardiac fibrillation in zebrafish embryos and arrhythmogenic Ca^{2+} signals in murine and human cardiomyocytes carrying mutations associated with CPVT. Altogether, we identified two highly interesting candidates for further preclinical and clinical testing of MiCUp-based antiarrhythmic therapy.

Material and Methods

Primary drug screen in permeabilized HeLa cells.

Drug screening was performed as described previously (Arduino *et al*, 2017). Briefly, HeLa cells stably expressing a mitochondrial matrix-targeted aequorin (AEQ_{mt}) were grown in Dulbecco's modified Eagle's medium (DMEM) with high-glucose (Sigma-Aldrich), 10% FBS (Sigma-Aldrich) and 100 µg/ml geneticin (Life Technologies; 10131019). On the day of the experiment, active aequorin was reconstituted from apoaequorin in the mitochondrial matrix by incubating cells with 3 µM coelenterazine derivative n (Biotium) for 3 hr at room temperature. Then, Ca^{2+} was depleted from intracellular stores by incubation with 200 nM thapsigargin (VWR) for 20 min and cells were permeabilized with 60 µM digitonin (Sigma-Aldrich) for 5 min. Experiments were performed in an intracellular-like buffer containing (in mM) 140 KCl, 1 KH_2PO_4/K_2HPO_4, 1 $MgCl_2$, 20 HEPES, 1 Na^+-pyruvate, 1 ATP/$MgCl_2$, 2 Na^+-succinate and 0.1 EGTA as a Ca^{2+} chelator (pH 7.2 with KOH) at a density of ~70,000 cells/well in a white 96-well compound plate. The NIH Clinical Collection library, consisting of ~700 compounds (10 µM, in 0.1% (v/v) DMSO) was screened in biological duplicates. DMSO (0.1%) was used as a vehicle control and Ru360 (10 µM, VWR), a classical inhibitor of MCU, was used as an experimental control to prove that aequorin luminescence is selective for MCU-mediated mitochondrial Ca^{2+} uptake. Permeabilized cells were incubated in the presence of compounds for 5 min at room temperature and Ca^{2+}-stimulated light signals upon a bolus application of 4 µM free Ca^{2+} was recorded at 469 nm every 0.1 s with a luminescence counter (MicroBeta^2 LumiJET Microplate Counter, PerkinElmer). Drug screens were analyzed as described previously (Arduino *et al*, 2017). Briefly, after smoothing the dynamics of mt-Ca^{2+}-dependent luminescence obtained for each compound, both peak (maximal amplitude of the luminescence signal) and uptake rate (left slope) were automatically determined. Based on these parameters a score (S_{drug}) was assigned to each compound as shown in Figure 1. Compounds were considered as MiCUps when S_{drug} was higher than 2,5.

SR-mitochondria Ca^{2+} transfer.

Ca^{2+} transfer from the SR into mitochondria was measured as described in Schweitzer et al. (Schweitzer *et al*, 2017). In brief, HL-1 cardiomyocytes (Claycomb *et al*, 1998) were plated in a 96-well plate, loaded with Rhod-2, AM and permeabilized with 100 mM digitonin in internal solution (in mM: 1 BAPTA, 20 HEPES, 100 L-Aspartic acid potassium salt, 40 KCl, 0.5 $MgCl_2$, 2 maleic acid, 2 glutamic acid, 5 pyruvic acid, 0.5 KH_2PO_4, 5 MgATP, and 0.46 $CaCl_2$, (pH=7.2 with KOH). Fluorescence at Ex= 540±9 nm and Em= 580±20 nm was recorded on an Infinite® 200 PRO multimode reader (Tecan, Maennedorf, Switzerland). After 22 sec caffeine was injected to a final concentration of 10 mM.

Cytosolic Ca^{2+} measurements on HL-1 cardiomcyocytes

For the measurement of Ca^{2+} release, HL-1 cells were loaded with 5 µM fura-2, AM for 1h at 37°C, before washing with external solution (in mM: 140 NaCl, 6 Kcl, 2 $CaCl_2$, 1 $MgCl_2$, 10 glucose, 20 HEPES, pH=7.4 with NaOH). After 30 min incubation to allow for total de-esterification of the dye, cells were washed and measured in an Infinite® 200 PRO multimode reader (Tecan, Maennedorf, Switzerland) at Ex= 340±9 nm and 380±9 nm and Em=510±20 nm. Test compounds were added 5 minutes prior to the experiment. Caffeine to a final concentration of 10 mM was added 22 sec after start of the recording. EC50 values were calculated using Quest Graph™ EC50 Calculator (AAT Bioquest, Inc.) at https://www.aatbio.com/tools/ec50-calculator.

Isolation of ventricular cardiomyocytes from $RyR2^{R4496C/WT}$ mice.

Ventricular cardiomyocytes of 8–16 weeks old mice were isolated by retrograde perfusion through the aorta as described previously (O'Connell *et al*, 2007; Schweitzer *et al*, 2017). After cervical dislocation, the heart was excised and placed on a Langendorff mode perfusion system. Tissue was digested by perfusion with Liberase™ TM (Roche Diagnostics, Penzberg, Germany) at a final concentration of 0.075 mg/ml for 6 min. After mechanical separation of the ventricles by trituration, cardiomyocytes were consecutively transferred into Tyrode's solution with 0.1, 0.5, and finally 1 mM $CaCl_2$ to reintroduce physiological Ca^{2+} concentrations. Only excitable, rod-shaped, quiescent cells were used for experiments.

Human iPSC cardiomyocytes.

Human iPSCs from a from a 60-year-old male donor presenting with a severe form of CPVT and control cells from a 32-year-old female Caucasian without history of cardiac disease scheduled for plastic surgery were generated as described previously (Moretti *et al*, 2010). Spontaneously beating areas were explanted after 2-5 months and enzymatically dissociated into single cardiomyocytes. Single cells were plated on fibronectin-coated glass bottom dishes (MatTek, Ashland, MA, USA) and used for experiments at approximately 7 days after dissociation (Schweitzer *et al*, 2017). Human iPSC generation was performed under a human research subject protocol approved by the institutional review boards and the ethic committee of the Klinikum rechts der Isar, Technical University of Munich. Written informed consent was obtained from the affected patient and healthy volunteer.

Confocal Ca^{2+} imaging.

Ca^{2+} waves were analyzed by confocal microscopy as described previously (Schweitzer *et al*, 2017). In brief, cardiomyocytes were loaded with 1 µM Fluo-4, AM (Thermo Fisher, Germany) and Ca^{2+} transients were elicited by electric field stimulation using a S48 square pulse Stimulator (Grass Technologies, Warwick, RI, USA) on an inverted confocal microscope (Leica TCS SP5 or Zeiss LSM 880). Line scan series were generated along the long axis of a myocyte. After reaching steady-state, pulsing was stopped and cells were analyzed for the occurrence of spontaneous diastolic Ca^{2+} waves.

Zebrafish husbandry and phenotype rescue experiments

Zebrafish of the mutant line TG(myl7:eGFP)/*tremblor* (*tre*^{tc318}) were maintained and bred as described elsewhere (Westerfield, 2000). Embryos collected from heterozygous *tre* crosses were kept in E3 buffer (in mM: 5 NaCl, 0.33 $MgSO_4$, 0.17 KCl, 0.33 $CaCl_2$) and exposed to the substances starting at 6 hours post fertilization (hpf). Embryos were dechorionated with 30 µg/ml protease from *Streptomyces griseus* at 26 hpf and cardiac function was analyzed at 30 hpf by visual examination of the embryonic hearts under a fluorescence stereomicroscope (Euromex DZ5040).

Statistical analysis

Data are presented as mean ± SEM. Normality of data was determined by Shapiro-Wilk test, and tests for statistical significance were conducted as indicated. Post hoc tests were Dunn's test for Kruskal-Wallis tests and Tukey's multiple comparisons test for ANOVA. (*$p< 0.05$; **$p< 0.01$, and ***$p< 0.001$).

Results

Screening for novel MiCUps

Since pharmacological enhancement of mt-Ca^{2+} uptake can prevent arrhythmogenesis in cardiomyocytes (Shimizu *et al*, 2015; Schweitzer *et al*, 2017), but agonists of mt-Ca^{2+} uptake are still scarce and experimental, we set out screen for novel, potent MiCUps for preclinical and clinical testing. We have previously developed a permeabilized HeLa cell-based screening approach for the identification of small molecule inhibitors of mt-Ca^{2+} uptake and successfully identified effective compounds (Arduino *et al*, 2017). Here we applied this screening approach for the identification of enhancers and screened the NIH Clinical Collection (NCC) consisting of ~700 compounds with a history of use in human clinical trials. Drug effects on luminescence-based mt-Ca^{2+} dynamics were quantified by scoring each drug at 10 µM (S_{drug}) based on its effect on the light peak when compared to vehicle (DMSO) and experimental (Ru360) controls (**Fig. 1A**). Compounds were then selected as MiCUps if they exerted at least a 2.5-fold increase in mt-Ca^{2+} level (**Fig. 1B**). Four hits, which had never been linked to mt-Ca^{2+} homeostasis before, were obtained and further investigated. Those included the bioactive biphenolic phytochemical honokiol, the antimicrobial cephalosporine cefatrizine, the cholesterol uptake inhibitor ezetimibe, and disulfiram, a drug used to treat chronic alcoholism. Their effect was further validated by analysis of the dose dependency of the mt-Ca^{2+} uptake over a wider range of concentrations (**Fig. 1C**). This revealed dose-dependent enhancement for honokiol, ezetimibe and disulfiram but not for cefatrizine which was thus considered as a false positive hit from the primary screen.

Ezetimibe and disulfiram enhance SR-mitochondria Ca^{2+} transfer in cardiomyocytes

In cardiomyocytes a specialized mechanism of SR-mitochondria Ca^{2+} transfer was recently described involving a tight coupling between the ryanodine receptor (RyR), VDAC2 and MCU (Min *et al*, 2012; De la Fuente *et al*, 2016). Because this direct SR-mitochondria Ca^{2+} transfer was proposed to be the molecular prerequisite for the antiarrhythmic effect of MiCUps (Shimizu *et al*, 2015; Schweitzer *et al*, 2017; Wilting *et al*, 2020), we tested the potential of the newly identified MiCUps ezetimibe, disulfiram and honokiol to specifically enhance SR-mitochondria Ca^{2+} transfer in permeabilized HL-1 cardiomyocytes (Claycomb *et al*, 1998; Schweitzer *et al*, 2017). Rapid mitochondrial uptake of Ca^{2+} released from the SR by a caffeine pulse was significantly enhanced by ezetimibe and disulfiram and reached maximum values of $\Delta F/F_0$=0.41±0.04 at 50 nM for ezetimibe and 0.37±0.04 at 100 nM for disulfiram compared to 0.14±0.01 in vehicle-treated control cells, while no significant effect of

honokiol could be observed (**Fig. 2A,B**). Strikingly, generation of dose-response curves revealed that the two active substances, ezetimibe and disulfiram, enhanced mt-Ca^{2+} uptake at markedly lower concentrations (ezetimibe: EC_{50}=25.5 nM, disulfiram: EC_{50}=36.8 nM) compared to the established MiCUps, the MCU activator kaempferol (Montero *et al*, 2004) (EC_{50}=3.9 µM) and the VDAC2 modifier efsevin (Wilting *et al*, 2020) (EC_{50}=2.9 µM). To exclude a putative false-positive result due to a potential effect of ezetimibe and/or disulfiram on SR Ca^{2+} release we next measured cytosolic Ca^{2+} levels in intact ezetimbe- and disulfiram-treated HL-1 cardiomyocytes using fura-2 and analyzed basal Ca^{2+} levels and Ca^{2+} release after superfusion with 10 mM caffeine (**Fig. 2C**). We observed a baseline fura-2 fluorescence ratio ($R_{340nm/380nm}$) of 0.75±0.01 for vehicle-treated cells, 0.72±0.01 for cells treated with 1µM ezetimibe and 0.79±0.01 for cells treated with 1 µM disulfiram. Release of Ca^{2+} from the SR induced a change in fluorescence (ΔR) of 1.07±0.05 for vehicle-treated cells, 1.02±0.05 for cells treated with 1 µM ezetimibe and 0.97±0.05 for cells treated with 1 µM disulfiram (**Fig. 2C**). In conclusion, the above data indicates that both, ezetimibe and disulfiram, specifically enhance mt-Ca^{2+} uptake in HL-1 cardiomyocytes without affecting baseline cytosolic Ca^{2+} levels or SR Ca^{2+} release and have significantly lower EC_{50} values then the established MiCUps kaempferol and efsevin.

Ezetimibe and disulfiram suppress arrhythmia in a zebrafish model of Ca^{2+}-overload induced arrhythmia

We recently demonstrated that zebrafish embryos of the transgenic line *tremblor* (*tre^{tc318}*), lacking a cardiac isoform of the sodium-calcium exchanger NCX, represent a suitable *in-vivo* model for Ca^{2+} overload-induced cardiac arrhythmia (Shimizu *et al*, 2015). Homozygous *tre* embryos display a hypercontracted heart that shows only chaotic contractions within the myocardium (Langenbacher *et al*, 2005). This phenotype can be rescued by treatment with efsevin (Shimizu *et al*, 2015). We therefore tested the newly identified MiCUps ezetimibe and disulfiram for their potential to restore rhythmic cardiac contractions in this model (**Fig. 3A**). Addition of 0.1 µM ezetimibe restored rhythmic cardiac contractions in 35.1±6.8% of *tre* embryos (p=0.001 compared to vehicle) and this value was increased to 53.9±3.2% at 1 µM (p<0.001 compared to vehicle) (**Fig. 3B**). However, treatment with up to 10 µM ezetimibe did not further enhance this rescue. In agreement with the dose-response curves in HL-1 cardiomcyocytes slightly higher concentrations of disulfiram were needed to obtain a similar phenotype rescue in *tre* embryos. While 0.1 µM disulfiram did not induce a significant effect, 43.2±5% of embryos displayed synchronized contractions at 1 µM (p<0.001 compared to vehicle) and 60.1±9.4% at 5 µM (p<0.001 compared to vehicle). However, zebrafish embryos treated with disulfiram showed signs of intoxication such as a lack of pigmentation and a disturbed morphology, which was not

observed in ezetimibe-treated embryos (**Fig. 3C**). Taken together, low μM concentrations of both drugs can efficiently restore rhythmic cardiac contractions in *tre* embryos but disulfiram appears to have toxic effects at effective concentrations above 1μM.

Ezetimibe and disulfiram suppress arrhythmogenesis in cardiomyocytes of a murine tachycardia model

We next tested both compounds in isolated cardiomyocytes of a murine model for CPVT (Cerrone *et al*, 2005). Freshly isolated cardiomyocytes from $RyR^{R4496C/WT}$ mice were loaded with fluo-4 and analyzed on a confocal microscope for the occurrence of diastolic Ca^{2+} waves, the most indicative measure for arrhythmogenesis in cardiomyocytes (**Fig. 4A**). These Ca^{2+} waves originate from the spontaneous release of Ca^{2+} through mutated RyRs and represent the origin of ectopic cardiac excitations that cause arrhythmia (Allen *et al*, 1984). Consistent with the phenotype of CPVT, these events became only detectable after treatment of cardiomyocytes with the β-adrenoreceptor agonist isoproterenol (ISO) and occured at a rate of 0.61±0.08 waves/min. Both MiCUps dose-dependently reduced the number of Ca^{2+} waves to levels comparable to unstimulated cells, i.e. 0.05±0.03 waves/min for ezetimibe and 0.26±0.16 waves/min for disulfiram at 1 μM (**Fig. 4B**). Interestingly, and comparable to our zebrafish data, disulfiram displayed toxic effects at higher concentrations (10 μM) reflected by an elevation of basal cytosolic Ca^{2+} levels. Cells treated with 10 μM disulfiram showed very high fluo-4 fluorescence (51.5±4.8FU compared to 15.3±0.5FU under ISO alone) and extensive spontaneous activity, which prevented further analysis (**Supplementary Fig. 1**).

To confirm that this striking effect in CPVT cardiomyocytes is solely attributable to the enhanced mt-Ca^{2+} uptake induced by the two MiCUps we crossbred RyR^{R4496C} mice with $MCU^{-/-}$ mice, which lack the central pore forming subunit of the MCU complex (Pan *et al*, 2013). Strikingly, application of the highest effective doses, 10 μM ezetimibe and 1 μM disulfiram, on isolated $RyR^{R4496C/WT}/MCU^{-/-}$ cardiomyocytes failed to reduce Ca^{2+} waves in both cases (**Fig. 4C**), indicating that the MCUP is the effective target of ezetimibe and disulfiram.

Apart from diastolic Ca^{2+} waves, systolic Ca^{2+} activity was suggested as a potential trigger for arrhythmia in CPVT (Němec *et al*, 2010, 2016). We therefore also analyzed systolic Ca^{2+} transients of our recordings for the occurrence of secondary systolic Ca^{2+}-elevations (SSCEs) and found that both, ezetimibe and disulfiram significantly reduced SSCEs (**Fig. 4D, E**). A clear dose-dependence was observed for ezetimibe, however, higher concentrations of disulfiram induced higher spontaneous Ca^{2+} activity, which might again be attributed to the enhanced baseline Ca^{2+} observed under disulfiram (**Supplementary Fig. 1**).

Ezetimibe and disulfiram suppress arrhythmogenesis in human iPSC-induced CPVT cardiomyocytes

Finally, we tested both substances for their ability to suppress arrhythmogenic Ca^{2+} waves in human cells to estimate the translatability of our data and the potential of ezetimibe and disulfiram to serve as candidates for a human therapy (**Fig. 5**). To this aim, we used iPSC-derived cardiomyocytes from a CPVT patient. Comparable to murine CPVT cells, addition of ISO induced prominent Ca^{2+} waves in iPSC-derived cardiomyocytes from the CPVT patient (**Fig. 5A, B**) but not in cells from a healthy control (**Fig. 5B**). Strikingly, in CPVT cells addition of ezetimibe and disulfiram reduced Ca^{2+} waves from 5.87±1.80 under ISO alone to 0.10±0.07 under ezetimibe ($p<0.01$) and 0.05±0.05 under disulfiram ($p<0.01$), respectively.

Discussion

MiCUp screen

We have previously demonstrated that the VDAC2 agonist efsevin as well as the MCU agonist kaempferol potently suppress arrhythmia in murine and human models of CPVT (Shimizu *et al*, 2015; Schweitzer *et al*, 2017). However, in regard of a clinical application of these substances, it is of note that both enhance SR-mitochondria Ca^{2+} transfer with an EC_{50} of around 5 µM, a concentration that is likely to favor off-target effects. Furthermore, data concerning efsevin's bioavailability, pharmacodynamics, stability, and toxicity are largely missing. Though kaempferol was used in clinical studies before, it was only used at low dose and as a nutritional supplement and was shown to bind multiple targets including the NF-κB (Kadioglu *et al*, 2015), the fibroblast growth factor (Lee *et al*, 2018), and other signaling pathways (Yao *et al*, 2014; Kim *et al*, 2015; Wu *et al*, 2017).

Altogether, these data establish the MCUP as a promising candidate target for future preclinical and clinical testing to develop a human antiarrhythmic therapy, but efsevin and kaempferol represent poor candidates for clinical use. The MCUP has been intensively studied over the past decade and several studies have already identified effective blockers of MCU (Woods & Wilson, 2020; Nathan *et al*, 2017; Di Marco *et al*, 2020; Kon *et al*, 2017; Arduino & Perocchi, 2018), while agonists still remain scarce. We therefore screened the NIH Clinical Collection (NCC) consisting of ~700 compounds with a history of use in human clinical trials to identify novel specific enhancers of mt-Ca^{2+} uptake. Three compounds, honokiol, disulfiram, and ezetimibe were selected as hits based on their stimulatory effect on mt-Ca^{2+} uptake in primary drug screens as well as dose-dependent measurements in permeabilized HeLa cells.

We then further tested these compounds for their ability to selectively enhance the transfer of Ca^{2+} from the SR into mitochondria in cardiomyocytes as the mechanism proposed to be the molecular

prerequisite for the antiarrhythmic effect of MiCUps (Shimizu *et al*, 2015; Schweitzer *et al*, 2017; Wilting *et al*, 2020). Interestingly, honokiol, which displayed the most pronounced effects in HeLa cells, was inactive in this system, while ezetimibe and disulfiram consistently enhanced mt-Ca^{2+} uptake and were further tested for their antiarrhythmogenic potential in translational models.

Taken together we successfully identified two novel, potent MiCUps by applying a combination of a HeLa-based chemical screening followed by cardiomyocyte-specific target validation. These novel enhancers are candidates for the use in further preclinical and eventually clinical tests on the efficacy of MiCUps for the treatment of cardiac arrhythmia, but also valuable compounds for further basic research on the MCUP and preclinical research for other indications. Enhancing mt-Ca^{2+} uptake was recently suggested to be beneficial to facilitate cerebral blood flow after traumatic brain injury (Murugan *et al*, 2016) and to promote metabolism/secretion coupling in type 2 diabetes (Bermont *et al*, 2020).

Cardiac selectivity of novel MiCUps

In this and previous studies we successfully applied MiCUps on different models from cell cultures to *in vivo* systems, but never observed gross effects on other tissues than the heart (Shimizu *et al*, 2015; Schweitzer *et al*, 2017). It has been proposed that, although most components of the MCUP are ubiquitously expressed throughout the organism, tissue selectivity is determined by composition and subcellular localization of individual components and channel subunits. Here, we observed differences in drug effects between cell types. For example, honokiol was active in HeLa cells, but did not show activity in HL-1 cardiomyocytes. Furthermore, the ezetimibe and disulfiram concentrations needed to activate mt-Ca^{2+} uptake significantly vary between the two systems. A possible explanation could be differences in tissue-specific MCU activity (Fieni *et al,* 2012), MCUP composition (Patron *et al*, 2019; Raffaello *et al*, 2013) or physiological adaption (Lambert *et al*, 2019). Since the target protein of the identified MiCUps within the MCUP remains elusive, it is conceivable that the MCUP in cardiac cells lacks the component required for honokiol binding or that this component is only present at a very low level. *Vice-versa* it is possible that the specific mt-Ca^{2+} complex composition that is present in cardiomyocytes is a better target for ezetimibe and disulfiram. Alternatively, different subcellular localization of MCUP components in the two cell types might account for the observed differences. By using caffeine as a trigger and BAPTA in the intracellular solution, we specifically analyze local transfer of Ca^{2+} from the SR into mitochondria in HL-1 cardiomyocytes. In contrast, global addition of 4 µM Ca^{2+} was used as a trigger in HeLa cells. Since both channels of the MCUP, VDAC2 and MCU, preferentially accumulate in areas of the mitochondrion which interact with the SR (De la Fuente *et al*,

2016; De La Fuente *et al*, 2018; Min *et al*, 2012) and the concentration of Ca^{2+} released from the SR reaches concentrations of up to 1mM in close vicinity to the Ca^{2+} release sites, this could explain why lower concentrations of ezetimibe and disulfiram are active in cardiomyocytes. Finally, the existence of two different MCU subpopulations with distinct subunit composition and Ca^{2+} sensitivity, one in the SR-mitochondria interface and one outside these junctions could account for the system-dependent activities. Such subpopulations could be established to differentiate between local and global Ca^{2+} signals. In this scenario, honokiol might only target the latter population, while ezetimbe and disulfiram are more selective for the SR-associated population.

The discussed differences in composition and localization of the different MCUP components could thus explain the observed cardio-selectivity of MiCUps. Therefore, MiCUps could act as specific enhancers of mt-Ca^{2+} uptake in the heart, while being relatively inert in other tissues. However, future studies are needed to evaluate this hypothesis. The identified substances from this study might serve as tools to address these questions.

Novel MiCUps for preclinical and clinical testing

We identified two compounds, ezetimibe and disulfiram, which enhance mt-Ca^{2+} uptake at significantly lower concentrations than efsevin and kaempferol and could thus serve as candidate drugs for preclinical and eventually clinical trials on the efficacy of MiCUps for the treatment of cardiac arrhythmia. In contrast to common antiarrhythmic drugs, which target ion channels in the cell membrane and thereby modulate the cardiac action potential to suppress propagation of ectopic signals, MiCUps act intracellularly by inhibiting the generation of arrhythmogenic triggers. Due to this mechanism of action, which does not directly interfere with the cardiac action potential, MiCUps are expected to be less prone to proarrhythmic side effects than commonly used antiarrhythmic drugs of Vaughan Williams class I, III, and IV. Both, ezetimibe and disulfiram, are FDA and EMA approved and currently in use. Ezetimibe is used as a blocker of the Niemann-Pick C1-like 1 (NPC1L1) (Garcia-Calvo *et al*, 2005) protein in epithelial cells of the small intestine to reduce uptake of cholesterol. It is thus already used for the prevention and treatment of cardiovascular disease. Although ezetimbe is well-tolerated, it is however not first-line therapy, due to a lower efficiency compared to the commonly used statins. Ezetimibe is membrane permeable (Alhayali *et al*, 2018), orally bioavailable, and plasma concentrations reach a maximum approx. 2 hours after intake. It is enterohepatically metabolized (Kosoglou *et al*, 2005). However, plasma concentrations needed to activate mt-Ca^{2+} uptake remain to be determined.

Disulfiram is an inhibitor of acetaldehyde dehydrogenase and is used for the treatment of alcohol abuse, but serious side effects limit the use of the drug. Most relevant to our findings, previous preclinical studies already demonstrated an antiarrhythmic potential of disulfiram (Fossa & Carlson, 1983; Fossa *et al*, 1982), which might now be explained by activation of mt-Ca^{2+} uptake. However, disulfiram also induced severe malformations in zebrafish and led to enhanced Ca^{2+} activity during diastole. This might at least in part be explained by a direct destabilizing effect of disulfiram on the RyR during diastole, which would be in agreement with a recently identified modulatory effect of disulfiram on the skeletal muscle isoform RyR1 (Rebbeck *et al*, 2017). Finally, disulfiram was shown to release Ca^{2+} from mitochondria at higher concentrations (Chávez *et al*, 1989). Therefore, further investigations on drug efficacy and safety are definitely needed for the use of disulfiram.

Taken together, we have identified two novel MiCUps that are already in clinical use. However, before clinical tests for the treatment of human arrhythmia can be performed with these substances, additional studies on their routes of administration, effective *in-vivo* concentrations, and efficacy in the prevention or acute treatment of arrhythmia need to be determined.

Acknowledgments

The authors thank Brigitte Mayrhofer and Shuyue Zhang for technical assistance. This work was supported by the Deutsche Forschungsgesellschaft DFG SCHR 1471/1-1 to J.S and Transregio Research Unit 152 (to A.M., T.G.); the Munich Center for Systems Neurology (SyNergy EXC 2145 / ID 390857198 to F.P.); The Bert L & N Kuggie Vallee Foundation (to F.P. and D.M.A.), the ‘ExNet-0041-Phase2-3 („SyNergy-HMGU“)‘ through the Initiative and Network Fund of the Helmholtz Association (to F.P.).

References

Alhayali A, Selo MA, Ehrhardt C & Velaga S (2018) Investigation of supersaturation and in vitro permeation of the poorly water soluble drug ezetimibe. *Eur. J. Pharm. Sci.* **117:** 147–153

Allen DG, Eisner DA & Orchard CH (1984) Characterization of oscillations of intracellular calcium concentration in ferret ventricular muscle. *J. Physiol.* **352:** 113–28

Arduino DM & Perocchi F (2018) Pharmacological modulation of mitochondrial calcium homeostasis. *J. Physiol.* **596:** 2717–2733

Arduino DM, Wettmarshausen J, Vais H, Navas-Navarro P, Cheng Y, Leimpek A, Ma Z, Delrio-Lorenzo A, Giordano A, Garcia-Perez C, Médard G, Kuster B, García-Sancho J, Mokranjac D, Foskett JK, Alonso MT & Perocchi F (2017) Systematic Identification of MCU Modulators by Orthogonal Interspecies Chemical Screening. *Mol. Cell* **67:** 711–723.e7

Baughman JM, Perocchi F, Girgis HS, Plovanich M, Belcher-Timme CA, Sancak Y, Bao XR, Strittmatter L, Goldberger O, Bogorad RL, Koteliansky V & Mootha VK (2011) Integrative genomics identifies MCU as an essential component of the mitochondrial calcium uniporter. *Nature* **476:** 341–5

Benjamin EJ, Virani SS, Callaway CW, Chamberlain AM, Chang AR, Cheng S, Chiuve SE, Cushman M, Delling FN, Deo R, de Ferranti SD, Ferguson JF, Fornage M, Gillespie C, Isasi CR, Jiménez MC, Jordan LC, Judd SE, Lackland D, Lichtman JH, et al (2018) Heart Disease and Stroke Statistics—2018 Update: A Report From the American Heart Association. *Circulation* **137:** e67–e492

Bermont F, Hermant A, Benninga R, Chabert C, Jacot G, Santo-Domingo J, Kraus MR-C, Feige JN & De Marchi U (2020) Targeting Mitochondrial Calcium Uptake with the Natural Flavonol Kaempferol, to Promote Metabolism/Secretion Coupling in Pancreatic β-cells. *Nutrients* **12:** 538

Bers DM (2002) Cardiac excitation-contraction coupling. *Nature* **415:** 198–205

Bers DM (2008) Calcium cycling and signaling in cardiac myocytes. *Annu. Rev. Physiol.* **70:** 23–49

Cerrone M, Colombi B, Santoro M, di Barletta MR, Scelsi M, Villani L, Napolitano C & Priori SG (2005) Bidirectional ventricular tachycardia and fibrillation elicited in a knock-in mouse model carrier of a mutation in the cardiac ryanodine receptor. *Circ. Res.* **96:** e77-82

Chávez E, Zazueta C & Bravo C (1989) Extensive Ca2+ release from energized mitochondria induced by disulfiram. *J. Bioenerg. Biomembr.* **21:** 335–45

Claycomb WC, Lanson NA, Stallworth BS, Egeland DB, Delcarpio JB, Bahinski A & Izzo NJ (1998) HL-1 cells: a cardiac muscle cell line that contracts and retains phenotypic characteristics of the adult cardiomyocyte. *Proc. Natl. Acad. Sci. U. S. A.* **95:** 2979–84

Fieni F, Lee SB, Jan YN & Kirichok Y (2012) Activity of the mitochondrial calcium uniporter varies greatly between tissues. *Nat. Commun.* **3:** 1317

Fossa AA & Carlson GP (1983) Antiarrhythmic Effect of Disulfiram in Various Cardiotoxic Models. *Pharmacology* **26:** 164–171 Available at: http://www.ncbi.nlm.nih.gov/pubmed/6836004 [Accessed October 29, 2018]

Fossa AA, White JF & Carlson GP (1982) Antiarrhythmic effects of disulfiram on epinephrine-induced cardiac arrhythmias in rabbits exposed to trichloroethylene. *Toxicol. Appl. Pharmacol.* **66:** 109–17

Garcia-Calvo M, Lisnock J, Bull HG, Hawes BE, Burnett DA, Braun MP, Crona JH, Davis HR, Dean DC, Detmers PA, Graziano MP, Hughes M, MacIntyre DE, Ogawa A, O'Neill KA, Iyer SPN, Shevell DE, Smith MM, Tang YS, Makarewicz AM, et al (2005) The target of ezetimibe is Niemann-Pick C1-Like 1 (NPC1L1). *Proc. Natl. Acad. Sci.* **102:** 8132–8137

Kadioglu O, Nass J, Saeed MEM, Schuler B & Efferth T (2015) Kaempferol Is an Anti-Inflammatory Compound with Activity towards NF-κB Pathway Proteins. *Anticancer Res.* **35:** 2645–50

Kim SH, Park JG, Lee J, Yang WS, Park GW, Kim HG, Yi Y-S, Baek K-S, Sung NY, Hossen MJ, Lee M, Kim J-H & Cho JY (2015) The Dietary Flavonoid Kaempferol Mediates Anti-Inflammatory Responses via the Src, Syk, IRAK1, and IRAK4 Molecular Targets. *Mediators Inflamm.* **2015:** 1–15

Kirichok Y, Krapivinsky G & Clapham DE (2004) The mitochondrial calcium uniporter is a highly selective ion channel. *Nature* **427:** 360–4

Kon N, Murakoshi M, Isobe A, Kagechika K, Miyoshi N & Nagayama T (2017) DS16570511 is a small-molecule inhibitor of the mitochondrial calcium uniporter. *Cell death Discov.* **3:** 17045

Kosoglou T, Statkevich P, Johnson-Levonas AO, Paolini JF, Bergman AJ & Alton KB (2005) Ezetimibe: a review of its metabolism, pharmacokinetics and drug interactions. *Clin. Pharmacokinet.* **44:** 467–94

De la Fuente S, Fernandez-Sanz C, Vail C, Agra EJ, Holmstrom K, Sun J, Mishra J, Williams D, Finkel T, Murphy E, Joseph SK, Sheu SS & Csordás G (2016) Strategic positioning and biased activity of the mitochondrial calcium uniporter in cardiac muscle. *J. Biol. Chem.* **291:**

De La Fuente S, Lambert JP, Nichtova Z, Fernandez Sanz C, Elrod JW, Sheu S-S & Csordás G (2018) Spatial Separation of Mitochondrial Calcium Uptake and Extrusion for Energy-Efficient Mitochondrial Calcium Signaling in the Heart. *Cell Rep.* **24:** 3099–3107.e4

Lambert JP, Luongo TS, Tomar D, Jadiya P, Gao E, Zhang X, Lucchese AM, Kolmetzky DW, Shah NS & Elrod JW (2019) MCUB Regulates the Molecular Composition of the Mitochondrial Calcium Uniporter Channel to Limit Mitochondrial Calcium Overload During Stress. *Circulation* **140:** 1720–1733

Langenbacher AD, Dong Y, Shu X, Choi J, Nicoll DA, Goldhaber JI, Philipson KD & Chen J-N (2005) Mutation in sodium-calcium exchanger 1 (NCX1) causes cardiac fibrillation in zebrafish. *Proc. Natl. Acad. Sci. U. S. A.* **102:** 17699–704

Lee C-J, Moon S-J, Jeong J-H, Lee S, Lee M-H, Yoo S-M, Lee HS, Kang HC, Lee JY, Lee WS, Lee H-J, Kim E-K, Jhun J-Y, Cho M-L, Min J-K & Cho Y-Y (2018) Kaempferol targeting on the fibroblast growth factor receptor 3-ribosomal S6 kinase 2 signaling axis prevents the development of rheumatoid arthritis. *Cell Death Dis.* **9:** 401

Di Marco G, Vallese F, Jourde B, Bergsdorf C, Sturlese M, De Mario A, Techer-Etienne V, Haasen D, Oberhauser B, Schleeger S, Minetti G, Moro S, Rizzuto R, De Stefani D, Fornaro M & Mammucari C (2020) A High-Throughput Screening Identifies MICU1 Targeting Compounds. *Cell Rep.* **30:** 2321–2331.e6

Min CK, Yeom DR, Lee K-E, Kwon H-K, Kang M, Kim Y-S, Park ZY, Jeon H & Kim DH (2012) Coupling of ryanodine receptor 2 and voltage-dependent anion channel 2 is essential for Ca^{2}+ transfer from the sarcoplasmic reticulum to the mitochondria in the heart. *Biochem. J.* **447:** 371–9

Montero M, Lobatón CD, Hernández-Sanmiguel E, Santodomingo J, Vay L, Moreno A & Alvarez J (2004) Direct activation of the mitochondrial calcium uniporter by natural plant flavonoids. *Biochem. J.* **384:** 19–24

Moretti A, Bellin M, Welling A, Jung CB, Lam JT, Bott-Flügel L, Dorn T, Goedel A, Höhnke C, Hofmann F, Seyfarth M, Sinnecker D, Schömig A & Laugwitz K-L (2010) Patient-specific induced pluripotent stem-cell models for long-QT syndrome. *N. Engl. J. Med.* **363:** 1397–409

Murugan M, Santhakumar V & Kannurpatti SS (2016) Facilitating Mitochondrial Calcium Uptake Improves Activation-Induced Cerebral Blood Flow and Behavior after mTBI. *Front. Syst. Neurosci.* **10:**

Nathan SR, Pino NW, Arduino DM, Perocchi F, MacMillan SN & Wilson JJ (2017) Synthetic Methods for the Preparation of a Functional Analogue of Ru360, a Potent Inhibitor of Mitochondrial Calcium Uptake. *Inorg. Chem.* **56:** 3123–3126

Němec J, Kim JJ, Gabris B & Salama G (2010) Calcium oscillations and T-wave lability precede ventricular arrhythmias in acquired long QT type 2. *Hear. Rhythm* **7:** 1686–94

Němec J, Kim JJ & Salama G (2016) The link between abnormal calcium handling and electrical instability in acquired long QT syndrome - Does calcium precipitate arrhythmic storms? *Prog. Biophys. Mol. Biol.* **120:** 210–21

O'Connell TD, Rodrigo MC & Simpson PC (2007) Isolation and culture of adult mouse cardiac myocytes. *Methods Mol. Biol.* **357:** 271–96

Pan X, Liu J, Nguyen TT, Liu C, Sun J, Teng Y, Fergusson MM, Rovira II, Allen M, Springer DA, Aponte AM, Gucek M, Balaban RS, Murphy E & Finkel T (2013) The physiological role of mitochondrial calcium revealed by mice lacking the mitochondrial calcium uniporter. *Nat. Cell Biol.* **15:** 1464–72

Patron M, Granatiero V, Espino J, Rizzuto R & De Stefani D (2019) MICU3 is a tissue-specific enhancer of mitochondrial calcium uptake. *Cell Death Differ.* **26:** 179–195

Raffaello A, De Stefani D, Sabbadin D, Teardo E, Merli G, Picard A, Checchetto V, Moro S, Szabò I & Rizzuto R (2013) The mitochondrial calcium uniporter is a multimer that can include a dominant-negative pore-forming subunit. *EMBO J.* **32:** 2362–76

Rebbeck RT, Essawy MM, Nitu FR, Grant BD, Gillispie GD, Thomas DD, Bers DM & Cornea RL (2017) High-throughput screens to discover small-molecule modulators of ryanodine receptor calcium release channels. *SLAS Discov.* **22:** 176–186

Robert V, Gurlini P, Tosello V, Nagai T, Miyawaki A, Di Lisa F & Pozzan T (2001) Beat-to-beat oscillations of mitochondrial [Ca2+] in cardiac cells. *EMBO J.* **20:** 4998–5007

Rog-Zielinska EA, Johnston CM, O'Toole ET, Morphew M, Hoenger A & Kohl P (2016) Electron tomography of rabbit cardiomyocyte three-dimensional ultrastructure. *Prog. Biophys. Mol. Biol.* **121:** 77–84

Schweitzer MK, Wilting F, Sedej S, Dreizehnter L, Dupper NJ, Tian Q, Moretti A, My I, Kwon O, Priori SG, Laugwitz K-L, Storch U, Lipp P, Breit A, Mederos y Schnitzler M, Gudermann T & Schredelseker J (2017) Suppression of Arrhythmia by Enhancing Mitochondrial Ca 2+ Uptake in Catecholaminergic Ventricular Tachycardia Models. *JACC Basic to Transl. Sci.* **2:** 737–746

Shimizu H, Schredelseker J, Huang J, Lu K, Naghdi S, Lu F, Franklin S, Fiji HD, Wang K, Zhu H, Tian C, Lin B, Nakano H, Ehrlich A, Nakai J, Stieg AZ, Gimzewski JK, Nakano A, Goldhaber JI, Vondriska TM, et al (2015) Mitochondrial Ca(2+) uptake by the voltage-dependent anion channel 2 regulates cardiac rhythmicity. *Elife* **4:**

De Stefani D, Raffaello A, Teardo E, Szabò I & Rizzuto R (2011) A forty-kilodalton protein of the inner membrane is the mitochondrial calcium uniporter. *Nature* **476:** 336–40

Waldeck-Weiermair M, Deak AT, Groschner LN, Alam MR, Jean-Quartier C, Malli R & Graier WF (2013) Molecularly distinct routes of mitochondrial Ca2+ uptake are activated depending on the activity of the sarco/endoplasmic reticulum Ca2+ ATPase (SERCA). *J. Biol. Chem.* **288:** 15367–79

Westerfield M (2000) The Zebrafish Book. *Eugene***:** University of Oregon Press.

Wilting F, Kopp R, Gurnev PA, Schedel A, Dupper NJ, Kwon O, Nicke A, Gudermann T & Schredelseker J (2020) The antiarrhythmic compound efsevin directly modulates voltage-dependent anion channel 2 by binding to its inner wall and enhancing mitochondrial Ca 2+ uptake . *Br. J. Pharmacol.*

Woods JJ & Wilson JJ (2020) Inhibitors of the mitochondrial calcium uniporter for the treatment of disease. *Curr. Opin. Chem. Biol.* **55:** 9–18

Wu Y, Zhang Q & Zhang R (2017) Kaempferol targets estrogen-related receptor α and suppresses the angiogenesis of human retinal endothelial cells under high glucose conditions. *Exp. Ther. Med.* **14:** 5576–5582

Yao K, Chen H, Liu K, Langfald A, Yang G, Zhang Y, Yu DH, Kim MO, Lee M-H, Li H, Bae KB, Kim H-G, Ma W-Y, Bode AM, Dong Z & Dong Z (2014) Kaempferol targets RSK2 and MSK1 to suppress UV radiation-induced skin cancer. *Cancer Prev. Res. (Phila).* **7:** 958–967

Fig. 1

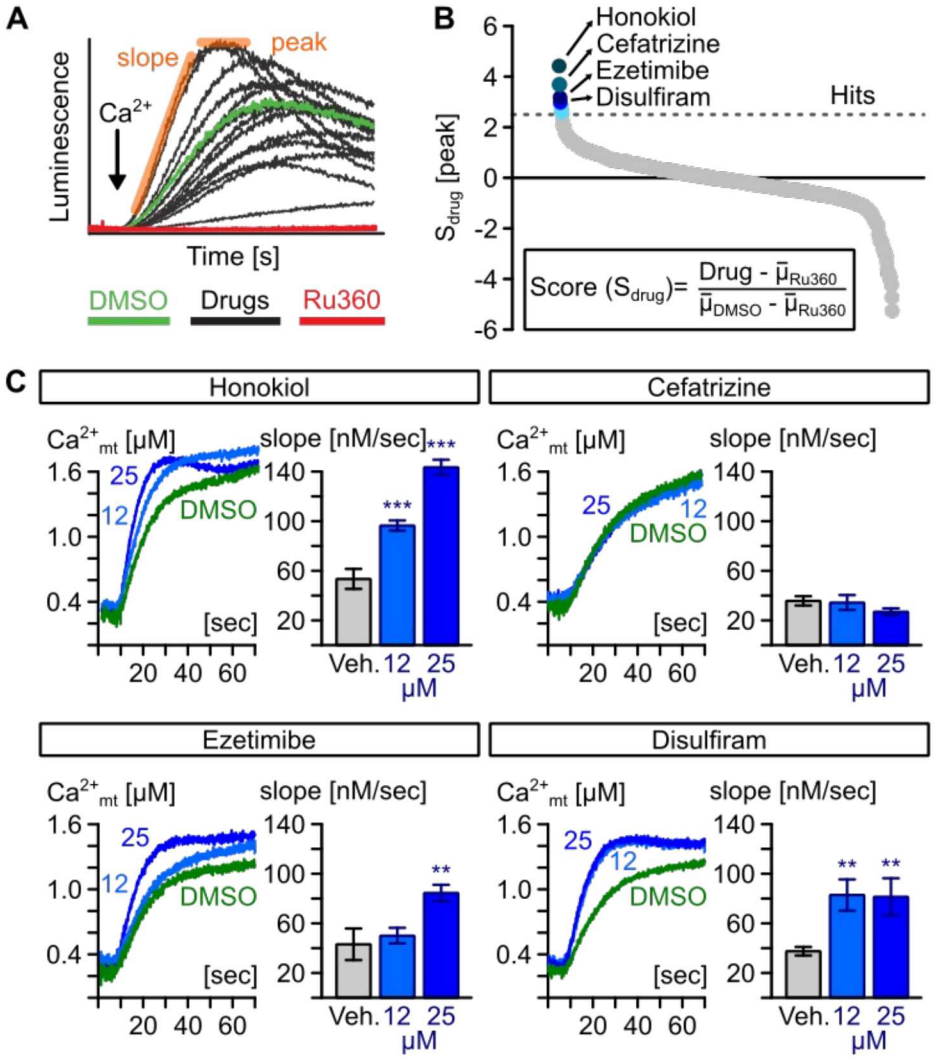

Figure 1. Identification of novel MiCUps by chemical screening. (**A**) Example of Ca^{2+}-dependent, mitochondrial aequorin-based light kinetics in digitonin-permeabilized HeLa cells upon the addition of 4μM free Ca^{2+} (black arrow) in the presence of candidate drugs (10 μM), experimental (10 μM Ru360), and vehicle controls (0.1% (v/v) DMSO). (**B**) Ranking of compounds based on S_{drug} scores. Drugs with S_{drug} scores higher than 2.5-fold in peak value compared to DMSO were selected as hits. (**C**) Representative traces of averaged mitochondrial Ca^{2+} kinetics and quantification of mt-Ca^{2+} uptake rate in mitochondria of permeabilized HeLa cells treated with different concentrations (12 and 25 uM) of honokiol, cefatrizine, ezetimibe and disulfiram and 0.1% (v/v) DMSO (vehicle; Veh.) (ANOVA).

Fig. 2

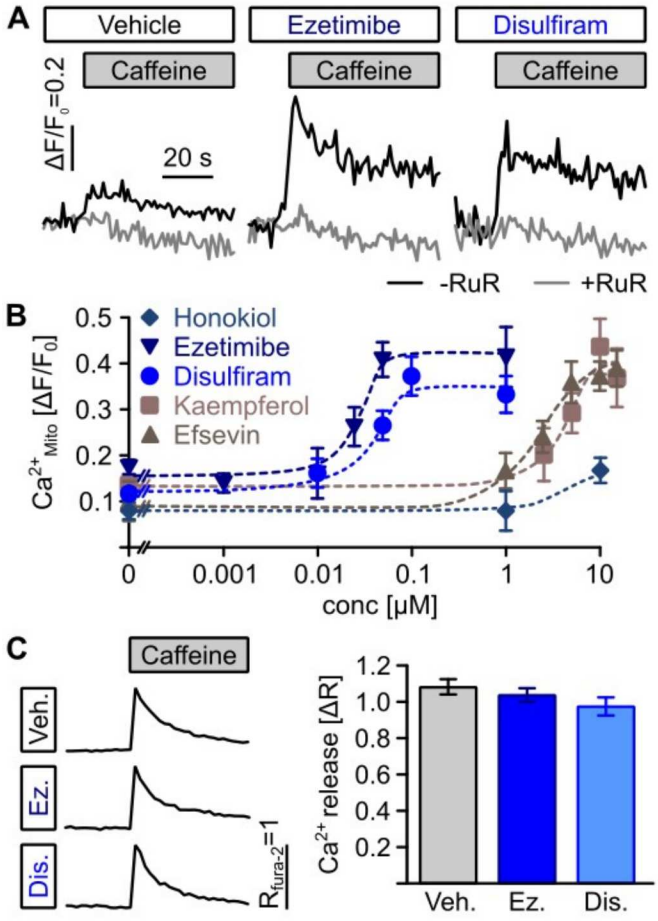

Figure 2. Direct transfer of Ca^{2+} from the sarcoplasmic reticulum into mitochondria in cardiomyocytes. (**A**) Representative recordings of mt-Ca^{2+} uptake (black line) in permeabilized HL-1 cardiomyocytes. Superfusion with 10 mM caffeine induced uptake of Ca^{2+} released form the SR into mitochondria. This uptake was enhanced by 1 μM ezetimibe and 1 μM disulfiram and was blocked by 10 μM of the mt-Ca^{2+} uptake blocker ruthenium red (RuR). (**B**) Ezetimibe and disulfiram enhanced SR-mitochondria Ca^{2+} transfer dose-dependently and at significantly lower concentrations then the established MiCUps kaempferol and efsevin (ezetimibe: EC_{50}=25.5 nM, disulfiram: EC_{50}=36.8 nM, kaempferol: EC_{50}=3.7 μM, efsevin: EC_{50}=2.9 μM). (**C**) Ezetimibe and disulfiram did not alter SR Ca^{2+} release as assessed by fura-2 fluorescence in intact HL-1 cardiomyocytes after addition of 10 mM caffeine (no statistical significance, ΔR=1.07±0.05, for vehicle, ΔR=1.02±0.05 for ezetimibe, ΔR=0.97±0.05 for disulfiram, n=34, ANOVA).

Fig. 3

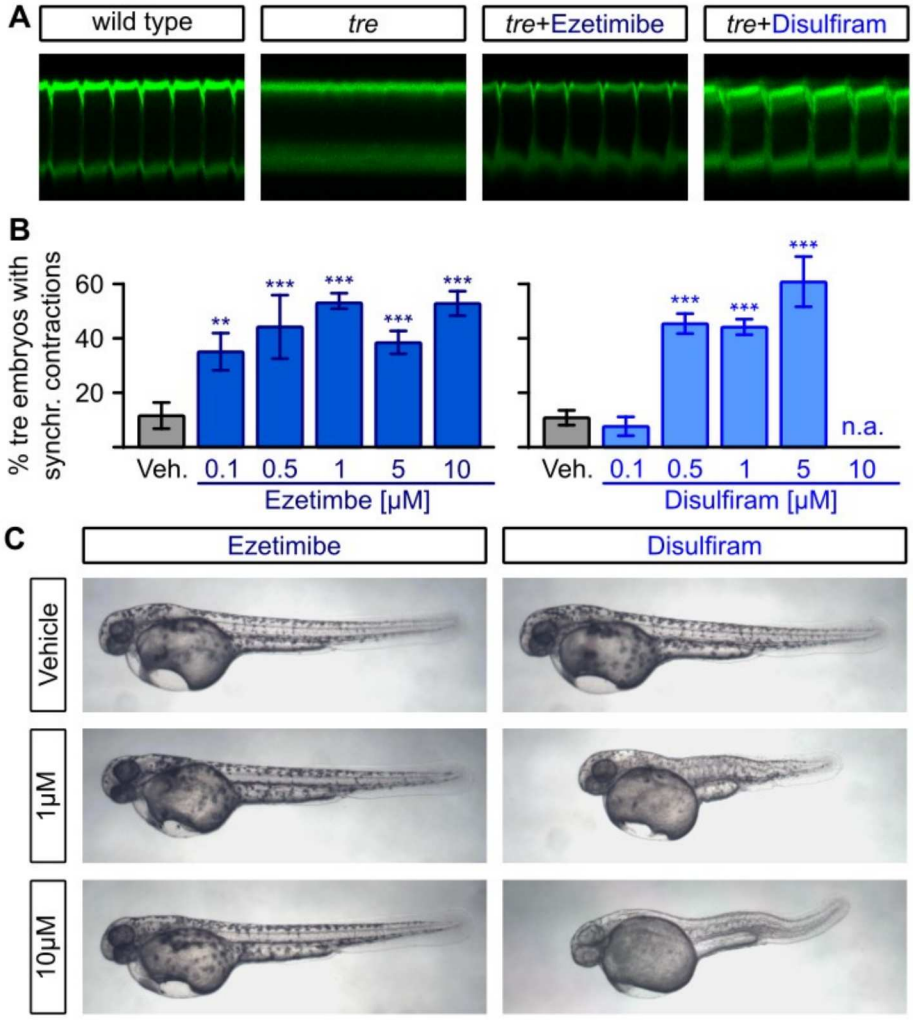

Figure 3. Restoration of rhythmic cardiac contractions in the zebrafish arrhythmia model *tremblor*. (**A**) Representative confocal linescan recordings through atria of beating GFP-labeled hearts from living zebrafish embryos (TG(myl7:eGFP)) at one day after fertilization. Rhythmic cardiac contractions can be observed in wild-type but not *tremblor* (*tre*) embryos. Treatment of *tre* embryos with 1 µM ezetimbe of 1 µM disulfiram restored rhythmic cardiac contractions. (**B**) Quantification of the percentage of *tre* embryos with synchronized contractions for different concentrations of ezetimibe and disulfiram revealed a dose-dependent rescue of the *tre* phenotype from 11.61±4.76 % (n=12) to a maximum of 53.88±3.23% (n=5, ANOVA) at 1µM ezetimibe and from 11.29±2.95% (n=9) to 60.08±9.40% (n=3, ANOVA) at 5 µM disulfiram. (**C**) Treatment of zebrafish embryos with ezetimibe did not alter gross morphology of embryos, while disulfiram induced severe malformations of the body and a lack of pigmentation.

Fig. 4

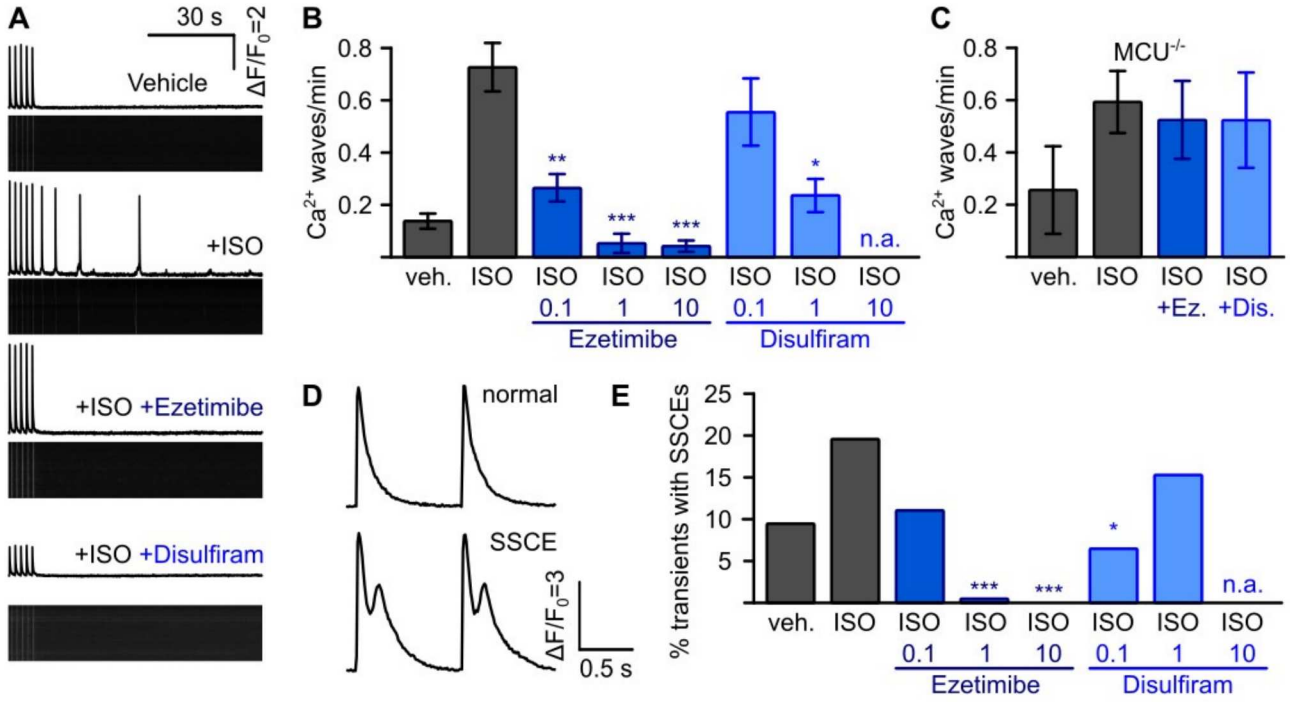

Figure 4 Suppression of arrhythmogenesis in freshly isolated murine RyR$^{C4496R/WT}$ cardiomyocytes by ezetimbe and disulfiram. (**A**) Representative confocal linescan recordings of intracellular Ca^{2+} in freshly isolated ventricular cardiomyocytes from RyR$^{C4496R/WT}$ mice. Cells were continuously pulsed at 0.5 Hz and spontaneous Ca^{2+} waves were analyzed during 1.5 min after pulsing was stopped. Addition of isoproterenol (ISO) induced spontaneous Ca^{2+} waves which could be blocked by the addition of ezetimibe or disulfiram. (**B**) Quantitative analysis of the experiments in A. Addition of ISO raised the propensity for spontaneous Ca^{2+} waves from 0.14±0.04 waves per minute (n=109 cells from 13 mice) to 0.73±0.09 (n=149 cells from 15 mice) in RyR$^{C4496R/WT}$ mice. Addition of ezetimibe lowered waves to 0.27±0.06 under 0.1 (n=64 cells from 7 mice), 0.06±0.04 under 1 (n=23 cells from 3 mice) and finally 0.04±0.03 under 10 µM ezetimibe (n=31 cells from 5 mice) and to 0.56±0.14 under 0.1 (n=36 cells from 4 mice), and 0.24±0.07 under 1 (n=31 cells from 5 mice) for disulfiram (Kruskal-Wallis-Test). (**C**) Disruption of mt-Ca^{2+} uptake by genetic ablation of MCU in MCU$^{-/-}$ / RyR$^{C4496R/WT}$ mice abolished the effect of ezetimibe and disulfiram indicated by comparable values of 0.52±0.15 (n=42 from 5 mice, p>0.999, Kuskal-Wallis-Test) for ISO + 10 µM ezetimibe and 0.52±0.18 (n=47 from 6 mice, p>0.999, Kuskal-Wallis-Test) for ISO + 1 µM disulfiram compared to 0.59±0.12 (n=107 from 10 mice) under ISO alone. (**D**) Representative recording from electrically induced systolic Ca^{2+} transients showing normal transients (upper trace) and transients with secondary systolic Ca^{2+} elevations (SSCEs). (**E**) SSCEs were observed in 9.36% (171/1827 transients; n=121 cells from 15 mice) of all transients in the vehicle control and rose to 19.38% after addition of ISO (386/1992 transients; n=134 cells from 16 mice). Addition of ezetimibe dose-dependently suppressed SSCEs to a minimum of 0.00% under 10 µM ezetimibe (0/783 transients; n=53 cells from 6 mice). Disulfiram decreased SSCEs to 6.51 at 0.1 µM (28/430 transients; n=28 cells from 4 mice), while cells treated with 1µM showed SSCEs in 15.29% of all transients (65/425 transients; n=29 cells from 4 mice, Fisher's exact test). n.a. … not analyzable.

Fig. 5

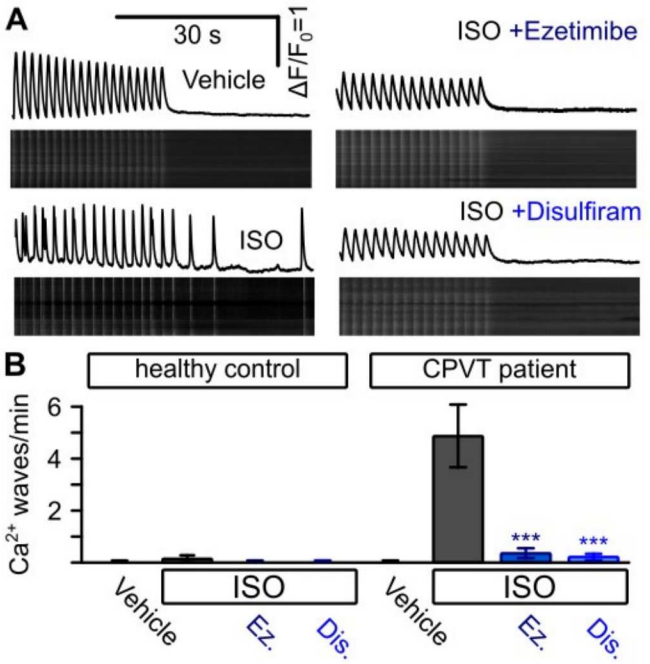

Figure 5 Suppression of arrhytmogenic Ca^{2+} signals in iPSC-derived cardiomyocytes from a CPVT patient. (**A**) Representative confocal linescan recordings of intracellular Ca^{2+} in iPSC-derived cardiomyocytes from a CPVT patient. Cells were continuously pulsed at 0.5 Hz and spontaneous Ca^{2+} waves were analyzed during 30 sec after pulsing was stopped. Addition of isoproterenol (ISO) induced spontaneous Ca^{2+} waves which could be blocked by the addition of ezetimibe or disulfiram. (**B**) Quantitative analysis of the experiments in A and cells from a healthy control. While in cells from a healthy individual addition of ISO did not induce a significant amount of spontaneous Ca^{2+} waves (only in one out of 20 cells examined), it induced the occurrence of waves in CPVT cells (0 waves per minute for vehicle control, n=11, 5.87±1.80 under ISO, n=16, Kruskal-Wallis test), which could be suppressed by the addition of ezetimibe or disulfiram (0.10±0.07 waves per minute for ezetimibe, n=13, 0.05±0.05 waves per minute for disulfiram, n=13, Kruskal-Wallis test)